



Kroner, Frank (2010) *Development of a high throughput screen for the expression of membrane proteins and their purification and crystallisation*. PhD thesis.

<http://theses.gla.ac.uk/1722/>

Copyright and moral rights for this thesis are retained by the author

A copy can be downloaded for personal non-commercial research or study, without prior permission or charge

This thesis cannot be reproduced or quoted extensively from without first obtaining permission in writing from the Author

The content must not be changed in any way or sold commercially in any format or medium without the formal permission of the Author

When referring to this work, full bibliographic details including the author, title, awarding institution and date of the thesis must be given.

Development of a
high throughput screen
for the expression of membrane proteins
and their purification and crystallisation

by
Frank Kroner



University
of Glasgow

A thesis submitted for the degree of
Doctor of Philosophy
in the Faculty of Physical Sciences,
University of Glasgow
December 2009

Declaration

This thesis has been written in accordance with the University of Glasgow regulations, has not been presented for a degree at any other university and is original except where indicated otherwise by reference in the text.

© Frank Kroner

Signed

Date

.....

.....

Frank Kroner

15th December 2009

This work is dedicated
to my father
(1948–1994)

Abstract

Every biological cell is surrounded by a membrane, which functions as a barrier to the environment and as a support matrix for membrane proteins. Membrane proteins facilitate the transport of manifold substrates across the membrane and are involved in fundamental cellular processes, such as signalling or energy generation to name a few. The key to the function of membrane proteins lies in their three dimensional structure, which can be determined by single crystal X-ray crystallography. However, membrane proteins are one of the most difficult protein classes to work with, which is reflected by the small number of available membrane protein structures. Protein crystallography requires milligram amounts of pure protein, which has to be expressed and purified to monodispersity to allow crystallisation. As membrane proteins have to be inserted into the membrane, recombinant expression yields are often low. In order to obtain enough protein for purification and crystallisation studies, the expression of membrane proteins requires screening for the best expression conditions. Purification of membrane proteins requires, due to their amphipathic character, the use of detergents to solubilise the membrane protein. The optimal combination of detergent and membrane protein is crucial for stability in aqueous solution in order to allow purification to monodispersity. Furthermore, the detergent has a high influence on the crystallisation of membrane proteins.

An approach to overcome the challenges of membrane protein structural biology is to work in a high throughput (HTP) manner to increase the chances of success. The aim is to find the most promising targets out of a library of membrane proteins and in the presented work a small-scale HTP expression screen was developed in order to find the optimal expression conditions for each membrane protein from a target library of 12 *E. coli* inner membrane proteins. The targets were then expressed in the determined optimal conditions in sufficient amounts to allow purification. All membrane proteins were subjected to a purification pipeline, which employed a subset of parameters, that have proved to be the most successful to date in membrane protein purification for structural studies. Five membrane proteins were purified to monodispersity and were submitted to crystallisation trials. Crystals of two targets were obtained, which diffracted to 7 Å and 15 Å. Furthermore, the data collected on the expression and purification behaviour of the 12 membrane proteins, will help to optimise the starting parameters for the screening of future targets.

Acknowledgments

I would like to thank my supervisors Prof. Neil W. Isaacs and Dr. Karen McLuskey, for their invaluable advice, guidance and encouragement during the course of my project.

I was very fortunate to have the possibility to work in the context of the Membrane Protein Structure Initiative (MPSi) and learned a lot at various conferences, meetings and a research exchange.

Thanks also goes to members of the PX lab past and present, in particular Isobel Black, Dr. Mads Gabrielsen, Dr. Allan Riboldi-Tunicliffe, Dr. Claire Waterston, Matt Horseham, Prof. Richard Cogdell, June Southall for their helpful advice and in general making the lab a good place to work. All of the above were generous with their time and teaching and often up for out-of-the-lab activites from BBQs, Go Ape adventures to one or more pints in the Aragon or Brel.

I also want to acknowledge Dr. Daniel Daley of the university of Stockholm for kindly providing the membrane protein-GFP fusion constructs used in this work.

A big thank you to all the wonderful people I met here in Glasgow in the past three years, especially to “Team Germany”, Michi, Mona, Daniela, Tobi, Johannes, Mareike, Kasia, Bärbel and Georg for many unforgotten adventures in the Scottish highlands and shared good and bad times. Thanks to my former flat-mate Anna for listen for one year to my moans and sorrows about work and else. Furthermore, I would like to thank the wider Chemistry Department, especially “Team France” comprising Raphaelle and Florence. Special thanks to Antonio Ferra and Catherina Henriques (Team Portugal) for dumping me in time for a new lab week after fantastic weekends up north on Ben Nevis, Ardnamurchan and elsewhere. I am also very grateful to my friends back home, who did not forget me in these three years: Claudio, Lynn, Matthias and Linda and especially helped me to get through my first six weeks of continuous rain in Glasgow.

Thanks to my parents and family for supporting me and helping me wherever they could in the last 29 years! Without their love and help I would not be where I am today. Finally I want to thank Astrid for enduring me, while getting more and more stressed during the write up of this thesis.

Abbreviations

ABC-transporter	ATP-binding cassette-transporter
ATP	Adenosine triphosphate
CMC	Critical micelle concentration
CSC	Critical solubilisation concentration
cv	Column volume
Da	Dalton
DDM	<i>n</i> -Dodecyl β-D-maltoside
DM	Dodecyl-maltopyranoside
DNA	Deoxyribonucleic acid
DTT	Dithiothreitol
<i>E. coli</i>	<i>Escherichia coli</i>
EDTA	Ethylenediamintetraacetic acid
EM	Electron microscopy
FCS	Fluorescence correlation spectroscopy
Ffh	Fifty-four homolog
Fos-choline-14	Tetradecylphosphocholine
FRAP	Fluorescence recovery after photobleaching
GFP	Green fluorescent protein
GTP	Guanidine triphosphate
HIV	Human immunodeficiency virus
HTP	High throughput
IMAC	Immobilised metal affinity chromatography
IMP	Integral membrane protein
IPTG	Isopropyl-β-D-thiogalactoside
LB medium	Lysogeny broth (or Luria Bertani)
LBA medium	LB medium supplemented with antibiotics
LDAO	Lauryldimethyl amine oxide
LDS	Lithium dodecyl sulphate
MFS	Major facilitator superfamily
MM	MagicMedia (Invitrogen)
mRNA	Messenger ribonucleic acid

MW	Molecular weight
MWCO	Molecular weight cut off
NBD	Nucleotide binding domain
NiNTA	Nitriloacetic acid
OG	n-Octyl- β -D-glucopyranoside
PDB	Protein Data Bank
PDB ID	Protein Data Bank Identification
PDC	Protein-detergent complex
PEG	Polyethylene glycol
RNA	Ribonucleic acid
SB medium	Super broth medium
SDS	Sodium dodecyl sulphate
SDS-PAGE	SDS-Polyacrylamide gel electrophoresis
SPT	Single-particle tracking
SRP	Signal recognition particle
TB	TB overnight express medium (Novagen)
Tfb	Transformation buffer
TMD	Trans membrane domain

List of Contents

Abstract.....	III
Acknowledgements.....	IV
Abbreviations.....	V
List of Figures.....	XIII
List of Tables.....	XVI

Chapter 1

Introduction	1
1.1 The biological membrane.....	1
1.1.1 Membrane structure	2
1.1.1.1 Phospholipids as building blocks of membranes.....	2
1.1.1.2 From fluid mosaic to the “picket fence” model of membranes.....	4
1.1.2 Membrane function.....	6
1.2 Membrane proteins.....	6
1.2.1 Biogenesis of inner membrane proteins	7
1.2.2 Transmembrane domains.....	9
1.2.3 Classification of membrane proteins	10
1.2.4 Function of membrane proteins	11
1.2.4.1 The ATP-binding cassette transporter superfamily	12
1.2.4.2 The major facilitator superfamily	14
1.3 Structural biology of membrane proteins.....	16
1.3.1 Introduction	16
1.3.2 Overexpression of inner membrane proteins.....	17
1.3.3 Purification of inner membrane proteins	19
1.3.3.1 Physical properties of detergents.....	19
1.3.3.2 The use of detergents in membrane protein biochemistry.....	21
1.3.4 Crystallisation of membrane proteins.....	25
1.4 High throughput approach.....	27
1.5 Aims of the study	29
1.6 Target membrane proteins.....	30

Chapter 2

Materials and Methods	31
2.1 Introduction	31
2.2 Target GFP-fusion construct	31
2.3 Molecular biology methods.....	33
2.3.1 Preparation of competent cells	33
2.3.2 Transformation of plasmid DNA into host cells	35
2.4 Protocols for protein expression and purification	36
2.4.1 Medium-scale protein expression.....	36
2.4.2 Cell density measurements	37
2.4.3 Protein analysis.....	38
2.4.3.1 The measurement of protein concentration	38
2.4.3.2 Sodium dodecyl sulphate polyacrylamide gel electrophoresis.....	39
2.4.3.3 Mass spectrometry.....	39
2.4.3.4 Fluorescence intensity	39
2.4.4 Cell lysis and membrane preparation	40
2.4.5 Solubilisation of membrane proteins.....	40
2.4.6 Immobilised metal affinity chromatography	41
2.4.7 Protein Dialysis.....	42
2.4.8 TEV-protease production & cleavage	42
2.4.8.1 Expression and purification of Tobacco etch virus-protease	43
2.4.8.2 Cleavage of GFP-fusion protein with tobacco etch virus-protease	44
2.4.9 Size exclusion chromatography	44
2.5 Crystallisation experiments	45
2.5.1 Initial screening	45
2.5.2 Optimisation screens.....	46
2.6 X-ray analysis.....	46

Chapter 3

Expression of target membrane proteins.....	47
3.1 Introduction	47
3.2 Development of a small-scale high throughput expression screen	49

3.2.1	Screen set up design	49
3.2.2	Transformation	51
3.2.3	Starter culture	53
3.2.4	Expression cultures.....	54
3.2.5	Collection of expression data	55
3.2.6	Limitations of small-scale expression screening	58
3.3	The choice of parameters	59
3.4	Final small-scale high throughput expression screen protocol	61
3.4.1	Transformation in the HTP-expression screen	64
3.4.2	Cell growth	65
3.4.3	Sample preparation and data collection.....	65
3.4.4	Results	67
3.5	Medium-scale expression	70
3.6	Trends from expression data	71
3.6.1	Trends in the performance of media.....	72
3.6.2	Trends in the performance of cell lines	73
3.6.3	Trends in the performance of single cell lines in different media	75
3.6.3.1	Protein expression and cell growth in C41(DE3).....	75
3.6.3.2	Protein expression and cell growth in BL21 Star (DE3).....	76
3.6.3.3	Protein expression and cell growth in BL21(DE3)pLysS	77
3.6.3.4	Protein expression and cell growth in Rosetta(DE3)pLysS	78
3.7	Conclusion.....	79

Chapter 4

Purification of target membrane proteins	81	
4.1	Introduction	81
4.2	Solubilisation.....	83
4.3	First NiNTA-column	84
4.4	Dialysis.....	86
4.5	Cleavage with <i>Tobacco etch virus</i> protease	86
4.6	Second NiNTA-column.....	88
4.7	Size-exclusion chromatography	89

4.8 Purification status of targets	91
4.8.1 XylE	92
4.8.2 PgpB	95
4.8.3 CcmC	99
4.8.4 YdhC	101
4.8.5 CodB	104
4.8.6 ChbC	107
4.8.7 PnuC	111
4.8.8 Lgt	113
4.8.9 YhbE	119
4.8.10 XylH	120
4.8.11 FtsX	125
4.8.12 YdeD	127
4.9 Conclusion	128

Chapter 5

Crystallisation.....	129
5.1 Introduction	129
5.2 Crystallisation trials	130
5.3 Crystallisation of XylH	132
5.4 Crystallisation of PgpB	139
5.5 Conclusion	146

Chapter 6

Discussion and future perspectives.....	148
--	------------

Chapter 7

Appendix	152
7.1 DNA and protein sequences	152
7.1.1 CcmC	152
7.1.1.1 DNA sequence	152

7.1.1.12 Protein sequence.....	152
7.1.2 CodB.....	153
7.1.2.1 DNA sequence.....	153
7.1.2.2 Protein Sequence	153
7.1.3 FtsX	154
7.1.3.1 DNA sequence.....	154
7.1.3.2 Protein sequence.....	155
7.1.4 Lgt.....	155
7.1.4.1 DNA sequence.....	155
7.1.4.2 Protein sequence.....	155
7.1.5 PnuC	156
7.1.5.1 DNA sequence.....	156
7.1.5.2 DNA sequence.....	156
7.1.6 XylE.....	157
7.1.6.1 DNA sequence.....	157
7.1.6.2 Protein sequence.....	157
7.1.7 XylH	158
7.1.7.1 DNA sequence.....	158
7.1.7.2 Protein sequence.....	158
7.1.8 YdeD.....	159
7.1.8.1 DNA sequence.....	159
7.1.8.2 Protein sequence.....	159
7.1.9 ChbC.....	160
7.1.9.1 DNA sequence.....	160
7.1.9.2 Protein sequence.....	160
7.1.10 PgpB	161
7.1.10.1 DNA sequence.....	161
7.1.10.2 Protein sequence.....	161
7.1.11 YhbE.....	162
7.1.11.1 DNA sequence.....	162
7.1.11.2 Protein sequence.....	162
7.1.12 YdhC.....	163
7.1.12.1 DNA sequence.....	163
7.1.12.2 Protein sequence.....	163

7.2	Mass spectrometry peptide sequencing results	164
7.2.1	PgpB	164
7.2.2	XylH	165
7.3	Formulations of crystallisation screens	166
7.3.1	MemStart	166
7.3.2	MemSys	167
7.3.3	MemGold	168
7.3.4	Peg/Ion 1/2	172
7.3.5	JCSG 1/2	174
7.3.6	Hampton Crystal Screen 1/2	176
7.3.7	Detergent Screen 1/2	178
7.3.8	Additive screen	180
References	182

List of Figures

Figure 1.1	The most common phospholipids in membranes	2
Figure 1.2	A simplified schematic of a membrane	4
Figure 1.3	Membrane protein biogenesis in <i>E. coli</i>	7
Figure 1.4	Examples of the helix-bundle fold and β -barrel fold of membrane proteins	9
Figure 1.5	Structure of the <i>E. coli</i> vitamin B12 importer BtuCD	13
Figure 1.6	Crystal structure of <i>E. coli</i> LacY.	14
Figure 1.7	Schematic view of detergent and lipid monomers and aggregates	19
Figure 1.8	Schematic display of the solubilisation process of membrane proteins with detergents	22
Figure 1.9	Different types of membrane protein crystals	25
Figure 2.1	Expression vector set-up of target membrane proteins	31
Figure 2.2	Calibration curve for the plate reader Fluostar Optima	38
Figure 3.1	The grid system used throughout the HTP screen.	50
Figure 3.2	The 96-well micro-tube cluster plate used as transformation block	51
Figure 3.3	Transfer of samples from 96-well transformation block to the 24-well agar plates	52
Figure 3.4.	Agar plates containing transformants after incubation	53
Figure 3.5	Inoculation of 48-well expression blocks with starter cultures	54
Figure 3.6	Preparation scheme of samples from the expression blocks for fluorescence and OD ₆₀₀ measurements	57
Figure 3.7	Workflow graphic of the small-scale HTP screen	63
Figure 3.8.	Schematic representation of the transformation block and agar plates	64
Figure 3.9	The collection of samples from expression blocks into analysis blocks	66
Figure 3.10	Overall expression results for all 12 membrane protein-GFP fusions	68
Figure 3.11	Temperature dependence of cell growth and expression in different media averaged over all targets and cell lines	72
Figure 3.12	Temperature dependence of cell growth and expression in different cell lines averaged over all targets and media	73
Figure 3.13	Data of fluorescence intensity and cell density of C41(DE3) in different media, averaged over all targets	75
Figure 3.14	Fluorescence values for average target expression and cell growth in BL21 Star (DE3)	76
Figure 3.15	Fluorescence values for average target expression and cell growth in BL21(DE3)pLysS	77
Figure 3.16	Fluorescence values for average target expression and cell growth in Rosetta(DE3)pLysS	78
Figure 4.1	Scheme of the membrane protein purification pipeline.	82

Figure 4.2	Optimisation of imidazole gradient for the elution of ChbC	84
Figure 4.3	Example of collected fractions after the first affinity column	85
Figure 4.4	SDS-Pages from samples from the TEVP cleavage of Lgt and from the following affinity column.	87
Figure 4.5	Elution of green coloured GFP-His ₈ from the second affinity column	88
Figure 4.6	Effect of different detergents on the monodispersity of XylH in solution.	90
Figure 4.7	XylE-GFP fusion elution trace of the first affinity column	92
Figure 4.8	SDS-Page of samples from the first NiNTA column of XylE purification	93
Figure 4.9	Precipitation of XylE-GFP fusion in the pooled fractions in the pooled fractions from the first affinity column	93
Figure 4.10	Samples from the second affinity column of XylE-purification	94
Figure 4.11	Elution trace of PgpB-GFP fusion from the first NiNTA-column	95
Figure 4.12	SDS-PAGE of samples from the PgpB-GFP fusion elution trace	96
Figure 4.13	SDS-PAGE of samples from the cleavage and the second affinity column in PgpB purification	97
Figure 4.14	Gel filtration trace of PgpB in DDM.	97
Figure 4.15	Gel of the final purification samples from PgpB	98
Figure 4.16	Elution trace of CcmC-GFP fusion from the first NiNTA-column	99
Figure 4.17	SDS-PAGE of samples from CcmC-GFP purification	100
Figure 4.18	SDS-PAGE of CcmC-GFP fusion from dialysis, cleavage samples and from fractions from the second affinity column in CcmC purification	100
Figure 4.19	Elution trace of YdhC-GFP from first NiNTA column	101
Figure 4.20	SDS-PAGE of samples from fractions from the first affinity column of YdhC-GFP fusion	102
Figure 4.21	SDS-Page of samples from dialysis, cleavage and second affinity column with YdhC	102
Figure 4.22	Gel filtration trace of YdhC in Fos-Choline 14	103
Figure 4.23	SDS-PAGE of samples from gel filtration run with YdhC	103
Figure 4.24	Elution trace of CodB-GFP fusion from the first affinity column	104
Figure 4.25	SDS-PAGE of samples from the first part of CodB purification	105
Figure 4.26	SDS-PAGE of samples from the second part of CodB purification	105
Figure 4.27	SDS-PAGE of samples from fractions from second affinity column in the purification of CodB	106
Figure 4.28	First affinity column trace of ChbC	107
Figure 4.29	SDS-PAGE of solubilisation samples and fractions from the first affinity column of ChbC	108
Figure 4.30	SDS-PAGE of ChbC samples from the supernatant of the cleavage and fractions from the second affinity column	108
Figure 4.31	On-column detergent optimisation for ChbC	110
Figure 4.32	Elution trace of PnuC from the first affinity column	111

Figure 4.33	SDS-PAGE of samples from PnuC solubilisation and from the peak fractions of the first affinity column	112
Figure 4.34	Samples from dialysis and from second NiNTA column from PnuC purification	112
Figure 4.35	Elution trace of Lgt from first affinity column	113
Figure 4.36	SDS-PAGE of first purification steps of Lgt	114
Figure 4.37	Gels of samples from the cleavage test for Lgt and from fractions from the following affinity columns	115
Figure 4.38	Elution trace of Lgt from first NiNTA column with optimised imidazole gradient	116
Figure 4.39	SDS-PAGE of samples from the solubilisation of Lgt and from peak fractions of the first affinity column	117
Figure 4.40	Gel filtration trace of Lgt in DDM	117
Figure 4.41	SDS-PAGE of gel filtration peak fractions of Lgt	118
Figure 4.42	Elution trace of YhbE-GFP fusion from the first affinity column	119
Figure 4.43	Elution trace of XylH-GFP fusion with optimised imidazole gradient from the first affinity column	120
Figure 4.44	SDS-PAGE of solubilisation and elution fractions from XylH-GFP	121
Figure 4.45	SDS-PAGE of samples from dialysis, cleavage and second affinity column of XylH purification	122
Figure 4.46	On-column detergent optimisation for XylH	123
Figure 4.47	Elution trace of FtsX-GFP fusion from the first affinity column	125
Figure 4.48	SDS-PAGE of initial samples from FtsX-GFP purification steps	126
Figure 4.49	SDS-PAGE of samples from the second half of the attempted FtsX purification	127
Figure 4.50	Elution trace of YdeD-GFP from the first affinity column	127
Figure 5.1	Initial crystals in MemStart/Sys screen condition C9	133
Figure 5.2	Suspected XylH crystals grown in the initial condition C9	133
Figure 5.3	Diffraction image of XylH obtained at the Diamond Light Source	134
Figure 5.4	Homemade screen I for XylH	136
Figure 5.5	Homemade screen II for XylH	137
Figure 5.6	Grown crystals in initial MemSys screen with PgpB in DDM	139
Figure 5.7	PgpB and detergent crystals in condition 27 of MemGold screen	140
Figure 5.8	Diffraction image of the PgpB crystal	141
Figure 5.9	Format of the 96-well homemade optimisation screen III for PgpB	142
Figure 5.10	Homemade screen IV for PgpB	143
Figure 5.11	Examples of the PgpB crystals found in homemade screens III and iV	144
Figure 5.12	Diffraction image of PgpB crystal in in-house X-ray source	144

List of Tables

Table 1.1	Physical properties of the detergents SDS, LDAO, Fos-Choline 14 and DDM	24
Table 1.2	The 12 <i>E. coli</i> inner membrane proteins chosen for the study	30
Table 2.1	The commercial <i>E. coli</i> strains employed, their usage, antibiotic resistances and suppliers	33
Table 2.2	The antibiotics used, together with their stock concentration, working concentration and solvent	33
Table 2.3	Media, antibiotics and buffers used in the RbCl-method	34
Table 2.4	Composition of buffers and media used for autoinduction expression	36
Table 2.5	Buffers and materials used for IMAC purification	41
Table 2.6	Buffers and materials employed for protein dialysis	42
Table 2.7	The buffers and labware used for the expression and purification of TEVP	43
Table 2.8	The buffer and the required materials used for size-exclusion chromatography	44
Table 2.9	The commercially available crystallisation screens used in this study	45
Table 3.1	Abbreviations for the parameters used in the small-scale HTP expression screen	61
Table 3.2	The blocks and plates employed for the small scale HTP screen	61
Table 3.3	The best expression condition for each of the screened 12 membrane proteins	69
Table 3.4	Ranking of the targets after expression screen according to their fluorescence values	69
Table 3.5	Ranking of targets from small-scale and medium scale expression	70
Table 5.1	Crystallisation screens for Lgt, XylH, ChbC and PgpB set-up after second affinity column	130
Table 5.2	Crystallisation screens for ChbC and YdhC, set-up after gel filtration	131
Table 5.3	Initial crystal screens for XylH in Fos-Choline 14	132
Table 5.4	Complete list of optimisation screens for XylH	138
Table 5.5	Initial screens for PgpB after purification by gel filtration chromatography	139
Table 5.6	Optimisation screens for PgpB	145
Table 6.1	Comparison of target properties with the expression and purification performance	150

Chapter 1

Introduction

Part one of the introduction to this study on membrane proteins introduces the fundamental biology of membranes and membrane proteins. The function of biological membranes, their building blocks and macromolecular assembly are described. Membrane proteins use the membrane as a matrix for their manifold functions, some of which are reviewed after their biogenesis, classification and common structural folding patterns are introduced. The second part of the introduction considers the structural biology of membrane proteins, involving all relevant steps for this study from recombinant overexpression to purification and crystallisation. Part three gives an overview of the benefits of high throughput methods in structural biology followed by the aim of this study. The final section introduces the target library of the addressed membrane proteins.

1.1 The biological membrane

The creation of membranes was a crucial step in evolution. Membranes prevent the free molecular diffusion of compounds and this enabled the development of the first self-replicating forms of life on Earth. The membrane itself evolved into the most important platform of the cell for energy generation, signalling, protection, transport of nutrients and facilitates countless other functions.

The formation of phospholipid bilayers was first described by Gorter and Grendel in 1925 (Gorter and Grendel 1925) and in 1935 Davson and Danielli proposed a model of the cell membrane, in which the phospholipid bilayer was embedded between two layers of globular protein (Danielli and Davson 1935). The model could explain the observed surface tension of lipid bilayers. The Davson-Danielli model was predominant for 37 years until in 1972 Singer and Nicolson published the fluid mosaic model (Singer and Nicolson 1972). They eliminated the flanking protein layers of the Davson-Danielli model, which were not supported by new experimental evidence and included transmembrane proteins (Singer and Nicolson 1972). Refinements of the fluid mosaic model allow a clearer picture of the cell membrane today, but many aspects, such as compartmentation or lipid rafts, are still a matter of debate.

1.1.1 Membrane structure

1.1.1.1 Phospholipids as building blocks of membranes

The primary building blocks of biological membranes are phospholipids (Alberts *et al.* 1983). They are in most cases derived from glycerol-3-phosphate, which is connected via ester bonds to two long hydrophobic hydrocarbon tails and to a hydrophilic phosphate head-group. The amphipathic character of a phospholipid is influenced by the length and saturation state of the fatty acids, which form the hydrophobic tail (Voet *et al.* 2002). The fatty acids contain 14–24 carbon atoms, with one tail group of the phospholipid usually having one or more *cis*-double bonds while the other tail is saturated. The phosphate functions as a linker to various hydrophilic head-groups (Alberts *et al.* 1983; Voet *et al.* 2002). Figure 1.1 shows a representation of the most common phospholipids in biological membranes.

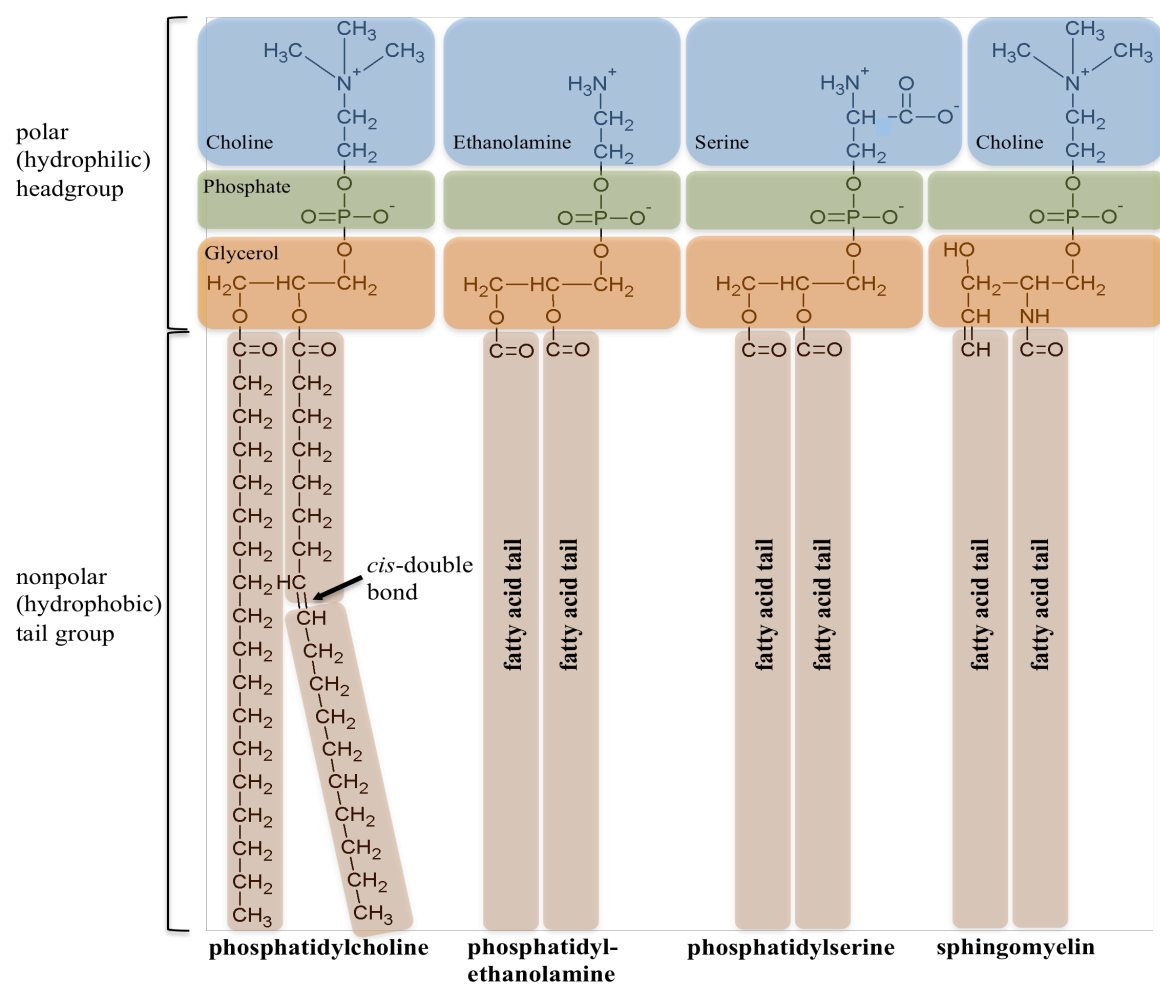


Figure 1.1: The most common phospholipids in membranes. For the ease of display the fatty acid tails are represented in straight columns. Fatty acid tails often contain *cis*-double bonds, which lead to a kink in the chain as shown for phosphatidylcholine. The figure was created with Microsoft Powerpoint.

Lipids have a complex phase behaviour in aqueous solution and different aggregation states are observed (Feigenson 2006; van Meer *et al.* 2008). Driven by the hydrophobic effect, a lipid bilayer can be formed in water by exposing the hydrophilic head-groups to the solvent and shielding the hydrophobic tails. Lipids can form liposomes in water, which consist of a continuous phospholipid bilayer (Alberts *et al.* 1983; van Meer *et al.* 2008).

The fluidity of the membrane is influenced by the length and saturation state of the fatty acid hydrocarbon chains and also dependent on the amount of other membrane components such as cholesterol (Alberts *et al.* 1983; Rawicz *et al.* 2000). The rigid steroid ring system of cholesterol hinders the movement of the fatty acid tails of the phospholipids. Cholesterol functions as a softening agent and widens the temperature range of membrane fluid phase (Alberts *et al.* 1983). Most biological membranes have transition temperatures between 10 and 40 °C. Ectothermic organisms such as bacteria or fish can adapt to temperature changes of the environment by altering the lipid composition of their membranes.

New membranes are built in all cells through the extension of the existing membrane (Voet *et al.* 2002). In eukaryotic cells the membrane lipids are in most cases synthesised in the membrane of the endoplasmic reticulum and are directed in vesicles to the plasma membrane (Alberts *et al.* 1983). Prokaryotic organisms, such as *Escherichia coli* (*E. coli*), feature a cell wall followed by the periplasm, which is separated in Gram-negative bacteria from the cytoplasm by an inner membrane. Membrane lipids are synthesised in bacteria directly at the membrane surface. The thickness of membranes varies around an average of 6 nm but is adjusted to the shape and size of its components, especially integral membrane proteins (Voet *et al.* 2002).

1.1.1.2 From fluid mosaic to the “picket fence” model of membranes

The macromolecular assembly of the lipid bilayer is still a matter of debate. The proposed fluid mosaic model of Singer and Nicolson is based on the principles of Brownian motion and predicted lateral and rotational freedom and random distribution of molecular components in the membrane (1972). A membrane was described as a two-dimensional orientated solution of integral membrane proteins in the viscous phospholipid bilayer. Membrane proteins would be evenly distributed and able to freely diffuse in the membrane (Singer and Nicolson 1972; Vereb *et al.* 2003). However, increasing experimental evidence challenged this model. The fluid mosaic model could not explain the observation that the diffusion rate of lipids in the cell membrane is reduced by up to 5–100 times in comparison to synthetic bilayers. Furthermore the great structural variety of phospholipids together with their asymmetric distribution in the membrane, indicate molecular heterogeneity and the possibility of membrane microdomain formation (Swaisgood and Schindler 1989; Lee *et al.* 1993; Shaikh *et al.* 2001; Fujiwara *et al.* 2002).

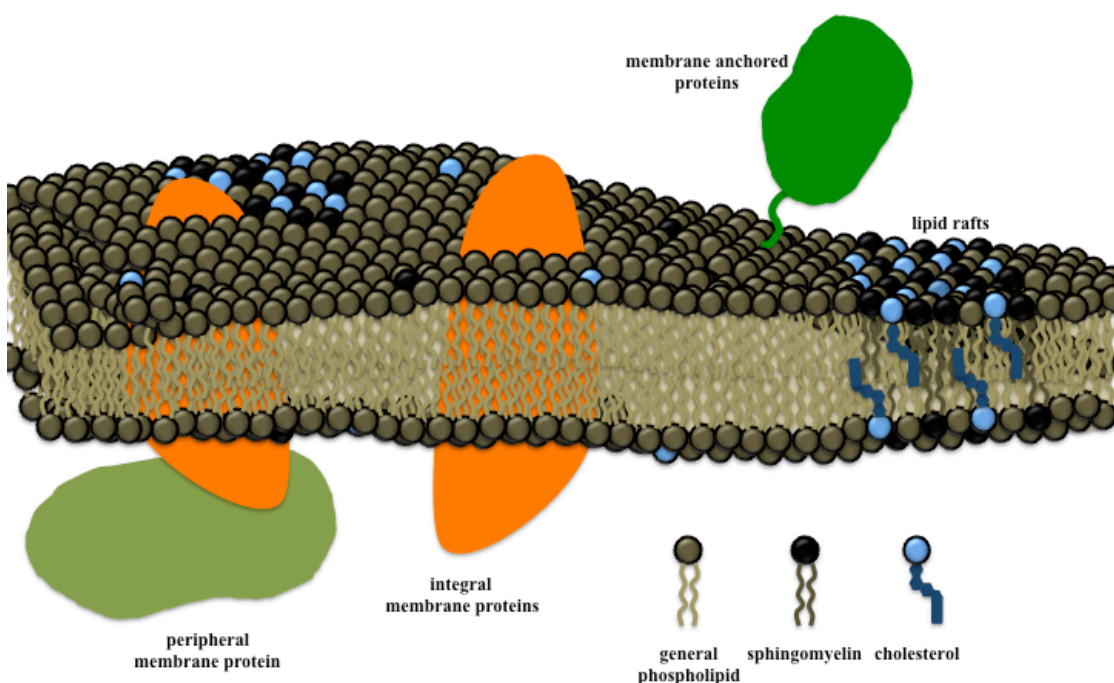


Figure 1.2: A simplified schematic of a membrane. The lipid bilayer is made up from phospholipids, sphingomyelins and cholesterol and is spanned by integral membrane proteins. As described in section 1.2.3, peripheral membrane proteins are non-covalently attached to the membrane by interaction with its components. Proteins can also be anchored to the membrane by a hydrophobic polypeptide sequence or a transmembrane domain. Lipid microdomains or rafts are rich in cholesterol and sphingolipids and are present in a liquid-ordered phase. The figure was created using Microsoft Powerpoint.

These findings led to the development of the “picket fence” model by the group of Kusumi (Fujiwara *et al.* 2002). This model is based on the assumption that inner membrane proteins (IMP), which can be anchored to the cytoskeleton, generate cages confining membrane components. The transmembrane helices are the pickets of the fence, which is formed by IMPs. The membrane components can diffuse very fast laterally inside these membrane compartments, but are hindered in long-range movements by various interactions that give rise to membrane domains. However, membrane proteins can still migrate from domain to domain by hopping or jumping the domain barriers, as was revealed by single-particle tracking (SPT) experiments (Kusumi *et al.* 1993). Furthermore, the model is able to explain increasing observations of domain formations induced through lipid-lipid interactions, lipid-protein interactions, protein-protein interactions and interactions with the cytoskeleton (Kusumi *et al.* 1993; Sprong *et al.* 2001; Baumgart *et al.* 2003; Daumas *et al.* 2003).

However, the model cannot explain the cause and origin of all various confinements that have been described and so it is constantly being refined. Especially the existence of lipid microdomains, or rafts, is difficult to incorporate into the “picket fence” model. These rafts were first described in 1988 (Simons and van Meer). The Keystone Symposium on Lipid Rafts and Cell Function in March 2006 found a common definition for these microdomains: “Membrane rafts are small (10–200 nm), heterogeneous, highly dynamic, sterol- and sphingolipid-enriched domains that compartmentalise cellular processes. Small rafts can sometimes be stabilised to form larger platforms through protein-protein and protein-lipid interactions” (Pike 2006). Although the existence of lipid rafts can be shown in model membranes, their presence in an intact biological cell still needs to be proven (Baumgart *et al.* 2007).

They are supposed to be involved in numerous processes, such as protein sorting, apoptosis, signal transduction (Brown and London 1998) or even virus infection processes for influenza and human immunodeficiency virus (HIV) (Ono and Freed 2001; Sun and Whittaker 2003; Jolly and Sattentau 2005).

Techniques such as fluorescence recovery after photobleaching (FRAP), SPT, and fluorescence correlation spectroscopy (FCS) were developed to investigate the macromolecular assembly of lipids and membranes and as they are improved we might obtain a clearer picture of membrane structure *in vivo* (Destainville *et al.* 2008).

1.1.2 Membrane function

The main function of every membrane is the formation of a barrier that separates the cell from the environment. Membranes also divide the internal cell volumes into comparable isolated compartments. In eukaryotic cells the membranes of the endoplasmic reticulum, Golgi apparatus, mitochondria and other membrane-bound organelles separate the inside of the specific organelles from the cytoplasm. The membrane makes the passing of polar or electrically charged molecules very difficult. This enables the cell to keep its chemical composition independently of the surrounding environment, in a range necessary to maintain its metabolism (Voet *et al.* 2002).

However, cell metabolism relies on a steady-state equilibrium, making the import or export of nutrients, ions and other chemicals necessary. The membrane therefore also functions as a matrix or platform for membrane proteins. They enable a controlled flow of compounds across the membrane and play multiple other important roles in the cell's ability to respond to changes in the environment (Alberts *et al.* 1983).

1.2 Membrane proteins

In most genomes, around 20–30 % of all predicted genes encode membrane proteins (Krogh *et al.* 2001). Biological membranes provide a matrix for membrane proteins, which catalyse most of the specific functions associated with membranes. Depending on the cellular location, the average amount of membrane protein varies around a mean of 50 % (w/w) (Alberts *et al.* 1983). This section describes the biogenesis of membrane proteins followed by their classification, common structural principles and their manifold functions.

1.2.1 Biogenesis of inner membrane proteins

The biogenesis of inner membrane proteins (IMP) follows a partly conserved co-translational pathway (Luirink *et al.* 2005). In *E. coli*, the targeting of the nascent polypeptide chain to the membrane involves a signal recognition particle (SRP) and the SRP-receptor (Collinson 2005). The inner membrane complex SecYEG is responsible for the insertion of the IMP into the membrane in *E. coli* (Luirink *et al.* 2005; Saier *et al.* 2008). The membrane protein YidC is involved in the late stages of IMP biogenesis in conjunction with SecYEG. YidC is also a membrane insertase for Sec-independent membrane proteins (Serek *et al.* 2004). A mechanism of membrane protein biosynthesis in *E. coli* was proposed based on biochemical data supported by electron microscope (EM) and X-ray structures of the SecYEG complex (Breyton *et al.* 2002; Van den Berg *et al.* 2004; Luirink *et al.* 2005). Figure 1.3 shows the three-step mechanism and more details of the participating proteins are given below.

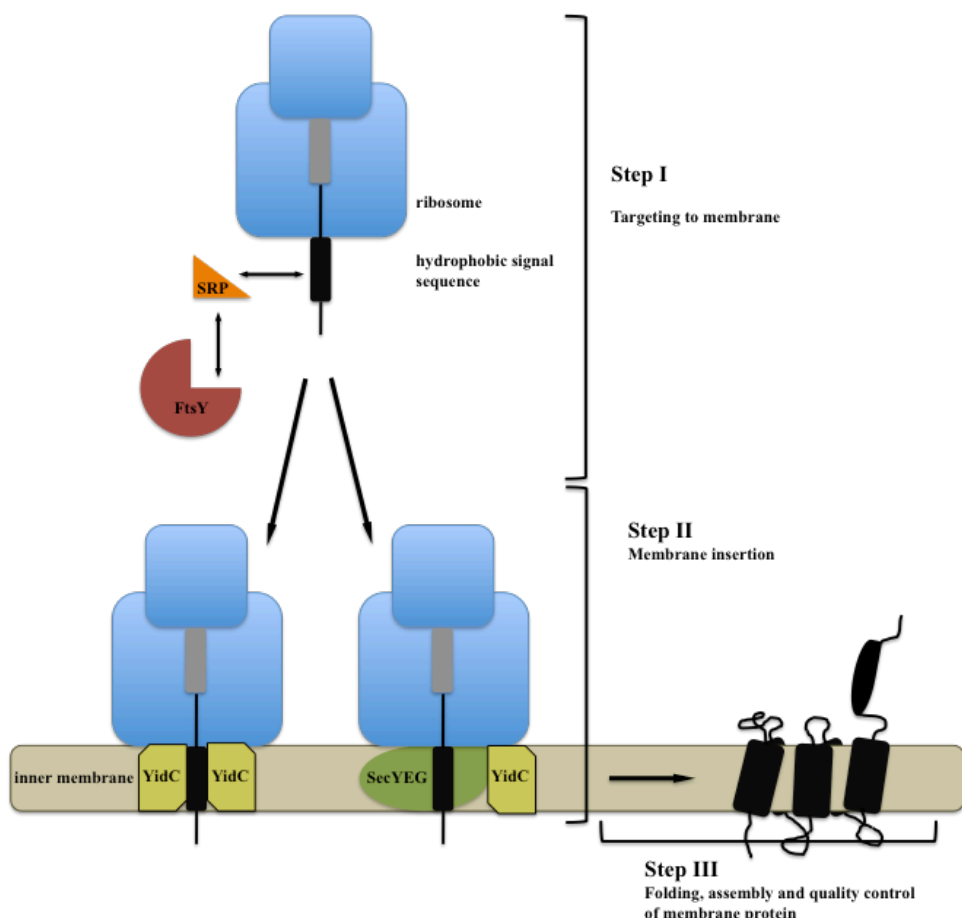


Figure 1.3: Membrane protein biogenesis in *E. coli*. In Step 1 the SRP binds to the nascent polypeptide chain and the SRP mediates together with FtsY (SRP-receptor) the targeting to the membrane. The second step involves the insertion of the polypeptide chain into the membrane, either by YidC or by a complex from SecYEG and YidC. The membrane protein is released from the translocon in the third step and folds in the membrane. The protein is degraded, if defects are detected.

In the first step, the SRP mediates co-translational targeting to the membrane by interacting with hydrophobic target sequences of the nascent polypeptide, shortly after the first residues exit the ribosome. The SRP in *E. coli* is one of the simplest and consists of only one protein Ffh (fifty-four homolog), a homolog to the eukaryotic SRP54 protein (Luirink *et al.* 2005). The SRP contains a 4.5S RNA component, which is homologous to parts of the mammalian SRP 7SL RNA (Luirink *et al.* 2005; Nouwen *et al.* 2007; Driessen and Nouwen 2008). The SRP-receptor FtsY binds to the ribosome-SRP complex. The receptor contains only one subunit, which is a homolog of the mammalian SRα-receptor (Luirink *et al.* 1994). FtsY supports the targeting to the membrane through its affinity for lipids and possibly to the translocon component SecY (Luirink *et al.* 1994). FtsY is supposed to act together with the SRP as a GTP-dependent chaperone, feeding the nascent polypeptide chain into the SecYEG complex or the YidC translocase (Scotti *et al.* 1999; Rapoport 2007; Driessen and Nouwen 2008).

In the second step, the nascent protein is transferred to a Sec/YidC-translocon, or to a YidC-translocase, by a poorly understood mechanism (Serek *et al.* 2004). Although the exact function of YidC is unclear, it is believed to act as an insertion and folding chaperone for membrane proteins (Luirink *et al.* 2005). The SecYEG complex belongs to the class of type II general secretory translocases and is universal. Homologues have been found in every bacterium, archaeon and eukaryote that has a fully sequenced genome (Kinch *et al.* 2002). SecYEG has also been reported to facilitate the export of some secretory proteins such as DsbA, β-lactamase and several autotransporters (Takamatsu *et al.* 1997; Sijbrandi *et al.* 2003). The insertion of IMP in the membrane and the export of proteins by the Sec-system are driven by ATP/GTP hydrolysis and stimulated by the proton motive force (Geller 1991; Rapoport *et al.* 1996; Nouwen *et al.* 2007; Driessen and Nouwen 2008).

In the third step the transmembrane segments of the polypeptide are laterally integrated in the membrane by the SecYEG translocon, with the help of YidC. Once in the membrane the new membrane protein folds and assembles into its native structure. Incorrectly folded proteins are detected, degraded and removed (Luirink *et al.* 2005).

1.2.2 Transmembrane domains

The membrane-spanning domains of proteins have a high content of amino acids with nonpolar side chains, due to the hydrophobic membrane environment (Alberts *et al.* 1983). The nonpolar side chains of the amino acids in transmembrane domains (TMD) are exposed to the membrane in order to shield the polar peptide bonds of the protein's polypeptide chain from the hydrophobic membrane environment. The peptide backbone of the TMD cannot access the aqueous phase and can only form hydrogen bonds between its peptide groups (Voet *et al.* 2002). The transmembrane domain folds that facilitate internal hydrogen bond formation are either α -helices or β -barrels. These motifs are retained also for multipass transmembrane proteins where the polypeptide chain crosses the membrane multiple times (Alberts *et al.* 1983; Voet *et al.* 2002). Figure 1.4 (A) shows a structure of the helix-bundle membrane protein CIC, an *E. coli* antiporter of chloride ions and protons and Fig. 1.4 (B) the *E. coli* sucrose porin, which forms a β -barrel.

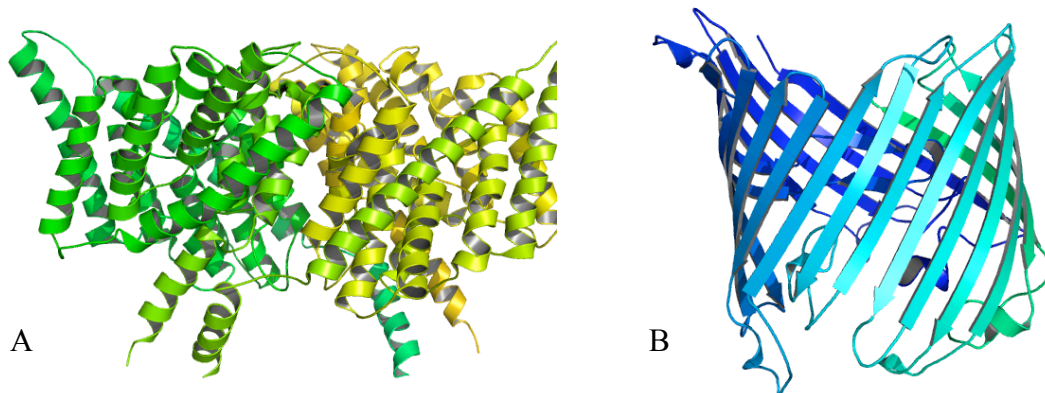


Figure 1.4: Examples for the helix-bundle fold (A) and β -barrel (B) fold of membrane proteins. A shows the structure of the *E. coli* CIC Cl^-/H^+ antiporter (PDB ID 1KPK), while B displays the β -barrel fold of the *E. coli* sucrose porin (PDB ID IA0S). The figure was created with PyMOL software.

The preference for structural motifs is dependent on the cellular location of the membrane protein. The transmembrane-helix bundle is the fundamental structural motif of plasma membrane proteins, as was finally revealed by the high resolution structures of bacteriorhodopsin in 1996 (EM) and 1997 (X-ray) (Grigorieff *et al.* 1996; Pebay-Peyroula *et al.* 1997). In contrast membrane proteins located in the bacterial, mitochondrial and chloroplast outer-membrane generally, but not exclusively, have a β -barrel motif (Buchanan 1999; Schulz 2000).

The group of helix-bundle proteins is more diverse and nearly all medically important membrane proteins such as receptors, transporters, channels, etc are found in this group (Heijne 2007). The hydrophobic part of transmembrane helices is made of apolar amino acids such as leucine, isoleucine, alanine, valine and phenylalanine. Furthermore tryptophan and tyrosine, two normally rare aromatic residues, are enriched near the ends of the transmembrane helices, in the parts of the protein that are embedded in the lipid head-group regions (Heijne 1999). The few charged or polar residues that are found between the apolar amino acids are usually facing the inside of the helix bundle and are responsible for specific functions (Heijne 2007).

1.2.3 Classification of membrane proteins

Membrane proteins can be classified into integral and peripheral membrane proteins, depending on their association with the membrane. Integral membrane proteins are amphiphatic. They consist of at least one hydrophobic membrane spanning segment and can extend out of the membrane, with their hydrophilic part of the polypeptide chain. Integral membrane proteins are tightly associated with the membrane through hydrophobic interactions with the fatty acid tails of the lipids (Alberts *et al.* 1983; Heijne 2007). Peripheral membrane proteins do not extend into the hydrophobic bilayer and are linked to the membrane usually by non-covalent interactions with other membrane proteins or lipid head-groups. They can easily be separated from the membrane by gentle extraction procedures, such as changes in pH or with changes in the ionic strength of the solute (Alberts *et al.* 1983). Proteins that are attached to the membrane, with for example a glycosylphosphatidylinositol (GPI) anchor, form a third class. (Alberts *et al.* 1983; Voet *et al.* 2002).

1.2.4 Function of membrane proteins

Membrane proteins are involved in a wide range of important cellular functions. Virtually any object that enters or leaves a cell, whether a nutrient, a virus or a waste product, must penetrate one or more enclosing membranes. Membrane proteins mediate this process and only a small number of compounds, such as oxygen and nitrogen, can enter a cell without the help of a membrane protein (Rees *et al.* 2009). To grasp the magnitude of transport across membranes, a good example is the glucose uptake of an actively growing *E. coli* cell. In order to feed its metabolic demands, it is estimated that a single cell needs to import up to 10^6 glucose molecules per second (Phillips and Quake 2006; Rees *et al.* 2009). Furthermore the pumping of molecules across membranes is estimated to consume 10–60 % of ATP required by bacteria and humans, depending on conditions (Skou 1998; Rees *et al.* 2009).

The list of membrane protein functions includes transport of ions, metabolites and larger molecules such as entire proteins and RNA. Membrane proteins are essential in chemical signalling to propagate electrical impulses that are required, for example, in the nervous system and muscle contraction. In addition, membrane proteins are used as anchors to attach to neighbouring cells, the extracellular matrix or to simply bind enzymes at specific cellular locations. Not only is the transport across the membrane regulated by membrane proteins, but also the intracellular vesicular transport and the control of lipid composition of the membrane and the maintenance of the shape of organelles and the cell itself (Alberts *et al.* 1983; Heijne 1999). With the crucial role of membrane proteins in energy generation the list goes on (Heijne 2007).

Work in this thesis deals with *E. coli* inner membrane proteins, especially transporters of the ATP binding cassette (ABC) superfamily and of the major facilitator superfamily (MFS). The following introduces these two superfamilies with regard to their distribution, medical importance, general architecture and transport mechanisms.

1.2.4.1 The ATP-binding cassette transporter superfamily

The largest group of primary transporters is the ATP-binding cassette (ABC) transporter superfamily (Ames *et al.* 1992; Higgins 1992). Members of this family are present in organisms from all kingdoms of life (Rees *et al.* 2009). ABC exporters are found in both eukaryotes and prokaryotes, although importers were only found in prokaryotic organisms (Rees *et al.* 2009). In *E. coli*, ABC transporters form the largest membrane protein family with up to 80 distinct sub-families, representing 5 % of the genome (Linton and Higgins 1998). In contrast only about 50 different ABC transporters have been identified in humans (Dean *et al.* 2001). The human ABC transporters are involved in cholesterol and lipid transport, multidrug resistance, antigen presentation, mitochondrial Fe homeostasis and the ATP-dependent regulation of ion channels (Rees *et al.* 2009). Mutations in these proteins lead to diseases such as cystic fibrosis (King *et al.* 2004), hypercholesterolaemia and diabetes. Multidrug resistance of tumour cells is an important challenge to overcome in cancer therapy (Higgins 2007), while ABC transporters in prokaryotes are responsible for increasing antibiotic resistance (McKeegan *et al.* 2002).

The first structure of an ABC transporter to be published was the *E. coli* vitamin B12 importer, BtuCD (Locher *et al.* 2002). Several other ABC transporter structures shed light on the molecular assembly and the general mechanism of ABC transporters. They minimally comprise four domains, two transmembrane domains (TMD) and two nucleotide binding domains (NBD) (Hollenstein *et al.* 2007). The latter are located in the cytoplasm and are highly conserved, whereas the transmembrane domain sequences are variable. The variance in the TMD sequences reflect the requirements for different transported substrates (Rees *et al.* 2009). Additional elements can fuse to the TMD and to the NBDs and probably have regulatory functions. In the case of prokaryotic importers these extra domains are highly substrate specific binding proteins (Biemans-Oldehinkel *et al.* 2006). Figure 1.5 shows as an example the ABC transporter structure of BtuCD, with its two TMDs and two NBDs, together with its periplasmic binding domain BtuF (Hvorup *et al.* 2007).

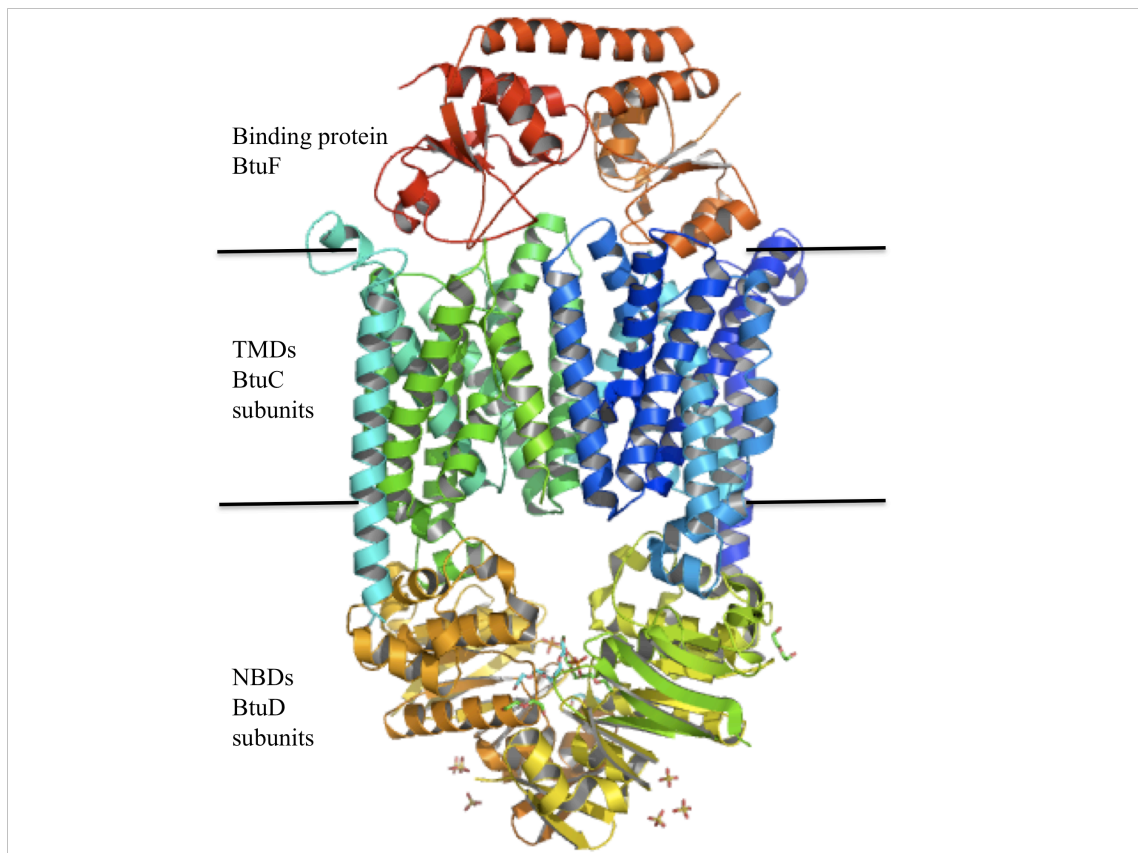


Figure 1.5: Structure of the *E. coli* vitamin B12 importer BtuCD together with its periplasmic binding domain BtuF in ribbon presentation. The horizontal lines indicate the approximate membrane boundaries. Figure created with PyMOL software (PDB ID 2QI9).

The transport itself is powered by the hydrolysis of ATP. Its mechanism is based on alternating access and release of the substrate to push it across the membrane, with enormous conformational changes between the inward- and outward-facing states of the transporter (Heijne 2007; Rees *et al.* 2009).

1.2.4.2 The major facilitator superfamily

The second largest membrane protein superfamily in *E. coli* is represented by the major facilitator superfamily (MFS). Up to 25 % of all known membrane transport proteins in prokaryotes belong to this superfamily of secondary transporters, which comprises 58 distinct families with about 15,000 sequenced members identified so far (Saier 2003; Law *et al.* 2008). MFS transporters exist in all kingdoms of life and comprise targets of significant medical and pharmaceutical importance (Law *et al.* 2008).

Three different kinetic transport schemes are found in MFS transporters. The first are uniporters, transporting only one substrate driven by its concentration gradient. The second group comprises symporters, which transport two or more substrates at the same time in the same direction by using the energy stored in the electrochemical gradient of one substrate. Antiporters make up the third class and are transporting two or more substrates in different directions across the membrane (Law *et al.* 2008).

Individual MFS transporters have a strict substrate specificity. But as a group, they show a broad spectrum of transported compounds ranging from ions, sugars and sugar phosphates, drugs, neurotransmitters, amino acids to peptides and many more other molecules (Law *et al.* 2008). The most intensively studied MFS symporter is the *E. coli* lactose/proton symporter LacY, whose structure was determined in 2003 (Abramson *et al.*). Figure 1.6 shows the structure of the *E. coli* symporter LacY. MFS antiporters are less well understood, but the structures of the *E. coli* sn-glycerol-3-phosphate:phosphate (GlpT) and EmrD transporters help to shed light on the function of MFS antiporters (Huang *et al.* 2003; Yin *et al.* 2006).

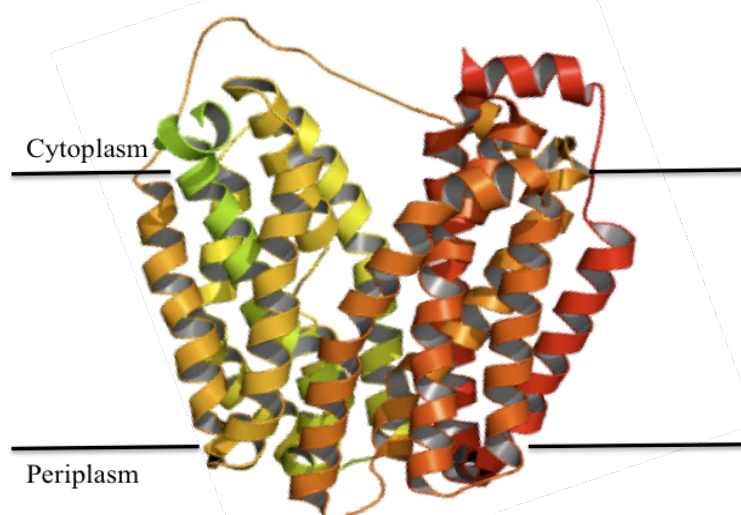


Figure 1.6: Crystal structure of *E. coli* LacY. Horizontal lines indicate the approximate membrane boundaries. The figure was produced with PyMOL software (PDB ID 1PV6)

A translocation pore, which is surrounded by two domains, is the common and highly conserved architecture shared by all MFS proteins and can be observed in the structure of LacY in Fig. 1.4. The high substrate variance in the MFS transporter family is enabled through changes in only few residues in the substrate-binding site and the translocation pathway. A rocker-switch mechanism was proposed for the transport of substrates across the membrane by MFS transporters (Lemieux *et al.* 2004; Smirnova *et al.* 2007; Law *et al.* 2008).

The named examples reflect only a small number of membrane protein functions. Their importance for fundamental cellular processes makes them desired targets in structural biology. To fully understand the function and the involvement of a membrane protein at an atomic level, its structure is an essential piece of information. However, membrane proteins belong to the most difficult proteins to work with and their structure determination remains a major challenge.

1.3 Structural biology of membrane proteins

1.3.1 Introduction

The function of any protein is determined by and is dependent upon its three-dimensional structure. Obtaining a detailed picture of a protein at an atomic level, is possible by the interpretation of diffraction images of X-rays obtained from many identical protein molecules present in a crystal. Single-crystal X-ray crystallography is today still the most powerful and successful technique for structure determination of proteins. However, the amphipathic nature of membrane proteins makes them one of the most difficult classes of protein structures to obtain. The publishing of the structure of the photosynthetic reaction centre in 1985 by Deisenhofer *et al.* marked the beginning of high resolution membrane protein structure determination (Deisenhofer *et al.* 1985). Since known, only a little more than 200 unique membrane protein structures have been obtained (White 2008; McLuskey *et al.* 2009). The challenges in obtaining membrane protein structures are illustrated by the difference in deposited structures between soluble and membrane proteins in the protein data bank (PDB), where structural information on proteins is archived. Despite exponential growth of the number of membrane protein structures in the PDB, membrane proteins account for less than one percent of all deposited structures (Heijne 2007; McLuskey *et al.* 2008).

X-ray crystallography relies on the availability of well-ordered protein crystals. Despite the reduced amounts of protein needed today, through increased use of high-throughput (HTP) methods and robotics for crystallisation experiments, many problems with membrane proteins arise during expression and purification. In general, structural studies require milligram amounts of pure and monodisperse membrane protein (Carpenter *et al.* 2008). Substantial difficulties are encountered, however, in the expression and purification of large quantities of stable membrane proteins. The following sections describe the challenges in membrane protein structure determination from their expression and purification to their crystallisation

1.3.2 Overexpression of inner membrane proteins

In the majority of cases, the natural amount of membrane protein is not sufficient for structural studies and the target of choice needs to be overexpressed. The recombinant overexpression of IMPs is not straightforward and has to overcome a number of difficulties. Often the expressed membrane protein is toxic to the cell and protein yields are low (Carpenter *et al.* 2008). Target specific, optimal expression conditions are dependent on a range of parameters, all of which need to be screened and optimised in order to obtain sufficient amounts of target for its purification. The variable parameters to choose from include different expression vectors, tags for purification, host organism, cell lines, expression media, induction methods, expression duration and temperature (McLuskey *et al.* 2008).

Unlike soluble proteins, which are accumulated in the cytoplasm in bacteria, membrane proteins have to be targeted and inserted into the membrane as described in section 1.2.1. In *E. coli*, the overexpressed targets are co-translationally integrated into the plasma membrane or aggregate as inclusion bodies in the cytoplasm (Wagner *et al.* 2007). The refolding of membrane proteins from inclusion bodies has proved very difficult for IMPs and the preferred option is their accumulation in the inner membrane (Drew *et al.* 2003). However, this is often accompanied by changes of the membrane integrity and toxicity to the host (Miroux and Walker 1996).

Available vectors for protein overexpression are genetically engineered to enhance the speed of expression and the required target DNA sequence is cloned into a vector to form a construct. Powerful promoters, developed for the expression of soluble proteins, lead to a fast increase of target mRNA levels after induction. This can result in the saturation of the cell's translocation machinery. Saturation hinders the cell's ability to carry out essential maintenance of membrane components and leads to a reduced amount of respiratory chain complexes in the membrane (Wagner *et al.* 2007). This triggers the less efficient acetate-phosphotransacetylase pathway for ATP production and the down regulation of the tricarboxylic acid cycle, leading to reduced bacterial growth, which is accompanied by low protein yields (Wagner *et al.* 2007). Furthermore, if the SecYEG complex cannot integrate all nascent membrane proteins into the membrane, they remain in the cytoplasm and are likely to aggregate to inclusion bodies (Wagner *et al.* 2007).

To date, the most commonly used induction method is based on the use of isopropyl- β -D-thiogalactoside (IPTG) (Berrow *et al.* 2006; Graslund *et al.* 2008). IPTG is a synthetic lactose analogue, that induces the *lac*-operon in *E. coli*. In constructs featuring a T7*lac*-promoter the target expression can be controlled and induced in lactose free growth medium by adding IPTG (Studier and Moffatt 1986). The optimal IPTG concentration and time of induction during bacterial growth to maximise protein yields, is target specific (Studier and Moffatt 1986; Studier 2005)

Studier developed a different approach with the invention of autoinduction medium (Studier 2005). The induction of target expression is mediated by glucose depletion. Autoinduction medium contains an optimised ratio of glucose and lactose. Once the cells have metabolised all the glucose in the medium (with glucose being a natural inhibitor to the T7*lac*-promotor), lactose needs to be metabolised and this then induces expression. The start of the target expression is therefore dependent on the rate of the cell's metabolism, making autoinduction suitable for expression screens where a large number of different cell lines, targets and other conditions are tested simultaneously (Studier 2005). Many more expression systems are available with all systems having their advantages and drawbacks, however the optimal expression system is dependent on the requirements of the specific membrane protein.

E. coli is the most common host organism for the recombinant overexpression of prokaryotic membrane proteins (Berrow *et al.* 2006; Graslund *et al.* 2008). Due to the often toxic nature of membrane proteins, the optimal expression host is target specific. The optimal growth medium and expression temperature is also dependent on the target membrane protein (Lundstrom 2006). The medium composition and the temperature during expression, aim at providing the perfect environment for the host cell to express the specific target and differences in media compositions and temperature have a high impact on protein yield. Therefore, despite recent work on the mechanisms of membrane protein overexpression and optimisations of protocols, a unique best strategy is still not available and the need to screen for the optimal conditions of each target remains (Surade *et al.* 2006; Wagner *et al.* 2007).

1.3.3 Purification of inner membrane proteins

The amphiphilic nature of membrane proteins requires the use of target specific detergents to solubilise and stabilise them in aqueous solution. The IMP has to be separated from the membrane by solubilisation with detergent in the first purification step. From this step onwards, the protein is always present as protein detergent complex (PDC) in solution. Therefore not the protein itself, but the PDC must be purified to monodispersity.

The detergent is the most important parameter for the successful solubilisation, purification and crystallisation of membrane proteins (Carpenter *et al.* 2008). The following sections give an introduction to the physical properties of detergents and their use in membrane protein biochemistry.

1.3.3.1 Physical properties of detergents

Detergents are part of the compound group called surfactants. They reduce interfacial surface tension in mixtures, such as oil and water, by adsorbing to interfaces (Rosen 2004). Detergents are amphipathic compounds that feature a well-segregated polar hydrophilic head-group and an apolar hydrophobic tail (Seddon *et al.* 2004). The hydrophilic head-group usually occupies more space than the tail, giving it a cone shaped appearance and allows the formation of circular micelles in water (Fig. 1.7 (A)) (Landau and Rosenbusch 1996). Lipids in contrast feature two tail groups that can lead, next to other aggregation states, to the formation of liposomes in solution, which consist of a continuous lipid bilayer (Fig 1.7 (B)) (Alberts *et al.* 1983; Privè 2007). A schematic of the shape of detergents, micelles, lipids and lipid bilayers are shown in Figure 1.7.

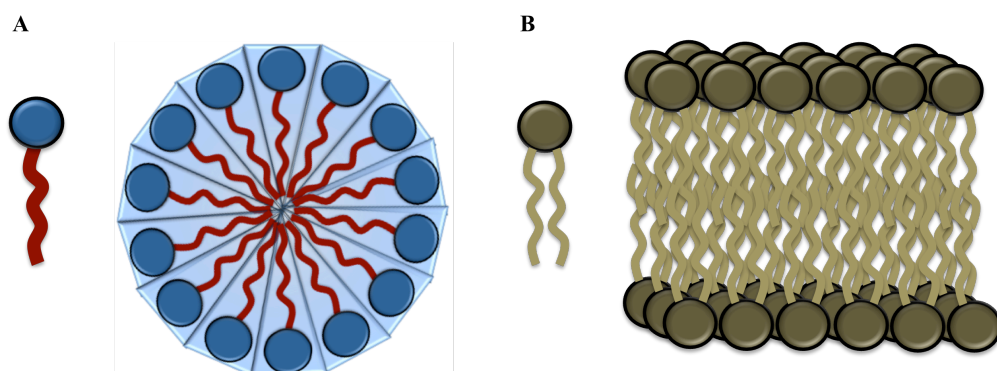


Figure 1.7: Schematic view of detergent (A) and lipid (B) monomers with polar head-groups and the hydrophobic tail groups. Driven by the hydrophobic effect, detergents form circular micelles due to their cone shape, while lipids can form bilayers that close in on each side, to form circular liposomes.

Pure detergent micelles contain from three to up to several hundred molecules, and are described by the unique aggregation number of a detergent (Privè 2007). The most important physical characteristic of a detergent is the critical micelle concentration (CMC) (Helenius *et al.* 1979; Rosen 2004). The CMC gives the minimal amount of detergent monomers required to form a micelle in solution (Helenius *et al.* 1979). The amphipathic character of the detergent monomer limits its solubility and the formation of micelles is driven by the hydrophobic effect, at concentrations above the CMC (Neugebauer 1990; Privè 2007). In micelles, the surface of the complex is smaller than in the monodisperse form, lowering entropy and making micelle formation thermodynamically favourable (Rosen 2004). Despite the formation of micelles above the CMC, there is always an amount of free monomers in solution, equalling the CMC concentration. The micelle detergent concentration can be determined as the total detergent concentration minus the CMC (Anatrace 2008). The CMC is most strongly influenced by the length of the alkyl tail group. The solubility of the detergent monomer is inversely proportional to the tail length. The CMC will roughly decrease by factor 10 for every two methylenes added to the aliphatic chain in a series based on the same head-group (Privè 2007). The CMC is for most detergents inversely proportional to the temperature, decreasing with increasing temperature (Anatrace 2008). A variety of methods can be employed to determine the CMC of a detergent, such as light scattering or, more quantitatively, by surface tension measurements (Mittal 1972).

Micelles have an asymmetrical form in solution. They feature rough surfaces, where the detergent monomers are disordered and can extend into the aqueous solution (Garavito and Ferguson-Miller 2001). Usually micelles have a size of a few nanometers and weigh less than 100 kDa. There is a continuous exchange of monomers between the monodisperse and the micelle state. The hydrophilic detergent head-group provides the water solubility and three different main types of head-groups exist, according to their polarity: ionic (cationic or anionic), nonionic or zwitterionic (Anatrace 2008).

1.3.3.2 The use of detergents in membrane protein biochemistry

Proteins need to be purified to the highest possible degree to allow crystallisation (Michel 1983; Rhodes 1993). In order to purify a membrane protein it has to be isolated from its native membrane environment. Membrane proteins can be solubilised with the help of detergents (Helenius *et al.* 1979). The amphipathic nature of detergents allows them to interact with hydrophobic membrane proteins and keep them water-soluble outside of their native bilayer environment (le Maire *et al.* 2000). When detergent is added slowly to the membrane suspension, the detergent monomers first partition into the bilayer and destabilise the membrane through detergent-lipid interactions. Mixed lipid-detergent complexes are formed and further addition of detergent leads finally to the dissolution of the bilayer and to membrane protein solubilisation (Almgren 2000; le Maire *et al.* 2000). A schematic of the solubilisation process of membrane proteins with increasing concentrations of detergent is shown in Fig. 1.8.

In the solubilisation step the so-called critical solubilisation concentration (CSC) dictates the minimal amount of detergent necessary to disrupt the membrane assembly into a state, dominated by the presence of micelle-protein complexes (Privè 2007). The CSC is dependent on the starting parameters of the solubilisation, especially on the lipid content.

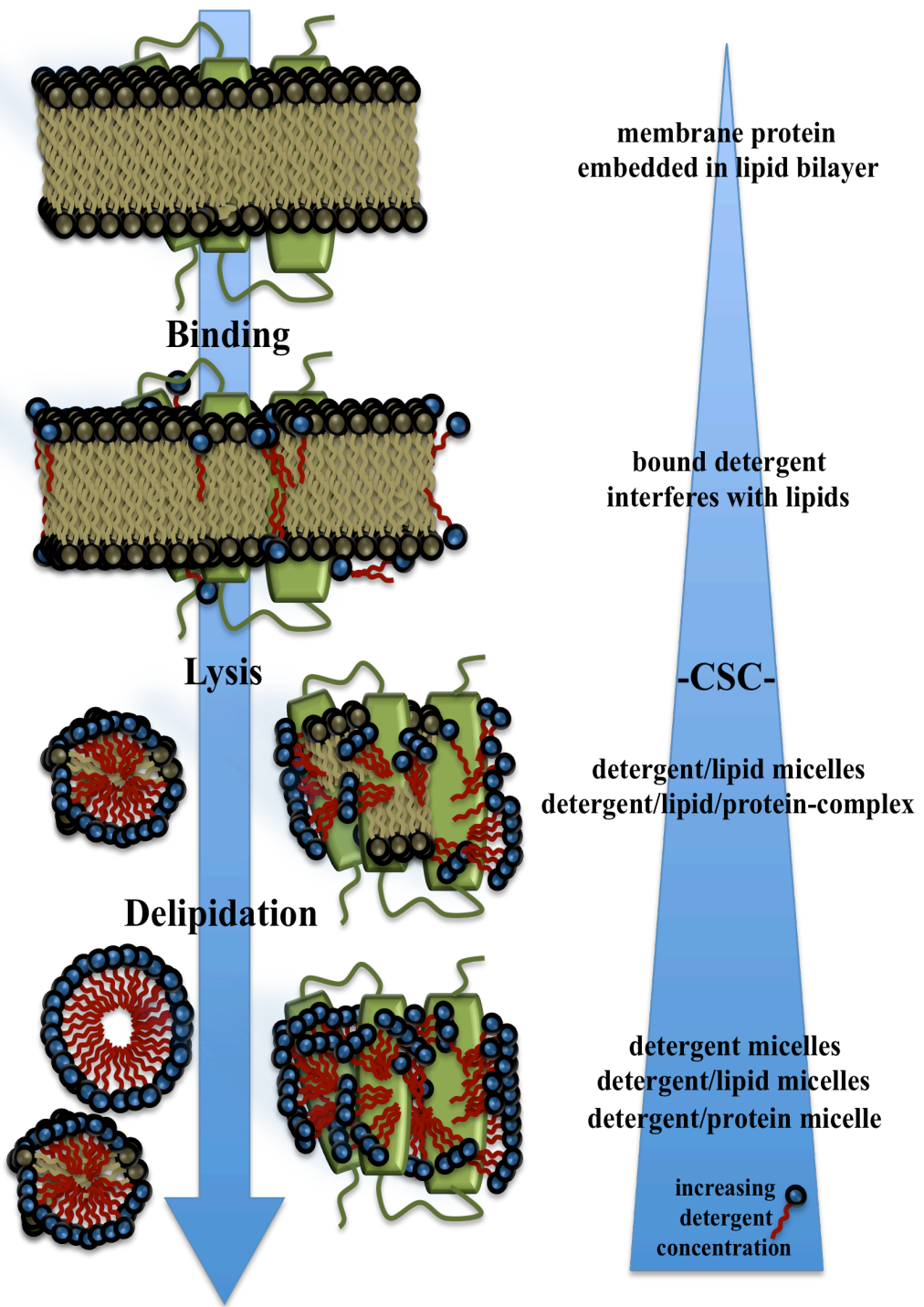


Figure 1.8: Schematic display of the solubilisation process of membrane proteins with increasing concentrations of detergent. The added detergent binds first to the membrane and interferes with the lipids. At higher detergent concentrations these interactions increase and break the membrane structure, when detergent concentrations close or higher than the CSC are reached. Lysis of the ordered membrane bilayer occurs and detergent/lipid/protein-complexes as well as detergent/lipid-micelles are found in solution. The adding of more detergent finally leads to the complete delipidation and the dissolution of the membrane and detergent/protein-micelles are found in solution next to detergent/lipid-micelles and free detergent monomers in solution. However, the formation of micelles is always in equilibrium with free detergent monomers in solution.

The CSC is dependent on temperature and decreases with higher temperature. However, the instability of most membrane proteins requires working at low temperatures, usually 4 °C (Seddon *et al.* 2004). In most cases when the CSC is reached, a change in turbidity of the solution can be observed. Once the membrane protein is solubilised, a general rule of thumb is to work with detergent concentrations of at least twice the CMC in buffers (Anatrace 2008). However, the solubilisation of membrane proteins requires far higher detergent specific concentrations. A detergent to lipid ratio of at least ten to one is recommended (Anatrace 2008). The detergent n-octyl- β -D-glucopyranoside (OG) for example, has a CMC of 0.89 % and can often be used for solubilisation at a concentration of 1.2–1.5 %. In contrast, dodecyl- β -D-maltoside (DDM), is a milder detergent with a long alkyl chain and a CMC of 0.009 %, but needs to be added to a final concentration of 1.5 % (Privè 2007).

The detergent head-group mediates the solubility of the PDC in the aqueous phase. The higher the polarity of the head-group, the better the solubilisation (Privè 2007). Ionic detergents such as sodium dodecyl sulphate (SDS), cetyltrimethylammoniumbromide (CTAB), N-lauryl sarcosine and sodium cholate perform very well in extracting proteins from the membrane. On the other hand, ionic detergents are very harsh and disrupt not only protein-membrane interactions, but also protein-protein interactions, and are mainly used as denaturants in quantitative protein folding/unfolding studies (Lau and Bowie 1997; Sehgal *et al.* 2005). In structural studies of membrane proteins the most commonly employed detergents belong to the group of non-ionic detergents such as maltosides, glucosides and polyoxyethyleneglycols, featuring uncharged hydrophilic head-groups. These mild detergents are less effective in solubilisation and therefore need to be added in higher concentrations. However, they are generally non-denaturing and their mildness increases with the length of their alkyl chain (le Maire *et al.* 2000; Seddon *et al.* 2004). DDM is a relatively mild detergent and a good initial choice for solubilisation and purification of membrane proteins. In addition, DDM was used in many successful crystallisation trials yielding membrane protein crystals (Privè 2007).

The group of zwitterionic detergents lies between the ionic and the non-ionic detergents in regard to mildness. They are electrically neutral as they feature both, a positive and negative charge in their head-group. Examples of zwitterionic detergents are the socalled Zwittergents, Fos-Cholines, 3-[(3-cholamidopropyl)dimethylammonio]-1-propanesulfonate (CHAPS/CHAPSO) as well as amine oxides. Lauryldimethyl amine oxide (LDAO) was, for example, successfully used in the structural characterisation of the photosynthetic reaction centre (Deisenhofer *et al.* 1985) and the outer membrane complex BtuB:TonB (Shultis *et al.* 2006).

Dodecylphosphocholine (Fos-Choline 12) is another zwitterionic detergent and has proven to be particularly successful in membrane protein structure NMR studies (Hwang *et al.* 2002; Oxenoid and Chou 2005). Physical properties of representatives of all detergent groups are shown in Table 1.1. The choice of detergent for membrane protein purification is always a compromise between solubilisation efficiency and protein stability (Seddon *et al.* 2004). Following the solubilisation of the target, purification can begin.

Type	Detergent	Aggregation Number	CMC [%]	Micelle size [kDa]	Schematic representation
Ionic	SDS	50-80	0.075	18	
Zwitterionic	LDAO	70	0.023	17-21	
Zwitterionic	Fos-Choline 14	108	0.005	47	
Non ionic	DDM	78-149	0.009	70	

Table 1.1: Physical properties of the detergents SDS (ionic), LDAO and Fos-Cholin 14 (zwitterionic) and DDM (non ionic) (Varela *et al.* 1995; Agostiano *et al.* 2004; Strop and Brunger 2005; Anatrace 2008).

The purification of membrane proteins employs the same established techniques as the ones developed for soluble proteins. Depending on the recombinant construct employed and its expressed counterpart, various purification techniques, such as ion exchange, affinity and size exclusion chromatography are available. However, the detergent often influences the effectiveness of these methods by, for example, interfering in the binding of protein purification tags to columns or changing their elution patterns. Instability leading to precipitation is often encountered, making a change of purification techniques necessary. The purity of the protein is assessed by an array of methods such as SDS-PAGE gel electrophoresis or mass spectrometry. Furthermore the monodispersity of a membrane protein sample, which can be estimated by analytical gel filtration or dynamic light scattering, is crucial to allow the formation of well-ordered single crystals, necessary for protein crystallography.

1.3.4 Crystallisation of membrane proteins

Similar to the purification stage, the membrane protein needs to be crystallised in a protein-detergent complex. The detergent micelle covers, like a belt, the hydrophobic parts of the membrane protein, with the polar detergent head-groups facing the aqueous phase. The purified protein-detergent complex (PDC) is submitted to crystallisation trials, in which it is screened against a large number of conditions that were successful in the crystallisation of membrane proteins. The vapour diffusion method in a sitting drop format is the most employed method to achieve the supersaturation state of the membrane protein solution, needed for nucleation of crystal growth (Carpenter *et al.* 2008). Polyethylene glycols, polyethylene glycol monomethylether or ammonium sulphate and phosphate salts are the common precipitants used in different combinations and concentrations in crystallisation screens (Hunte *et al.* 2003).

The amphipathic surface of membrane proteins allows the formation of two types of three-dimensional membrane protein crystals (Michel 1983). Type I crystals are ordered stacks of two-dimensional crystals grown in a phospholipid bilayer, which contains the ordered protein molecules within the membrane plane. Type II crystals are formed by membrane proteins integrated in detergent micelles. The crystal contacts are mediated in type II crystals by the polar surfaces of the membrane protein, which are not covered by the detergent micelle. Mixed type I and II crystals are possible, but most membrane proteins are found to crystallise in type II (Michel 1983; Hunte *et al.* 2003). The different types of three-dimensional membrane protein crystals are shown in Fig. 1.9.

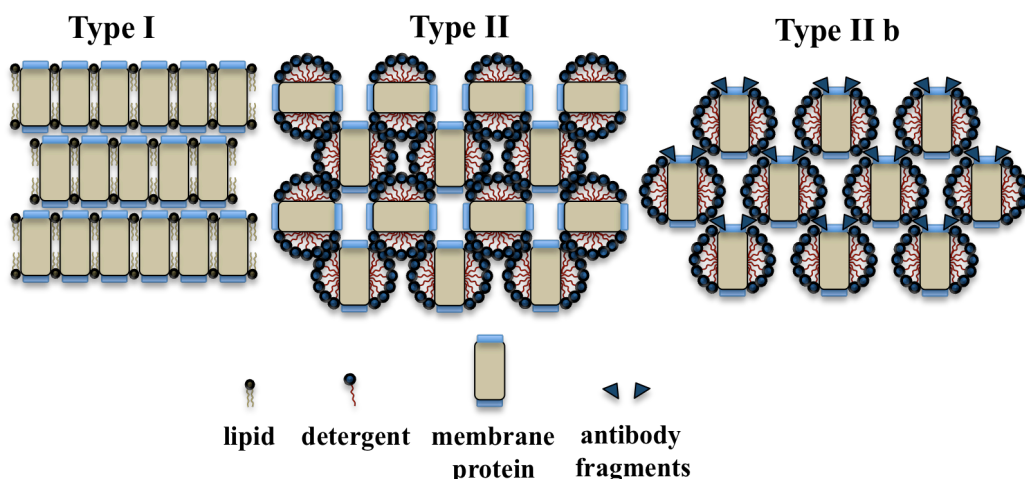


Figure 1.9: Different types of membrane protein crystals. Type I crystals are ordered stacks of two-dimensional crystals grown in lipid bilayers. In type II crystals the PDCs align in the shown pattern, so that crystal contacts can be formed by the hydrophilic protein parts, which can be enlarged with antibody framents (IIb). Figure based on (Hunte *et al.* 2003).

Although short chain detergents can contribute through interactions of their polar head-group to the stability of a formed crystal lattice, the detergent micelle requires space in the lattice and cannot contribute to rigid crystal contacts (Zulauf 1991). Therefore, membrane proteins that feature only small hydrophilic domains or very short solvent exposed loops, such as many transporters, are very difficult to crystallise (Hunte *et al.* 2003). One approach to improve the chances of crystal contact formation is to extend the hydrophilic domain through means of attachment of specific polar domains, such as antibody fragments (Ostermeier *et al.* 1995) or designed ankyrin repeat proteins (DARPINS) (Binz *et al.* 2004).

However, as for purification, choosing the right detergent has always been the key to success in membrane protein crystallisation (Hunte *et al.* 2003; Lacapère *et al.* 2007; Carpenter *et al.* 2008). Well-ordered crystals of the photosynthetic reaction centre from the purple bacterium *Rhodopseudomonas viridis* for example, could only be obtained in LDAO (Deisenhofer *et al.* 1985). Employment of the decyl homolog that differs only in two carbon atoms did not produce crystals. A similar effect was observed with the yeast cytochrome bc₁ complex, which was crystallised together with an antibody fragment in the detergent dodecyl-maltopyranoside (DM). No crystals grew in undecyl-maltopyranoside, which feature an alkyl chain that is only one carbon atom shorter than DM (Hunte *et al.* 2003).

The detergent micelle needs to fit optimally into the crystal lattice of the protein. Therefore, crystallisation is usually favoured with small detergent micelles (Michel 1983). This is in contrast to the solubilisation and stabilisation properties of detergents in regard to membrane proteins and the optimal protein-detergent combination has to be established.

A different method to obtain membrane protein crystals is lipidic cubic phase crystallography. Lipids can form bicontinuous three-dimensional bilayers in water, called lipidic cubic phases. The idea is that membrane proteins can diffuse in the bilayer, but are also able to form three-dimensional contacts, especially with their hydrophobic domains (Landau and Rosenbusch 1996). The crystals belong to the type I class of well ordered stacks of two dimensional layers. This technique has been successful for obtaining well-diffracting crystals for structure determination (Kolbe *et al.* 2000; Luecke *et al.* 2001) and an example is the structure of monomeric bacteriorhodopsin from purple membranes, which could be crystallised in lipidic cubic phases (Landau and Rosenbusch 1996).

In the case the initial crystallisation screens showed crystalline material, the crystallisation condition is refined in order to obtain better diffracting crystals. Small changes, such as pH, salt or precipitant concentration, additives, protein concentration and type and concentration of the detergent can considerably improve crystal quality and have to be tested empirically.

In order to stabilise crystals in the X-ray beam and to trap the protein in a conformational state, crystals are flash frozen in liquid nitrogen or directly in the dry airflow of the cryo-system on the goniometer head (Teng 1990). Finding the optimal cryo-protectant can have a big impact on the diffraction quality of the crystal. Membrane protein crystals are more vulnerable to freezing, as the solvent content is high and the presence of detergent enhances instability (Yoshikawa *et al.* 1998; Luecke *et al.* 2001; Hunte *et al.* 2003). Data collection and structure determination is in general the same as with soluble proteins. However, membrane protein crystals are usually very fragile and therefore difficult to handle (Carpenter *et al.* 2008). Membrane protein crystals diffract often only to low resolution and suffer from radiation damage during the diffraction experiments. Therefore, large numbers of crystals need to be screened, as even crystals from the same drop can vary considerably in diffraction quality (Carpenter *et al.* 2008). Access to high throughput facilities for the set up of crystallisation screens and to strong synchrotron radiation is very important to increase the chances of successful data collection.

1.4 High throughput approach

One way to overcome the problems of membrane protein structure determination is to try a large number of targets in the hope that a few will behave relatively well in expression, purification and crystallisation. Structural genomics projects for soluble and in increasing number also for membrane proteins specialise on the employment of established methods in high throughput (HTP) mode or the development of such techniques (Lundstrom 2006). HTP methods are used in all steps of the pipeline from cloning to crystallisation. The aim is to find promising targets in a short time frame with a minimum use of resources (Carpenter *et al.* 2008).

In the first instance the experiments are designed to work on a small-scale to reduce the necessary resources and to ease handling. Targets are often screened in 96-well or larger formats at the same time. Although not necessarily required, automation is possible for many steps and common for the generation of expression clone libraries (Stevens 2000). Studies on soluble proteins have shown that small-scale results are a useful indicator, if sufficient protein can be produced for large-scale structural studies and this approach is increasingly common for structural studies on membrane proteins (Berrow *et al.* 2006; Carpenter *et al.* 2008; Graslund *et al.* 2008).

In order to maximise the benefits of HTP techniques, all target constructs must be expressed in a synchronous fashion. In addition, the applied purification protocol must be as similar as possible and produce the high-quality material that is needed for crystallisation. This imposes restrictions on the screen set up and on the parameters involved (Stevens 2000). All methods have in common that they employ a sub set of parameters that were previously successful. The most feasible options for the large number of parameters need to be employed, such as cloning strategies, construct design, expression host, temperature and duration, growth media, culture size, purification tags and purification methods to only name a few. Furthermore, the parallel HTP production of protein targets, expressed under a range of conditions and purified with different techniques, will produce a self improving knowledge base about which parameters do work and which ones do not. These data can then lead to the further optimisation of starting parameters (Stevens 2000).

However, to obtain fast reliable results, especially for expression screens, a tool to monitor overexpression in a fast and easily accessible way is needed. One possibility is the measurement of fluorescence intensity of reporter proteins such as green fluorescent protein (GFP). The target is cloned into specialised constructs, containing the sequence of GFP and is coexpressed as a fusion protein. The measured fluorescence intensity correlates with the amount of expressed fusion protein (Drew *et al.* 2001; Daley *et al.* 2005).

1.5 Aims of the study

The structural characterisation of membrane proteins is very important for our understanding of some of the most fundamental cellular processes. The main bottleneck in membrane protein structure determination is the expression and the crystallisation, provided the membrane protein can be purified to monodispersity (Hunte *et al.* 2003; Loll 2003; Carpenter *et al.* 2008).

Therefore, a flexible small-scale HTP expression screen was developed to screen 12 membrane proteins (see section 1.6) in a short time frame for the best expression. Each target was screened for expression levels in 32 conditions. The results were used to express all these targets in larger cultures and to identify trends in expression behaviour. All membrane proteins were subjected to a purification scheme, which employed a subset of parameters such as choice of specific detergents and buffers, that proved to be the most successful to date in membrane protein structure determination. Targets that could be purified to monodispersity were submitted to crystallisation trials and initial crystals were optimised.

1.6 Target membrane proteins

The membrane proteins in this work are all members of the inner membrane proteome of *E. coli*. They were chosen from a library (Daley *et al.* 2005) of GFP-fusion constructs (see section 2.1) on the basis of four criteria. First, only membrane proteins with their C-terminus extending into the cytoplasm were selected. This is necessary as GFP folds properly and shows fluorescence, only if it is located in the cytoplasm (Feilmeier *et al.* 2000). Secondly, the biological function of the target membrane protein should be known. The third selection criterion required, that the membrane protein complex has at least four transmembrane helices, as the majority of determined membrane protein structures are from targets featuring four or more transmembrane helices (McLuskey, personal communication). The fourth and last criterion was that the GFP fluorescence in preliminary tests (Daley *et al.* 2005) was higher than a certain threshold (1.5 AU), indicating the general expression functionality of the target. The chosen membrane proteins are listed in Table 1.2, together with relevant physical properties and their biological function. The DNA and protein sequences of all targets are listed in the appendix (section 7.1).

Target	Amino acids	MW (kDa)	TMD-helices	Function
CcmC	245	27.7	6	Heme exporter
CodB	419	43.5	12	Cytosine transporter
FtsX	352	38.4	4	Involved in cell division
Lgt	291	33.0	5	Lipoprotein biosynthesis
PnuC	239	27.0	6	Nicotinamide mononucleotide transport
XylE	491	53.4	12	D-Xylose-proton symporter
XylH	393	41.0	10	Xylose ABC-transporter; Membrane part
YdeD	299	32.1	10	Aminoacid metabolite efflux pump
ChbC	452	48.2	10	N,N'-diacetylchitobiose permease
PgpB	254	28.8	6	Phosphatidylglycerophosphatase
YhbE	321	34.8	12	Transporter, EamA-like family
YdhC	417	43.2	10	Transporter, Major facilitator superfamily

Table 1.2: The 12 *E. coli* inner membrane proteins that were chosen for the study. The number of amino acids of each target is shown alongside molecular weight (MW), number of transmembrane domain (TMD) helices and function.

Chapter 2

Materials and Methods

2.1 Introduction

Throughout this project, work was carried out on 12 membrane proteins. The basic biochemical procedures were similar for each protein and this chapter gives an overview of the methods and materials used. Unless otherwise described, general molecular biology and laboratory techniques were performed as described in Sambrook *et al.* (1989). Optimisations of protocols specific to individual targets are mentioned in the relevant chapters. The workflow is described in the order of appearance during this study.

2.2 Target GFP-fusion construct

A library of *E. coli* membrane protein-GFP fusion constructs was established and the constructs for this work kindly provided by Dr. Daniel Daley *et al.*. The group cloned the target membrane protein DNA-sequences into a pGFP-e-vector with the restriction enzyme combination *XhoI/KpnI*, yielding a 14 amino acid-long linker sequence (SVPGESENLYFQQQF) (Daley *et al.* 2005). Figure 2.1 shows a schematic of the vector used.

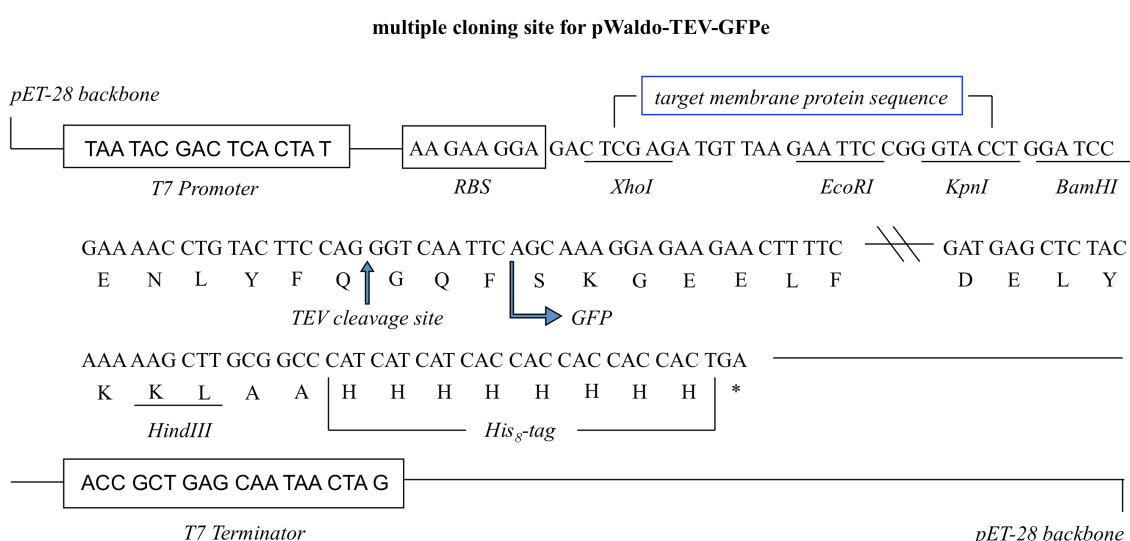


Figure 2.1: Expression vector set-up of target membrane proteins. The target DNA-sequence was inserted between the restriction sites *XhoI* and *KpnI*. Following expression, it is possible to cleave with TEV-protease the GFP-His₈ moiety from the target in the shown position.

The construct is a pET28-vector derivative that is based on the pWaldo vector (Waldo *et al.* 1999). An optimised pWaldo GFP vector (pGFPe) was developed by Rapp *et al.* (Rapp *et al.* 2004). pGFPe differs from pWaldo in featuring an extended multiple cloning site (5' *Xho*I and 3' *Eco*RI/*Kpn*I/*Bam*HI), as well as carrying a TEV protease site in the linker sequence. Furthermore it contains a His₈-tag at the GFP C-terminus for purification purposes. The GFP is linked to the C-terminus of the target protein and is only fluorescent, if the target fusion protein is folded correctly. Fusion protein aggregated in inclusion bodies will not be fluorescent (Waldo *et al.* 1999; Drew *et al.* 2001)

2.3 Molecular biology methods

2.3.1 Preparation of competent cells

Competent *E. coli* strains used in this study were initially bought (suppliers see Table 2.1) and subsequently made competent according to the RbCl-method (Hanahan 1983). The house-keeping strain DH5 α T1 was used to generate stocks of target plasmid DNA, while the other four strains listed in Table 2.1 were involved in recombinant overexpression of target membrane protein.

Strain & Genotype	Function	Antibiotic resistance	Supplier
DH5 α T1	house-keeping	none	
F- <i>endA1 glnV44 thi-1</i> <i>relA1 gyrA96 deoR</i> <i>nupG lacZdeltaM15</i> <i>hsdR17</i>			Invitrogen, Paisley, UK
BL21 Star (DE3)	expression	none	
F - <i>ompT hsdS B (rB-</i> <i>mB-) gal dcm rne131</i> (DE3)			Invitrogen, Paisley, UK
BL21(DE3)pLysS	expression	chloramphenicol	
F-, <i>ompT, hsdS_B (r_B-,</i> <i>m_B-), dcm, gal, λ(DE3),</i> pLysS, Cm ^r .			Invitrogen, Paisley, UK
Rosetta(DE3)pLysS	expression	chloramphenicol	
F- <i>ompT hsdS_B(r_B- m_B-)</i> <i>gal dcm (DE3)</i>			Novagen, San Diego, USA
pLysSRARE (Cam ^R)			
C41(DE3)	expression	none	
F - <i>ompT hsdSB (rB-</i> <i>mB-) gal dcm (DE3)</i>			Lucigen Corp. Middleton, USA

Table 2.1: The commercial *E. coli* strains employed, their usage, antibiotic resistances and suppliers.

The working concentrations of all antibiotics used throughout this study are listed below in Table 2.2. The detailed protocol of the RbCl-method is described in the following and the necessary media, chemicals and buffer compositions are listed in Table 2.3.

Antibiotic	Stock concentration [mg/mL]	Working concentration [μ g/mL]	Solvent
Ampicillin	100	100	dH ₂ O
Kanamycin	30	30	dH ₂ O
Chloramphenicol	34	34	Ethanol

Table 2.2: The antibiotics used, together with their stock concentration, working concentrations and solvent.

The RbCl-method for the preparation of competent cells starts with plating out 50 µL of the stock of a desired strain onto a Lysogeny Broth (LB) agar plate, containing the necessary antibiotics. The plate was incubated at 37 °C for 16 h. A single colony was picked with a sterile pipette tip to inoculate 5 mL of LB, containing the appropriate antibiotics (LBA). The culture was grown for 16 h at 37 °C and at 220 rpm in a shaking incubator. It was diluted 1:100 (2.5 mL in 250 mL culture) with LBA and further incubated until the optical density (OD₆₀₀) (see section 2.4.2 for details) reached 0.25–0.30. The cells were incubated on ice for 5 min, before being centrifuged at 4000×g for 5 min at 4 °C. The supernatant was discarded and the pellet resuspended in 100 mL Transformation buffer (Tfb) I buffer and incubated on ice for 5 min. The cell suspension was centrifuged at 4000×g for 5 min at 4 °C and the supernatant removed. The obtained pellet was resuspended in 10 mL Tfb II buffer and incubated on ice for 15 min. The cells were transferred to 50 µL aliquots in 1.2 mL tubes (1.2 mL micro-tube cluster plate, ABgene, Epson, UK) on dry ice and finally stored at –80 °C.

Reagent	Composition	Comments
Lysogeny Broth medium (LB)	1.0 % (w/v) tryptone 0.5 % (w/v) yeast extract 1.0 % (w/v) NaCl	Sterilized by autoclaving (15 psi for 15 min) prior to use.
LB agar	LB 1.5 % (w/v) micro-agar 1.0 % (w/v) glucose	Sterilized by autoclaving (15 psi for 15 min) prior to use. Glucose was added after autoclaving
Tfb I buffer	30 mM KOAc 100 mM RbCl 10 mM CaCl ₂ 50 mM MnCl ₂ 3 mM Hexamine cobalt Cl 15 % (w/v) glycerol	Adjusted to pH 5.8 (acetic acid)
Tfb II buffer	10 mM MOPS 75 mM CaCl ₂ 10 mM RbCl 15 % (w/v) glycerol	Adjusted to pH 6.5 (KOH)

Table 2.3: Media and buffers used in the RbCl-method for the preparation of competent cells (Hanahan 1983). Unless stated otherwise, all reagents were sterilized by filtration (0.22 µm filter).

2.3.2 Transformation of plasmid DNA into host cells

Plasmid DNA was transformed into the bacterial host using the following protocol. A 50 µL aliquot of competent cells was thawed on ice for 15 min. To this, 1.5 µL plasmid DNA (75 ng/µL), encoding the target membrane protein, was added and incubated on ice for 20 min. A 45 second heat shock at 42 °C was followed by a further incubation on ice for 2 min. Pre-warmed (37 °C) GS96 medium (MP biomedicals, Illkirch, France) was added to a final volume of 500 µL and the reaction mixture was incubated at 37 °C for 1 h. GS96 medium is optimised for bacterial growth under low oxygen levels. 25 µL of transformed cells were plated out on LBA agar and incubated overnight at 37 °C. Single colonies were picked with a sterile pipette tip for inoculation of starter cultures.

2.4 Protocols for protein expression and purification

2.4.1 Medium-scale protein expression

The over expression of the target membrane proteins was achieved by the autoinduction method described by Studier (2005). Although four different media were used in this study to test expression levels, the general protocol is identical and described in the following. The media compositions are listed in table 2.4.

Reagent	Composition	Comments
MagicMedia	Proprietary; supplied by Invitrogen, Paisley, UK	Sugar component added after autoclaving.
TB overnight express medium	Proprietary, supplied by Novagen, San Diego, USA	Sterilized by microwaving (2 min, 800 W).
LB autoinduction medium	1.0 % (w/v) tryptone 0.5 % (w/v) yeast extract 1 mM MgSO ₄ 2 % (v/v) 50×5052 buffer 5 % (v/v) 20×NPSC buffer	5052 buffer was added after autoclaving to preserve the heat sensitive sugar content.
SB autoinduction medium	3.2 % (w/v) tryptone 2.0 % (w/v) yeast extract 1 mM NaOH 1 mM MgSO ₄ 2 % (v/v) 50×5052 buffer 5 % (v/v) 20×NPSC buffer	5052 buffer was added after autoclaving to preserve the heat sensitive sugar content.
5052 (×50) buffer	25 % (w/v) glycerol 2.5 % (w/v) glucose 10 % (w/v) lactose	Sterilised by filtration.
NPSC (×20)-buffer	7.1 % (w/v) Na ₂ HPO ₄ 6.8 % (w/v) KH ₂ PO ₄ 1.4 % (w/v) Na ₂ SO ₄ 5.4 % (w/v) NH ₄ Cl	Adjusted to pH 6.75. Sterilised by filtration.

Table 2.4: Composition of buffers and media used for autoinduction expression (Studier 2005). Unless stated otherwise the components were sterilised prior to use by autoclaving for 15 min at a pressure of 15 psi.

Starter cultures were prepared by inoculating two 50 mL LBA cultures with two single colonies from a LB agar plate. Cells were grown for 16 h before being diluted 1:50 into 500 mL of desired sterile autoinduction medium in 2 L flasks, supplemented with the appropriate antibiotics. The different media employed were two commercial media,

MagicMedia (Invitrogen, Paisley, UK) and TB overnight express (Novagen, San Diego, USA) and two standard media, LB and the richer SB medium.

The main cultures (500 mL) were incubated in a shaking incubator (220 rpm) for 4 h at 37 °C and for a further 18 h at 25 °C. Cells were harvested by centrifugation at 4000×g at 4 °C for 20 min. The supernatant was removed and the cells were stored at -20 °C. In addition cells were grown in a 15 L fermenter using the same conditions as above.

2.4.2 Cell density measurements

The optical density at a wavelength of 600 nm (OD_{600}) can be used to determine the number of cells present in a bacterial suspension. The Beer-Lambert Law describes the relationship between absorbed light and concentration for dilute solutions:

$$A = \log I_0/I = \epsilon cl \quad \text{equation 1}$$

Where A = absorption, I = intensity of light after passing through the sample, I_0 = intensity of light before passing through the sample, ϵ = extinction coefficient, c = concentration and l = path length

A derivation of the Beer-Lambert-Law gives as optical density

$$(OD) = \log I_0/I = kc \quad \text{equation 2}$$

Where I_0 = intensity of light before passing through the sample, I = intensity of light after passing through the sample, k = apparatus dependent constant and c = concentration (Koch 1970; Lamanna 1973; Lawrence and Maier 1977).

The linear relationship between amount of cells and light scattering is only correct for dilute solutions, where effects of secondary scattering can be neglected. The necessary dilution factor of samples needs to be verified for the spectrophotometer used, in this case a Fluostar Optima platereader (BMG Labtech, Aylesbury, UK), and was tested with the following procedure. A frozen bacterial sample was thawed and resuspended in PBS buffer. This solution (100 %) was then subsequently diluted in a series of 10 % intervals, down to 10 % bacterial solution mixed with 90 % PBS. The dilutions were dispensed into a 96 well reading plate (Costar® 3799, Corning Inc., New York, USA). This type of plate was used throughout this study. The OD_{600} values of each dilution was measured and plotted against the dilution to give the calibration curve displayed in Fig. 2.2. The graph shows that the optical density correlates linearly with the amount of cells for an $OD_{600} < 1$ and the Beer-Lambert law is satisfied. In the developed expression screen, all samples were diluted prior to measurement to an OD_{600} below 1.

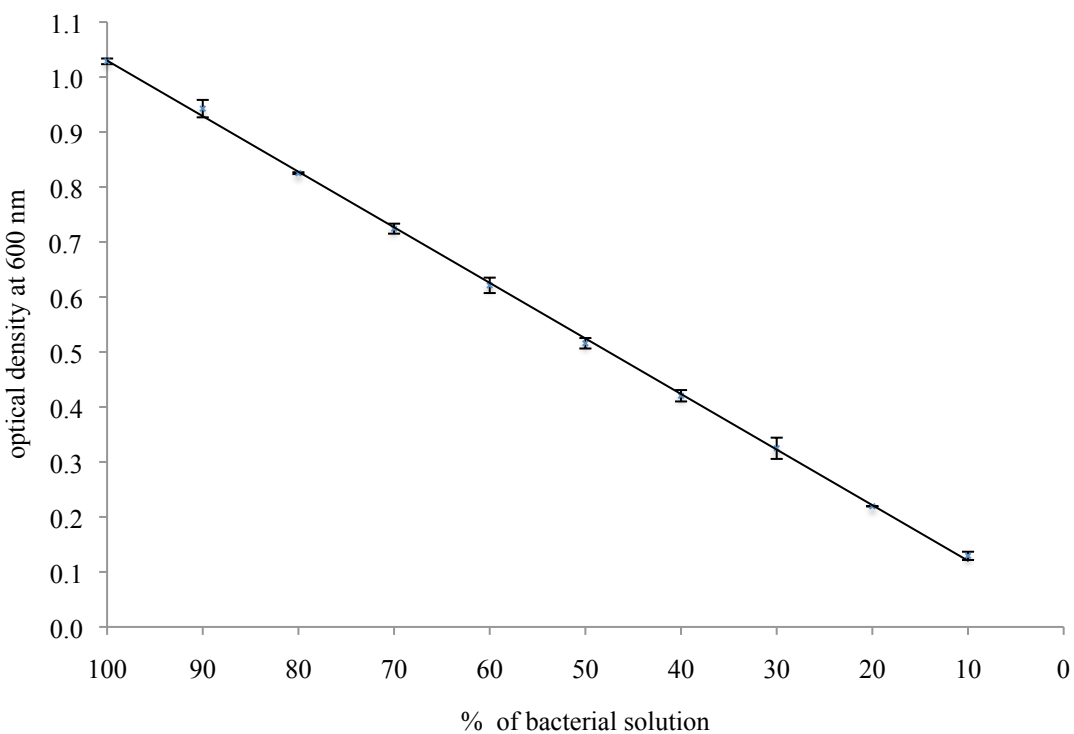


Figure 2.2: Calibration curve for the plate reader Fluostar Optima (BMG Labtech) with values of optical density at 600 nm versus percentage of bacterial solution. Three series of OD₆₀₀ measurements were averaged and the standard error is displayed.

2.4.3 Protein analysis

2.4.3.1 The measurement of protein concentration

The protein concentration was determined utilising the Beer-Lambert law (equation 1, section 2.4.2) by measuring the absorption of the protein solution with light at a wavelength of 280 nm with a Lambda 40 spectrophotometer (Perkin-Elmer, Waltham, USA). The extinction coefficient of each protein was calculated with the PROTPARAM tool of the EXPASY proteomics server (<http://www.expasy.ch>). PROTPARAM calculates the protein extinction coefficient from the amino acid sequence in conjunction with calculated values of tyrosine and tryptophan residues (Edelhoch 1967; Pace *et al.* 1995).

2.4.3.2 Sodium dodecyl sulphate polyacrylamide gel electrophoresis

The purity of a protein sample was analysed during purification with sodium dodecyl sulphate polyacrylamide gel electrophoresis (SDS-PAGE) based on a method developed by Laemmli (Laemmli 1970). The NuPAGE® Pre-Cast Gel System was used in combination with NuPAGE gels in MOPS running buffer (Invitrogen, Paisley, UK). Protein samples were added to lithium dodecyl sulphate (LDS) loading buffer (6X) (Invitrogen, Paisley, UK) supplemented with 1 mM DTT, in a 1:3 ratio (buffer: protein sample) and incubated at 37 °C for 30 min prior to loading. The volume loaded was dependent upon well size and protein concentration. Samples were loaded alongside SeeBlue Plus 2 Pre-Stained Standard (Invitrogen, Paisley, UK) to estimate the molecular weight of protein bands. Gels were run under constant voltage (200 V) for 55 min. Protein bands were stained with a solution composed of 45 % (v/v) methanol, 10 % (v/v) glacial acetic acid and 2.5 g/L Coomassie® Brilliant Blue R250. Gels were destained by slow shaking in water.

2.4.3.3 Mass spectrometry

Mass spectrometry analysis was used to verify the identity of the purified protein. Samples were sent to the *Sequencing Service* (School of Life Sciences, University of Dundee, UK), which performed mass spectrometry peptide sequencing following a trypsin digest.

2.4.3.4 Fluorescence intensity

The fluorescence from the GFP-fusion protein was used in expression tests to monitor expression levels of the target protein in different growth conditions. Fluorescence intensities (excitation 485 nm, emission 512 nm) of bacterial suspensions in a 96-well reading plate (Costar plate no. 3799, Corning Inc. New York, USA) were measured in a Fluostar Optima fluorimeter (BMG Labtech, Aylesbury, UK). In order to make a direct comparison between different conditions possible, the gain-value of the fluorimeter was optimised to enable maximum sensitivity and kept constant for all measurements. The detailed procedure is described in subsequent chapters.

2.4.4 Cell lysis and membrane preparation

The target membrane proteins are located in the inner membrane of the host organism. In order to isolate the inner membranes, the cells need to be broken. To lyse the cells, the frozen cell pellets were thawed on ice and resuspended in 50 mM Tris-HCl pH 7.5 using 50 mL of buffer per 10 g of cells. Complete protease inhibitor tablets (Roche Diagnostics Ltd., Burgess Hill, UK) (1 per 100 mL) and 10 mg of DNase (Sigma-Aldrich, Steinheim, Germany) were added. Cell lysis was performed for small volumes using a French pressure cell (Thermo Scientific, Waltham, USA) at 14000 psi in three passes. Larger volumes were lysed using a constant flow Cell Disrupter (Constant Systems Ltd., Daventry, UK). Three passes (22000 psi) broke the cell walls. Following lysis, the cell debris was sedimented by centrifugation at 8000×g for 20 min. The resulting supernatant was centrifuged again for 50 min at 250000×g to pellet the cell membranes. The supernatant was discarded and the membranes were resuspended in a small volume of 50 mM Tris-HCl pH 7.5 supplemented with 10 % (w/v) glycerol using a steel needle. The suspension was finally aliquoted (1.5 mL) into Eppendorf tubes, flash frozen in liquid nitrogen and stored at –80 °C.

2.4.5 Solubilisation of membrane proteins

The target proteins need to be isolated from their native membranous environment using detergents. In this study, *n*-dodecyl β-D-maltoside (DDM) (Anatrace, Maumee, USA) was used for all solubilisations. Membranes were thawed on ice and diluted in Buffer I (50 mM Tris-HCl pH 7.5 and 100 mM NaCl), using 50 mL for 20 g of wet cells. Assuming an extinction coefficient of 1 the total protein concentration was measured (A_{280}) and the membrane suspension diluted to reach a final concentration of 40 mg/mL. A 10 % (w/v) solution of DDM in the above buffer was added dropwise with stirring until a final concentration of 1.5 % (w/v) DDM was reached. The protein solution was gently stirred for 1 h at 4 °C. The unsolubilised material was sedimented by ultracentrifugation for 50 min at 250000×g. The target protein-detergent complex was now in the supernatant along with other membrane proteins that were solubilised by DDM. The desired membrane protein can be purified from this solution using the following purification methods.

2.4.6 Immobilised metal affinity chromatography

In this work a histidine tag attached to the membrane proteins was used, comprising eight histidine residues (His_8), for purification with immobilised metal affinity chromatography (IMAC). The aromatic ring of the imidazole side chain of the histidines binds to a Ni^{2+} -ion that is immobilised with a linker to the column matrix, such as nitriloacetic acid (NiNTA). A concentration gradient of imidazole is employed to elute the target protein off the column. The following describes the protocol for membrane protein purification based on the IMAC method used in this study. Buffers and materials are listed in Table 2.5.

Any precipitation was removed by centrifugation at $8,000\times g$ for 20 min. The supernatant was filtered ($0.22\ \mu\text{m}$) and loaded (2 mL/min) onto a pre-equilibrated (Buffer A) 5 mL HisTrap column (GE Healthcare, Amersham, UK). The column was washed with three column volumes (cv) of Buffer A followed by a step gradient elution, which was composed of four steps of increasing imidazole concentrations. Steps were performed on an Äkta purifier (GE Healthcare, Amersham, UK) with Buffers A and B (3 mL/min). In the first two concentration steps of 65 and 100 mM (each 3 cv) non specific binding proteins were eluted followed by target elution (5 cv) with 250 mM imidazole. The final step of 500 mM (5 cv) was used to clean the column of any remaining proteins. The eluate was collected in 2 mL fractions for the first two imidazole steps and in 1 mL fractions during target elution. The collected fractions were examined by SDS-PAGE. In addition, fractions containing target protein appeared green in colour due to GFP-fluorescence. These fractions were pooled and centrifuged for 20 min at $8000\times g$ to sediment any precipitate.

Buffers & Materials	Composition	Comments
Buffer A	20 mM Tris-HCl (pH 7.5) 150 mM NaCl 5 % (w/v) glycerol 0.04 % (w/v) DDM	Sterilised by filtration
Buffer B	20 mM Tris-HCl (pH 7.5) 150 mM NaCl 5 % (w/v) glycerol 0.04 % (w/v) DDM 1 M imidazole	Sterilised by filtration
5 mL HisTrap-column	NiNTA	Supplied by GE Healthcare
Äkta Purifier	Fast Protein Liquid Chromatography (FPLC)	Supplied by GE Healthcare

Table 2.5: Buffers and materials used for IMAC purification. Buffer A was also used to equilibrate desalting columns and for gel filtration columns.

2.4.7 Protein Dialysis

To remove imidazole from the purified protein sample, the protein was filled into pre-wetted dialysis tubing (Medicell International Ltd., London, UK), with a molecular weight cut off (MWCO) of 10 kDa. The protein solution in the tube was dialysed against 2 L of dialysis buffer for 16 h at 4 °C.

If a target proved unstable, PD-10 desalting columns (GE Healthcare, Amersham, UK) were used instead of dialysis. These columns were equilibrated with 25 mL of Buffer A. The protein sample was applied to the column in 2.5 mL and eluted with 3.5 mL Buffer A. After the removal of imidazole the solution was centrifuged at 8000×g for 20 min.

Buffers & Materials	Composition	Comments
Dialysis buffer	20 mM Tris-HCl (pH 7.5) 150 mM NaCl 0.04 % (w/v) DDM 1 mM dithiothreitol (DTT) 0.5 mM ethylenediamintetraacetic acid (EDTA)	Sterilised by filtration
Buffer A	20 mM Tris-HCl (pH 7.5) 150 mM NaCl 5 % (w/v) glycerol 0.04 % (w/v) DDM	Sterilised by filtration
Dialysis tubing	10 kDa MWCO	Medicell International Ltd.
PD-10 Desalting columns	Sephadex-25	GE Healthcare

Table 2.6: Buffers and materials employed for protein dialysis.

2.4.8 TEV-protease production & cleavage

To remove the histidine tagged GFP from the target fusion protein, *Tobacco etch virus* protease (TEVP) is used. TEVP is expressed as a protein featuring a His₆-tag. After the cleavage the His-tagged GFP and TEVP can be separated from the target protein by IMAC. TEVP is overexpressed and purified as described below.

2.4.8.1 Expression and purification of Tobacco etch virus-protease

The TEVP-construct, which carries the gene for ampicillin resistance, is transformed into BL21(DE3)pLysS cells as described in section 2.3.2. Single colonies were used to inoculate 50 mL LBA starter cultures and grown for 16 h at 37 °C and 220 rpm in a shaking incubator. Once inoculated the main cultures were grown at 37 °C and 220 rpm until the OD₆₀₀ reached 0.6–0.7. Protein expression was induced with 1 mM isopropyl-β-D-thiogalactopyranoside (IPTG) and the temperature lowered to 22 °C for a further 16 h. Cells were harvested by centrifugation at 4000×g for 20 min. The supernatant was removed and the cell pellet stored at –20 °C.

The frozen cells were thawed and resuspended in TEVP buffer A and a protease inhibitor tablet and DNase were added. Lysis was performed using a French pressure cell (14000 psi, 3 passes). The cell debris was separated by centrifugation (8000×g for 20 min) and the filtered supernatant applied to a pre-equilibrated (TEVP-buffer A) NiNTA-column. TEVP was eluted against a linear gradient (20 cv, 0–100 %) of TEVP-buffer A and B. The eluate was fractionated into glass tubes containing 1 mM DTT and 1 mM EDTA. Column runs were performed on an Äkta purifier. The fractions containing protein were determined using SDS-PAGE analysis and the relevant fractions were pooled. The protein concentration was determined, before 500 µL aliquots were flash frozen in liquid nitrogen and stored at –80 °C.

Buffers & Materials	Composition	Comments
TEVP buffer A	50 mM phosphate buffer (pH 8.0) 150 mM NaCl 10 % (w/v) glycerol 25 mM imidazole	Sterilised by filtration
TEVP buffer B	50 mM phosphate buffer (pH 8.0) 150 mM NaCl 10 % (w/v) glycerol 800 mM imidazole	Sterilised by filtration
5 mL HisTrap-column	NiNTA	Supplied by GE Healthcare
Äkta Purifier	Fast Protein Liquid Chromatography (FPLC)	Supplied by GE Healthcare

Table 2.7: The buffers and labware used for the expression and purification of TEVP.

2.4.8.2 Cleavage of GFP-fusion protein with tobacco etch virus-protease

The necessary amount of frozen TEVP (1:1 molar ratio target to protease) for the cleavage reaction was thawed and incubated with the target membrane GFP-fusion for 1 h at 30 °C. The resulting GFP-His₈ and TEVP-His₆ was separated from the now untagged membrane protein by IMAC.

2.4.9 Size exclusion chromatography

Size exclusion chromatography was used as the final protein purification step as well as to assess the monodispersity of the protein sample.

Before being applied to a gel filtration column, the protein solution was concentrated in a 100 kDa MWCO Vivaspin II concentrator (Sartorius Stedim Biotech, Aubagne, France) until a final volume of 500 µL was reached. The sample was then applied with a 500 µL loop onto a Superdex 200 10/300 gel filtration column (GE Healthcare, Little Chalfont, UK), which was pre-equilibrated with Buffer A. The target was eluted with 1.5 cv (36 mL) of Buffer A and collected in 1 mL fractions. Gel filtration runs were performed on an Äkta purifier (FPLC). Fractions were analysed by SDS-PAGE analysis and the samples containing protein were pooled and concentrated for use in crystallisation trials.

Buffers & Materials	Composition	Comments
Buffer A	20 mM Tris-HCl (pH 7.5) 150 mM NaCl 5 % (w/v) glycerol 0.04 % (w/v) DDM	Sterilised by filtration
Protein concentrator	Vivaspin II concentrator	Supplied by Sartorius Stedim
Gel filtration column	Superdex 200 30/10	Supplied by GE Healthcare
Äkta Purifier	Fast Protein Liquid Chromatography (FPLC)	Supplied by GE Healthcare

Table 2.8: The buffer and the required materials used for size-exclusion chromatography.

2.5 Crystallisation experiments

2.5.1 Initial screening

Protein samples were subjected to sparse matrix screens in concentrations from 4.7–12.3 mg/mL. Initial screening was performed at 22 °C using the sitting-drop vapour-diffusion method. The reservoir contained 50 µL and drop volumes (1:1 ratio of protein and reservoir solution) ranged from 500 nL to 1 µL. 96-well plates (MRC, SwissSci, Neuheim, Switzerland) for initial screens were prepared through dispensing of reservoir solution by a Hamilton Microlab Star robot (Hamilton Bonaduz AG, Switzerland) and then stored at 4 °C, until required. The drops of crystallisation experiments were set up automatically with a Cartesian Honeybee nanoliter dispensing system (Genomic Solutions Ltd., Huntington, UK). Initial 96-well screening plates were integrated into a Rhombix Crystal Plate Imager (Thermo Scientific Waltham, USA) for automatic monitoring or checked by microscope. All trays were incubated at 22 °C. Trays were checked for signs of crystal formation after one, three, five, seven, ten and fourteen days and weekly thereafter. The commercial screens used for initial screening are listed in Table 2.5.

Screen	Manufacturer
MemGold	Molecular Dimensions Ltd., Newmarket, UK
MemSys	Molecular Dimensions Ltd., Newmarket, UK
MemStart	Molecular Dimensions Ltd., Newmarket, UK
Hampton Crystal Screen 1 & 2	Hampton Research, Aliso Viejo, USA
Peg/Ion 1 & 2	Hampton Research, Aliso Viejo, USA
JCSGplus 1 & 2	Qiagen, Crawley, UK

Table 2.9: The commercially available crystallisation screens used in this study.

2.5.2 Optimisation screens

Conditions, which yielded crystalline material, were optimised. In the case of appearing crystals in initial screens, the successful conditions needed to be optimised. The primary method of optimisation was to screen around the initial hit, altering the precipitant concentration, the pH or the salt concentrations. Additive Screens 1/2 and Detergent Screens 1/2 (Hampton Research, Aliso Viejo, USA) were also used in the aim to improve crystal diffraction properties. Self-made optimisation screens were designed with the software *Screen Designer* (Hamilton Bonaduz AG, Switzerland) and set up with the Hamilton Microlab Star Robot. Further details of optimisations are given in subsequent chapters. Larger optimisation screens, using 24-well sitting drop Cryschem plates, were set up and sealed with Crystal Clear tape (Hampton Research, Aliso Viejo, USA). The plates contained 500–1000 µL reservoir solution with total drop volumes ranging from 1 to 5 µL and were set up by hand.

2.6 X-ray analysis

In order to test cryo conditions, 20 % (v/v) of ethylene glycol or PEG400 was added to a drop of reservoir solution. An empty cryo loop was dipped into the resulting cryo-protectant and placed in the beam. The frozen protectant was examined for the formation of a clear glass and chosen on this performance. Promising crystals were mounted with a loop of appropriate size, dipped for 5 seconds into the cryo-protectant and placed straight onto the goniometer head. Crystals were immediately flash frozen at –160 °C by the cryo cooling system (Oxford Cryosystems, Oxford, UK). The crystals were centred in the X-ray beam and exposed to X-rays. The in-house X-ray source was a Rigaku MicroMax 007 rotating anode generator coupled with a MarResearch 345 image plate detector. Crystals showing diffraction at low resolution were stored in liquid nitrogen for additional exposure to stronger synchrotron radiation. Crystals were routinely brought to the synchrotron beamlines BM-14 at the ESRF (Grenoble, France) and IO-2/4 at the Diamond Light Source (Oxford, UK).

Chapter 3

Expression of target membrane proteins

3.1 Introduction

The amount of naturally produced membrane protein is in many cases too low to obtain sufficient amounts of material for functional and structural studies. Most membrane protein targets therefore need to be overexpressed. However, most available expression systems have been developed to produce high amounts of cytosolic proteins in the host. In contrast to cytosolic proteins, the multi-step biogenesis of membrane proteins from targeting the nascent chain to the membrane, followed by insertion into and assembly in the membrane is a limiting factor in membrane protein overexpression (Drew *et al.* 2003; Dalbey and Chen 2004).

Membrane proteins can be optimised on the molecular level with parameters such as codon bias or the stability and translational efficiency of mRNA, with well established and documented methods (Peti and Page 2007). However, overexpressed membrane proteins are often toxic to the host and the overexpression itself has limitations. The saturation of the cell's ability to process the nascent membrane proteins can lead to the formation of aggregated material such as inclusion bodies. Although refolding of membrane proteins is possible and has been effective for β -barrel type outer membrane proteins, it is notoriously difficult or not possible for inner membrane proteins (Drew *et al.* 2003; Geertsma *et al.* 2008). When it comes to the expression of the target gene, no empirical rules or unique best conditions are known to date. The optimisation of parameters such as host strain, medium and expression temperature are thought to be target specific (Graslund *et al.* 2008).

Due to the high number of variables in the parameters involved, the task of finding the best expression conditions for a target protein is similar to other difficult multi-parameter problems such as protein crystallisation. The main issue is therefore, given finite resources, how to determine most effectively the best conditions to express the target protein (Berrow *et al.* 2006).

An economic and time saving way to explore protein expression is to work on a small-scale and, if a large number of targets or parameters are under study, to employ high throughput (HTP) methods. In order to be able to use these methods effectively an optimised laboratory set up needs to be developed. Such a HTP expression screen should be able to find the best expression conditions of a large number of targets in a short time frame. Furthermore, the results should guide whether expression levels are sufficient to proceed with purification and ideally crystallisation.

Below, the development of a small-scale HTP expression screen for the identification of the best expression conditions for 12 membrane protein-GFP targets is described and the results are presented and discussed. The screen utilises the fluorescence of the GFP-fusion proteins to estimate overexpression levels. The fast measurement of fluorescence, together with an optimised setup and employment of 96-well blocks, enables each target to be tested in four different cell lines, four different media and at two different growth temperatures in only four days. Therefore a total of 32 conditions were examined to identify the highest expression levels for each target and all together 384 results were obtained. In addition, cell density measurements together with the fluorescence data made a comparison of parameters influencing the expression possible and trends in the data can be examined.

Once the best expression condition was identified, all 12 targets were then expressed in larger cell cultures, initially in 500 mL flasks but up to 15 L fermenters when required.

3.2 Development of a small-scale high throughput expression screen

The main parameters involved in expression are the employed construct, cell lines, media and temperature. All membrane protein targets were previously cloned in proven and optimised GFP-fusion constructs (Drew *et al.* 2001; Daley *et al.* 2005), leaving the remaining three parameters to be tested. The development of the expression screen aimed at a flexible set up that is easy and fast to handle and allows rapid collection of expression data.

3.2.1 Screen set up design

The screen was designed to initially express 12 membrane protein GFP-fusions (P_1-P_{12}), by screening four cell lines (C_1-C_4), four medium compositions (medium 1–4) and two growth temperatures (T_1, T_2).

A lot of thought went into the optimisation of sample handling and data collection to generate a time efficient screening protocol. In early experiments the use of eppendorf tubes and single channel pipettes made the handling times so long, that a consistent treatment of every condition could not be guaranteed. Multi-channel pipettes were introduced and the necessary plastic labware in the shape of multi-well blocks had to be sourced to allow the combination of the small-scale approach with a HTP method. Based on a 96-well system, a number of 96, 48 and 24-well blocks and reading plates of different sizes were sourced, tested for their suitability and coordinated throughout the screen. The blocks and plates used are listed in Table 3.2.

The most important step in the screen design was the development of a grid system that combines the benefits of blocks and eight channel multi-pipettes to allow an easy workflow when pipetting from one block to another, reducing handling times. This grid system was maintained throughout the whole experiment and is described in detail below and is shown in an example 96-well block in (Fig. 3.1).

The 96-well (12 columns \times 8 rows) block layout is divided into four quadrants (I–IV). Rows A–D and columns 1–6 are represented by quadrant I, rows E–H and columns 1–6 by quadrant II. The columns 7–12 are represented by quadrant III (rows A–D) and by quadrant IV (rows E–H). To make best use of the multi-pipette, the four cell lines were allocated to the rows of each quadrant and the first six protein targets (P_1-P_6) were added sequentially to the columns

(1–6) of the first quadrant. The same set up was repeated for the second quadrant with the other half of the targets (P_6 – P_{12}). Furthermore the cell lines were grouped in neighbouring rows according to their antibiotic resistances. The multi-pipette could then be employed column wise throughout the entire screen.

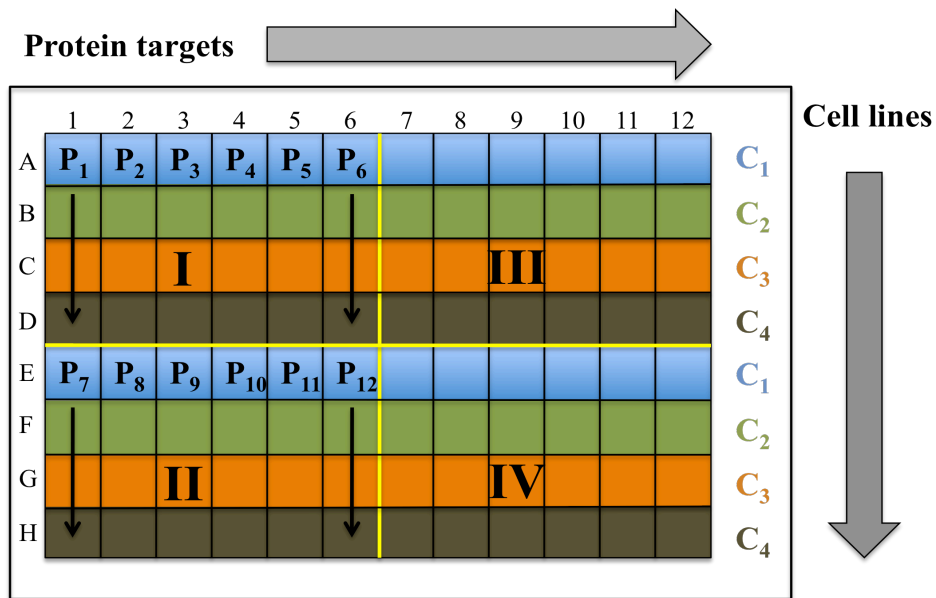


Figure 3.1: The grid system used throughout the HTP screen. The cell lines (C_1 – C_4) are in the rows (A–H) of the 96-well block and the target proteins (P_1 – P_{12}) in the columns (1–6). The block is divided into four quadrants I–IV.

3.2.2 Transformation

To insert the target GFP-fusion construct into the host cell of choice, the transformations were carried out using the grid system shown in Fig. 3.1. Initially the competent cells were aliquoted in 1.2 mL micro-tubes fitting a 96-well Cluster Plate (AB-0595, ABgene, Epson, UK) denoted as transformation block (Fig. 3.2). Unless stated otherwise, the transformation block was placed on ice during all handling procedures.

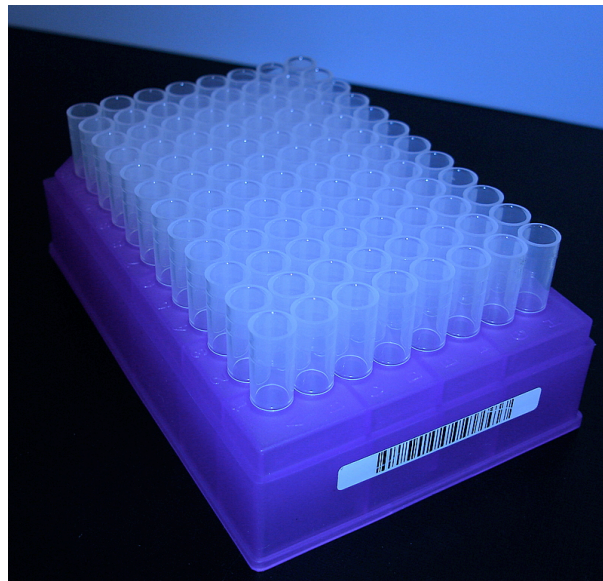


Figure 3.2: The 96-well micro-tube cluster plate that was used as transformation block.

The target DNA was stored and assorted in tubes that make the employment of a multi-pipette possible. The tubes were organised in two lines (P_1-P_6 and P_7-P_{12}) and then transferred row by row into quadrant I (P_1-P_6) and II (P_7-P_{12}) of the assembled transformation block. Working in a sterile environment is essential. Furthermore it is recommended to visually inspect the tips to ensure each tip has sucked up the correct amount of solution.

As the transformation is required, it was typically carried out in duplicate to give maximum chance of success using the second half of the transformation block (quadrants III and IV). Following the transfer of the targets DNA and incubation on ice, the rack was placed in a water bath at 42 °C for the heat shock treatment. The block was again placed on ice for cell recovery before the wells were supplemented with GS96 medium.

On such a small-scale, lack of aeration can be a major problem in all steps involving cell growth in blocks. In the transformation step this was overcome by using GS96 medium instead of more commonly used Super Optimal Culture (SOC) medium. GS96 medium is optimised in general for cell growth under low oxygen levels (see section 2.3.2). The medium was prepared with the required antibiotics for the specific cell lines added before dispensing into the transformation block. This procedure is less error prone than adding the antibiotics to each well of the block and is facilitated by the grouping of cell lines with the same resistances. In this study, cell lines of rows A and B did not carry any resistance plasmid in contrast to the two cell lines of rows C and D, which were resistant to chloramphenicol. Furthermore, the construct carries kanamycin resistance and this was added to all media.

After the GS96 medium was added, the transformation block was incubated at 37 °C for 1 h. As the transformation was carried out in quadrants I and II (and often III and IV) of the transformation block, the required amount of transformant could easily be transferred from the wells of each quadrant to the wells of a 24-well agar plate (Costar 3524, Corning Inc., New York, USA) (Fig. 3.3). The two resulting agar plates I and II (III and IV) were incubated at 37 °C overnight.

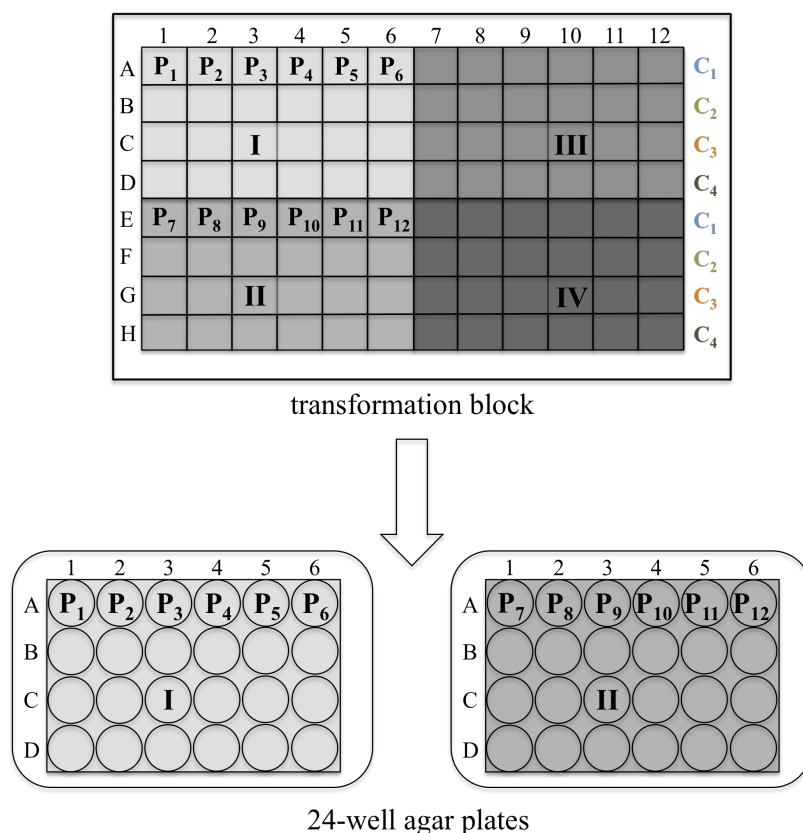


Figure 3.3: Transfer of samples from the 96-well transformation block to the 24-well agar plates.

3.2.3 Starter culture

The preparation of starter cultures requires the picking of single colonies from the agar plates. This selection step allows a visual control of the transformation efficiency and makes it easier to trace back any errors at an earlier stage. Photographs were typically taken to document transformation efficiency for each target. Figure 3.3 shows an example of an agar plate with the resulting colonies that were used to inoculate the starting cultures.

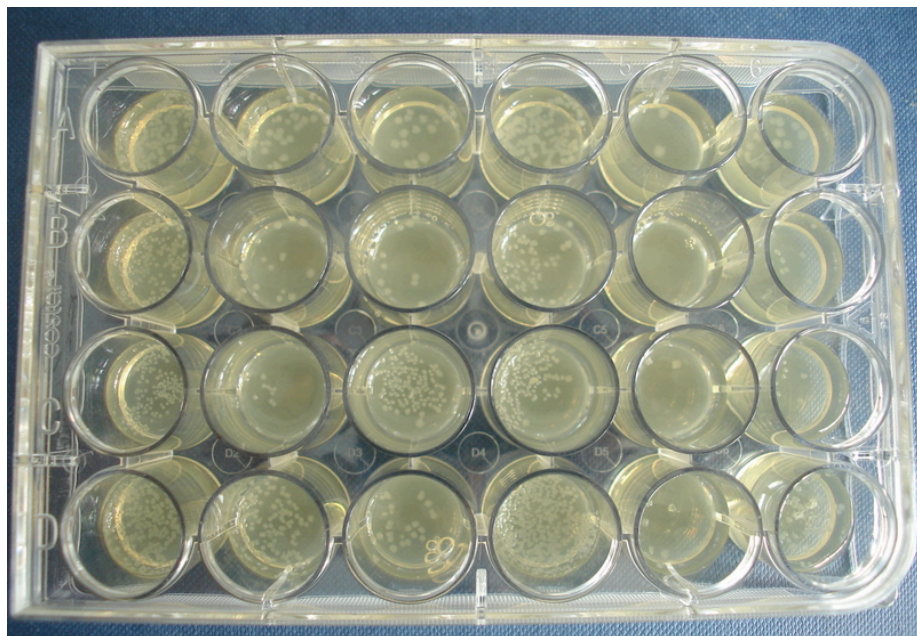


Figure 3.4: An agar plate containing transforms after incubation at 37 °C for 16 h. Single colonies can be identified in each well and were picked for the inoculation of starter cultures.

The 96-well starter culture block (2.2 mL storage plate Mark II, AB-0932, ABgene, Epsom, UK) was prepared by adding 500 µL of GS96-medium supplemented with the appropriate antibiotics to the wells of quadrants I and II. Single colonies were picked with a sterile pipette tip from the agar plate resembling quadrant I to inoculate the corresponding wells in quadrant I of the starter culture block. The procedure was repeated for the second agar plate and quadrant II to maintain the grid system. In general all blocks were covered with a gas permeable adhesive seal (AB-0718, ABgene, Epsom, UK) to avoid cross contamination prior to incubation in a shaking incubator, at 200 rpm and 37 °C overnight.

3.2.4 Expression cultures

The main expression cultures were set up to comprise two expression blocks per tested medium, one block for each temperature (T1,T2). The employed 48-well expression blocks were 6 mL deep well blocks (DWB)s (6.0 mL storage plate AB-0988, ABgene Epsom, UK) that feature bigger wells than typical 96-well blocks, therefore easing the lack of aeration and allowing to grow the cells in 2.5 mL of media per well. Inoculation was carried out by transferring 50 µL of quadrants I and II of the starter culture block into the expression blocks, maintaining the grid system as shown in Fig. 3.5.

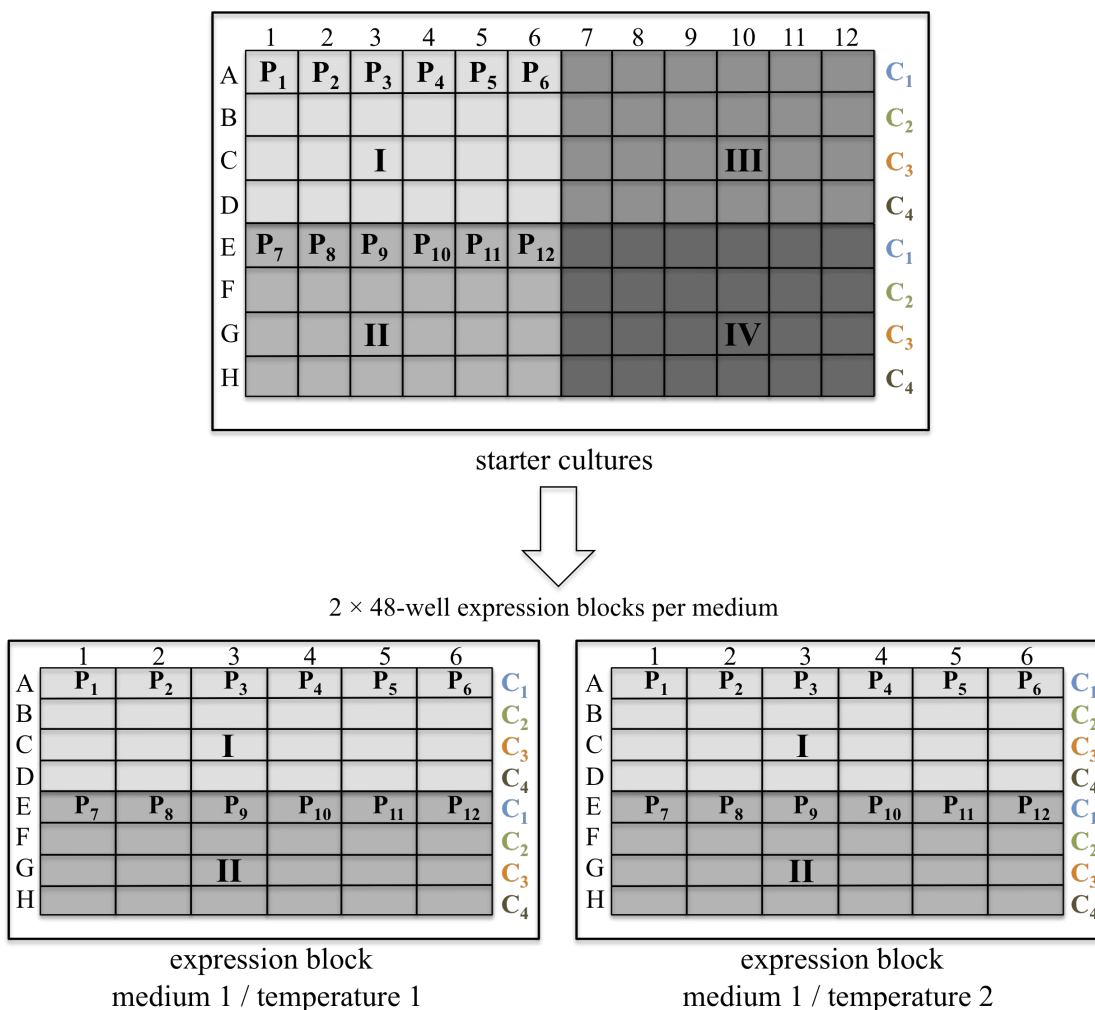


Figure 3.5: Inoculation of 48-well expression blocks with starter cultures. For each medium two expression blocks were prepared, one for each temperature tested.

The expression blocks were covered with the same type of breathable seals used for the starter culture block and always incubated in a shaking incubator at 220 rpm to improve aeration. The system of preparing one expression block per tested temperature in a particular medium makes the protocol very flexible. More media compositions or temperatures could be screened by simply inoculating more appropriate blocks.

The choice of induction system was the use of auto-induction medium, as it simplifies the protocol and handling times of the blocks. It was estimated and compared with other studies e.g (Berrow *et al.* 2006) that the time necessary for glucose depletion and subsequent induction start would be approximately four hours past the incubation start. All main expression blocks were incubated at 37 °C for 4 h and then transferred to the expression temperature of choice for the remaining 18 hours of incubation. Incubation for 4 h at 37 °C allows the cells to reach high densities in the mid-to-late log phase, prior to induction and is a commonly used approach in protein expression (for recent examples see (Berrow *et al.* 2006; Graslund *et al.* 2008).

3.2.5 Collection of expression data

The GFP-fluorescence of the targets was used as a measure of their overexpression levels. The measurement of whole-cell fluorescence intensity (FI) data (excitation 485 nm, emission 512 nm) corresponds well with the amount of overexpressed membrane protein-GFP fusion (Waldo *et al.* 1999). Focusing on obtaining the most important information in order to speed up data collection and mining, the primary aim was to identify the best expression condition for each target. This was achieved by fluorescence intensity measurements, but OD₆₀₀ data was also collected to give information about cell growth and viability in different conditions. This allowed the identification of trends in the data of both fluorescence and cell density to aid in optimising the starting parameters for future targets.

Preliminary experiments were thorough in examining the influences of different cell lines, media and sample preparations on the outcome of fluorescence and cell density measurements. In general, the observed differences between different cell lines and media were not large enough to influence the overall results. Relative values between different conditions were sufficient to identify the best expression conditions.

The key aspect is to work at sufficiently high dilutions of the samples to make fluorescence and cell density values more reliable. Diluting the samples to OD₆₀₀ values of below one, avoids both dampening the fluorescence signal through the cells, and deviations in cell density measurements through secondary scattering. In the employed OD₆₀₀ range a linear relationship between the amount of cells and the optical cell density could be established, as shown in section 2.4.2.

Fluorescence and optical density measurements are dependent on the chosen instruments. Relative comparisons are only possible if the same instruments, settings and sample preparations are employed. Therefore, all samples were treated identically and the same spectrophotometer (FLUOstar OPTIMA, BMG Labtech, Aylesbury, UK) was used throughout the study. The gain value of the spectrophotometer needs to be adjusted to achieve maximum sensitivity in fluorescence readings. If known, the samples with the highest expected fluorescence should be measured first and the determined gain value kept constant for all measurements. OD₆₀₀ readings were taken directly after fluorescence measurements in the same reading plate (Costar 3799, Corning Inc., New York, USA).

The optimised sample preparation protocol is described in the following and displayed in Fig. 3.6. From each well of the expression blocks, 100 µL samples were transferred with a multi-pipette into a 96-well analysis block (2.2 mL storage plate Mark II (AB-0932), ABgene, Epsom, UK) maintaining the grid system. 100 µL of quadrants I and II of the expression block at temperature 1 were transferred to quadrants I and II of the analysis block, while quadrants I and II from the second expression block at temperature 2 were transferred to quadrants III and IV of the analysis block, leading to one 96-well analysis block for each tested medium. The cells were then pelleted by centrifugation and the supernatant removed. The analysis blocks could then be sealed and stored at -20 °C if required. The cell pellets were resuspended in PBS buffer using a ten-fold dilution until a homogeneous sample was obtained. Resuspension takes time, but the freezing of the sample blocks enables the preparation and measurement of one block after another, without time considerations. Furthermore this step removes the influence of different media on the measurements. Finally, 100 µL of the homogeneous cell suspension is transferred to a 96-well reading plate for fluorescence intensity and OD₆₀₀ measurements.

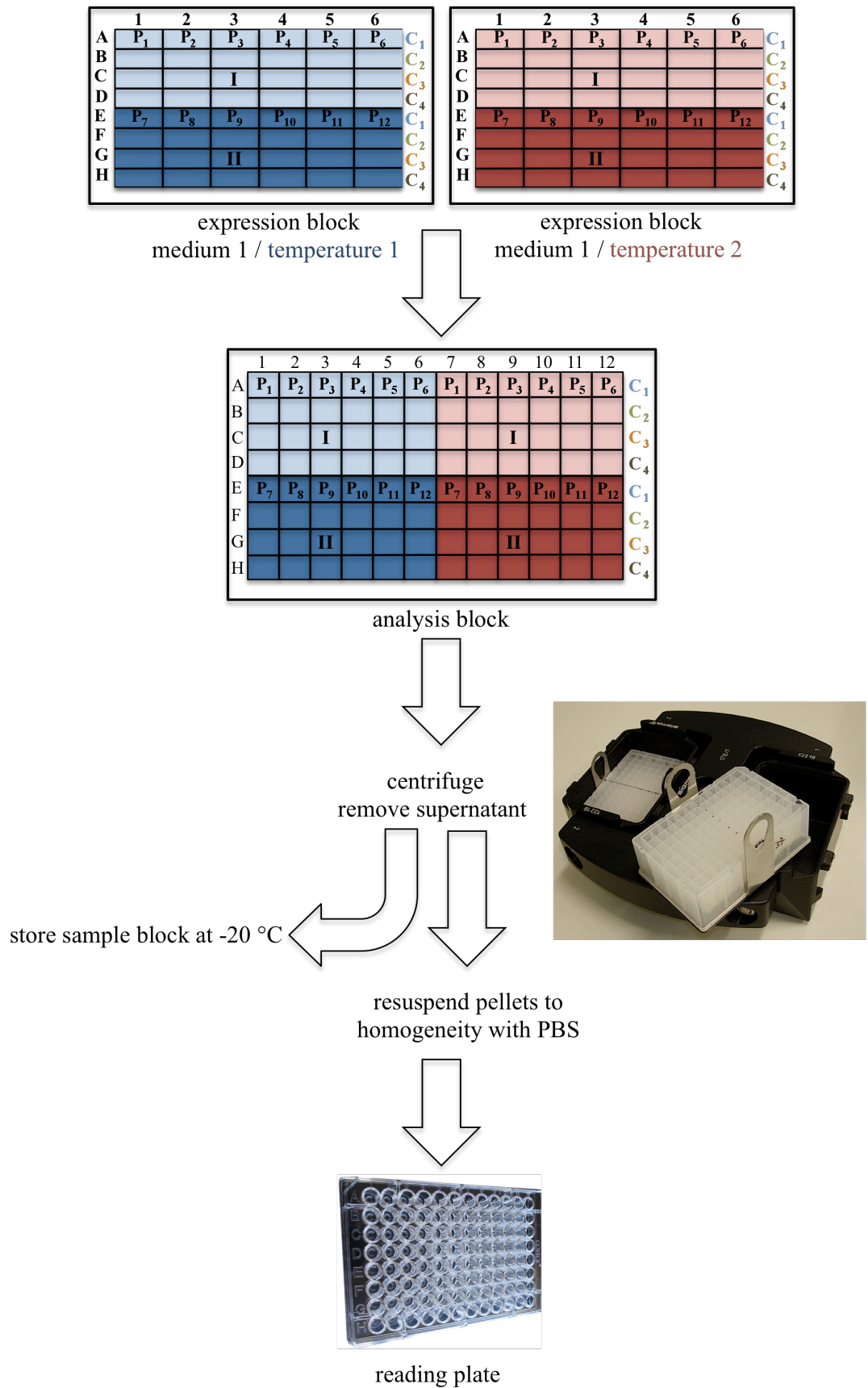


Figure 3.6: Preparation scheme of samples from the expression blocks for fluorescence and OD₆₀₀ measurements. Temperature 1 is represented by blue and temperature 2 by red colour.

3.2.6 Limitations of small-scale expression screening

In order to work with a large number of targets in a high throughput approach, compromises in the choice of the screened parameters are necessary to enable the fast and simultaneous determination of best expression conditions for the targets.

Therefore the screen aims to employ the most successful conditions to date already in the general set-up. Despite this, there will be a number of false negative clones, that mean targets, that did not express under the screen conditions or in the screen set-up, but could possibly be expressed under different conditions or in larger culture volumes. For example, how recombinant membrane protein expression is influenced by the screen set-up and the degree of aeration, is an unknown factor. These parameters do not always scale with culture volume (Graslund *et al.* 2008). The overall results are also dependent on the differences in sample preparation and purification between different scales of culture volumes (Graslund *et al.* 2008).

The screen uses the GFP-fluorescence to estimate target protein overexpression levels in the tested conditions relative to others, which is sufficient for the purpose of the screen.

However it has to be kept in mind, that whole-cell GFP-fluorescence intensity measurements are limited to the quantification of the amount of folded protein in the sample. Information about the overall expression, including the aggregated fraction, is not resolved. Low fluorescence levels could either stand for low protein expression or could indicate a large aggregated fraction (Geertsma *et al.* 2008). The expression behaviour of such a particular target could possibly be optimised in order to reduce the amount of aggregated target protein in the cells.

The developed expression screen aims to find the conditions with the highest amounts of folded target accumulated in the membrane, which can be easily solubilised for purification. Following the examination of the most promising targets in purification and crystallisation it is well worth to reanalyse the data and screen suspected false negative targets with a different set-up. In the end the successful optimisation of bacterial expression is protein dependent and interestingly, even after extensive screening of expression conditions, 30 % of *E. coli*'s own proteins can only be obtained in aggregated form when overexpressed in *E. coli* (Vincentelli *et al.* 2003; Graslund *et al.* 2008; Sahdev *et al.* 2008)

3.3 The choice of parameters

The parameters for expression were chosen on the basis of a database, which summarises all key parameters of successful membrane protein structure determinations and was established by McLuskey (personal communication), and by comparison with other structural genomic projects.

The popularity of the bacterium *Escherichia coli* as expression host is due to its fast growth to high cell numbers in inexpensive media coupled with well-known genetics and a large number of available expression vectors and mutant host strains (Jana and Deb 2005; Peti and Page 2007). The *E. coli* strains chosen for this work were BL21 Star (DE3), BL21(DE3)pLysS, Rosetta(DE3)pLysS and C41(DE3). All these strains are commonly used in structural genomics projects and were genetically optimised for protein overexpression and feature different characteristics, which are shortly described in the following (Berrow *et al.* 2006; Graslund *et al.* 2008). The strain BL21 Star (DE3) is mutated in RnaseE, reducing the degradation of mRNA in the cell and protein expression may be increased (Kido *et al.* 1996; Lopez *et al.* 1999). Host cells of the pLysS system carry an extra plasmid coding for T7 lysozyme, which functions as inhibitor of T7 polymerase. It enables a much tighter expression control and reduces basal expression, which can be toxic to the host (Studier and Moffatt 1986). Rosetta(DE3)pLysS was originally intended to facilitate the expression of eukaryotic genes and harbours the genes for rarely used t-RNAs in *E. coli* on the pLysS-plasmid, helping to overcome codon bias problems (Baneyx 1999). The fourth cell line was C41(DE3). This member of the so-called Walker strains, was selected on an empirical basis and is more resistant to the expression of toxic and membrane proteins (Miroux and Walker 1996; Terpe 2006).

In terms of media, two standard laboratory media Lysogeny Broth (LB) (Bertani 1951) and the richer Super Broth (SB) were chosen for comparison with the two commercially available auto-induction media TB overnight express (from here on referred to as TB) (Novagen, San Diego, USA) and MagicMedia (Invitrogen, Paisley, UK). TB and MagicMedia were optimised for the expression of cytosolic proteins but had not yet been tested in regard to membrane protein overexpression. LB is the most commonly used medium for recombinant overexpression of proteins in laboratories combining good bacterial growth with cheap ingredients (Berrow *et al.* 2006; Graslund *et al.* 2008). SB is an enriched LB medium. LB and SB media were used as auto-induction media based on a method developed by Studier (2005). Therefore all used media in this study were auto-induction media.

Bacterial growth will vary at a given time in different wells of a HTP expression screen, depending on the cell lines and the targets and induction at a certain optical density is difficult to monitor and to handle. The main advantage of auto-induction medium is the induction of protein expression by nutrient depletion of glucose. Auto-induction allows efficient screening of many clones in parallel for expression, as cultures have only to be inoculated and grown to saturation. Furthermore auto-induction medium is buffered to prevent a decrease of pH in the medium, which is caused by the accumulation of metabolic products. The buffering can increase cell yields and might therefore also increase protein yields (Studier 2005).

In regard to temperature, the standard temperature for optimal cell growth of the *E. coli* host at 37 °C was compared to the lower temperature of 25 °C. Expression at lower temperature reduces the risk of inclusion body formation and is supposed to relieve some of the cell's metabolic stress, giving the cell's protein production system more time to fold and process the expressed proteins (Schein and Noteborn 1988).

The test was developed and used with the above mentioned parameters but can easily be adapted to test other or even more variables. In a set of any 12 targets, the employment of more blocks would make the testing of more different media, other temperatures and more fluorescence measurements at different time points possible.

3.4 Final small-scale high throughput expression screen protocol

The discussed development of the small-scale HTP expression screen led to the final screen protocol incorporating the chosen parameters (Table 3.1) for the test of expression levels of 12 membrane proteins and is described in the following.

The expression screen tests the expression level of each target in four different cell lines, four different media and at two different temperatures. The four cell lines C41(DE3), BL21 Star (DE3), BL21(DE3)pLysS and Rosetta(DE3)pLysS are for matters of clarity denoted as C₁–C₄. The used media were LB, SB, TB overnight express (TB) and MagicMedia (MM). All media were employed as auto-induction medium. The tested temperatures were 37 °C and 25 °C. The protein targets are denoted as P₁–P₁₂ (Table 1.2). All abbreviations are listed in Table 3.2.

Symbol	Parameter
C ₁	C41(DE3)
C ₂	BL21 Star (DE3)
C ₃	BL21(DE3)pLysS
C ₄	Rosetta(DE3)pLysS
LB	Lysogeny Broth media / auto-induction
SB	Super Broth media / auto-induction
TB	TB overnight express
MM	MagicMedia
P ₁ –P ₁₂	Membrane protein GFP-fusions (see Table 1.2)

Table 3.1 Abbreviations for the parameters used in the small-scale HTP expression screen.

Multi-well blocks in the format of 96, 48 and 24-well blocks (Table 3.2) were used in the expression screen together with an eight-channel multi-pipettes (Rainin, Mettler Toledo Beaumont Leys, UK) for the fast transfer of liquids between the blocks.

Name	Wells	Type / manufacturer
Transformation block	96	1.2 mL Micro-Tube Cluster Plate (AB-0595) ABgene
Agar plates	24	Costar 3524, Corning Inc.
Starter cultures	96	2.2 mL storage plate Mark II (AB-0932) ABgene
Expression block	48	6.0 mL storage plate (AB-0988) ABgene
Analysis block	96	2.2 mL storage plate Mark II (AB-0932) ABgene
Reading plate	96	Costar 3799, Corning Inc.

Table 3.2: The blocks and plates employed for the small-scale HTP expression screen.

The screen yields data on 32 expression conditions per target in four days. In order to allow a fast handling of blocks, the developed grid system (see Fig. 3.1) was used throughout the entire screen.

Fig. 3.7 shows a flowchart of the screen including all employed multi-well blocks, their denotation and the main volumes that are transferred. The positions of the names of the specific cell lines in the rows of the blocks are displayed in the first step and although not visualized in the following steps, they are not altered. Furthermore, Fig. 3.7 illustrates with the steps for each day the overall time frame of the expression screen.

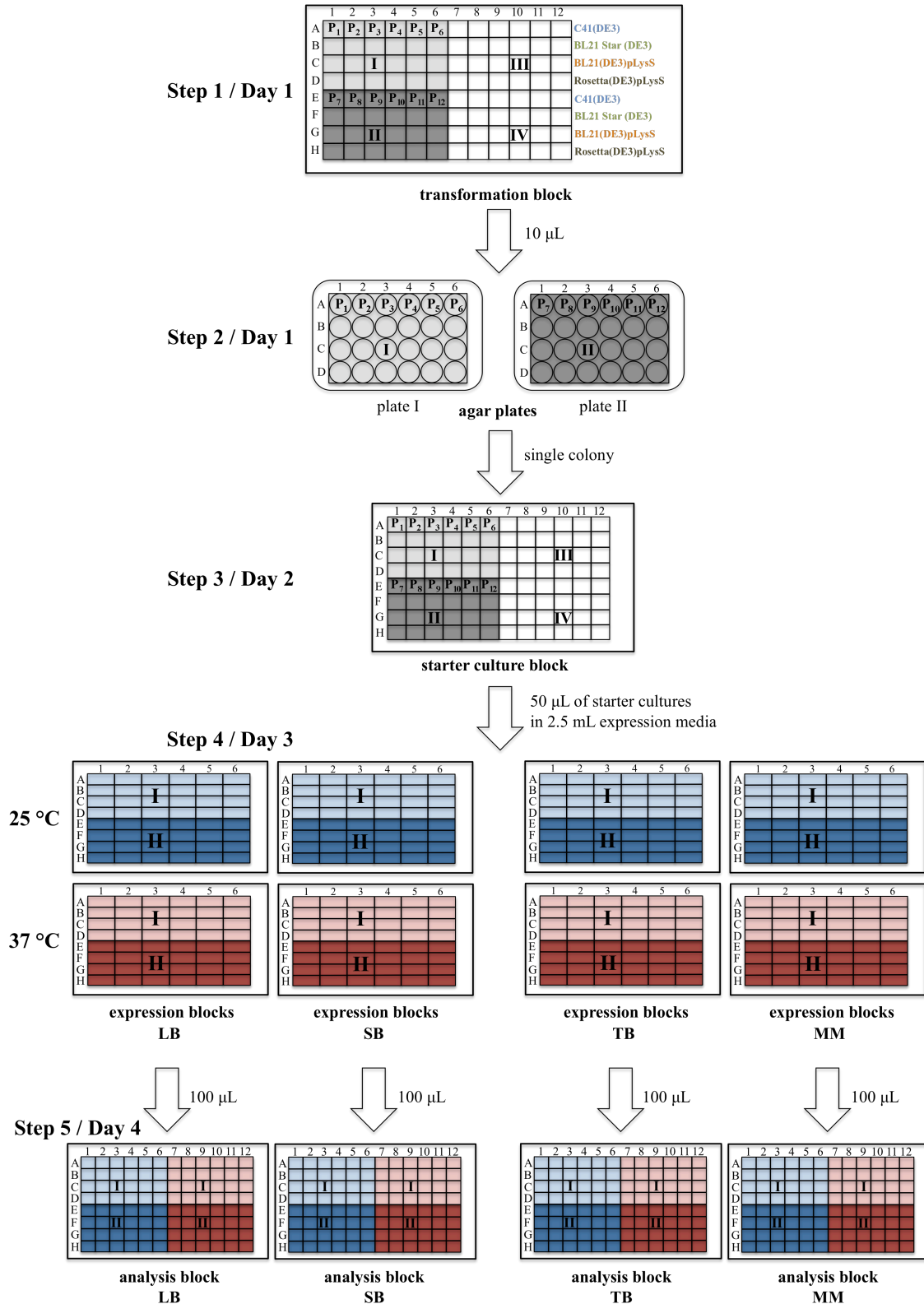


Figure 3.7: Workflow graphic of the small-scale HTP screen. Step 1: Transformation block showing all four quadrants (I-IV) together with the position of the membrane proteins P₁-P₁₂ and cell lines. Step 2: Quadrants I and II are copied to 24-well agar plates. Step 3: Single colonies of the agar plates are used to inoculate the starter culture block. Step 4: The starter cultures are diluted into two 48-well expression blocks per medium, one for each temperature. Step 5: Samples from the two 48-well expression blocks per medium are transferred in the shown arrangement into one 96-well analysis block giving finally one analysis block per tested medium.

3.4.1 Transformation in the HTP-expression screen

The transformation of target plasmid DNA into the host cells marks the beginning of the screen and in step 1, the required competent cells are thawed and the transformation block is assembled with 48 microtubes (quadrant I and II) on ice. 10 µL of competent cells, are aliquoted according to the different cell lines into the rows A–D of quadrant I and repeated for the rows E–H of quadrant II. Then 1 µL (~ 20 ng/µL of DNA) of each target, P₁–P₆ and P₇–P₁₂, is pipetted into columns 1–6 of sections I and II, respectively. A graphic view of the transformation block set up and of the resulting agar plates, which reflect the quadrants I and II of the transformation block, are shown in Fig. 3.8.

The transformation block is incubated on ice for 20 min. The cells are transformed by heat-shock for 45 sec at 42 °C, by placing the transformation block in a water bath. After recovery on ice for 3 min, 500 µL of pre-warmed (42 °C) GS96 medium is added to each microtube and incubated for 1 h at 37 °C (no shaking required). In step 2, two sterile 24-well agar plates are prepared with the appropriate antibiotics and pre-warmed to 37 °C. Maintaining the grid system from step 1, 10 µL of each microtube of quadrant I is plated out on the first agar plate and the same for quadrant II on the second agar plate. The plates are incubated for 16 h at 37 °C and stored at 4 °C until required.

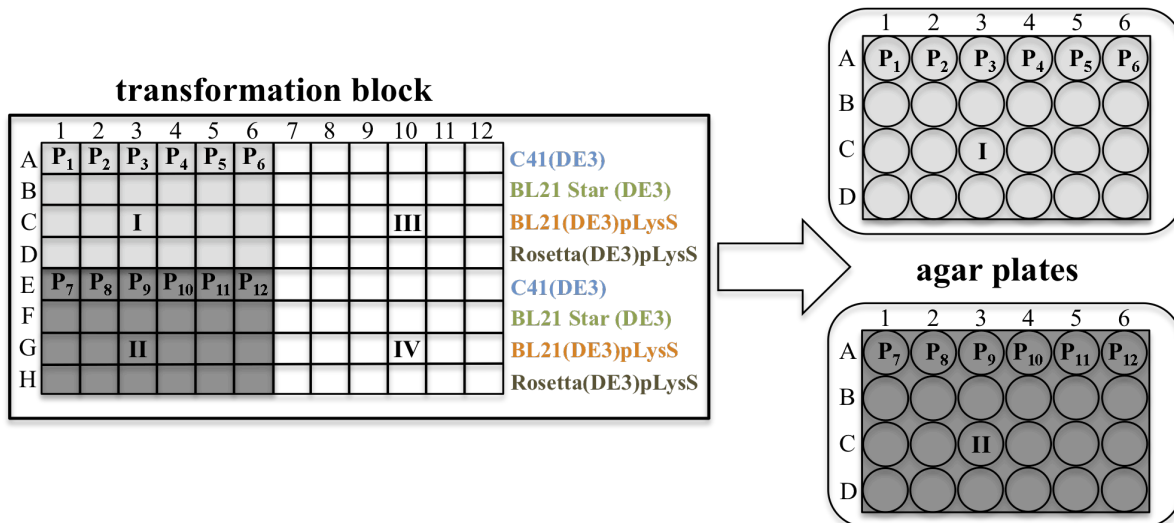


Figure 3.8: Schematic representation of the transformation block and agar plates.

3.4.2 Cell growth

Starter cultures are prepared by adding 500 µL of GS96 medium to quadrants I and II of a 96-well deep well block (DWB), maintaining the grid system (step 3). Corresponding single colonies from the agar plates are picked to inoculate quadrant I and quadrant II of the starter culture DWB, respectively. The starter culture block is sealed with a gas permeable adhesive seal and incubated for 16 h in a shaking incubator operating at 37 °C and 180 rpm.

The main expression blocks in step 4 consist out of two 48-well DWB for each medium used, one for growth at 25 °C and one for 37 °C. Every 48-well expression block is prepared by adding 2.5 mL of the required medium and supplemented with the appropriate antibiotics (Table 2.2). The expression blocks are inoculated by adding 50 µL of each well of quadrants I and II of the starter culture block to the corresponding wells of all eight expression blocks. The expression blocks are first incubated for 4 h at 37 °C and 220 rpm. After 4 h, the blocks intended for the lower temperature are removed and incubated at 25 °C for a further 18 h, while one block per medium remains at 37 °C for the same amount of time.

3.4.3 Sample preparation and data collection

Samples are collected for fluorescence intensity and OD₆₀₀ measurements by transferring 100 µL samples in one 96-well analysis block for each medium as shown in Fig. 3.9 at the end of this section, resulting in four analysis blocks (step 5). The cells in the analysis blocks are harvested by centrifugation at 5000×g for 5 min. The supernatant is removed and the blocks are sealed before being stored at –20 °C until required.

Prior to data collection the analysis blocks are thawed and the samples diluted to an OD₆₀₀ below 1.0. This is done by adding 900 µL of PBS (phosphate buffered saline) pH 7.4 to each well. The samples are mixed thoroughly by pipetting to achieve homogeneity. Subsequently 100 µL of each well are transferred to a 96-well reading plate and placed in the fluorimeter (FLUOstar OPTIMA, BMG Labtech) (see also sample preparation scheme in Fig. 3.6). After incubating the plate for 5 min at 37 °C with shaking, the fluorescence intensity is measured (excitation 485 nm, emission 512 nm).

The gain value of the fluorimeter is optimised to enable maximum sensitivity and is kept constant for all measurements to make a comparison of different blocks possible. The measurement of OD₆₀₀ follows directly after the fluorescence reading in the same plate and fluorimeter.

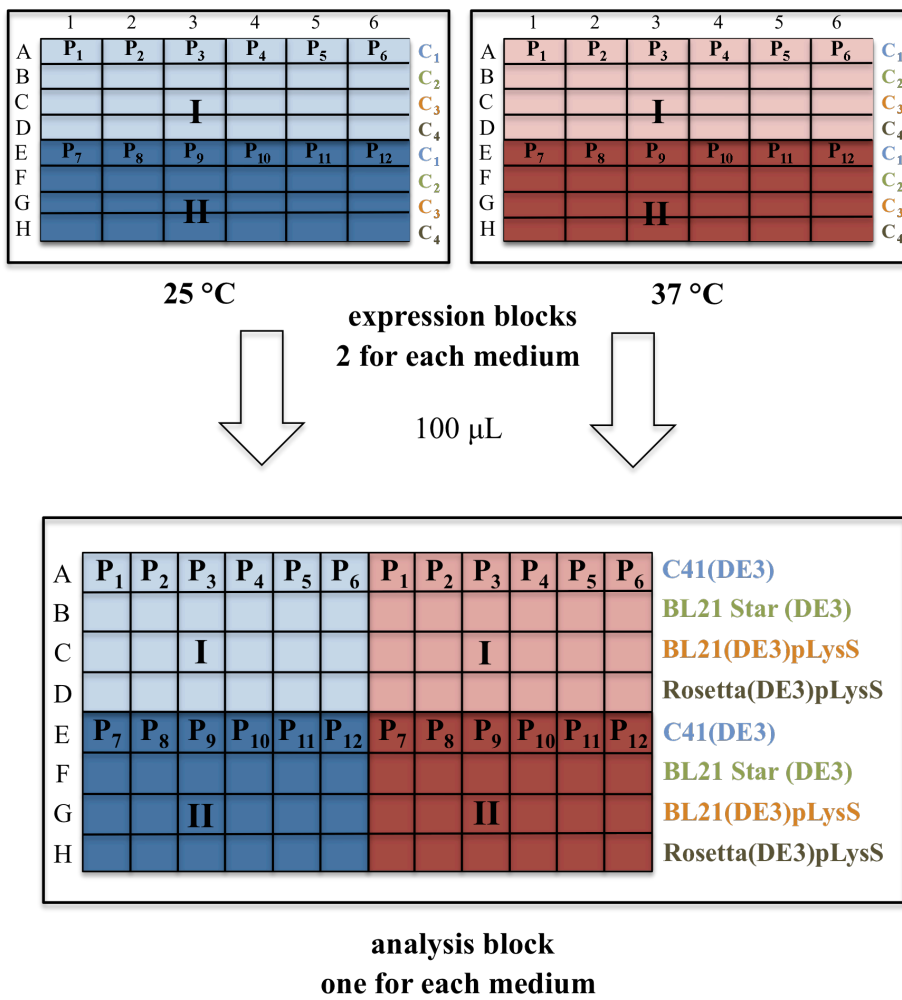


Figure 3.9: The collection of samples from the expression blocks into one analysis block. Analysis blocks are centrifuged to harvest the cells, the supernatant is discarded and the blocks are sealed and stored at -20° C.

3.4.4 Results

The main advantage of the small-scale HTP screen is the vast amount of data gathered on the expression behaviour of the target membrane proteins, with relatively low amounts of reagents and in a short time. This allows not only the best expression condition for each target to be identified, but also makes it possible to mine trends in the data, which in turn can be used to further optimise the starting parameters.

Samples were transferred from each of the expression blocks into the corresponding analysis blocks after 22 h of incubation. Whole-cell fluorescence intensity data was collected from each of the four analysis blocks after sample preparation and transfer to a reading plate.

The results from the fluorescence intensity measurements are shown in a schematic in Fig. 3.10. The target names (Table 1.2) are displayed in a column, the cell lines in the rows and each row is subdivided in growth media and temperatures. The fluorescence intensity values are shown as pictograms for better visualisation. One square equals 100000 fluorescence counts while one dot stands for 20000. Values were rounded down to the next multiple of 20000. Targets with whole-cell fluorescence values $0 < 20000$ are displayed as 20000. Conditions in which target expression led to cell death are denoted by \ominus . The expression of XylE (target No. 6), for example, led to cell death in the cell line BL21 Star (DE3) in all the media tested when expression was run at 25 °C.

A quick look at the overall 384 expression results in Fig. 3.10 already reveals some of the trends in the data, which are described in the following sections. With regard to cell lines, most targets express best in Rosetta(DE3)pLysS, followed by BL21(DE3)pLysS, C41(DE3) and BL21 Star (DE3). While XylE is the target with the highest expression level of the whole screen in BL21(DE3)pLysS at 25 °C in SB medium, it appears to be toxic at the same temperature to the strain BL21 Star (DE3) in all the media used. The influence of temperature is clearly visible with higher expression levels at 25 °C in nearly all cases. The differences in fluorescence values between media are less distinctive, but most targets expressed best in SB medium at 25 °C. The data from Fig. 3.11 shows the best expression conditions for each target, which are listed in Table 3.3.

Target / Cell line	CcmC	CodB	FtsX	Lgt	PnuC	XylE	XylH	ChbC	YdeD	PgpB	YdhC	YhbE	Temperature & Media
C41(DE3)	•	•	•	•	•	■■••	■•••	■■••	■•••	■■••••	■■•••	•	25 °C SB
	•	•	•	•	•	•	•	•	•	•	•	•	37 °C
	•	•	•	•	•	■	■	•	■	■■••	■	•	25 °C LB
	•	•	•	•	•	•	•	•	•	•	•	•	37 °C
	•	•	•	•	•	■■••	■•••	■■	■•	■	•	•	25 °C TB
	•	•	•	•	•	•	•	■	•	•	•	•	37 °C
	•	•	•	•	•	■■	••••	■■••	■•••	■■••	■	•	25 °C MM
	•	•	•	•	•	•	•	■	•	■	•	•	37 °C
	•	•	•	•	•	•	•	•	•	•	•	•	•
BL21 Star (DE3)	•••	•	■	•	■••	∅	■•	■••••	•••	■••••	•	•	25 °C SB
	•	•	•	•	•	•	•	•	•	•	•	•	37 °C
	•	•	•	•	•	•	•	•	•	•	•	•	25 °C LB
	•	•	•	•	•	•	•	•	•	•	•	•	37 °C
	•	•	•	•	•	•	•	•	•	•	•	•	25 °C TB
	•	•	•	•	•	•	•	•	•	•	•	•	37 °C
	•••	•	•••	•	•	∅	•	•••	•••	•••	•	•	25 °C MM
	•	•	•	•	•	•	•	•	•	•	•	•	37 °C
	•	•	•	•	•	•	•	•	•	•	•	•	•
BL21(DE3) pLysS	■■••	■	■■••••	■	■■■■■■■■■■	■■■■■■■■■■	••	■•	■•••	■■••	•••	••	25 °C SB
	•••	•••	•••	•••	■	■	•	•	•	•	•	•	37 °C
	■	•••	■	•••	•••	■■■■■■■■■■	•••	•••	•••	•••	•••	•	25 °C LB
	•••	•••	•••	•••	•••	•••	•••	•••	•••	•••	•••	•	37 °C
	•	•	•	•	•	■■■■■■■■■■	•••	•••	•••	•••	•••	•	25 °C TB
	•	•	•	•	•	•	•	•	•	•	•	•	37 °C
	■	■	■■••	■	■■■■■■■■■■	■■■■■■■■■■	•••	■■••	■■••	■■••	■■••	••	25 °C MM
	•••	•••	•••	•••	•••	•••	•••	•••	•••	•••	•••	•	37 °C
	•	•	•	•	•	•	•	•	•	•	•	•	•
Rosetta (DE3)pLysS	•••	■■■■■■■■■■	■■■■■■■■■■	■■■■■■■■■■	■■■■■■■■■■	■	■■••	■■■■■■■■■■	■•••	■••••	■■■■■■■■■■	■•••	25 °C SB
	•	■	■	■	■	•	•	•	•	•	•	•	37 °C
	•••	■■■■■■■■■■	■■■■■■■■■■	■■■■■■■■■■	■■■■■■■■■■	■■■■■■■■■■	■■■■■■■■■■	■■■■■■■■■■	■■■■■■■■■■	■■■■■■■■■■	■■■■■■■■■■	■	25 °C LB
	•	•	•	•	•	•	•	•	•	•	•	•	37 °C
	•	■■■■■■■■■■	•	■■■■■■■■■■	■■■■■■■■■■	■■■■■■■■■■	■■■■■■■■■■	■■■■■■■■■■	■■■■■■■■■■	■■■■■■■■■■	■■■■■■■■■■	■	25 °C TB
	•	•	•	•	•	•	•	•	•	•	•	•	37 °C
	•••	•••	•••	•••	•••	•••	•••	•••	•••	•••	•••	•••	25 °C MM
	•	•	•	•	•	•	•	•	•	•	•	•	37 °C
	•	•	•	•	•	•	•	•	•	•	•	•	•
■ = 100000													
• = 20000													

Figure 3.10: Overall expression results for all 12 membrane protein-GFP fusions (listed in columns). A square symbolises a whole-cell fluorescence value of 100000 and a dot 20000 fluorescence counts. Temperature is displayed in blue for 25 and red for 37 °C. The fluorescence value for example of CcmC (target No. 1), expressed in BL21(DE3)pLysS in SB media at 25 °C is read as 220000 AU. Values were rounded down to the nearest multiple of 20000. Values 0 < 20000 are shown as 20000. Cases in which cell death occurred are denoted as ∅. Fluorescence values are measured in arbitrary units.

Target	Media	Cell line	Temperature [°C]
CcmC	SB	BL21(DE3)pLysS	25
CodB	SB	Rosetta(DE3)pLysS	25
FtsX	SB	Rosetta(DE3)pLysS	25
Lgt	LB	Rosetta(DE3)pLysS	25
PnuC	SB	BL21(DE3)pLysS	25
XylE	SB	BL21(DE3)pLysS	25
XylH	SB	Rosetta(DE3)pLysS	25
YdeD	LB	Rosetta(DE3)pLysS	25
ChbC	SB	Rosetta(DE3)pLysS	25
PgpB	SB	C41(DE3)	25
YdhC	SB	Rosetta(DE3)pLysS	25
YhbE	SB	Rosetta(DE3)pLysS	25

Table 3.3: The best expression condition for each of the screened 12 membrane proteins.

In order to identify the best expressing targets, they can be ranked according to their fluorescence values (Table 3.4). As Table 3.4 shows, there is a considerable difference between the best expressing target XylE and the worst, YhbE, with XylE showing four times higher fluorescence values than YhbE. The ranking was used to start the scale-up expression with the targets showing the highest fluorescence values.

Rank	Target	Maximal fluorescence value (AU)	Medium	Cell line
1	XylE	637820	SB	BL21(DE3)pLysS
2	PnuC	580610	SB	BL21(DE3)pLysS
3	CodB	478850	SB	Rosetta(DE3)pLysS
4	FtsX	466140	SB	Rosetta(DE3)pLysS
5	ChbC	342620	SB	Rosetta(DE3)pLysS
6	Lgt	314060	LB	Rosetta(DE3)pLysS
7	PgpB	288650	SB	C41(DE3)
8	YdhC	287660	SB	Rosetta(DE3)pLysS
9	CcmC	232870	SB	BL21(DE3)pLysS
10	XylH	215450	SB	Rosetta(DE3)pLysS
11	YdeD	198040	LB	Rosetta(DE3)pLysS
12	YhbE	156990	SB	Rosetta(DE3)pLysS

Table 3.4: Ranking of target membrane proteins after the HTP small-scale expression screen according to their best whole-cell fluorescence intensity value and together with the respective medium and cell line.

3.5 Medium-scale expression

After identifying the best expression condition for each target, all membrane proteins were expressed in 500 mL cell cultures in 2 L flasks. Fluorescence values were measured from samples taken before harvesting after 22 h. Table 3.5 shows the ranking of the best expressing proteins in 500 mL cultures, compared to the ranking in the small-scale test. XylE expresses best in both rankings. However, as the results in Table 3.6 show, a real correlation in the rankings of the targets expressed on a small-scale or in larger cell cultures is not found. FtsX is the target with the biggest drop in fluorescence values in the ranking, compared to other targets. In contrast, targets such as PgpB or CcmC, rank higher in the scale-up expression than in the small-scale screen. Only XylE and XylH keep their places in the ranking. Therefore it is target specific how the cell culture volume affects membrane protein expression in this study. In conclusion the small-scale HTP screen identifies the best expression conditions, in order to produce enough protein for further purification and crystallisation studies, but a ranking of the targets is not transferable to larger cell cultures. It was possible to obtain enough protein for further purification studies of all targets, following their expression in the identified optimal conditions. The scale-up expression ranking was then used to focus the work on purification, to start with the most promising membrane proteins: XylE, PgpB and CcmC.

Ranking	Scale-up expression	Small-scale expression HTP screen
1	XylE	XylE
2	PgpB	PnuC
3	CcmC	CodB
4	YdhC	FtsX
5	CodB	ChbC
6	ChbC	Lgt
7	PnuC	PgpB
8	Lgt	YdhC
9	YhbE	CcmC
10	XylH	XylH
11	FtsX	YdeD
12	YdeD	YhbE

Table 3.5: Ranking of targets from small-scale and medium-scale expression.

3.6 Trends from expression data

The large amount of expression data gathered, makes it possible to examine the behaviour of single parameters or combinations thereof. For example, the influence of one particular cell line or growth medium at different temperatures on cell growth and target expression can be examined. The highest fluorescence observed, identifies the best expression condition in the screen, while the cell density (OD_{600}), which was measured (see section 2.4.2) simultaneously with the fluorescence intensity, allows insight into relations between protein production and cell growth under all tested conditions. In the following figures the OD_{600} data is shown next to the fluorescence values to make a direct comparison possible between the cell growth and how much protein these cells yielded in relation to others.

In general, the best expression temperature found for all targets was 25 °C. Ten out of twelve membrane proteins expressed best in SB medium and the remaining two in LB medium. With regard to cell line, eight targets gave the highest fluorescence readings in Rosetta(DE3)pLysS, followed by three targets in BL21(DE3)pLysS and only one in C41(DE3). Overall, the combination Rosetta(DE3)pLysS in SB medium at 25 °C was the most successful of the screen, with six targets expressing best in this condition.

The following sections look at trends, which are averaged over all targets, in regard to how particular parameters such as media or cell lines perform at different temperatures and in relation to each other.

3.6.1 Trends in the performance of media

The first set of questions one could ask are, in which medium are, on average, the highest fluorescence values obtained? Does this correlate with the cell growth and does the temperature influence this trend? When averaging the fluorescence intensity (Fig. 3.11 (A)) and the optical density data (Fig. 3.11 (B)) of the expression screen over all targets and cell lines, it is possible to look at the performance of the tested media in relation to each other at different temperatures (Fig. 3.11). The analysis reveals which medium produces on average the highest amount of cells and if this correlates to the measured fluorescence levels.

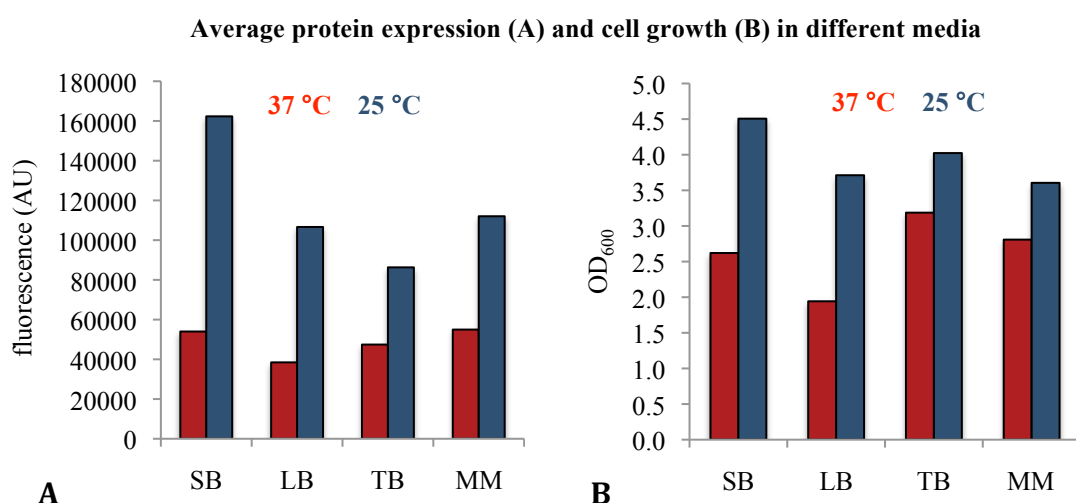


Figure 3.11: Temperature dependence of cell growth (B) and expression (A) in different media, averaged over all targets and cell lines. SB is the best medium at 25 °C with the highest fluorescence and cell density values. MagicMedia (MM) yields the highest fluorescence readings at 37 °C, but TB medium the highest cell density at this temperature.

The medium obtaining the highest fluorescence readings and cell density values is SB medium at 25 °C. The performance of the medium is however temperature dependent and at 37 °C, MagicMedia (MM) performs slightly better than SB medium in regard to expression of target GFP-fusion protein and amount of cells. Despite the best cell growth at 37 °C and the second best at 25 °C, TB medium ranks only third in the fluorescence readings at both temperatures. LB medium has the lowest cell growth and expression of all media at 37 °C. In contrast, cell growth in LB medium at 25 °C is ranking between the media MM (lower) and TB (higher). However cells growing in LB

medium at 25 °C express more target protein-GFP fusion than in TB medium and only slightly less than in MM medium.

In general, temperature has a greater effect on protein expression than on cell growth when comparing fluorescence and cell density. The commercial media TB and MM are less influenced by different temperatures than LB and SB medium, especially with regard to cell growth.

3.6.2 Trends in the performance of cell lines

The second set of questions deals with how the cell lines on average cope with different temperatures. Which cell line grows best and does this cell line also express more target proteins than the other cell lines? To address these questions, the expression data were averaged over all targets and all media. The resulting data, which are presented in figures for fluorescence intensity (Fig. 4.12 (A)) and cell density (Fig. 4.12 (B)), make it possible to compare trends between the four cell lines used in the screen dependent on the temperature.

Average protein expression (A) and cell growth (B) in different cell lines

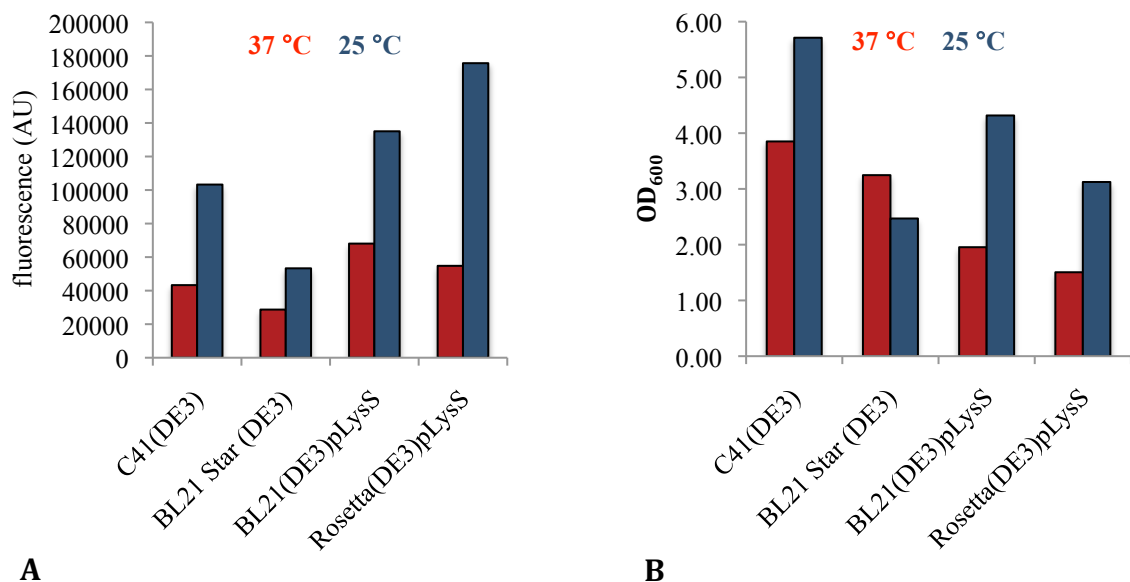


Figure 3.12: Temperature dependence of cell growth (OD₆₀₀) (B) and protein expression (fluorescence) (A) in different cell lines, averaged over all targets and media. Rosetta(DE3)pLysS is expressing the most target protein GFP-fusion. BL21 Star (DE3) is the only cell line growing better at higher temperature, although yielding more protein at lower temperature. C41(DE3) grows to the highest cell densities in the study, but only ranks third in terms of fluorescence. Temperature dependency is more distinct in protein synthesis than in cell growth.

All cell lines express more target GFP-fusion protein at 25 °C, as the increased fluorescence values show at this temperature. The cell line Rosetta(DE3)pLysS shows the highest fluorescence values at 25 °C followed by BL21(DE3)pLysS, C41(DE3) and BL21 Star (DE3). BL21 Star (DE3) is the only cell line that grows better at 37 °C than at 25 °C, however it still expresses more target protein at 25 °C, although less than any other cell line.

With regard to cell growth, it is revealed that the cell line growing to the highest cell densities at both temperatures, C41(DE3), ranks only third in protein expression. In contrast Rosetta(DE3)pLysS ranks third in cell growth at 25 °C and fourth at 37 °C, but gives the highest fluorescence readings at 25 °C and the second highest at 37 °C. Rosetta(DE3)pLysS has the best ratio of produced target membrane protein per cell from the tested cell lines in the expression screen. The fact that eight out of twelve targets express best in Rosetta(DE3)pLysS confirms this result. Therefore the amount of cells does not necessarily correspond with higher fluorescence and hence target protein expression in the screen.

3.6.3 Trends in the performance of single cell lines in different media

A further question arises in regard to how single cell lines perform in different media and at different temperatures. The data were analysed and averaged over all targets to make a comparison of cell line performances in different media and growth temperatures possible and the results are presented for each cell line in the following sections.

3.6.3.1 Protein expression and cell growth in C41(DE3)

The average performance of the cell line C41(DE3) in regard to target protein expression (Fig. 3.13 (A)) and cell growth (Fig. 3.13 (B)) shows that SB medium stands out from the other three media with the highest expression and cell growth at 25 °C.

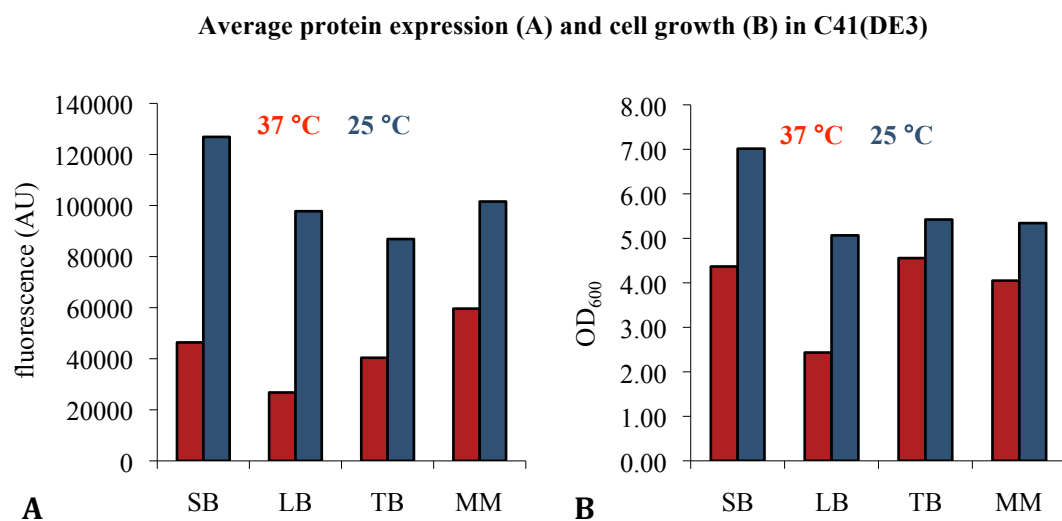


Figure 3.13: Data of fluorescence intensity (A) and cell density (OD_{600}) (B) of C41(DE3) in different media averaged over all tested membrane proteins. C41(DE3) grows and expresses best at 25 °C in SB medium. LB, TB and MM media all perform on a similar level at lower temperature.

The growth of C41(DE3) and the expression of target protein is less influenced by temperature in the media TB and MM. MagicMedia yields the highest fluorescence values at 37 °C, while LB medium performs worst. C41(DE3) cells grow in TB medium to the highest cell density at 37 °C and second highest at 25 °C, but the expression levels rank only third at 37 °C and last at 25 °C.

3.6.3.2 Protein expression and cell growth in BL21 Star (DE3)

A different trend is observed for BL21 Star (DE3). This cell line grows in all media, especially the commercial media TB and MM, the best at 37 °C (Fig. 3.14 (B)). In SB and LB media the cell growth does not differ much between temperatures. Despite the trend in cell growth, the highest protein expression (Fig 3.14 (A)) in all media is found at 25 °C, with BL21 Star (DE3) expressing the most target protein in SB medium. LB medium has the lowest cell growth and protein expression at both temperatures relative to all other media tested.

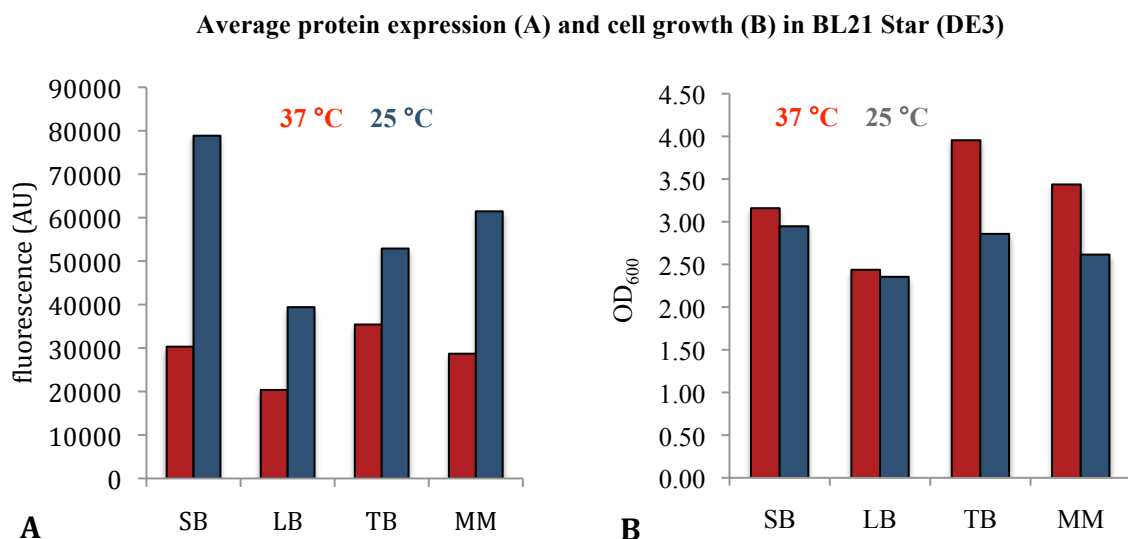


Figure 3.14: Fluorescence values (A) for average target expression and cell growth (OD₆₀₀) (B) values in B21 Star (DE3). The data was averaged over all 12 membrane protein targets. BL21 Star (DE3) is the only cell line growing best in all media at 37 °C, despite having the highest protein expression at 25°C. The most successful media in terms of fluorescence is SB followed by MM, TB and LB.

A comparison between C41(DE3) and BL21 Star (DE3) shows, that C41(DE3) reaches considerably higher values for cell growth and protein expression, especially in SB medium, than BL21 Star (DE3). Possible explanations for the low cell growth and protein expression are discussed in the conclusion of this chapter.

3.6.3.3 Protein expression and cell growth in BL21(DE3)pLysS

The fluorescence and the cell density data was averaged over all targets for the cell line BL21(DE3)pLysS. The resulting graphs show that cell growth (Fig. 3.15 (B)) of BL21(DE3)pLysS and target expression (Fig. 3.15 (A)) is highly influenced by temperature. The influence of temperature is especially observed for the cell growth of BL21(DE3)pLysS in the media SB, LB and MM at 25 °C, where cell density levels are considerably higher than at 37 °C. The growth of BL21(DE3)pLysS is less affected by temperature in TB medium, but the expression levels are the lowest in this medium. BL21(DE3)pLysS grew best and produces the most membrane protein in SB medium, followed by MM medium, at 25 °C.

Average protein expression (A) and cell growth (B) in BL21(DE3)pLysS

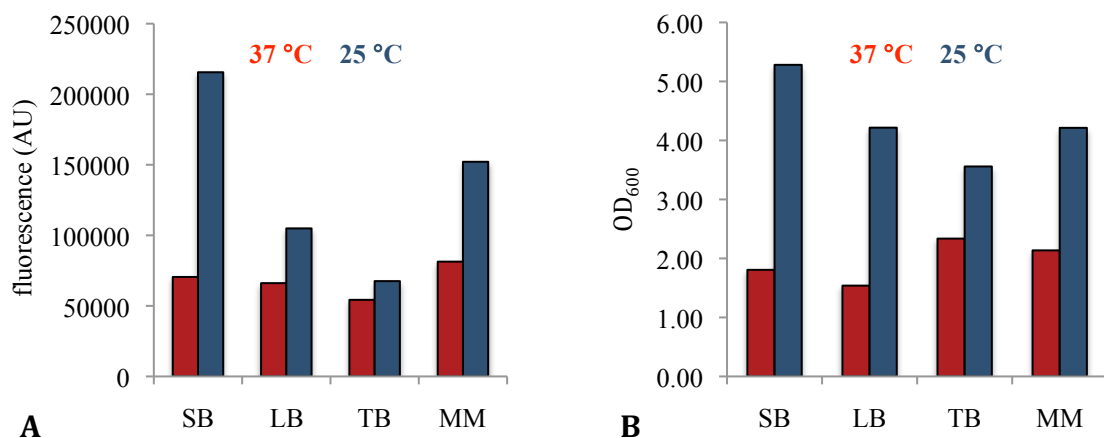


Figure 3.15: Fluorescence values (A) for average expression and cell growth (OD₆₀₀) (B) in BL21(DE3)pLysS. The data was averaged over all 12 membrane protein targets. Performance is very temperature dependent and BL21(DE3)pLysS yields the most protein in SB media at 25 °C.

3.6.3.4 Protein expression and cell growth in Rosetta(DE3)pLysS

Similar to BL21(DE3)pLysS, a strong influence of the temperature on the expression levels of target protein (Fig. 3.16 (A)) and the cell growth (Fig. 3.16 (B)) of Rosetta(DE3)pLysS can be observed. Rosetta(DE3)pLysS grew best in TB medium. Although cell growth in SB medium is ranks only third behind TB and LB media at 25 °C, more target protein is expressed with SB medium followed by LB and TB media. The best ratio of the tested cell lines with the amount of cells to expressed target protein is therefore only obtained in SB medium at 25 °C.

Average protein expression (A) and cell growth (B) in Rosetta(DE3)pLysS

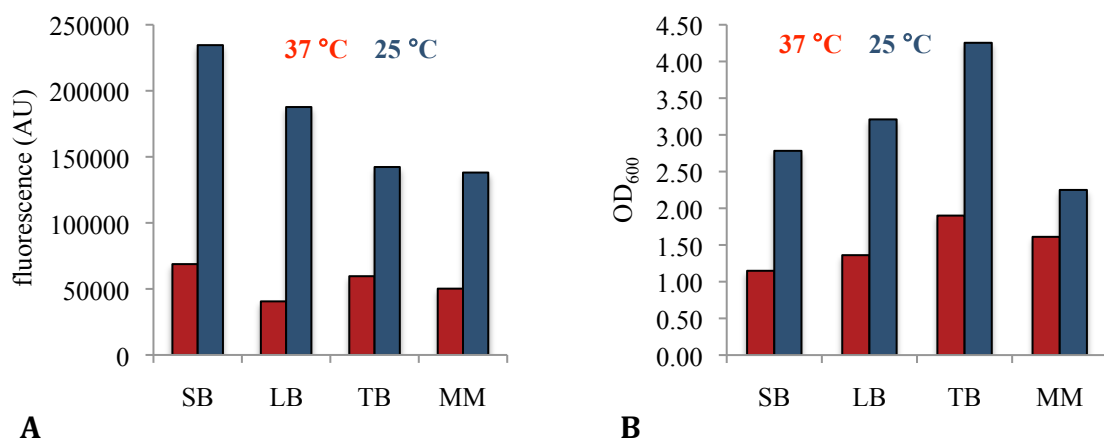


Figure 3.16: Fluorescence values (A) for average expression and cell growth (OD_{600}) (B) in Rosetta(DE3)pLysS. The data was averaged over all 12 membrane protein targets. A strong influence of temperature is observed for cell growth and even more for protein synthesis. Rosetta(DE3)pLysS grows best in TB medium at 25 °C but yields more protein in SB medium at the same temperature.

3.7 Conclusion

The developed small-scale HTP screen identified the best expression conditions for the 12 membrane protein GFP-fusions out of 32 conditions per target. The data from 384 expression results obtained, was used to search for trends in the parameters. It was found that the expression temperature is the most important parameter to optimise, followed by the choice of cell line and media. Low temperature can reduce the metabolic stress of the cells and was observed to lead to higher target expression in all cell lines grown in all media. The results, with regard to cell lines, suggest that the two main aspects for successful membrane protein expression in *E. coli* are, first how well potential basal expression is suppressed and second how quickly expression takes place. All cell lines use the fast and powerful T7 expression system. However the cell line C41(DE3) features several mutations in its *lacUV5* promoter. These mutations reduce the expression efficiency of C41(DE3) cells to a level similar as those obtained with the wild type promoter (Wagner *et al.* 2007). Therefore C41(DE3) is protected by its low speed of protein synthesis, which gives the cell more time to translocate the nascent membrane proteins into the membrane. C41(DE3) yields the highest cell densities and the third highest fluorescence values. The two pLysS strains using the stringent control of basal expression by T7Lysozyme to their advantage, allowing them to reach a considerably high level of cell density before induction starts. Wagner *et al.* (2007) found that the effects of the mutations in the *lacUV5* promoter of the Walker strains (i.e. C41(DE3)) and the finely tuned dampening of T7RNAP activity by T7Lysozyme can lead to the same result of reducing recombinant mRNA levels. This is in accordance with the good results of the pLysS-strains in this study, which showed higher fluorescence values than C41(DE3). The absence of a stringent control of target basal expression levels could also explain, why the cell line BL21 Star (DE3) showed the lowest levels of cell growth and target expression of all cell lines tested. As all tested membrane proteins originate from *E. coli*, codon bias should not be an issue. It can only be speculated, if the presence of rare t-RNAs during transcription in Rosetta(DE3)pLysS does influence, or is even responsible for the superior membrane protein expression of this strain.

It was observed that growth and expression results differ widely between different media and cell lines. Although SB medium was optimal for cell growth only for C41(DE3) and BL21(DE3)pLysS strains, all cell lines expressed the most target protein

at 25 °C in SB medium. Growth in TB medium led to the highest cell density in BL21 Star (DE3) and Rosetta(DE3)pLysS and averaged over all cell lines, TB medium ranks second in cell growth, but last in protein expression at 25 °C. The cell growth in the commercial media TB and MM is less influenced by temperature, however, TB medium expresses less protein at 25 °C than LB medium and MM medium is only slightly better.

Future runs of the developed small-scale HTP expression screen will benefit from the results obtained. Parameters that did not show positive results could be exchanged. Therefore future screens could not employ the commercial media TB and MM or the cell line BL21 Star (DE3). Instead other media such as M9 minimal medium or self made TB medium could be tested. In regard to cell lines the second Walker strain C43(DE3), or newly available pLysS strains like C41(DE3)pLysS should be screened. The tested temperatures will be lowered further.

The small-scale HTP expression screen developed here, was described as part of the publication “A protocol for high throughput methods for the expression and purification of inner membrane proteins.” by McLuskey *et al.* (2008). The results obtained and trends identified will be published elsewhere.

Chapter 4

Purification of target membrane proteins

4.1 Introduction

The small-scale screen determined the optimal expression conditions for each target, in which they were subsequently overexpressed in 500 mL cultures. The cells were lysed and the membranes prepared according to the methods described in section 2.4.4.

Based on the construct design, a combination of the methods for solubilisation and purification described in chapter 2.4.5–9 was employed. Similar to the HTP approach for protein expression, the number of targets makes a compromise on the employed parameters in the purification protocol necessary. A purification pipeline (Fig. 4.1), therefore tries to employ the most successful parameters revealed from previous studies on membrane protein purifications (Privè 2007). The initial choice of detergent is very important. The purification scheme uses the detergent DDM, which is the most commonly employed detergent in purification of membrane proteins and the most successful in crystallisation trials (Privè 2007; Newstead *et al.* 2008). However, instability of any membrane protein solubilised in a PDC with DDM does not necessarily mean that a target cannot be purified and crystallised in a different detergent. Targets showing instability in DDM can be screened in different detergents, after the membrane proteins that were identified to be stable in DDM have been examined. Compromising by using only one detergent, makes the purification results comparable between targets and this can then be used to find stable targets that can be purified to monodispersity with a single purification pipeline in a relatively short time frame. Monodispersity is a key requirement for crystallisation.

As mentioned in section 2.2 the construct harbours, in its multiple cloning site, the DNA-sequence corresponding to the membrane protein of interest followed, by a linker sequence, the *gfp* sequence and a histidine tag at the C-terminus. The linker sequence contains a cleavage site for *Tobacco etch virus* protease (TEVP) (section 2.4.8). Therefore, the target protein can be cleaved from the GFP-reporter protein. A schematic of the purification pipeline is shown in Fig. 4.1. and all the purification steps are described in detail in the following sections.

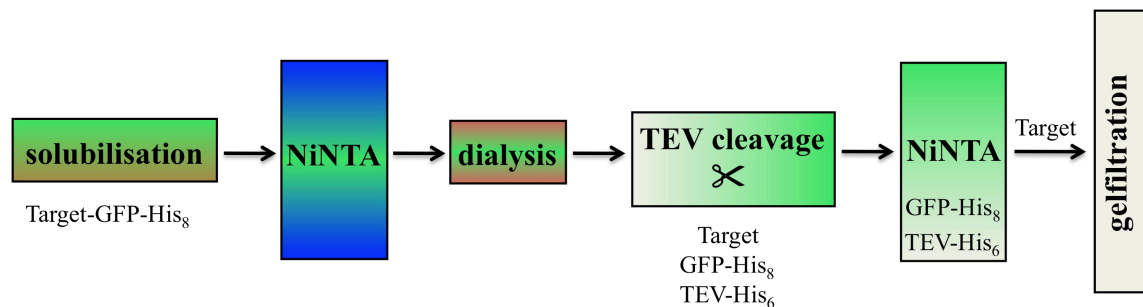


Figure 4.1: Scheme of the membrane protein purification pipeline used.

The solubilised target-GFP fusion binds with its histidine tag to the first affinity column. It can be eluted from the column with an imidazole step gradient. The imidazole is then removed by dialysis and the GFP-His₈ moiety is cleaved off the target by TEVP. The His-tagged proteins (GFP-His₈/TEVP-His₆) bind to the next NiNTA column, while the target is found in the flow through. The final purification step is size-exclusion chromatography.

4.2 Solubilisation

The purification starts with the solubilisation of the membrane proteins with the detergent DDM as shown in Fig. 1.8. The CSC of a detergent is very much dependent on the lipid content of the preparation, leading to different required detergent concentrations for successful solubilisation. It is possible to use the protein content of the membrane suspension as a surrogate of the difficult to determine lipid concentration (Privè 2007). A fast absorbance (A_{280}) measurement of the membrane suspension can estimate its protein content and can be used to calculate the required amount of detergent. This assumption for the lipid content is valid as long as the membranes are always from the same source and prepared according to the same protocol (Privè 2007). Therefore, following resuspension of the membranes in Buffer I, the protein content was estimated with an A_{280} measurement. The membrane suspension was diluted with Buffer I to the desired protein/lipid concentration, which was optimised as described below and the required amount of detergent, was added. The initial protocol aimed at a membrane suspension with an estimated protein concentration of 20 mg/mL. The solubilisation levels with different amounts of detergent were determined by SDS-PAGE. It was found that solubilisation with 1.5 % DDM is sufficient to solubilise all membrane proteins used in this study in a membrane suspension with a protein/lipid concentration of 40 mg/mL. This effectively reduces the amount of detergent required by a factor of two, as it was possible to use twice as much membrane suspension with the same amount of detergent. The membrane suspension was therefore diluted with Buffer I to a protein/lipid concentration of 40 mg/mL and 1.5 % DDM was added. The remaining unsolubilised membranes were removed by ultracentrifugation after 1 h of slow stirring at 4 °C. The target protein, now solubilised as PDC, remained in the supernatant, which was filtered and subjected to the first affinity chromatography column.

4.3 First NiNTA-column

The filtered supernatant contains all membrane proteins that could be solubilised with the detergent DDM. To purify the target, the solubilised proteins were applied onto a NiNTA-column, where the histidine tag of the fusion protein binds to the column. The detailed procedure for this is described in section 2.4.6. The column is washed to remove non-binding proteins and then subjected to a step gradient of imidazole. The first two elution steps with 50 and 100 mM imidazole concentrations remove the non-specifically bound proteins. Other proteins can bind weakly to the column, if they are for example naturally rich in histidines. The 100 mM step proved to be too high, as the target protein was partially eluted (Fig. 4.2 A). The peak fractions of the 50 and the 100 mM steps could be combined and the purification continued. Different gradient steps were tested and it was found that a step of 65 mM is sufficient for the removal of non-specific binding proteins. At an imidazole concentration of 65 mM, none of the targets in this study were partially eluted. Figure 4.2 displays an example of elution traces with 50/100 mM (A) and 65 mM imidazole (B) in the purification of the target ChbC.

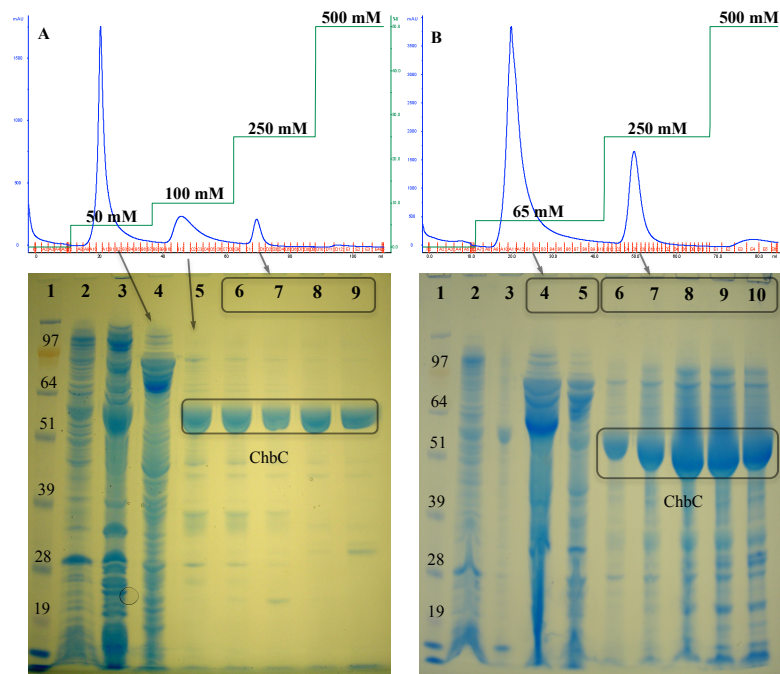


Figure 4.2: Optimisation of imidazole gradient for the elution of ChbC from the first affinity column. **(A)** Elution trace and gel with initial starting protocol (1.5 L of cell culture). Lanes 5–7 correspond to the fractions of the 100 mM imidazole peak and show that target protein is already eluted. Lanes 8–9 show the fractions from the main protein elution peak with a 250 mM imidazole step. **(B)** Elution trace and gel after optimisation of the imidazole gradient (2 L of cell culture). The gel shows that at 65 mM (lane 4–5) only small amounts of target protein is eluted. Lanes 6–10 show the fractions of the main protein peak eluted with a 250 mM imidazole step.

The target was eluted with a 250 mM imidazole step in 1 mL fractions. The fractions containing fusion-protein showed a green colour (Fig. 4.3). The protein content of the samples was checked by SDS-PAGE.

Large-scale preparations deriving from cell pellets of 3 L cell culture of the two targets XylH and PgpB lead to precipitation in the collection tubes due to concentration problems. This was eased with a higher fraction volume, but the sharp elution of the target proteins still lead to precipitation in most cases. Therefore, an amount of cell pellet harvested from a maximum of 2 L of cell culture was used for all subsequent protein preparations.

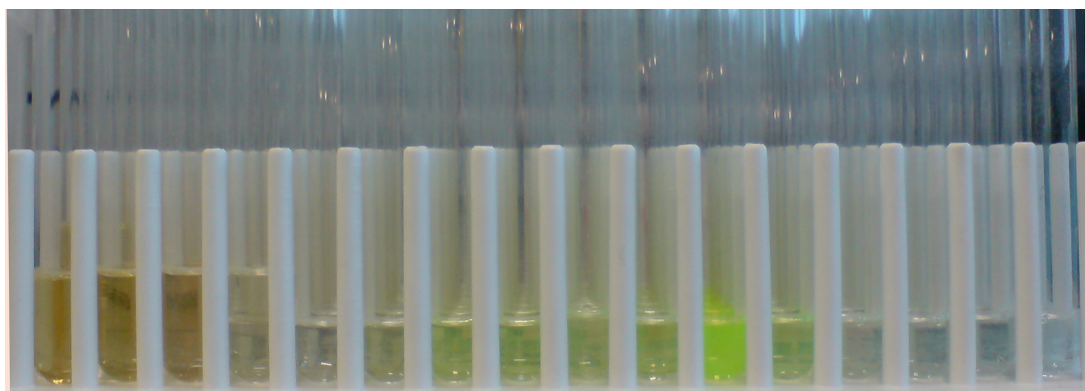


Figure 4.3: Example of collected fractions after the first affinity column. The first four fractions show the flow through with the unbound part of the sample, followed by the first imidazole step and the elution of non-specific binding proteins. The bright green fractions contain target protein eluted with 250 mM imidazole.

4.4 Dialysis

The fractions containing the target protein were pooled and dialysed overnight at 4 °C to remove excess imidazole (see section 2.4.7). This step was a good indicator for the stability of the membrane proteins in solution. Nearly all targets showed precipitation after dialysis. Depending on the stability of the targets to the TEVP cleavage, the dialysis requirements were optimised. In general, heavy precipitation in the dialysis step (4 °C) lead to complete precipitation of the membrane protein during the cleavage reaction (30 °C).

Small to medium losses could be avoided in the case of XylH by the use of desalting columns. The desalting columns were equilibrated with 25 mL of buffer A (see table 2.5). The target was applied in a 2.5 mL sample and the protein was eluted with 3.5 mL buffer A, while imidazole was retained on the column. However success with desalting columns proved to be target specific. In the case of the target PgpB, protein yields could not be improved. In either case, after dialysis or desalting column, precipitate was removed by centrifugation at 8000×g for 20 min before the supernatant was subjected to the cleavage reaction.

4.5 Cleavage with *Tobacco etch virus* protease

This step proved to be the major bottleneck in the purification protocol. The cleavage reaction at 30 °C for 1 h rigorously tested the thermal stability of the targets. The general trend throughout all purifications found, that if a target was already precipitating to some extent in previous steps, it would precipitate completely in the cleavage reaction.

In single cases, such as Lgt (see Fig. 4.4) the effect of temperature and duration was examined, but this only influenced the amount of precipitation to a small extent. Figure 4.4 is described in detail in the Lgt specific section 4.6.8.

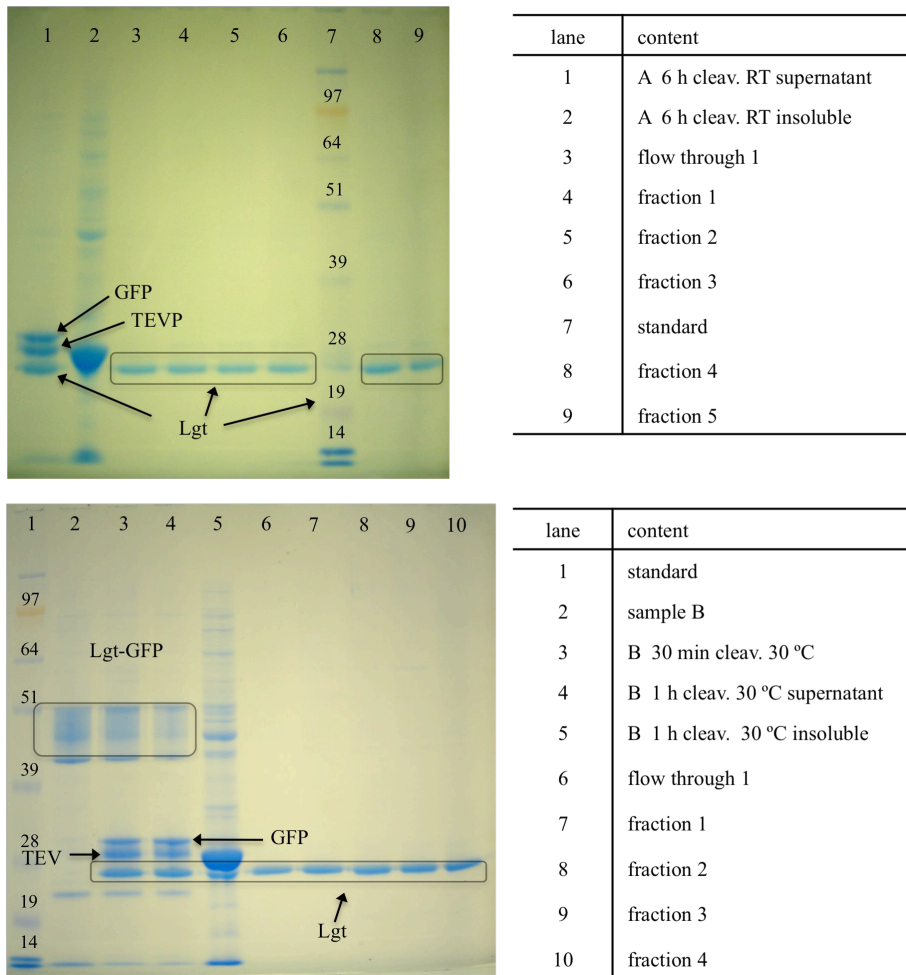


Figure 4.4: SDS-PAGES of samples from the TEVP cleavage of Lgt and from the following affinity column. Sample A of Lgt-GFP fusion was cleaved for 6 h at room temperature (RT) and a second sample B was cleaved for 1 h at 30 °C. Two gel samples were taken from B, one after 30 min and one after 1 h. The cleavage at RT for 6 h is complete, while in the cleavage reaction at 30°C still uncut fusion protein is detectable. See chapter 4.6.8 for details.

Due to the influence of detergents on TEVP performance (Mohanty *et al.* 2003; Lundbäck *et al.* 2008), the enzyme was used in a 1:1 molar ratio with respect to the target protein. The protease began to precipitate in increasing amounts after 30 min, possibly influencing target protein aggregation as well. The precipitation of TEVP could not be avoided by going to a lower temperature, as longer cleavage times were then required. Therefore the TEVP cleavage functioned on the one hand as a necessary step to remove the reporter-GFP and on the other as an important stability assessment for thermal and long-term stability of the target proteins.

Centrifugation at 8000×g for 20 min removed precipitated protease together with any aggregated target protein, and their samples were analysed by SDS-PAGE to assess the completion of the cleavage reaction. The supernatant now contained the untagged target membrane protein as well as GFP-His₈ and TEVP-His₆.

4.6 Second NiNTA-column

The cleavage products were subjected to a second affinity column. GFP-His₈ and TEVP-His₆ bind to the NiNTA-column, while the untagged target protein elutes in the flow through. The binding of GFP-His₈ to the column was clearly visible and a picture of such a column is displayed in Fig. 4.5. The his-tagged GFP and TEVP can be eluted by a 250 mM imidazole step and the column can be recovered.



Figure 4.5: Elution of green coloured GFP-His₈ from the second affinity column.

The advantage of the second affinity column lies in the possibility to separate the target protein from all proteins, that are still present in the sample solution, that bound to the first NiNTA-column. This is especially true for the notoriously problematic contamination with acriflavine resistance protein B (AcrB) (Veesler *et al.* 2008).

AcrB is an *E. coli* multidrug efflux pump that features a histidine rich cluster at its C-terminus that binds to NiNTA columns. AcrB has been shown to crystallise from preparations where it is present as a contaminant of less than 5 %. This makes it invisible on a standard SDS-PAGE or mass spectrometry and leads to false positives in crystallisation trials (Veesler *et al.* 2008). The contamination is often only detectable after X-ray diffraction data has been collected and processed.

All targets after this second NiNTA-column showed high purity on a SDS-gel and were submitted to crystallisation trials. Gel electrophoresis, however, does not give information about the monodispersity of the purified protein and a further purification step to improve and assess homogeneity is necessary.

4.7 Size-exclusion chromatography

Despite showing a high degree of purity after the second affinity column, no initial crystal hits were obtained with samples purified without a final gel filtration step. In gel electrophoresis the samples are denatured, through sample preparation and the influence of SDS and show a single band on the SDS-PAGE. However when size-exclusion chromatography is employed, it can emerge that for the same protein sample different PDCs exist in solution. The sample could contain a mixture of mono- and multimeric assemblies of membrane proteins or partially aggregated fractions. In any of these cases, the resulting gel filtration trace shows multiple elution peaks. Large aggregated fractions are identified through their elution in the void volume of the column, due to their high molecular weight. However in this study, large aggregates did not emerge in any protein preparations tested. All the membrane proteins used in this study eluted as PDCs shortly after the column void volume at 8 mL. The information gained from gel filtration traces is based on the shape of the peak that indicates the monodispersity of the sample. The main difficulty was that the trace of the eluted PDCs showed multiple peaks, which can be caused by various aggregation states. Finding the optimal detergent for the target membrane protein is the crucial step to achieve a high degree of monodispersity, necessary for crystallisation.

Until now, all targets were solubilised by DDM. Only in the case of Lgt and PgpB could monodispersity be achieved with DDM. The targets XylH, ChbC and YhbC needed on-column detergent exchange. This is in accordance with results of all membrane protein studies that achieved good diffracting crystals, in which for 50 % of all target a different detergent was used for solubilisation, purification and for crystallisation (McLuskey *et al.* 2008). Figure 4.6 shows the effects of successful detergent optimisation in the case of XylH. The detergent optimisation of single targets is then described in their specific sections.

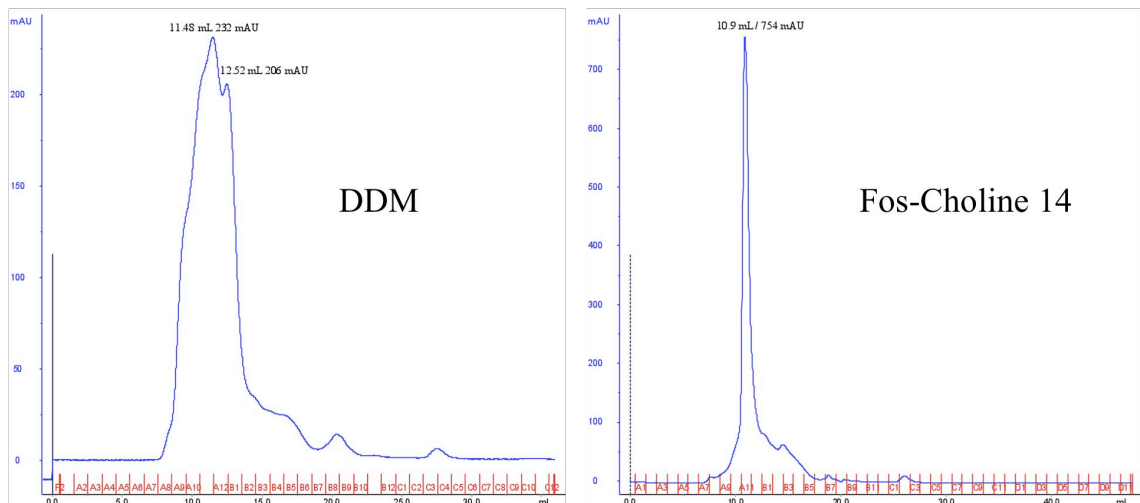


Figure 4.6: Effect of different detergents on the monodispersity of XylH in solution. The detergent DDM was exchanged to Fos-Choline 14 via a gel filtration column run.

The actual size-exclusion chromatography run was performed according to the protocol described in section 2.4.9. On-column detergent exchange was necessary if the gel filtration trace did not show monodispersity. The sample was again concentrated as before to a final volume of 100 μ L. The protein solution was then diluted with buffer A containing a different detergent, to a final volume of 500 μ L and applied onto the gel filtration column. The column was previously equilibrated with buffer A containing the new detergent. In the cases where on-column detergent exchange proved successful, the detergent was exchanged for all follow up preparations in the final gel filtration step.

4.8 Purification status of targets

The targets were taken through the purification pipeline in the order of the ranking derived from the scale-up expression results (Table 3.6). Therefore the target with the highest expression level entered the purification stage first. The following gives for each membrane protein, a short note about its function, physical properties and shows the relevant elution traces and gel pictures of each purification step.

All purification steps were verified and confirmed with SDS-PAGE gel electrophoresis. However the migration of membrane proteins in SDS-gels is specific to the target's structure and dependent on the amount of SDS that binds to the membrane protein. Cases have been reported in which the membrane protein migrates faster or slower than would be expected from its molecular weight (MW) and the causes are not fully understood (Rath *et al.* 2009). The majority of the targets of this study migrate faster than expected, leading to bands corresponding to lower apparent MW. However the comparison of gels before and after the cleavage helps to confirm the identity of the relevant bands of the target-GFP fusion and of the target alone.

4.8.1 XylE

XylE belongs to the major facilitator superfamily (MFS) of transporters and functions as a D-xylose/proton symporter. XylE is part of one of two systems in *E. coli* responsible for the uptake of D-xylose. The other system is the ABC transporter XylFGH, with XylH being also a target of this study (Davis and Henderson 1987; Griffith *et al.* 1992).

The membrane protein GFP-fusion has a MW of 83.1 kDa and XylE itself is, with 53.4 kDa and 12 transmembrane helices (Davis and Henderson 1987), the largest target in this study. Furthermore it was the best expressing target in both small-scale and medium-scale experiments, but sadly also the one with the largest amount of precipitation during purification. XylE was the first target to be purified. The cell pellet from 2 L of cell culture was lysed and the intensely green coloured membranes were prepared.

In the solubilisation step, DDM was added to the resuspended membranes in Buffer I, until the suspension clarified. The suspension was submitted to ultracentrifugation and the insoluble fraction obtained was not of green colour. The supernatant was applied to a NiNTA column. The elution trace in Fig. 4.7 of the first affinity column showed a major peak in the target elution gradient step of 250 mM imidazole.

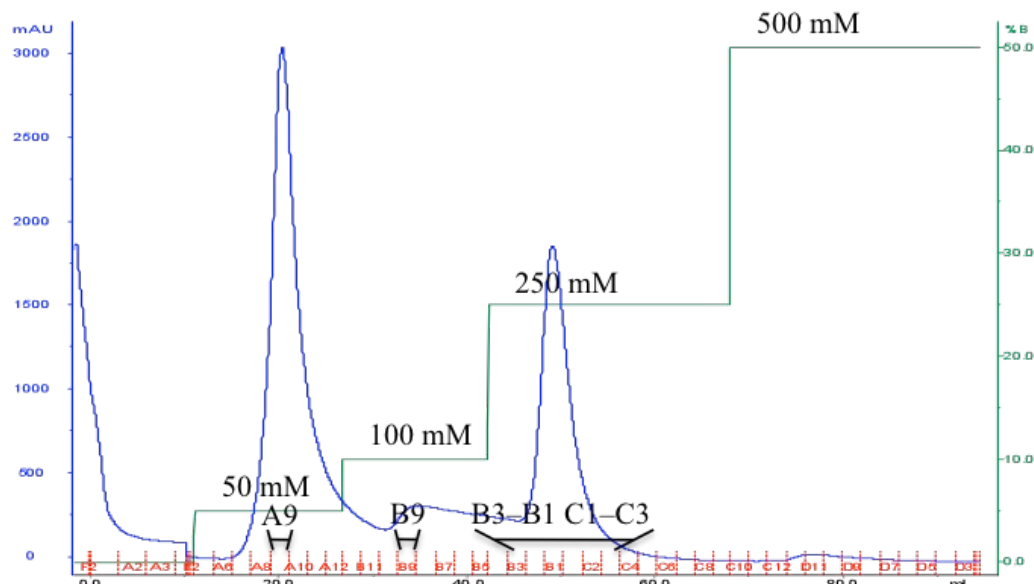


Figure 4.7: XylE-GFP fusion elution trace of the first affinity column. Employed imidazole concentration steps were 50, 100, 250, 500 mM. Membranes derived from 2 L of cell culture were used for the preparation.

The highlighted peak fractions in Fig. 4.7 were run on a SDS-PAGE, which is shown in Fig. 4.8. The 100 mM imidazole step already led to target elution, as the fractions had a green colour. However the quality of the gel in Fig. 4.8 is not sufficient to verify this finding.

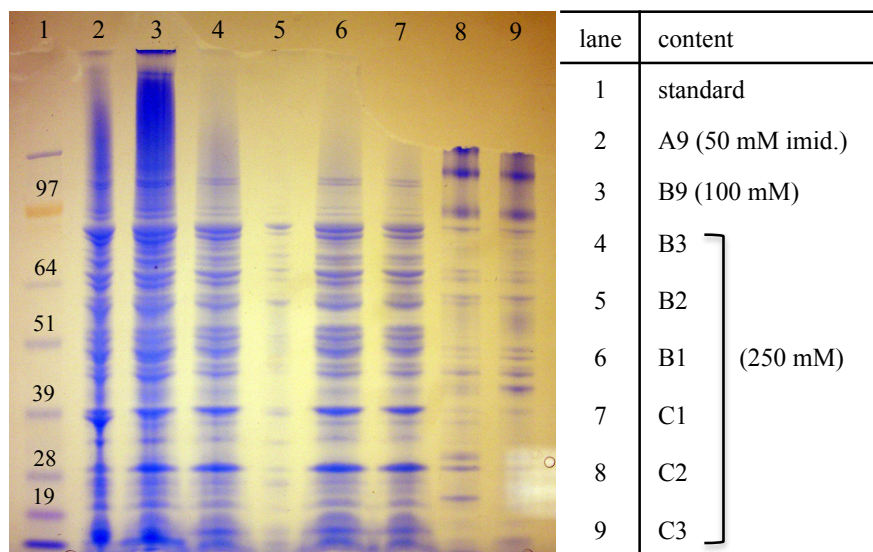


Figure 4.8: SDS-PAGE of first NiNTA column of Xyle purification. The GFP-fusion accounts for 83.1 kDa, but to link a specific band to the protein is not possible at this stage.

Xyle already started to precipitate in the fraction tubes after the first affinity column and the pooled, green coloured, fractions were centrifuged and the supernatant subjected to dialysis.



Figure 4.9: Precipitation of Xyle-GFP fusion in the pooled fractions from the first affinity column .The pooled fractions are shown before (left) and after (right) centrifugation.

More precipitation of the fusion protein was encountered in the dialysis and cleavage step. Gel samples from the supernatant (lane 6) and the insoluble fraction (lane 7) of the cleavage are shown on the SDS-PAGE in Fig. 4.10. A comparison shows that the cleavage was successful, as no high molecular weight bands are present in the supernatant. Lane 7 shows the amount of precipitation of XylE in the insoluble cleavage fraction. The supernatant was applied to the second affinity column but no bands corresponding to XylE could be detected in the first eleven fractions of the eluate from the column (not shown). Figure 4.10 shows fractions 12–15. In the last two fractions (lanes 9 and 10) the final elution of bound GFP and TEVP with 250 mM imidazole can be observed.

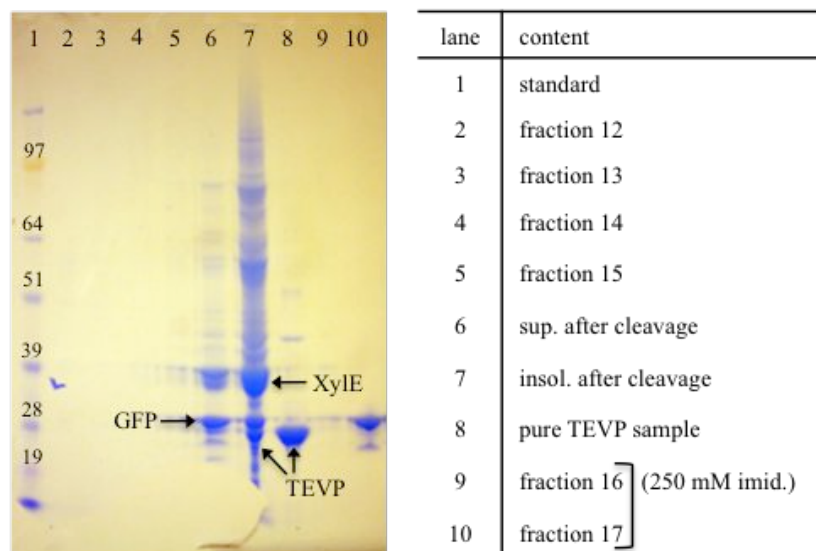


Figure 4.10: Samples from the second affinity column of XylE purification (lanes 2–5, 9–10). Lanes 6 and 7 show the cleavage fractions, while lanes 16 and 17 are from the elution of bound GFP and TEVP with 250 mM imidazole.

XylE was not considered as promising target due to the amount of precipitation and work on this target halted at this stage.

4.8.2 PgpB

The main function of phosphatidylglycerophosphatase B (PgpB) may be its diacylglycerol pyrophosphate (DGPP) phosphatase activity. DGPP plays an important role in phospholipid metabolism and cell signalling. Phosphatidate (PA), lyso-PA and phosphatidylglycerophosphate are reported to be other substrates of the enzyme. PA is a phospholipid intermediate used for the synthesis of phospholipids and triacylglycerols. PA regulates the activity of several lipid-dependent enzymes and is the source of signalling lipids, such as diacylglycerol (DG) and lyso-PA (Dillon *et al.* 1996). PgpB belongs to the PAP2 superfamily. It is reported to be located in both, the outer and the inner membrane with the phosphatase activity being higher in the cytoplasmic membrane, whereas PA and LPA activity is higher in the outer membrane (Icho 1988). PgpB features six transmembrane helices (Touze *et al.* 2008) and with a MW of 28.8 kDa it belongs to the “small” targets used in this study. PgpB ranks second in the scale-up expression and high amounts of protein could be observed in the elution trace (Fig. 4.11) of the first affinity column during its purification. The imidazole gradient employed was optimised to 65, 250 and 500 mM and no PgpB-GFP fusion can be found in fraction A12 on the corresponding SDS-PAGE shown in Fig. 4.12.

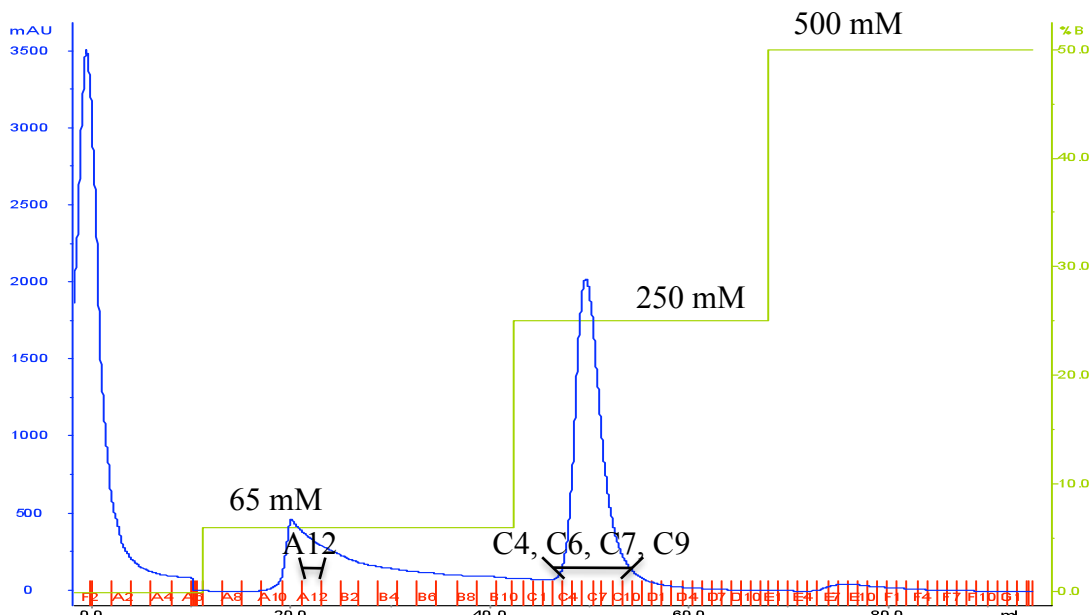


Figure 4.11: Elution trace of PgpB-GFP fusion from the first NiNTA column. The optimised imidazole gradient employed, comprised 65, 250 and 500 mM steps. The green fractions C5–C9 were pooled for further purification. Membranes from 2.5 L of initial cell culture were used for the preparation.

A SDS-PAGE (Fig. 4.12) of the fractions C4, C6, C7 and C9 confirmed the presence of PgpB-GFP in the green fractions of the first affinity column. These were pooled and dialysed overnight. The PgpB-GFP fusion migrates slightly faster than its actual size of 58.6 kDa and appears with an intense band at a corresponding size of 51 kDa in the gel of Fig. 4.12.

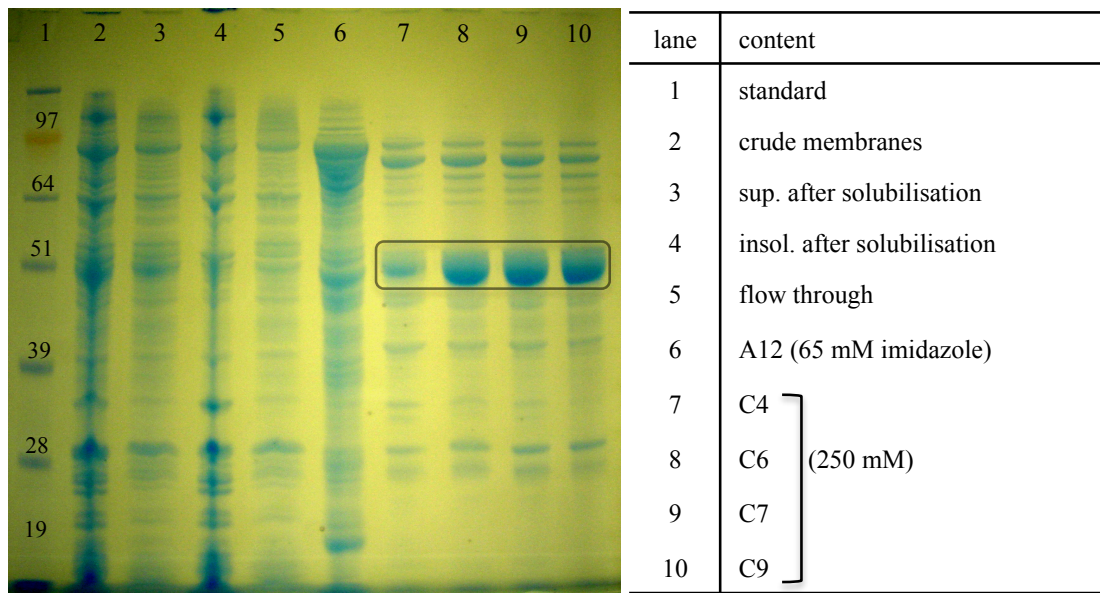


Figure 4.12: SDS-PAGE of samples from the PgpB-GFP fusion elution trace of Fig. 4.11. An intense band for the PgpB-GFP fusion (58.6 kDa) can be observed in the range of 51 kDa. The fractions corresponding to the framed samples were pooled for further purification.

The protein fusion showed only minor precipitation losses after dialysis, which could not be improved through the use of desalting columns. However PgpB proved to be thermally stable during the TEVP cleavage and no precipitation of the protein occurred. The gel in Fig. 4.13 shows in lane 2 a sample of the supernatant after cleavage, indicating the completion of the cleavage, as no PgpB-GFP fusion band is observed. The fractions of the second affinity column (lanes 3–8) show a band on the gel in the size range of PgpB at 28 kDa, and the highlighted fractions were pooled and subjected to gel filtration.

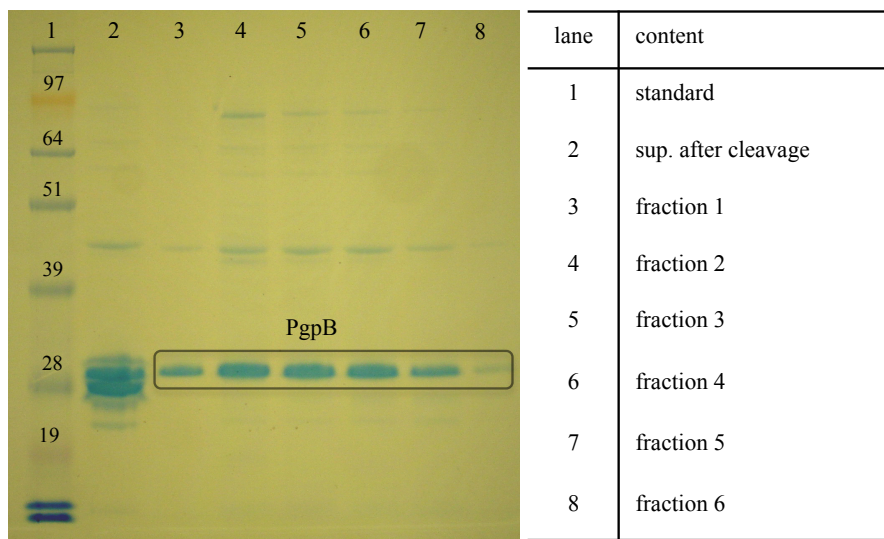


Figure 4.13: SDS-PAGE of samples from the cleavage and the second affinity column in PgpB purification. Lane 2 shows the completeness of the cleavage reaction as no band for the GFP-fusion can be observed. Fractions 1–6 in the highlighted lanes (3–8) contain PgpB as a band can be detected in the size range of PgpB at 28.8 kDa.

PgpB eluted from the gel filtration column in a single peak in 0.04 % DDM (Fig. 4.14) and no further detergent optimisation was undertaken.

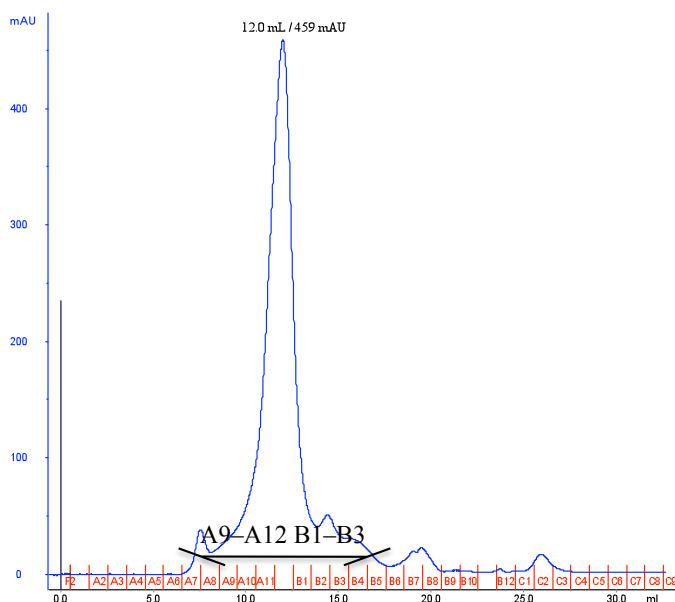


Figure 4.14: Gel filtration trace of PgpB in DDM. The peak fractions (A9–B3) were analysed with a SDS-PAGE in Fig. 4.15. PgpB eluted from the column in a single peak.

The gel samples from the peak fraction (A9–B3) of the elution trace show a high degree of purity on the gel in Fig. 4.15. Lane 2 shows the applied sample and the purest fractions A11 and A12 (lane 5 and 6), which were pooled and subjected to crystallisation trials.

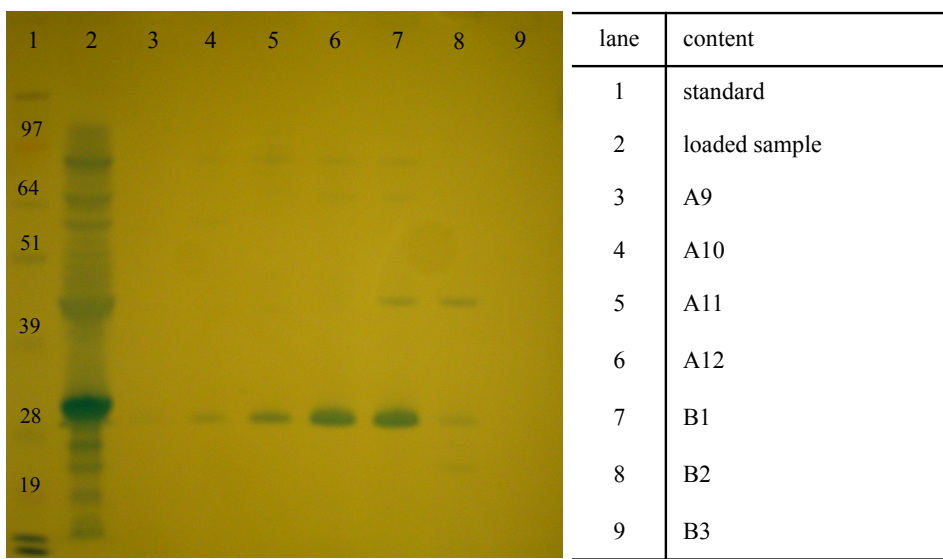


Figure 4.15: Gel of the final purification samples from PgpB. Lane 2 shows the concentrated sample that was applied to the gel filtration column. The purest samples in lanes 5 and 6, fractions A11 and A12 respectively, were pooled for crystallisation trials.

The overall yield after purification was 0.4 mg derived from 1 L of initial cell culture.

The purified PgpB sample was submitted for mass spectrometry peptide sequencing to *The Sequencing Service* (School of Life Sciences, University of Dundee). The sample fragmentation was analysed following trypsin digest and the identity of the protein was confirmed to be PgpB. The results of the peptide sequencing can be found in the appendix (7.2.1).

4.8.3 CcmC

The target CcmC is the integral membrane component of the CcmABC protoheme IX ABC transporter and involved in heme transfer for cytochrome c-maturation. It contains six transmembrane helices (Schulz *et al.* 1999; Ahuja and Thony-Meyer 2003). CcmC consists of 245 amino acids contributing to a size of 27.7 kDa. The GFP-fusion has a size of 57.5 kDa. Figure 4.16 displays the elution profile from the first NiNTA column with this protein. The imidazole gradient employed featured 50, 75, 100 and 250 mM steps. The highlighted fractions of each protein peak were analysed on a gel.

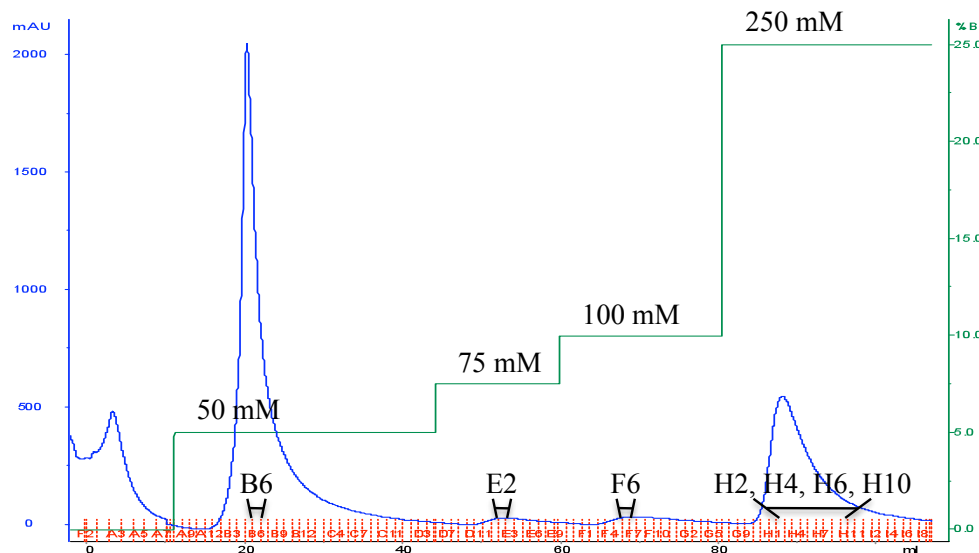


Figure 4.16: Elution trace of CcmC-GFP fusion from the first NiNTA-column. Gradient steps are 50, 75, 100 and 250 mM imidazole. Non-specific binding proteins are successfully removed in the first gradient step of 50 mM. Preparation based on membranes from 1.5 L cell culture.

The corresponding SDS-PAGE shows in Fig. 4.17 an enhanced protein band emerging at a size slightly lower than 51 kDa for the fractions in lanes 7–8, which is supposed to be the CcmC-GFP fusion protein. CcmC binds stronger to the affinity column than the previous targets as no band for the target can be observed in the fractions E2 and F6 from the 75 and 100 mM imidazole steps. Lane 2 shows the sample that was applied to the first NiNTA column after solubilisation and lane 3 the insoluble fractions after solubilisation. In Lane 4 there is a sample of the non-specific binding proteins that were removed in the first peak of Fig. 4.16 with 50 mM imidazole. The last four lanes show every second fraction collected from the peak elution of the CcmC-GFP fusion, eluted with 250 mM imidazole.

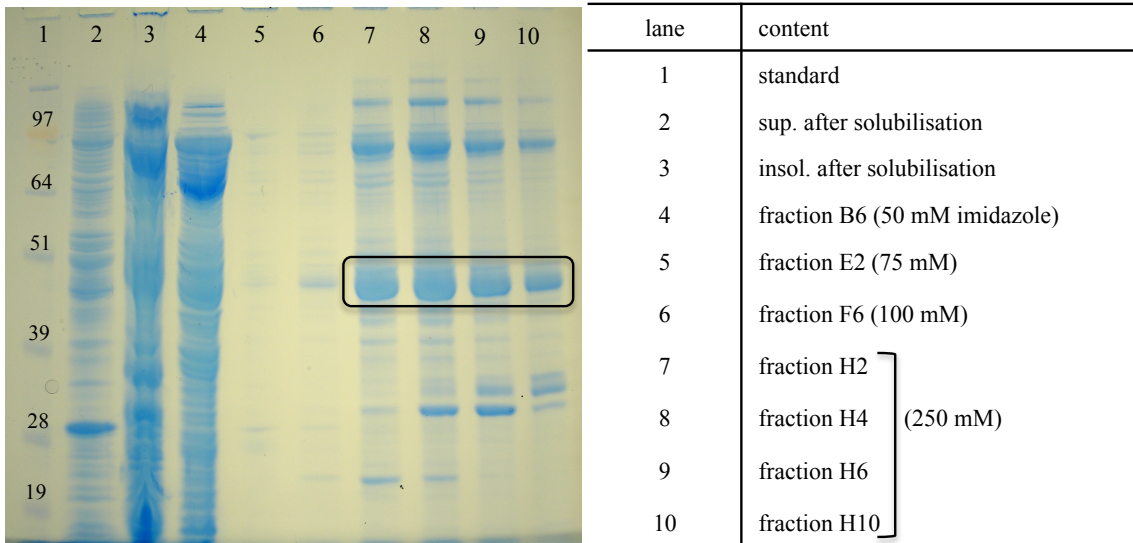


Figure 4.17: SDS-PAGE of purification samples from CcmC-GFP starting with solubilisation samples from the supernatant and the insoluble fraction followed by the samples from fractions from the NiNTA-trace of Fig. 4.16.

Substantial precipitation losses occurred in the dialysis step. More protein precipitated in the TEVP-cleavage and led to the elution of insufficient amounts of protein from the second affinity column, to continue purification. The SDS-PAGE of Fig. 4.18 shows the differences in gel bands after dialysis (lane 2) and after cleavage (lane 3). The cleavage reaction is nearly complete as the band for the GFP-fusion disappears almost completely. However, in the supernatant after cleavage (lane 3) only bands for GFP-His₈ and TEVP-His₆ can be observed leading to the conclusion that CcmC precipitated in the cleavage reaction. This is in accordance with the results from the samples collected from the flow through of the second affinity column (lanes 4–9), which show no bands on the gel corresponding to CcmC (27.7 kDa).

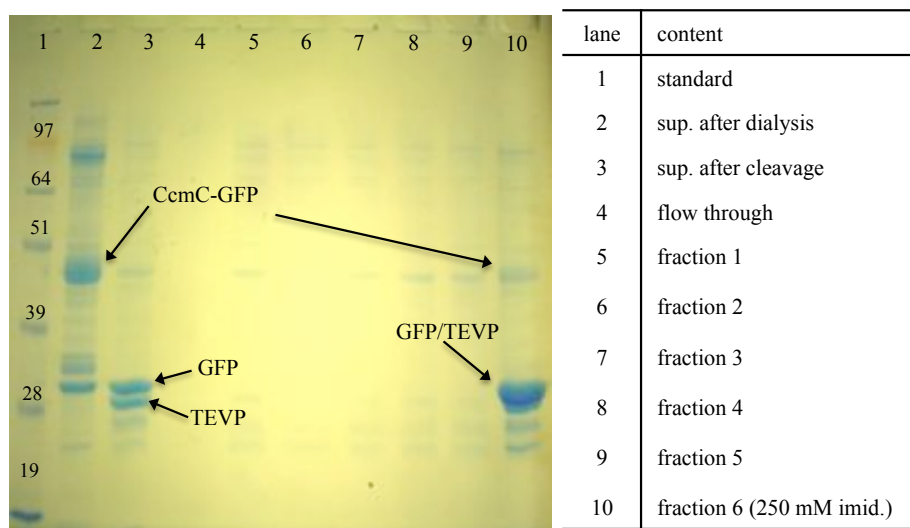


Figure 4.18: SDS-PAGE of CcmC-GFP fusion samples, collected after dialysis, cleavage (soluble fraction) and after second NiNTA column (fractions 1–6).

Lane 10 corresponds to the sample of bound GFP-His₈ (28 kDa) and TEV-P-His₆ (27 kDa), which were eluted with 250 mM imidazole. It also shows a third band at higher molecular weight, probably due to a small amount of still uncleaved fusion protein.

Work on CcmC was halted at this stage.

4.8.4 YdhC

Sequence similarity suggests that YdhC is involved in drug efflux. YdhC is an uncharacterised member of the major facilitator superfamily (Marger and Saier Jr 1993). It contains ten transmembrane helices and has a size of 43.2 kDa. It ranked in both expression rankings in the middle of the field and the elution trace in Fig. 4.19 indicates good protein yield. The imidazole gradient employed contained four steps 50, 75, 250 and 500 mM. The magnified peak fractions were analysed on a SDS-PAGE, which is shown in Fig. 4.20.

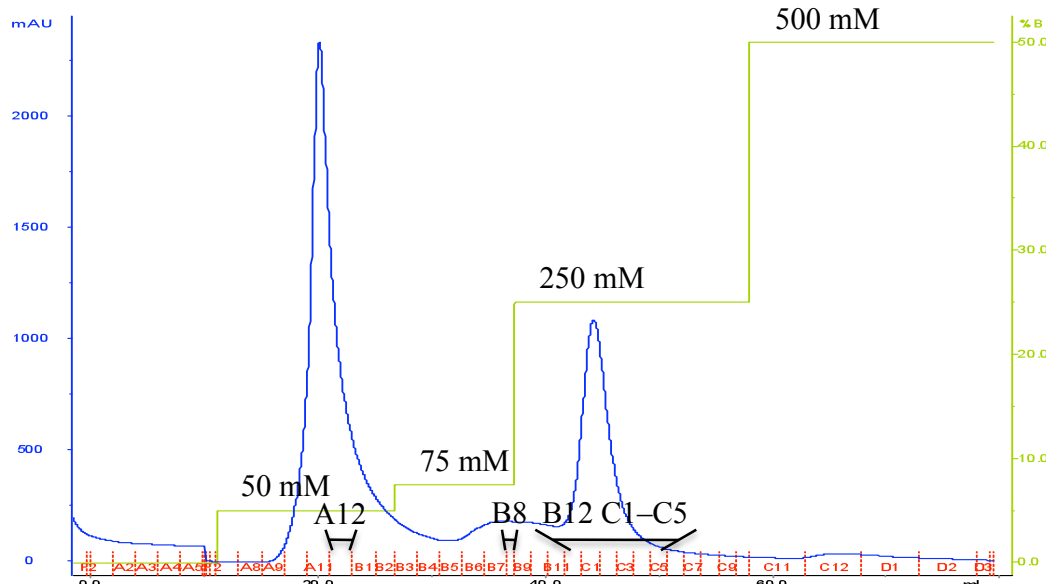


Figure 4.19: Elution trace of YdhC-GFP fusion from the first NiNTA-column with a 50, 75, 250 and 500 mM imidazole step gradient. The target was partially eluted at 75 mM imidazole. The main fraction was eluted at 250 mM. Preparation based on membranes derived of 1.5 L of cell culture.

YdhC-GFP fusion was partially eluted in the 75 mM imidazole step (fraction B8) and optimisation of the gradient was necessary. The gel shows an intense double band for the green coloured peak fractions (B12–C5) in the range of 51 kDa (highlighted bands).

This band disappears after cleavage, as a comparison of lanes 2 and 4 of the gel in Fig. 4.21 shows. All target protein containing fractions (B8–C5) were pooled and subjected to dialysis.

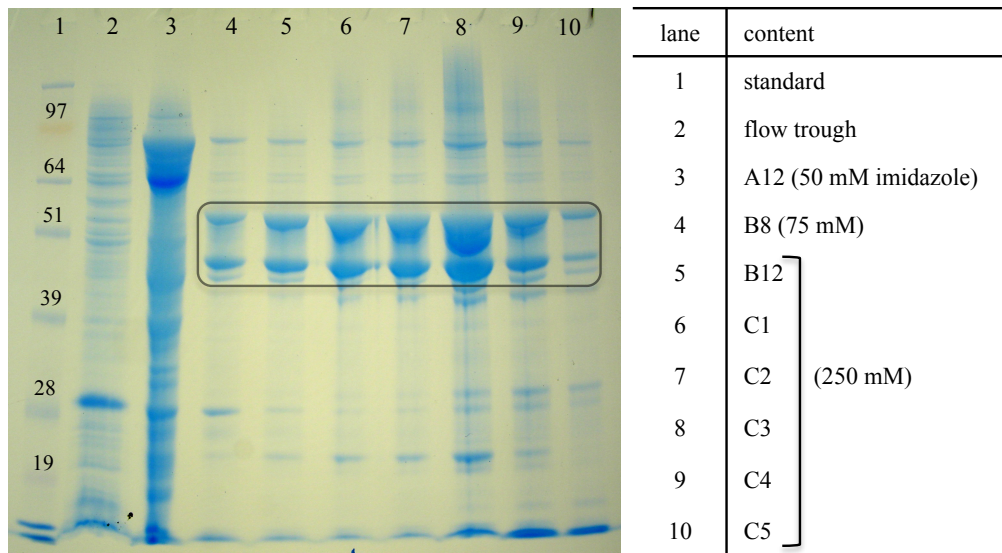


Figure 4.20: SDS-PAGE of fractions of the first affinity column of YdhC-GFP fusion purification. Partially elution of target protein occurs at 75 mM imidazole (fraction B8) as a comparison with the main elution peak in lanes 5–10 with 250 mM imidazole shows.

Precipitation losses occurred during dialysis. The gel sample of the supernatant and the insoluble fraction after dialysis (lane 2 and 3 Fig. 4.21) clearly show the extent of lost YdhC-GFP fusion protein.

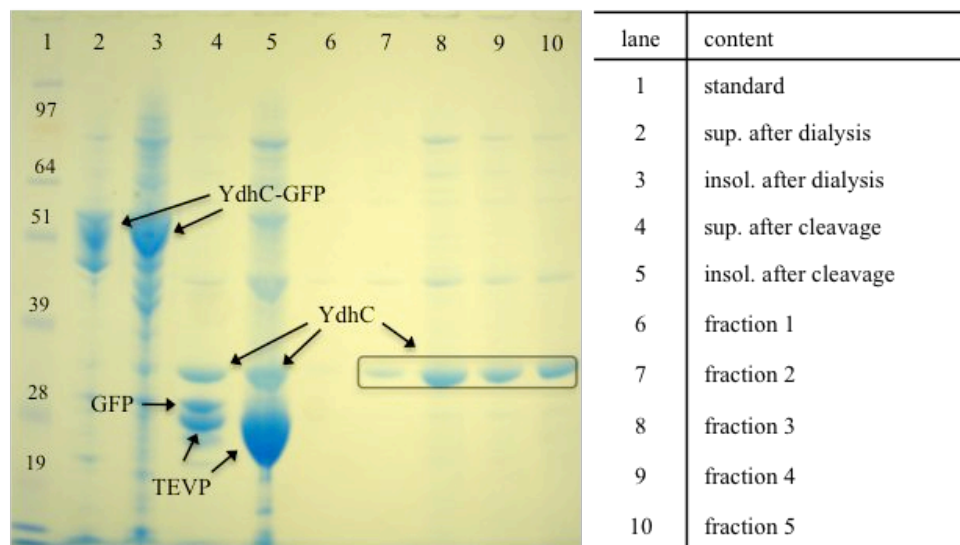


Figure 4.21: SDS-Page of samples taken from dialysis, cleavage and second affinity column in the second part of the YdhC purification. The losses endured in the dialysis and cleavage steps are visible in the insoluble fractions of both steps (lane 3 and 5). The fractions from the second affinity column show the cleaved target protein YdhC.

Although lane 4 indicates that the cleavage reaction was complete, lane 5 shows that a substantial amount of YdhC precipitated together with uncut fusion protein. However, the samples from the second affinity column in fractions 3–5 contained YdhC and were pooled and applied to a gel filtration column which was equilibrated in buffer containing 0.03 % Fos-Choline 14. The gel filtration trace obtained (see Fig. 4.22) features a single elution peak indicating the homogeneity of the sample.

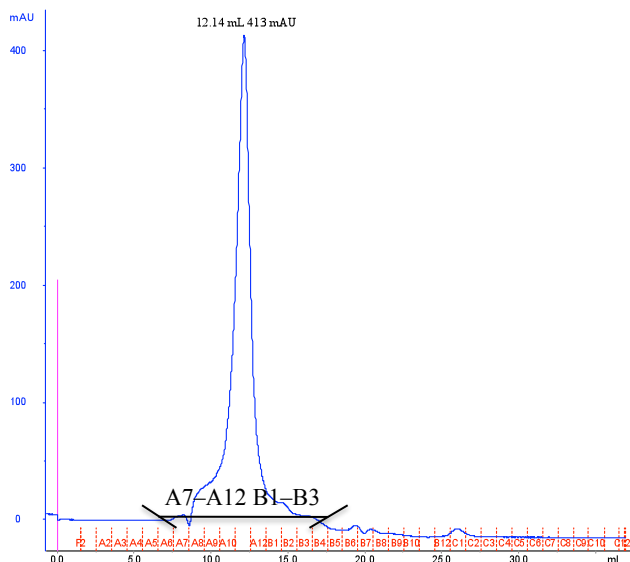


Figure 4.22: Gel filtration trace of YdhC in Fos-Choline 14. YdhC elutes from the column in a single peak. The fractions A7 to A12 and B1 to B3 were analysed on a gel, which is shown in Fig. 4.23.

The samples from the gel filtration fractions (A7–B3) show a reasonable degree of purity in the gel (Fig. 4.23) and the fractions A11 and A12 (lanes 6 and 7) were pooled for crystallisation trials.

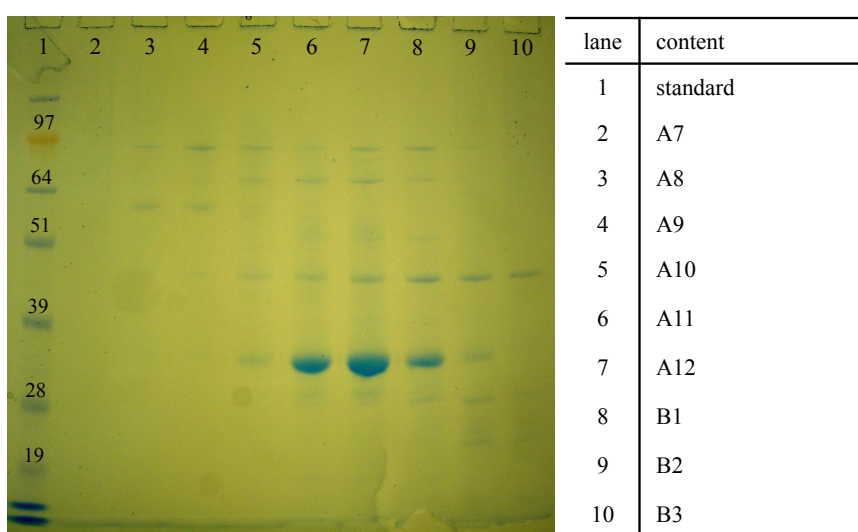


Figure 4.23: SDS-PAGE of samples from the gel filtration run with YdhC. Fractions A11 and A12 (lanes 6 and 7) were pooled and subjected to crystallisation trials.

The target YdhC was only purified once due to the time constraints of this study, but a yield of 0.4 mg from 1 L of initial cell culture was obtained. Follow up purifications should focus on the optimisation of the initial imidazole gradient and on minimising precipitation losses in the dialysis step through the use of desalting columns. Furthermore, temperature and duration of the TEVP cleavage could be tried to improve stability. Likewise for all other targets, if no initial crystal hits were obtained, more detergents should be screened.

4.8.5 CodB

CodB (43.6 kDa) belongs to the nucleobase cation symporter-1 (NCS-1) family. It is a putative cytosine/proton symporter and features 12 transmembrane helices (Danielsen *et al.* 1992; Danielsen *et al.* 1995). The first affinity column with this target protein employed an imidazole step gradient of 50, 70, 250 and 500 mM and the resulting elution trace is displayed in Fig. 4.24. Samples from the solubilisation were analysed together with the magnified fractions from the main peaks of the affinity column by gel electrophoresis and the gel obtained is shown in Fig. 4.25.

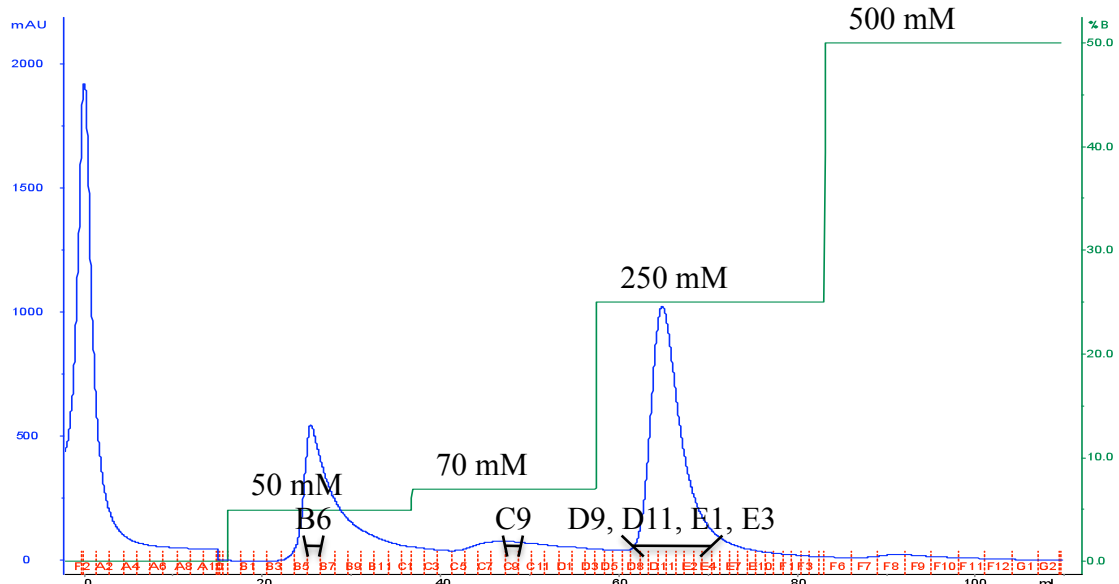


Figure 4.24: Elution trace of CodB-GFP fusion from the first affinity column. Cell pellet from 1.5 L of cell culture was used for this preparation. An imidazole step gradient of 50, 70, 250 and 500 mM was employed. The target eluted partially with 75 mM imidazole but the main fraction is eluted with 250 mM.

Samples from the fractions B6 (50 mM) and C9 (70 mM imidazole) reveal that the target has already been eluted, to a considerable amount, at low imidazole concentrations. Similar to the target YdhC, no sharp band can be observed for the GFP-fusion (73.2 kDa), but a double band in the region of 51 kDa is seen.

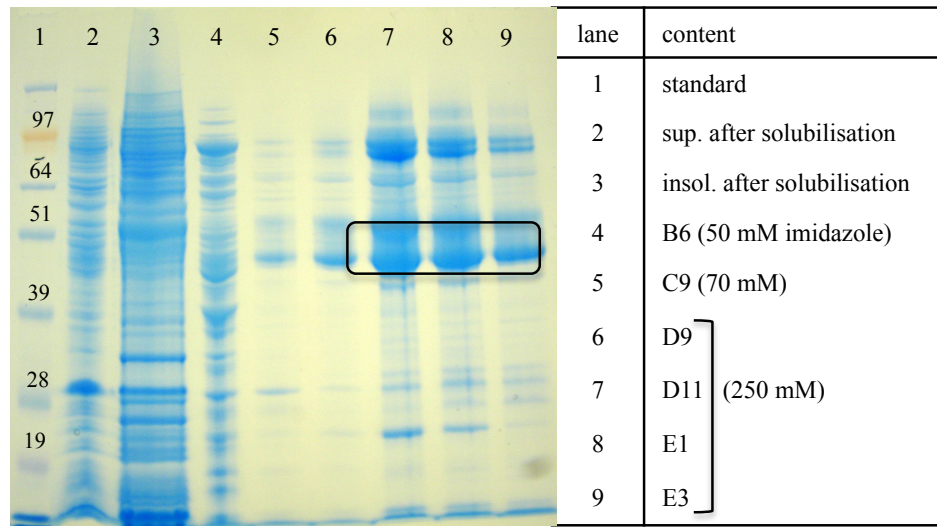


Figure 4.25: SDS-PAGE from samples of the first part of the CodB purification and from the peak fractions of the first affinity column. The highlighted bands are supposed to be CodB-GFP fusion protein. Lanes 2 and 3 show the samples of the soluble fraction after solubilisation and the insoluble fraction.

In the second part of the purification, substantial loss of protein in both the dialysis step and the cleavage step occurred. A comparison of soluble and insoluble fractions after centrifugation of both purification steps, followed by the first fractions of the second affinity column, are displayed in the SDS-PAGE in Fig. 4.26.

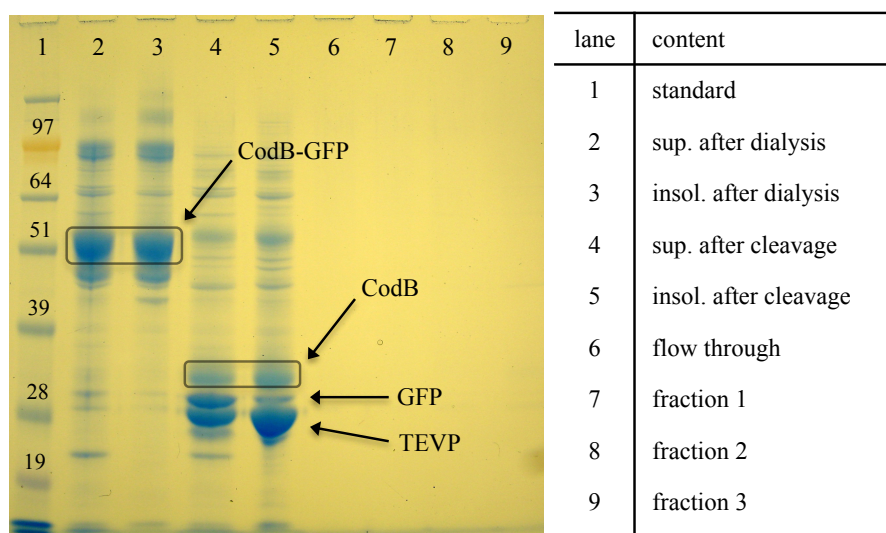


Figure 4.26: SDS-PAGE of samples from the second purification part of CodB. Lane 2 and 3 makes an estimation of losses after the dialysis step possible, while the same can be done for the cleavage fractions represented in lanes 4 and 5. Lanes 6–9 show the first three fractions of the second affinity column.

A comparison of the gel samples from the soluble and insoluble fraction from the dialysis step (lanes 2 and 3) visualises the amount of precipitated protein. The remaining CodB-GFP fusion was subjected to TEVP cleavage. The corresponding band for the fusion protein disappears in lanes 4 and 5 indicating that the cleavage was successful and the high thermal stability of CodB-GFP fusion. However the insoluble fraction after centrifugation of the cleavage products shows, that CodB alone is not stable and precipitates in high amounts.

Figure 4.27 shows very weak bands for CodB (lanes 1 and 3–8) in the SDS-PAGE samples from the second NiNTA-column. Imidazole at a concentration of 250 mM was used for the elution of GFP-His₈ and TEVP-His₆ from the column and is starting to show effects from lane 8 onwards. However Fig. 4.27 shows that CodB is not purified to a high degree at this stage and yields are very low.

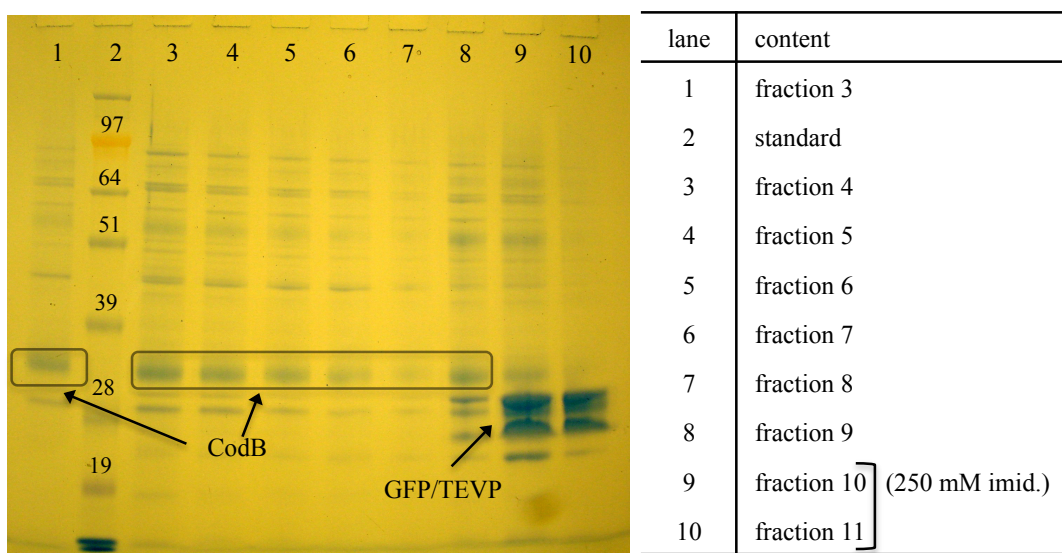


Figure 4.27: SDS-PAGE of samples from the fractions 3–11, eluted from the second affinity column during CodB purification. The last three fractions were eluted by a 250 mM imidazole step gradient.

An additional purification step in the form of ion exchange chromatography was added but led to the complete precipitation of the target. As a result of this, due to the losses in the dialysis and cleavage steps, CodB was classified as unstable and work stopped at this point.

4.8.6 ChbC

ChbC is classified as a *N,N'*-diacetylchitobiose permease. It is the membrane component of ChbABC, which belongs to the superfamily of the phosphoenol pyruvate (PEP)-dependent sugar transporting phosphotransferase system (PTS) (Keyhani and Roseman 1997). Like the targets described later in this study, XylH and YdeD, ChbC features ten transmembrane helices and is, with a mass of 48.2 kDa, the largest of these three targets. It expressed in the screens (rank 5 and 6) better than XylH and YdeD. An optimised imidazole gradient of 65, 250 and 500 mM was used for the first affinity column. The elution trace in Fig. 4.28 shows a single peak corresponding to the elution of high amounts of the ChbC-GFP fusion (77.9 kDa) in the 250 mM imidazole step.

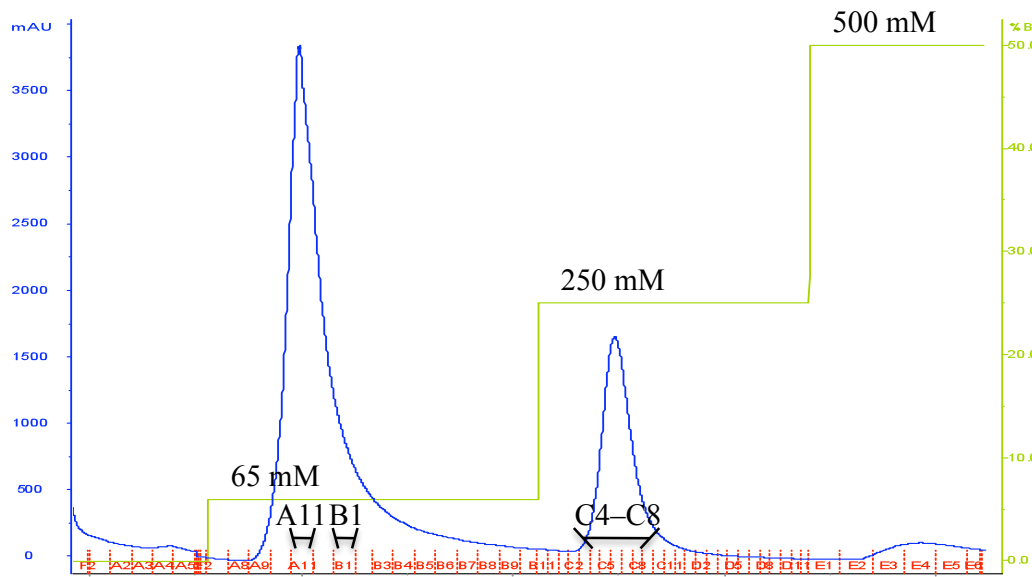


Figure 4.28: First affinity column trace of ChbC. Preparation based on membranes from 2 L of cell culture. The imidazole gradient encompassed the steps 65, 250 and 500 mM. All highlighted fractions were analysed by gel electrophoresis. The green coloured fractions C4–C8 were pooled for further purification.

The samples from fractions of the solubilisation step and the corresponding samples of the peak fractions of the first affinity column are displayed in the SDS-PAGE of Fig. 4.29. The highlighted bands mark the large amount of ChbC-GFP fusion in the green coloured fractions C4–C8. These fractions were pooled and dialysed overnight.

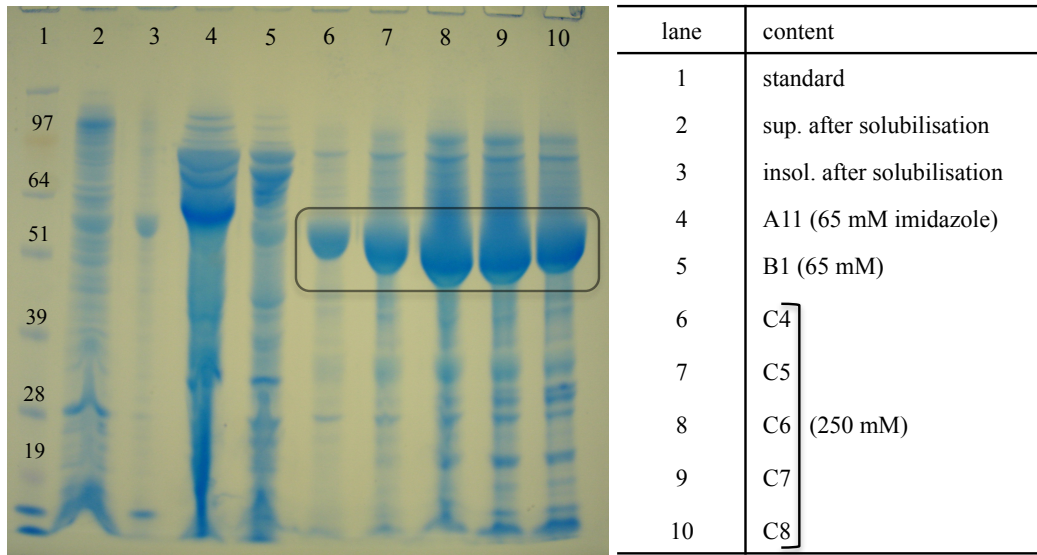


Figure 4.29: SDS-PAGE of solubilisation samples and fractions from the first affinity column of ChbC. The fractions correspond with the trace displayed in Fig. 4.38. An intense band in the size range of the ChbC-GFP fusion is observed in the green coloured fractions C4–C8 (lane 6–8).

The ChbC-GFP fusion did not precipitate in the dialysis step and only small amounts of aggregation were detected in the following TEVP cleavage. However samples from the cleavage reaction show that a large amount of the fusion protein was not successfully cleaved and the band for ChbC-GFP is clearly detectable in lane 2 of the gel in Fig. 4.30.

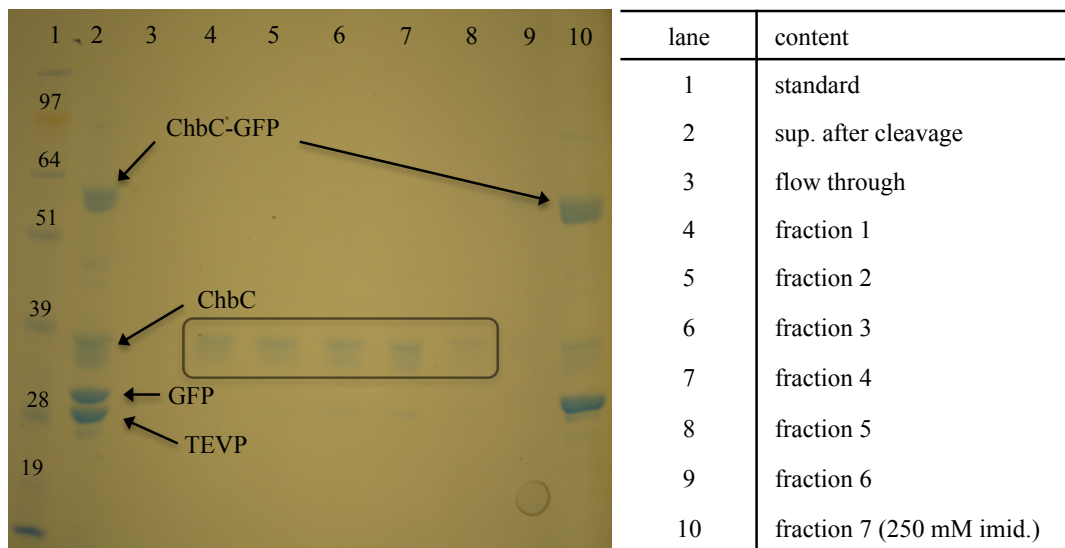


Figure 4.30: SDS-PAGE of ChbC samples from the supernatant of the cleavage and fractions from the second affinity column. Lane 2 indicates incomplete cleavage of the fusion, leading to its detection also in fraction 7. Here it is eluted together with the histidine tagged GFP and TEVP from the affinity column with 250 mM imidazole. ChbC is found in the fractions 1–5 and a frame highlights the bands.

The uncleaved fusion still features a histidine tag and therefore binds to the second column. It elutes together with the histidine tagged GFP and TEVP in the 250 mM imidazole step (lane 10). ChbC does not bind to the affinity column and is detected in fractions 1–8, which were pooled for further purification by size-exclusion chromatography.

The first gel filtration run of ChbC in DDM lead to the elution trace displayed in (A) of Fig. 4.31 on the following page, indicating a low degree of monodispersity of the sample. On-column detergent exchange to the previously successful Fos-Choline 14 did not improve the elution properties of ChbC (B). Finally with a new preparation the exchange from DDM to Cymal-5 (0.3 %) improved monodispersity. (C) shows the resulting elution trace of ChbC in Cymal-5 together with the resulting SDS-PAGE of the applied sample and the peak fractions. The purest fractions (A10 and A11) were pooled for crystallisation trials. The final protein yield for ChbC was 0.9 mg per litre of cell culture.

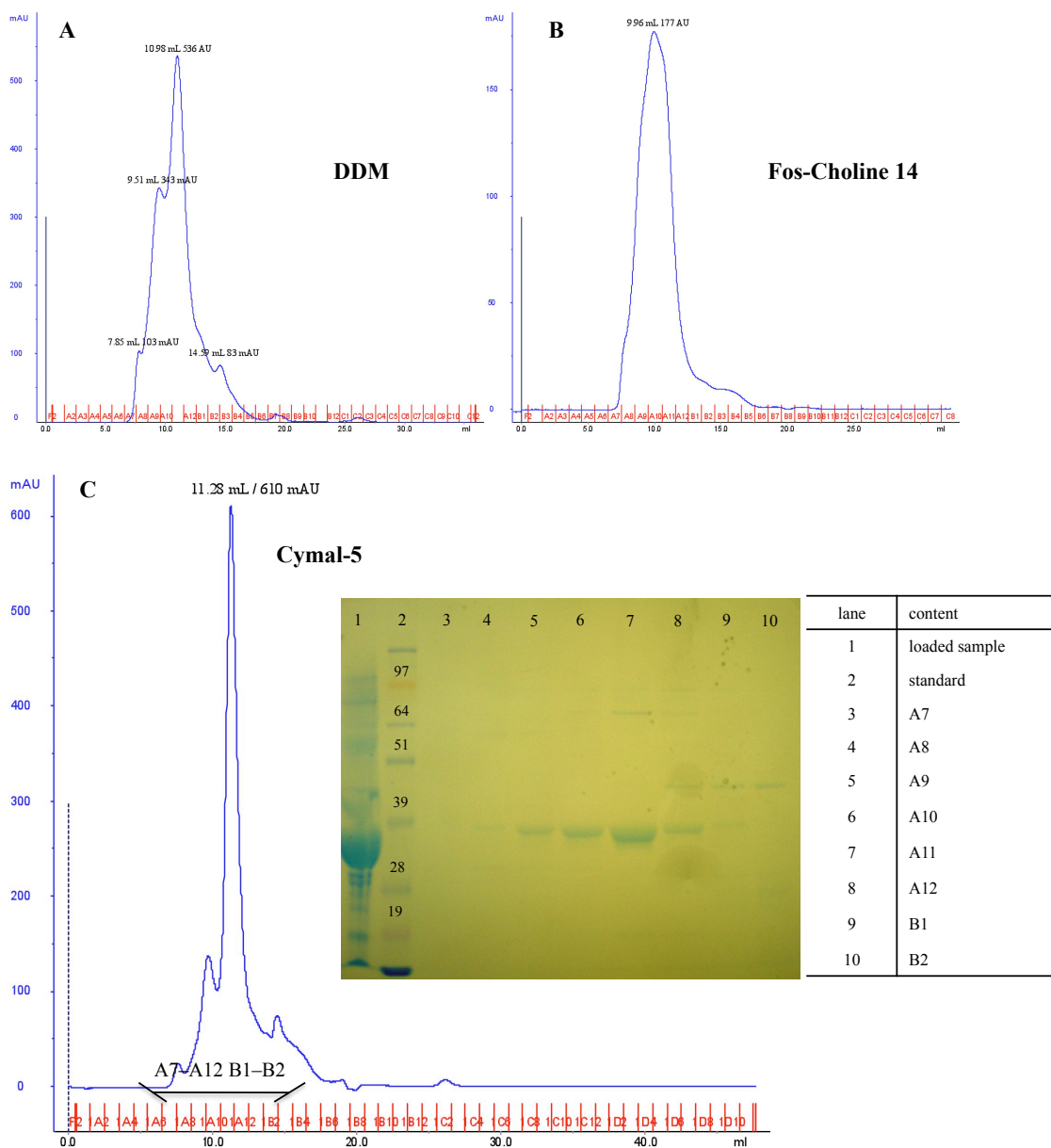


Figure 4.31: On-column detergent optimisation for ChbC. Multiple or broad peaks for the detergents DDM and Fos-Choline 14 are indicating low monodispersity of the sample. Monodispersity was improved with the employment of the detergent Cymal-5 and the samples of the peak fractions shown in the SDS-PAGE (lane 6 and 7) were pooled for crystallisation trials.

4.8.7 PnuC

PnuC is a member of the nicotinamide mononucleotide (NMN) uptake permease family. The function of PnuC in *E. coli* is not well defined, but due to its sequence homology with PnuC of *Salmonella typhimurium* it was suggested to be an integral membrane protein and essential for the NMN transport across the cytoplasmic membrane (Foster *et al.* 1990; Zhu *et al.* 1991).

PnuC features six transmembrane helices and has a MW of 27 kDa while the PnuC-GFP fusion protein has a MW of 56.5 kDa. Solubilisation yields of PnuC were low and the corresponding elution peak of the first affinity column was comparably small (Fig. 4.32).

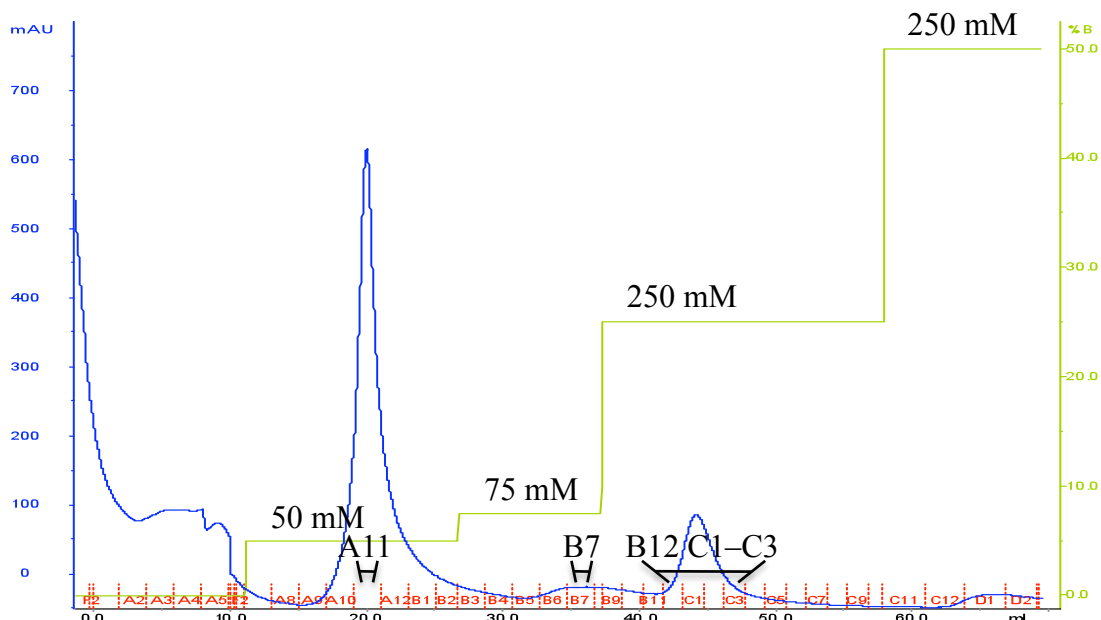


Figure 4.32: Elution trace of PnuC from the first affinity column. The used imidazole step gradient encompassed steps of 50, 75, 250 and 500 mM. Yield of PnuC was very low compared to other target preparations. The membranes used for this preparation were derived from 1.5 L of cell culture.

Samples from the highlighted peak fractions from the elution trace gave only weak bands on the gel shown in Fig. 4.33. The band in lane 5 shows that PnuC-GFP fusion was already partially eluted from the column with an imidazole concentration of 75 mM imidazole. The light green coloured fractions C1 and C2 were pooled and dialysed overnight.

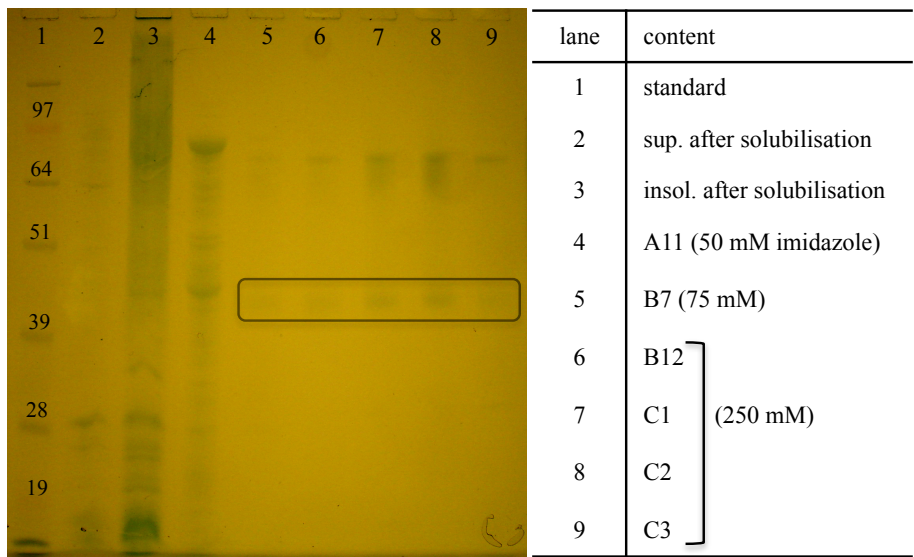


Figure 4.33: SDS-PAGE of samples from PnuC solubilisation and from the peak fractions from the first NiNTA-column. Very weak bands in a range of 45 kDa could correspond to the PnuC-GFP fusion.

Large amounts of protein precipitated in the dialysis step. A band resembling the PnuC-GFP fusion protein was observed in the insoluble dialysis fraction (Fig. 4.34). The remaining protein aggregated during TEVP cleavage and the gel in Fig. 4.34 shows that no protein could be detected after the second affinity column. PnuC was identified as unstable and no further work was carried out on this target.

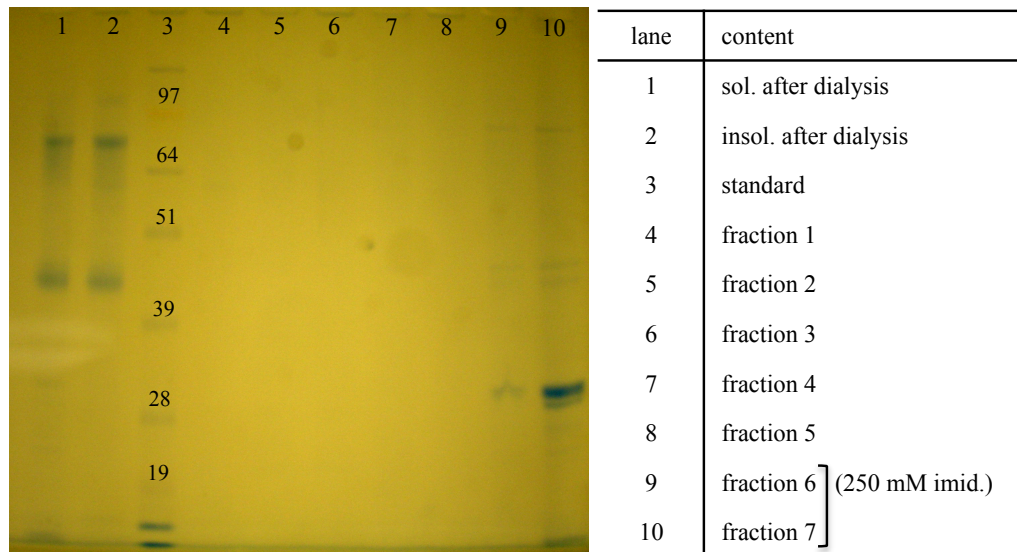


Figure 4.34: SDS-PAGE of samples from the dialysis fractions of PnuC (soluble/insoluble) and from the following NiNTA-column. Lane 9 and 10 show the obtained bands for the elution with 250 mM imidazole and most likely belong to GFP or TEVP. PnuC is untagged after the cleavage and should appear in the flow through (fractions 1–6).

4.8.8 Lgt

The first step of lipoprotein biosynthesis in gram-negative bacteria is catalysed by prolipoprotein diacylglycerol transferase (Lgt). Lgt utilises membrane lipids as substrates and transfers a diacylglycerol moiety onto a highly conserved cysteine in the signal peptide sequence (lipobox) of the prolipoproteins. Homologues of Lgt exist in gram-positive bacteria and their pathogenesis and cell cycle is highly influenced by surface lipoproteins (Hutchings *et al.* 2009).

Lgt (33 kDa) showed stability throughout the purification pipeline with only small losses after dialysis and TEVP cleavage. The imidazole step gradient of the first NiNTA column lead in the 100 mM step to partial elution of Lgt-GFP fusion (Fig. 4.35, B6). This is confirmed by the gel samples of the highlighted peak fractions in the SDS-PAGE shown in Fig. 4.36.

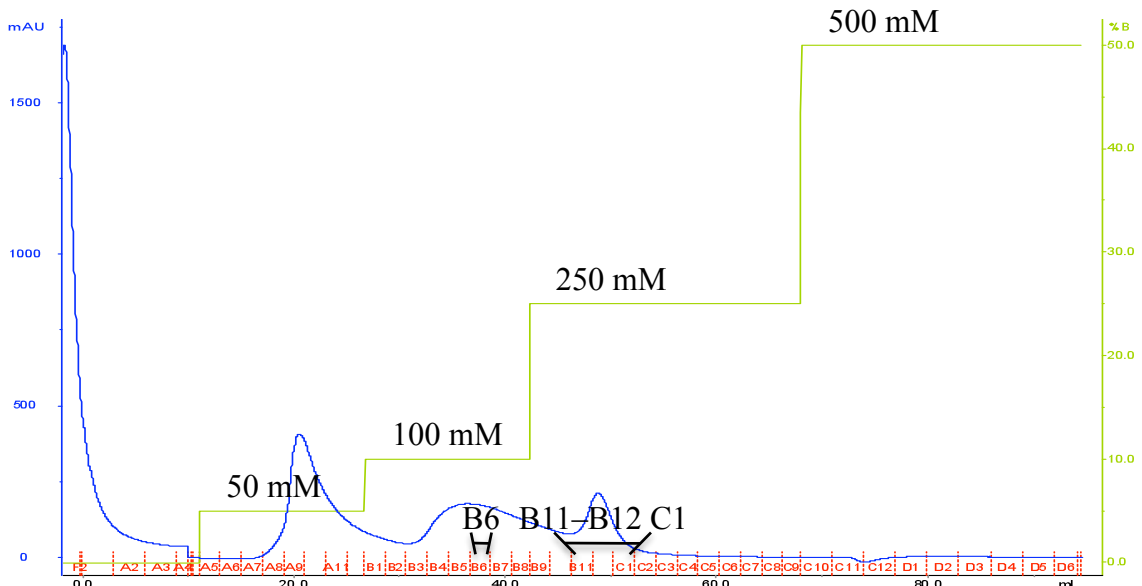


Figure 4.35: Elution trace of Lgt from first affinity column. Membranes derived from 1 L of cell culture were used in this preparation. The imidazole gradient employed was 50, 100, 250 and 500 mM. The target elutes already in the 100 mM imidazole step. Fractions B4–B7 were pooled and treated as sample A. Fractions B11, B12 and C1 were pooled to sample B.

The gel in Fig. 4.36 shows samples from the crude membranes, the solubilisation fractions and the fractions from the first NiNTA column. The difference of intensity in the bands between the soluble and insoluble solubilisation fractions (lane 4 and 5) demonstrates the successful solubilisation of the target out of the membrane.

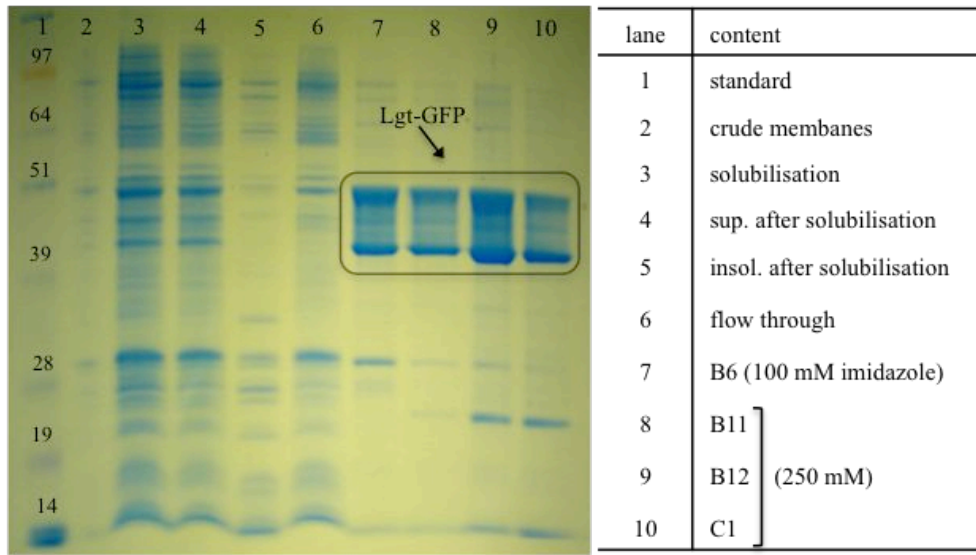


Figure 4.36: SDS-PAGE of first purification steps of Lgt, including samples from crude membranes, solubilisation and from the fractions of the main peaks of the first NiNTA column.

The target protein containing fractions were pooled (around B6 and C1) (Fig. 4.35) and treated as independent samples A and B.

The two samples A and B were, following dialysis, subjected to different cleavage conditions. Sample A was incubated with TEVP for 6 h at room temperature (RT), while sample B was incubated at 30 °C for 1 h. Samples A and B were then passed through a second affinity column and samples for a SDS-gel were collected. The gels in Fig. 4.37 show the results of the cleavage and the second affinity column, which give information about the cleavage completion and the impact on protein stability. A comparison of the samples from the cleavage supernatant and the insoluble fraction show that precipitation levels were low in both cleavage reactions, but sample A was completed. Cleavage products of sample B still contain uncleaved fusion protein.

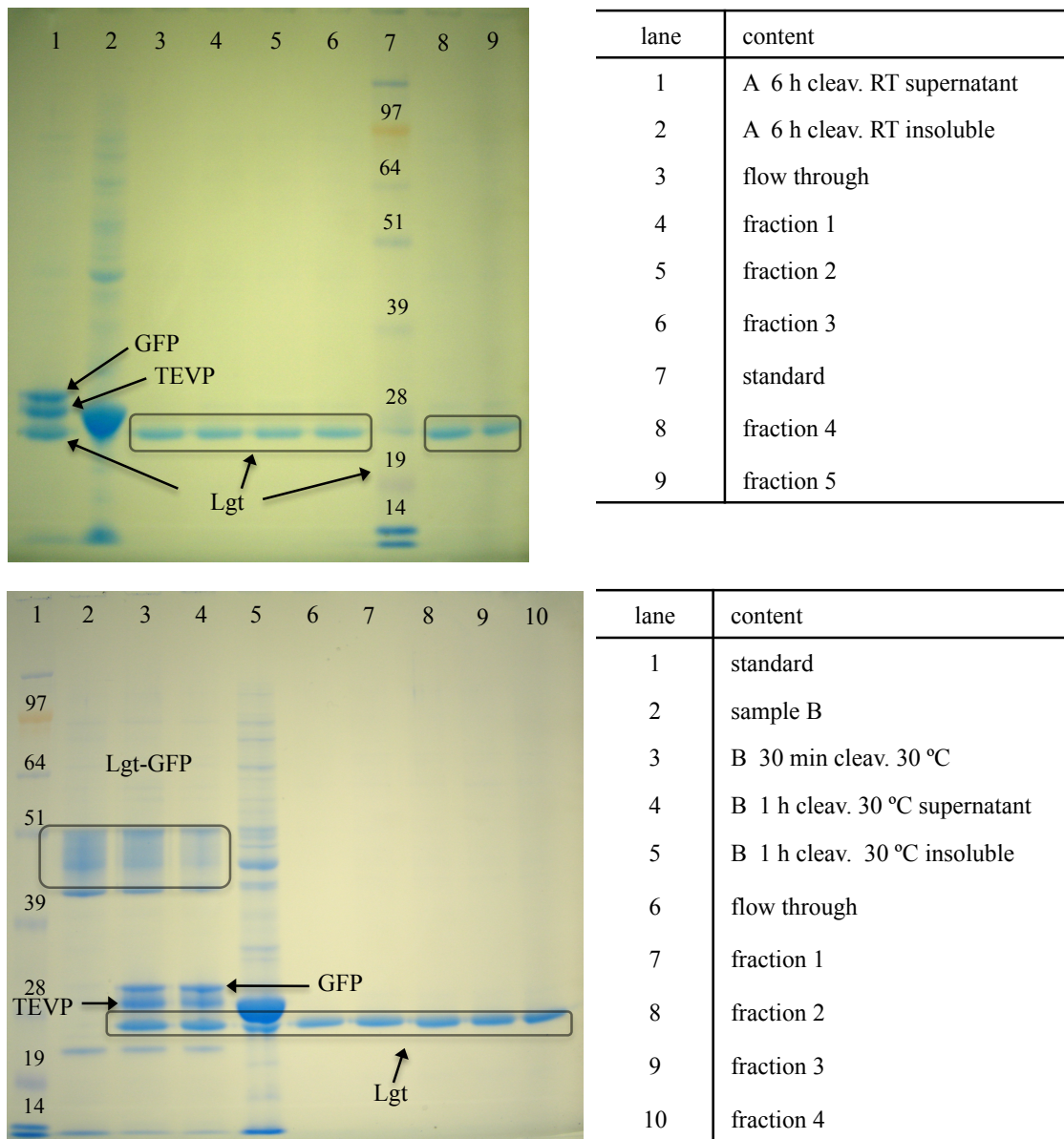


Figure 4.37: Gels of samples from the cleavage test for Lgt and from the following affinity column. The top gel shows the results of the 6 h room temperature (RT) cleavage of sample A. The lower gel displays the cleavage of sample B for 30 min respectively one hour at 30 °C. Cleavage of sample A is complete and precipitation levels were low in both samples A and B.

The gel samples from the second affinity columns showed a high degree of purity and the fractions from both columns were pooled and concentrated. The overall yield at this purification level from 1 L of cell culture was 0.85 mg. Four crystallisation screens were set up and are described in section 5.2. However, as none of the screens yielded initial crystal hits, a size-exclusion chromatography step was added to the purification protocol of Lgt in the following preparation.

The optimisation of the imidazole gradient was based on the common finding with the previous targets, that an imidazole step of 65 mM is sufficient for the removal of non-specifically bound proteins. The optimised gradient in the first purification step gave a better elution trace (Fig. 4.38). The non-specific binding proteins were now eluted in a 65 mM imidazole step, followed by target elution with 250 mM imidazole buffer. The yield, judged on the height of the 250 mM peak, is compared to other targets low, especially as this preparation used membranes from 2.5 L of cell culture.

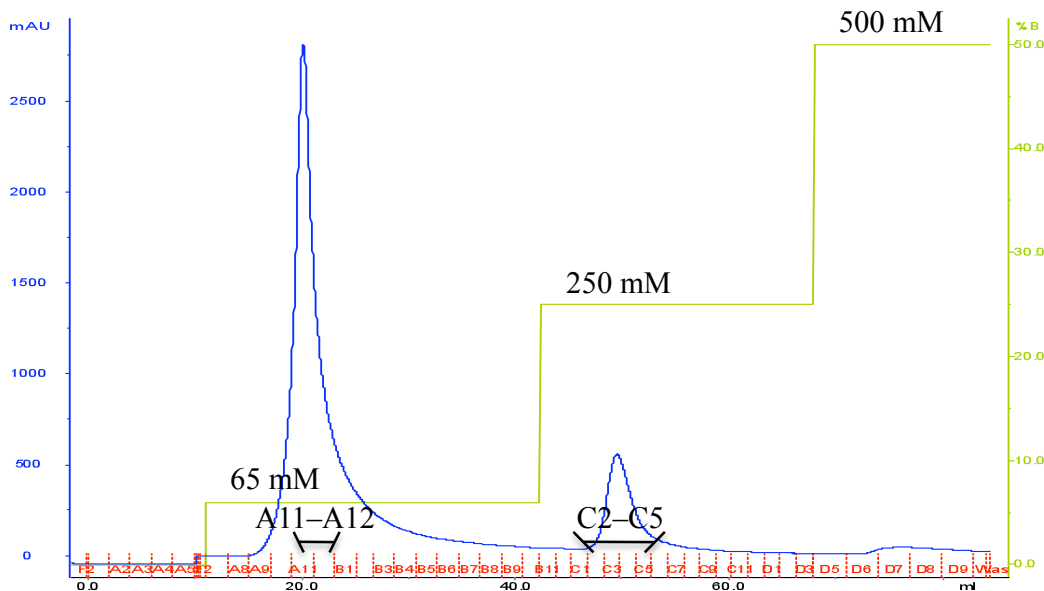


Figure 4.38: Elution trace from Lgt, obtained with optimised imidazole gradient of 65 mM, 250 mM and 500 mM. This preparation used membranes prepared from 2.5 L of cell culture. Fractions A10–B1 contained unspecific binding proteins followed by the green coloured fractions C3–C5.

Samples of the peak fractions from the first affinity column were analysed on a gel (Fig. 4.39) and they show that the Lgt-GFP fusion elutes in a single peak in the fractions C3–C5.

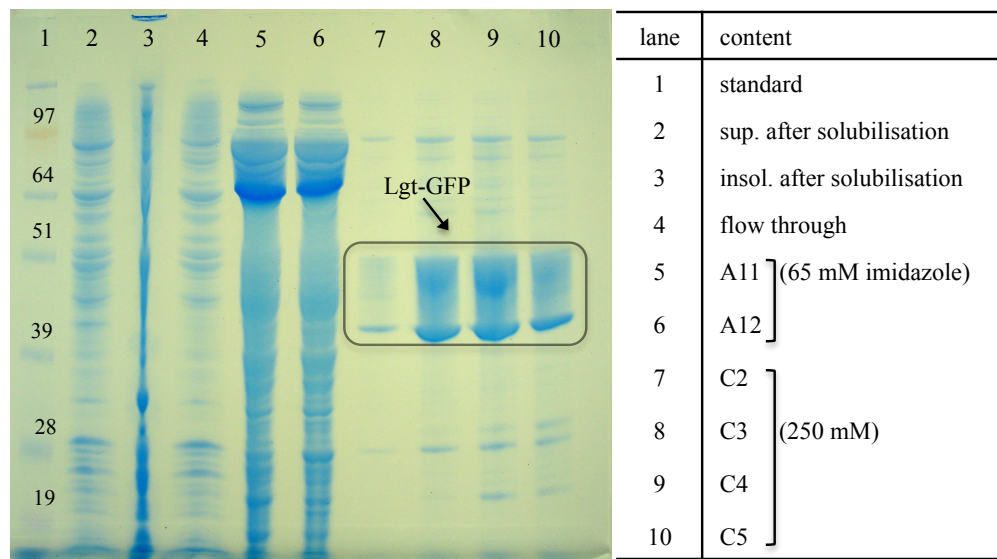


Figure 4.39: SDS-PAGE of samples from the solubilisation of Lgt and from peak fractions from the first optimised affinity column (trace Fig. 4.38) during purification of Lgt. Fractions C3–C5 were pooled.

The fractions C3–C5 were pooled and subjected to dialysis and TEVP-cleavage. The samples from the second affinity column showed the same high level of purity as observed before in Fig. 4.37. The degree of monodispersity of the protein sample was estimated by size-exclusion chromatography on a gel filtration column. The single peak in the gel filtration trace of Lgt (Fig. 4.40) indicates monodispersity of the protein sample.

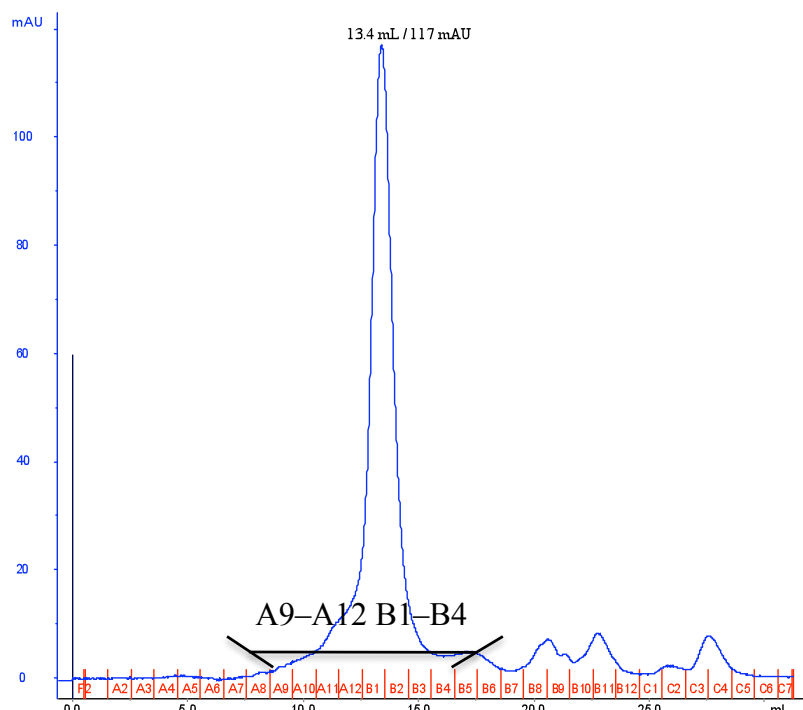


Figure 4.40: Gel filtration trace of Lgt in DDM. Lgt elutes in a single peak and the purity of the highlighted peak fractions were analysed on a SDS-PAGE shown in Fig. 4.41.

The protein containing fractions were identified via SDS-PAGE analysis. The gel in Fig. 4.41 shows a reasonable degree of purity of the peak fractions. Lane 2 contains the concentrated sample that was applied onto the gel filtration column. Lanes 6–8 show the peak fractions from the gel filtration with Lgt.

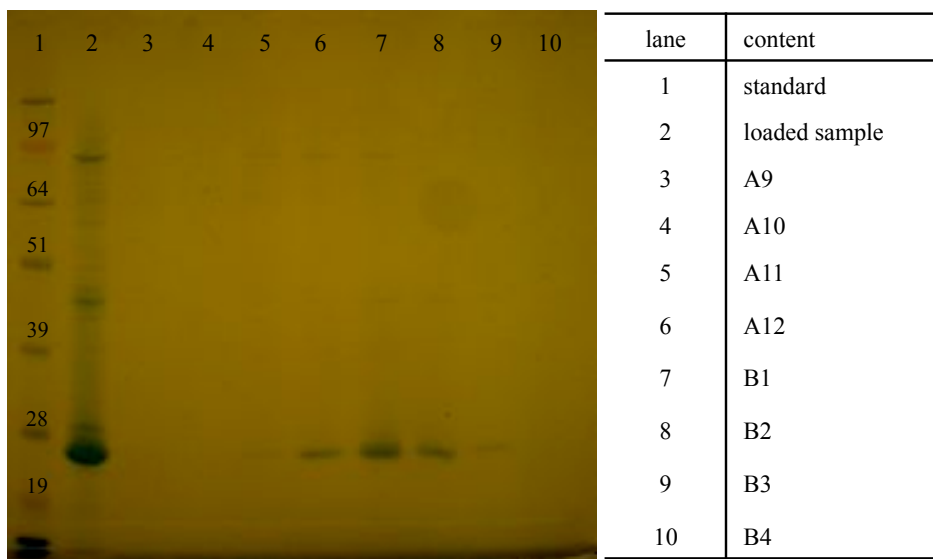


Figure 4.41: SDS-PAGE of gel filtration peak fractions of Lgt. Lane 2 shows the concentrated sample that was applied to the column. Fractions corresponding to lanes 6–8 contain pure Lgt.

Starting from 2.5 L of cell culture the preparation only yielded 0.37 mg of protein, which was not sufficient to set up crystallisation trials. Work focused on other, more promising targets, which had crystallised in the meantime.

4.8.9 YhbE

This target is an uncharacterised conserved membrane protein, which was identified as transporter in topology predictions. It belongs to the EamA-like family of transporters (<http://www.uniprot.org>; Daley *et al.* 2005).

YhbE (34.8 kDa) contains ten predicted transmembrane helices (Daley *et al.* 2005). Despite YhbE being ranked last in the small-scale expression screen and ninth in the scale-up expression, the initial affinity column yielded an average amount of protein judged on the peak height of the elution trace (Fig. 4.42).

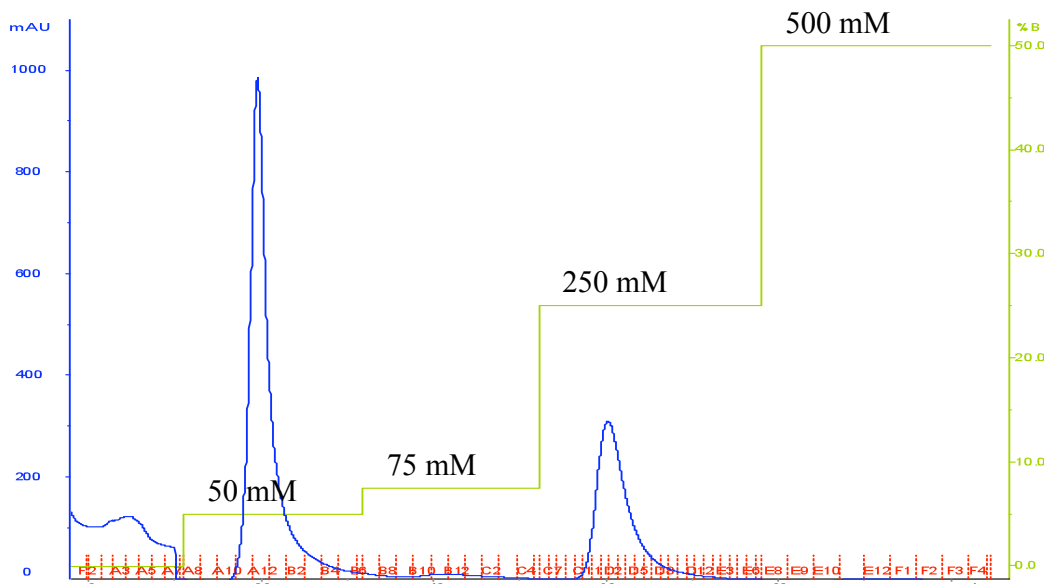


Figure 4.42: Elution trace of YhbE-GFP fusion from the first affinity column. A 50, 75, 250 and 500 mM imidazole step gradient was employed. Preparation used membranes derived from 1.5 L of cell culture. The protein precipitated completely in the collected fractions.

The target precipitated immediately in the fraction tubes after elution. YhbE did not show sufficient stability in DDM in solution and work was halted on this target. Screening of more detergents for solubilisation might improve the precipitation problems.

4.8.10 XylH

XylFGH is the second D-xylose transport system in *E. coli* and belongs to the ATP Binding Cassette (ABC) superfamily (Wu and Mandrand-Berthelot 1995). XylH is the membrane component of the ABC transporter XylFGH, while XylF is the periplasmic substrate-binding protein and XylG the ATP-binding protein (Sofia *et al.* 1994; Sumiya *et al.* 1995). *E. coli* can import D-xylose, which is the most abundant sugar in nature and metabolise it as a sole carbon source if necessary, through the pentose phosphate pathway (Song and Park 1998).

The overexpression of XylH (41.0 kDa) ranked tenth in both categories. Figure 4.43 displays the elution profile of the XylH-GFP fusion protein (70.6 kDa) followed by the SDS-PAGE showing samples from the solubilisation step and from the peak fractions of the first NiNTA column in Fig. 4.44. The preparation used membranes derived from 1 L of cell culture and judged on the 250 mM imidazole peak, the yield is high compared to other targets of this study.

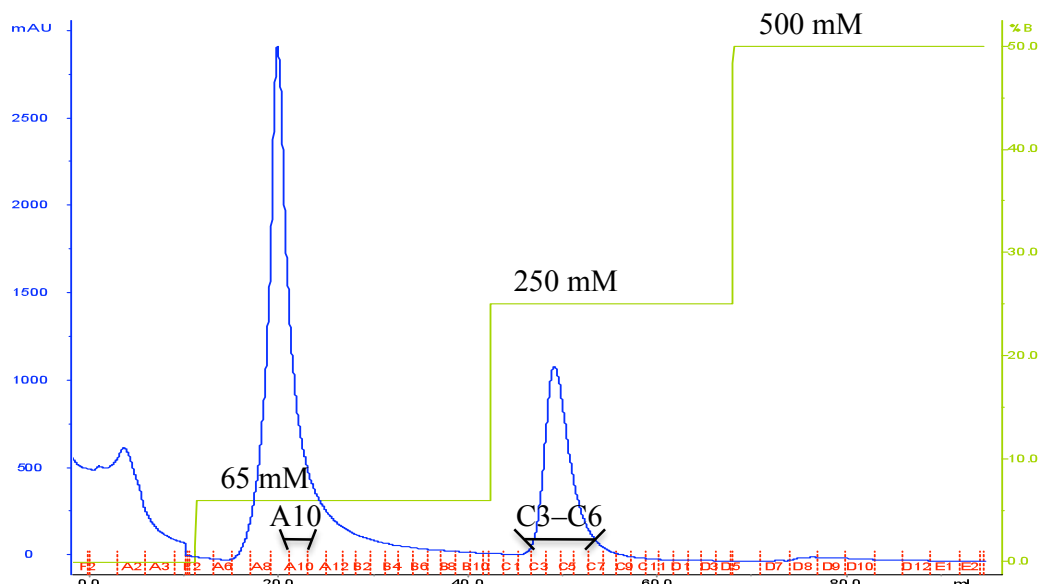


Figure 4.43: Elution trace of XylH-GFP fusion (70.6 kDa) with optimised imidazole gradient of 65 mM, 250 mM and 500 mM. The fractions C3–C6 showed green colour. This preparation is based on the membranes of 1 L of cell culture.

The applied step-gradient was optimised to 65 mM imidazole for the elution of the unbound fraction. An imidazole concentration above 65 mM, lead to partial elution of the fusion protein. The GFP-fusion eluted from the first affinity column with 250 mM imidazole in a single peak and the fractions C3–C6 showed green colour.

The samples from the fractions C3–C6 show, in the gel of Fig. 4.44, intense bands for overexpressed XylH-GFP fusion in the highlighted range of 51 kDa (migrating slightly faster than its actual size of 70.6 kDa).

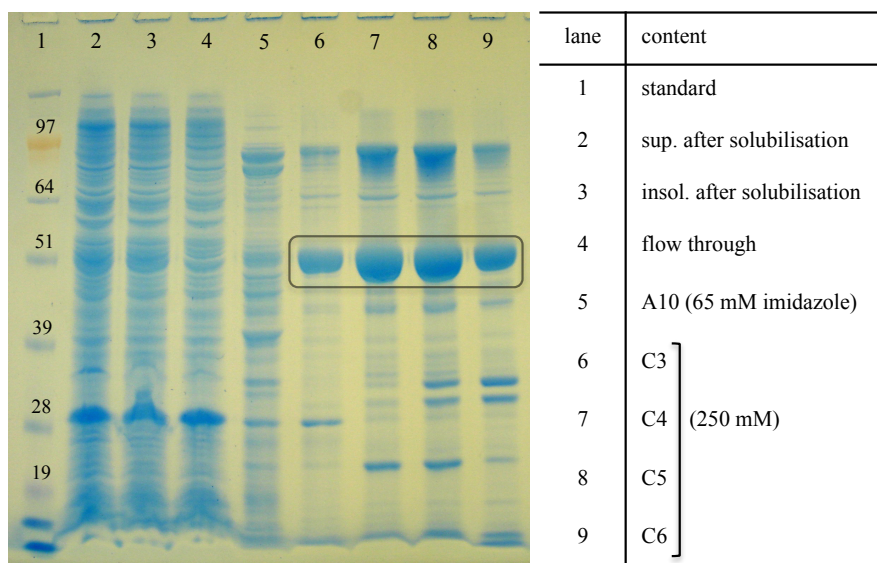


Figure 4.44: SDS-PAGE of solubilisation fractions from XylH-GFP, together with samples from the main peaks of the elution profile of Fig. 4.33. The green coloured fractions C3–C6 show an intensive band at 51 kDa accounting for XylH-GFP, which is highlighted.

The four fractions C3–C6 were pooled and dialysed overnight. Considerable precipitation losses of protein occurred in this step. In follow up preparations the dialysis was replaced by desalting columns as described in Chapter 4.2.3 and protein yield could be doubled. In contrast to PgpB, desalting columns were successful in reducing precipitation and the overall yield of XylH could be doubled.

XylH proved to be thermally stable during the TEVP-cleavage at 30 °C for 1 h. The gel samples in Fig. 4.45 show the completeness of the cleavage in lane 3 for the soluble fraction and the lack of precipitated XylH-GFP or XylH in the insoluble cleavage fraction (lane 4). The soluble fraction was applied to the second affinity column and the flow through was collected (fractions 1–6). Fractions 2–5 were pooled and concentrated for the final gel filtration purification step.

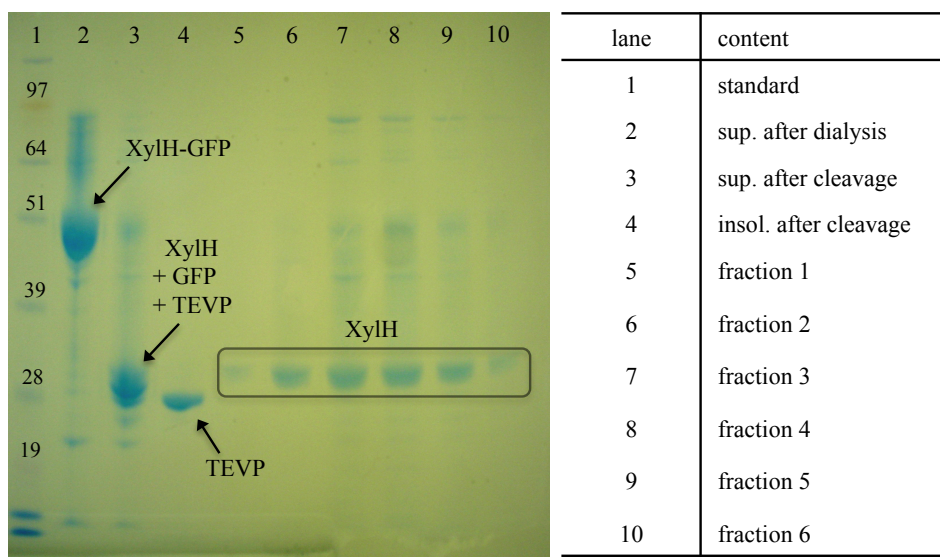


Figure 4.45: SDS-PAGE of samples from the XylH-GFP dialysis, cleavage and from the second affinity column. No precipitated XylH or XylH-GFP can be detected in the insoluble cleavage fraction (lane 4). The samples from the fractions from the second affinity column are shown in lanes 5–10 and contain XylH.

Initial size-exclusion chromatography in DDM gave an elution trace (Fig. 4.46 (A)) with a broad multiple peak indicating that the PDCs containing XylH, were not monodisperse in solution and detergent exchange was required. Figure 4.46 shows the gel filtration trace of all different detergents that were tried to improve the monodispersity of the XylH sample. Two more detergents were screened, (B) with 0.1 % Lauryldimethyl amine oxide (LDAO) and (C), with 0.03 % Fos-Choline 14 (see Table 4.1). LDAO did not improve monodispersity over DDM. The multiple peaks show that LDAO is detrimental to the PDC monodispersity of XylH. Fos-Choline 14 proved to be the right choice of detergent and the resulting elution trace (C), features a single sharp peak indicating a high degree of monodispersity of the sample. The corresponding SDS-PAGE from the peak fractions is shown next to the Fos-Choline 14 gel filtration trace. The gel in Fig. 4.47 shows a high degree of purity for the XylH containing fractions. The two fractions A11 and A12 were pooled, concentrated and submitted to crystallisation trials.

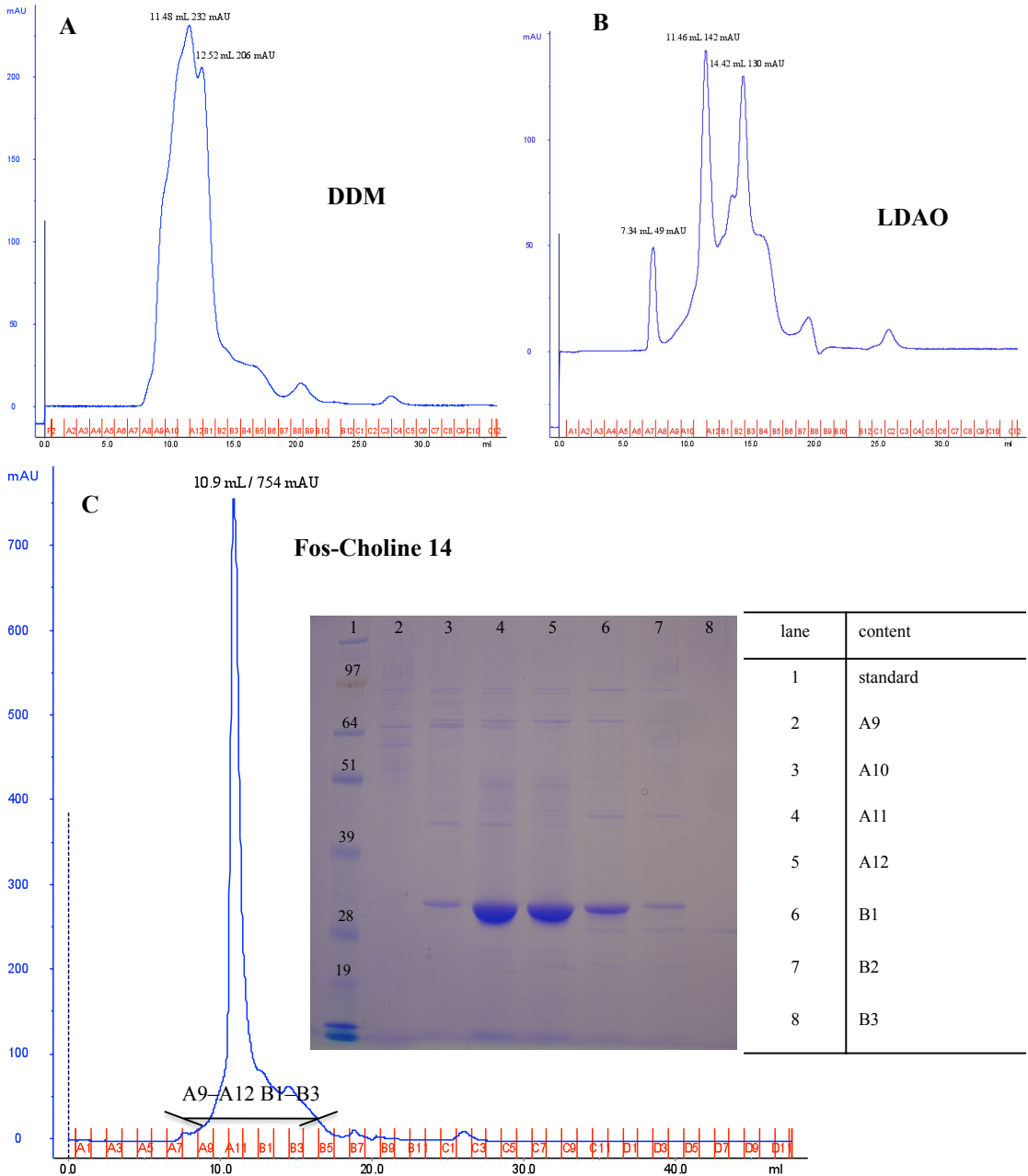


Figure 4.46: Optimisation of homogeneity for XylH by on-column detergent exchange. (A) The original gel filtration trace in 0.04 % DDM shows a broad peak indicating a low degree of monodispersity. (B) The change to 0.1 % LDAO did not improve homogeneity. (C) The detergent Fos-Choline 14 (0.03 %) was tested with material from a new preparation and a single elution peak indicates good monodispersity. The trace is displayed in conjunction with the corresponding SDS-PAGE from the peak fractions showing a high degree of purity.

DDM was subsequently exchanged in all preparations to Fos-Choline 14 on the gel filtration column. The final average protein yield after purification was 1.3 mg per litre of initial cell culture.

A later experiment showed that detergent exchange made on the first NiNTA-column of the purification protocol improved stability during dialysis of XylH. However, losses could be minimised by the use of desalting columns and the relatively expensive Fos-Choline 14 was introduced in the final purification step.

The identity of the protein in the purified solution was verified by mass spectrometry peptide sequencing. A protein sample was submitted to the *Sequencing Service* (School of Life Sciences of the University of Dundee), where the fragmentation after trypsin digest was analysed. The protein in the sample was identified as XylH and the obtained sequencing data is listed in the appendix (7.2.2).

4.8.11 FtsX

FtsX is, together with FtsE, related to the group of ABC importers. FtsX forms the membrane component. It is localised in the septal ring and is essential for cell division. Interestingly, *ftsE* mutant strains can only survive if NaCl is added to the growth medium, which led to the proposal that FtsEX transports an ion needed for cell division but not for growth per se (Schmidt *et al.* 2004).

Despite FtsX ranking third in the small-scale expression screen, its expression levels in larger cultures were the second lowest of all targets. This trend was continued in the purification of FtsX. Starting from membranes from 1.5 L of initial cell culture the resulting FtsX-GFP peak in the elution trace of Fig. 4.47 only reaches around 300 mAU.

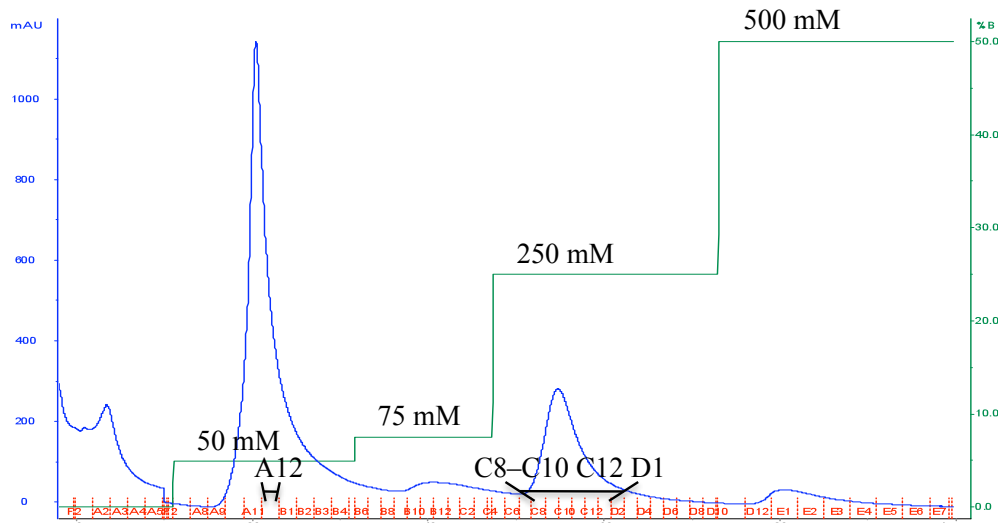


Figure 4.47: The elution trace of FtsX-GFP fusion from the first NiNTA column with an imidazole step gradient of 50, 75, 250 and 500 mM. Samples from the highlighted peak fractions were analysed on a SDS-PAGE gel Fig. 4.48.

The gel of the peak fractions does not give a clear band at 68.1 kDa, which could correspond to the fusion protein. In comparison with migrating characteristics of other tested targets, FtsX behaves differently in migrating only slightly faster in the gel (Fig. 4.48 and 4.49).

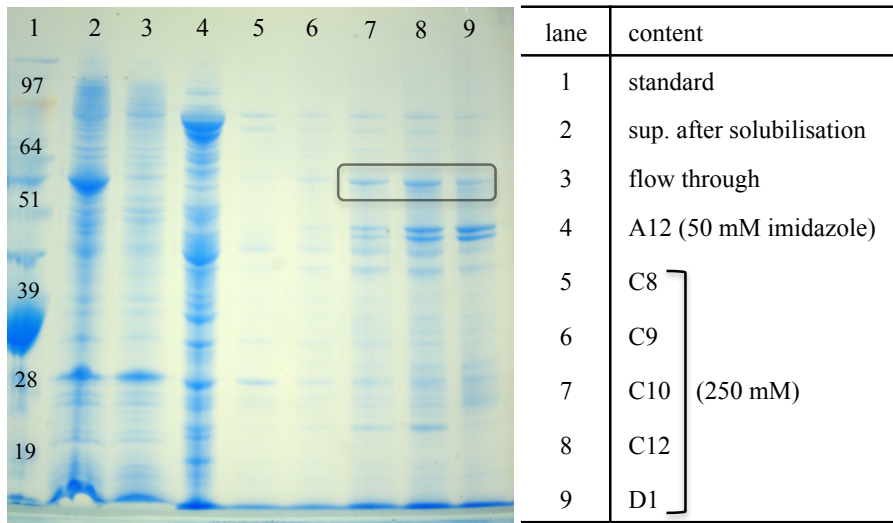


Figure 4.48: SDS-PAGE of initial samples from FtsX-GFP purification steps. The gel shows the sample of the supernatant after solubilisation and samples of the peak fractions corresponding to the trace of Fig. 4.47. The very weak presumed band for FtsX-GFP is highlighted.

While FtsX was stable during dialysis, it precipitated heavily in the TEVP cleavage step. A band for FtsX-GFP cannot be detected in lanes 9 and 10 of the gel in Fig. 4.49, where GFP and TEVP were eluted with 250 mM imidazole. This indicates either complete cleavage or precipitation. The gel samples from the fractions from the second affinity column show a very weak band that could be FtsX, but its stability and yields were very low. Work on this target was halted at this stage.

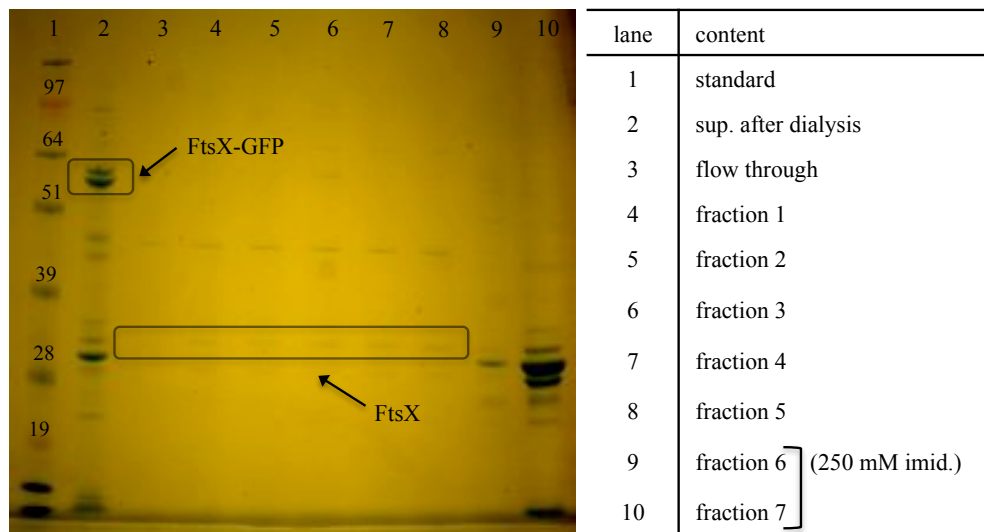


Figure 4.49: SDS-PAGE of the second half of attempted purification of FtsX. In lane 2 the band of the fusion protein (68.1 kDa) can be seen, which disappears after the cleavage. FtsX (38.5 kDa) bands are highlighted and the fractions of the last two lanes were eluted in 250 mM imidazole showing GFP (28 kDa) and TEVP (27 kDa).

4.8.12 YdeD

YdeD is an exporter of O-acetylserine and cysteine and belongs to the major facilitator superfamily. It features ten transmembrane helices and has with 299 amino acids a MW of 32.1 kDa (Dafler *et al.* 2000). YdeD ranked 11th in the small-scale expression screen and last in the scale-up expression. The ranking corresponds well with the low YdeD-GFP fusion protein content detected in the elution trace from the first affinity column (Fig. 4.50). Precipitation occurred already in the fractions from the first column.

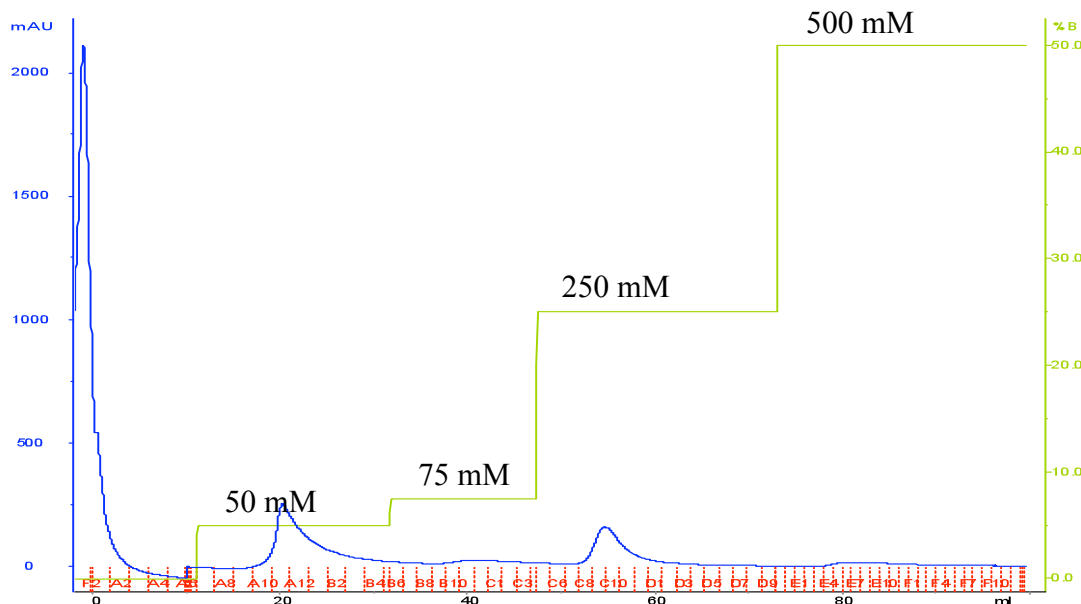


Figure 4.50: Elution trace of YdeD-GFP from the first affinity column. Employed imidazole gradient steps were 50, 75, 250 and 500 mM. The preparation is based on membranes derived from 1 L of initial cell culture. The protein yield is very low and precipitation occurred immediately after elution.

The remaining supernatant of the light green coloured fractions from the 250 mM imidazole step was pooled and subjected to dialysis, where the target completely precipitated. No further attempts to purify YdeD were undertaken, due to its instability.

4.9 Conclusion

Lgt was the only target from 12 membrane proteins entering the purification pipeline that did not show precipitation during purification. However, five targets could be purified to monodispersity, despite losses in yield due to precipitation. Two of the successful targets, Lgt and PgpB, were shown to be monodisperse in the initial solubilisation detergent DDM. The other three targets, XylH, ChbC, YdhC, were not monodisperse in DDM and detergent exchange was required. This finding is in line with literature stating that the optimal detergent is target specific for each membrane protein (Garavito and Ferguson-Miller 2001; Iwata 2003; Carpenter *et al.* 2008). This is especially important for these targets that did not show sufficient stability in DDM to allow purification. The target XylE, for example, had the highest expression levels in small- and medium-scale expression, but precipitated heavily during purification in DDM. The screening of more detergents for solubilisation and purification for the targets XylE, CcmC, FtsX, YdeD and YhbE could still lead to sufficient stability in solution to allow purification. The targets CodB and PnuC were stable in solution with DDM to a certain extent but the purification protocol would need optimisation in order to reduce precipitation and increase protein yields.

Work on the successful targets was given higher priority, in order to submit monodisperse membrane protein samples to crystallisation trials. A detailed discussion with a comparison of the purification results and possible trends can be found in Chapter 6. The results show that it is possible to address a set of membrane proteins from different families and functions, with a carefully chosen subset of parameters in a common purification pipeline and find targets that can be purified to monodispersity. These targets then enter crystallisation trials, before returning to the remaining targets and further optimise protocols.

Chapter 5

Crystallisation

5.1 Introduction

The crystallisation of proteins is a complex multi-parameter problem. The right crystallisation conditions for a protein cannot be predicted and need to be found empirically. The protein targets used in the presented study were tested in a large number of conditions with commercially available sparse matrix screens. The commercial screens used throughout this work for initial screening were a combination of MemStart/MemSys and MemGold. The screens were designed, after comparing the successful conditions for membrane protein crystallisation of all available membrane protein structures. These conditions have been grouped in both, a sparse matrix screen (MemStart, MemGold) and a systematic screen (MemSys). The latest screen is MemGold, which is based on the crystallisation information on 121 polytopic α -helical membrane proteins found in the PDB (Newstead *et al.* 2008). Promising conditions showing crystalline material are then optimised for example, by slight changes in the pH, salt and precipitant concentration in order to try to obtain better diffracting crystals. The crystallisation of membrane proteins is particularly difficult, due to their amphipathic character (see section 1.3.4), which requires detergent for stability in solution. The membrane protein has to be crystallised in a complex with detergent. Therefore, not only the membrane protein, but also the detergent strongly influences the outcome of the crystallisation trials. The detergent often hinders crucial crystal contacts between the hydrophilic domains of the membrane proteins. Crystal contacts between membrane proteins are generally more likely to be formed, when they are solubilised in detergents with a short alkyl tail. However, solubilisation and stabilisation properties of detergents, in regard to membrane proteins, are inverse proportional to the length of the detergent's alkyl chain, as discussed in section 1.3.3.2. Finding a target specific optimal detergent, that is not only good for monodispersity of the membrane protein sample, but also for crystallisation, adds another very important parameter to the multi-parameter problem of protein crystallisation.

5.2 Crystallisation trials

The targets Lgt, XylH, ChbC and PgpB showed enough purity after the second affinity column of the purification scheme to be submitted to crystallisation trials. The protein sample was concentrated for the set up of at least two 96-well screens (MemStart/Sys, MemGold). An initial protein concentration around 10 mg/mL was used, if the amount of purified protein was sufficient. This concentration has been recommended as a good starting point (Iwata 2003). The method of crystallisation used, was based on vapour diffusion in a sitting drop set-up. The crystallisation screens for each target are listed together with the protein concentration and the drop size in Table 5.1. All targets were initially solubilised with DDM.

Target	Screen	Protein concentration [mg/mL]
Lgt	MemStart/Sys	4.7
	MemStart/Sys	5.2
	MemGold	4.7
	MemGold	5.2
XylH	MemStart/Sys	11.0
	MemGold	11.0
ChbC	MemStart/Sys	7.5
	MemGold	7.5
PgpB	MemStart/Sys	5.0
	MemGold	5.0

Table 5.1: Crystallisation screens for Lgt, XylH, ChbC and PgpB, which were set up after the second affinity column. The employed crystallisation screens are shown together with the protein concentration for the targets Lgt, XylH, ChbC and PgpB after the basic purification protocol. All crystallisation experiments were set up in 500 nL (250 nL reservoir +250 nL protein sample) sitting drops.

No crystalline material was observed in any of the screens with any of the targets. The protein concentration used with ChbC (7.5 mg/mL) seemed to be in a good range as 50 % of the drops remained without precipitation. The other targets showed high amounts of precipitation in all of the drops.

Further purification with size-exclusion chromatography of XylH and ChbC revealed that half of these samples were not monodisperse in DDM. XylH and YdhC were

monodisperse in the zwitterionic detergent Fos-Choline 14, while ChbC was found to be monodisperse in Cymal-5. YdhC was after solubilisation and purification in DDM directly applied to an on-column detergent exchange and was monodisperse in Fos-Choline 14. The targets Lgt and PgpB proved to be monodisperse in DDM, but the purity of the samples before gel filtration might not have been good enough for crystallisation. PgpB for example showed less heavy precipitation in screens following size-exclusion chromatography, despite higher protein concentration in the drops.

The targets XylH, ChbC, PgpB and YdhC were subjected to crystallisation screens, after the added purification step of size-exclusion chromatography. The screens for ChbC and YdhC are listed in Table 5.2. The crystallisation trials for XylH and PgpB are described in their sections, 5.3 and 5.4 respectively.

The protein concentrations employed were in the range where 50 % of the drops remained clear after one week. In the case of YdhC sufficient protein sample was left, after setting up trials with MemGold and MemStart/Sys, so with the Peg/Ion 1/2 a third screen was also tested. The commercial Peg/Ion 1/2 screen is a systematic screen that tests the influence of different molecular weight polyethylene glycols (PEGs) together with polyvalent cations and anions. Unfortunately, none of the screens yields crystalline material, either for YdhC or for ChbC. The gel filtration traces of both targets showed a single elution peak in the optimised detergents. Therefore future screening should probably use higher protein concentrations. Another option is to screen more detergents, so long as these do allow monodispersity of the membrane protein-detergent complexes.

Target	Screen	Protein concentration [mg/mL]	Detergent
ChbC	MemStart/Sys	7.5	Cymal-5
	MemGold	7.5	Cymal-5
YdhC	MemStart/Sys	12.0	Fos-Choline 14
	MemGold	12.0	Fos-Choline 14
	Peg/Ion 1/2	12.0	Fos-Choline 14

Table 5.2: Crystallisation screens for ChbC and YdhC, set up after gel filtration purification. All drops had a volume of 500 nL (250 nL reservoir + 250 nL protein sample) in a 96-well sitting drop screen format. No initial crystal hits could be obtained for ChbC or YdhC.

5.3 Crystallisation of XylH

Fos-Choline 14 improved the monodispersity of XylH. The purified membrane protein was subjected to a new row of crystallisation trials and the protein concentration in the drops was further varied. The screens used for this stage and their parameters are listed in Table 5.3. The drops appeared to stay clear in most of the conditions. The protein concentration was varied in the screens MemStart/Sys and MemGold from 8.0 to 12.3 mg/mL, and only a slight increase in the amount of precipitation was observed. In the screens with the highest protein concentration, the additive 1,2,3-heptanetriol was tested. Small amphiphilic molecules such as 1,2,3-heptanetriol can reduce the size of detergent micelles and may help to enable crystal contacts (Michel 1983). However it did not show any effect with XylH.

Screen	Protein concentration [mg/mL]	Drop size [μL]	Additives
MemStart/Sys	8.0	0.5	1,2,3-heptanetriol (0.03 %)
	9.5	0.5	
	12.3	1.0	
MemGold	8.0	0.5	1,2,3-heptanetriol (0.03 %)
	9.5	0.5	
	12.3	1.0	

Table 5.3: Initial crystal screens for XylH in Fos-Choline 14. The screened protein concentration is shown alongside drop size (1 to 1 ratio of protein to reservoir solution) and additives. The condition C9 (0.1 M Tris pH 8.5, 1.5 M lithium sulphate) of the MemStart/Sys plate with protein concentration of 9.5 mg/mL showed initial hits.

All trays were checked under the microscope for the degree of precipitation or crystalline material, directly after the set up. It emerged that birefringent plate-like crystals had formed in the MemStart/Sys condition C9 of the plate with 9.5 mg/mL protein concentration. This condition contains 0.1 M Tris pH 8.5 and 1.5 M lithium sulphate. The plate-like crystals are shown in Fig. 5.1.

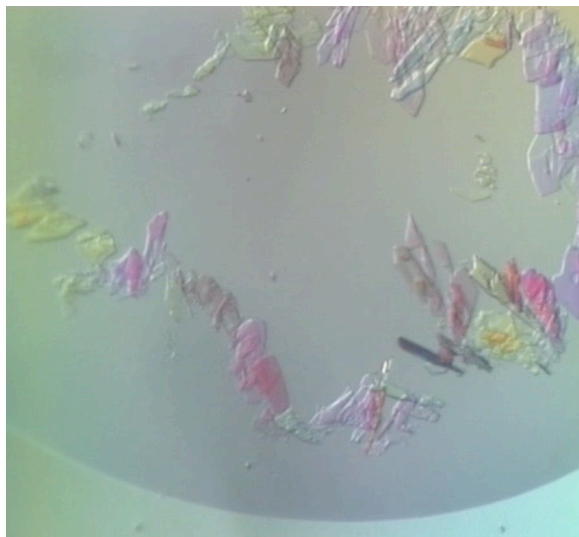


Figure 5.1: Initial crystals in MemStart/Sys screen condition C9 (0.1 M Tris pH 8.5, 1.5 M Li₂SO₄).

The crystals of Fig. 5.1 dissolved after 20 minutes and did not re-emerge. In order to verify, if the observed crystals were not salt, the reservoir solution was examined for the formation of salt crystals in the process of drying out. The observed crystals, of lithium sulphate were analysed under the microscope but appeared to have different shapes. Therefore, this condition was used to set up larger drops and optimisation screens with different pH or salt concentrations. A 24-well sitting drop plate with 2 µL (1:1 ratio protein sample/reservoir) drops of the MemStart/Sys C9 condition and XylH (9.5 mg/mL) showed two crystals in two drops after two weeks. The crystals were of different appearance and are shown in Fig. 5.2. They grew from a small amount of precipitation in otherwise clear drops.

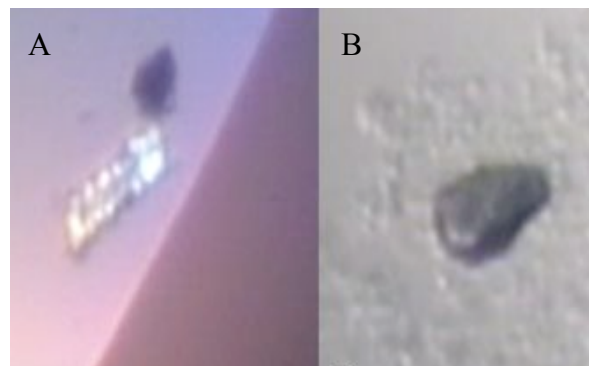


Figure 5.2: Suspected XylH crystals grown in the initial condition C9. Derived from a 24-well sitting drop plate with 2 µL (1:1 ratio protein sample/reservoir) drops. Crystal A diffracted to 7 Å, while crystal B did not show any diffraction at the I02 synchrotron beamline at Diamond Light Source.

In order to find a suitable cryo protectant, 20 % ethylene glycol or PEG 400 was added to the reservoir solution and the mixture was lifted with an empty loop and flash frozen in the dry air flow of the cryo-flow system. A clear glass was formed with ethylene glycol. Reservoir solution mixed with 20 % ethylene glycol was then used as cryo-protectant. The mounted crystal was dipped for two seconds into cryo-protectant and immediately placed and frozen in the cryo-flow on the goniometer head. Exposure to X-rays did not show any diffraction with crystals in the in-house X-ray source, a Rigaku MicroMax 007 rotating anode generator coupled with a MarResearch 345 image plate detector. No diffraction in the first instance was an indicator that both crystals may be protein and not salt. They were, therefore, stored in liquid nitrogen for later exposure to more intense synchrotron radiation.

The crystals were taken to the Diamond Light Source. Crystal B in Fig. 5.2 did not show any diffraction. However, crystal A diffracted at the I02 beamline to 7 Å. An example of the diffraction pattern of crystal A is shown in Fig. 5.3.

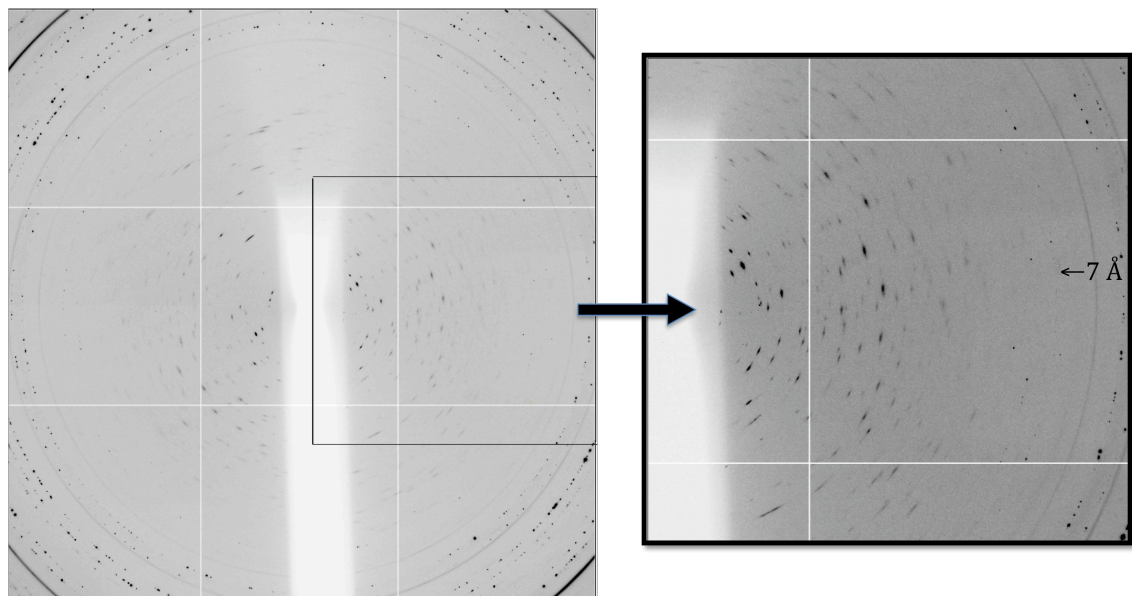


Figure 5.3: Diffraction image of XylH (crystal A) obtained at the Diamond Light Source Beamline IO2. A zoomed part of the image is displayed on the right.

Unfortunately the data were not of sufficient quality for interpretation and processing. The focus of the work was then to reproduce the initial crystal and to further optimise the conditions in order to obtain better diffracting crystals. No further crystals were found in any other drops of the successful crystallisation screen.

Further 24-well optimisations screens were set up, varying the conditions used in the initial screen. All the optimisation trays used, are listed in Table 5.4 at the end of this section. The first approach was to optimise the protein concentration. Increasing the protein concentration aims to bring the protein closer to the supersaturation state in the drop. All the drops in previous screens contained small amounts of precipitation and XylH proved very stable in solution. Precipitation increased from a protein concentration of 20 mg/mL upwards, but even in a tray with a protein concentration of 38 mg/mL no heavy precipitation was observed.

The second attempt to obtain more XylH crystals was to find a suitable additive that might be capable of changing the micelle size of the PDC, favouring crystal contacts and nucleation. Small organic molecules, additional detergents, multivalent salts, and chemicals can all have a significant impact on the formation and quality of membrane protein crystals (Michel 1983; Iwata 2003; Carpenter *et al.* 2008).

The additive 1,2,3-heptanetriol was added, as it can reduce the size of detergent micelles, but no effect was observed. Detergents, as additives, were screened with the two commercially available Detergent 1/2 screens. But despite leading to further precipitation, no signs of crystals emerged. Furthermore, the two sparse matrix screens Hampton Crystal 1/2 and JCSGplus 1/2 were tested as additive screens. The screens were added in ratios 1:10 and 1:1000 to premade screens containing the initial condition, in which XylH had crystallised before. The added screens only had a small influence on precipitation in the 1:10 ratio, but crystalline material could not be observed.

Membrane proteins have been shown to prefer crystallisation in a pH range between 5–9 (Iwata 2003; Newstead *et al.* 2008). The obtained XylH crystal appeared in the initial conditions at a pH of 8.5 and this condition contains no other precipitant other than lithium sulphate (1.5 M). The polyvalent cations and anions of salts can be essential for crystallisation, because they can stabilise crystal contacts by acting as linkers, but can also weaken ionic interactions between proteins if the concentration is too high (Iwata 2003). In order to explore the influence of the pH and the salt concentration a 24-well optimisation screen with 2 µL drops (1:1 ratio) based on the initial condition, was prepared with the pH ranging from 7.5–9 and with lithium sulphate concentrations from 1.25–2.00 M. Nearly all drops remained clear, indicating stability of XylH over a wide range of pH and salt concentrations.

The software Screen Designer and the Hamilton Star Lab robot were used to design and to dispense homemade 96-well trays in order to test more parameters in one screen and to identify trends. The first designed screen tested both, lithium sulphate and ammonium sulphate concentrations, from 1.1–1.8 M. It was found that lithium sulphate and ammonium sulphate can be substituted and the salt exchange may favour crystallisation (Iwata 2003). In addition to the different salts, each screen contained 0.1 M Tris in a pH range of 8.3–10.0. A schematic of homemade screen I is displayed in Fig. 5.4. Most drops stayed clear and no trend regarding the amount of precipitation could be observed.

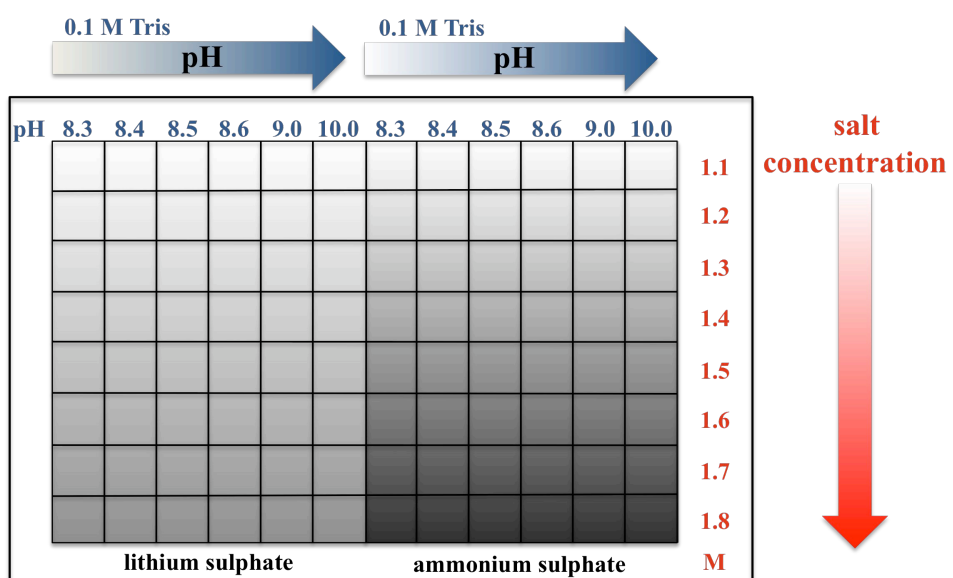


Figure 5.4: Homemade screen I for XylH, containing two different salts with lithium sulphate and ammonium sulphate in eight different concentrations. Tris-buffer (0.1 M) was used in six different pH steps.

The combination of salts was tested with the homemade screen II (Fig. 5.5). Ammonium sulphate concentrations from 0.6–2.8 M supplemented with a gradient of LiCl as additive from 0.001–0.2 M were screened. The protein concentration (10 mg/mL), buffer concentration (0.1 M Tris) and pH (8.5) were held constant.

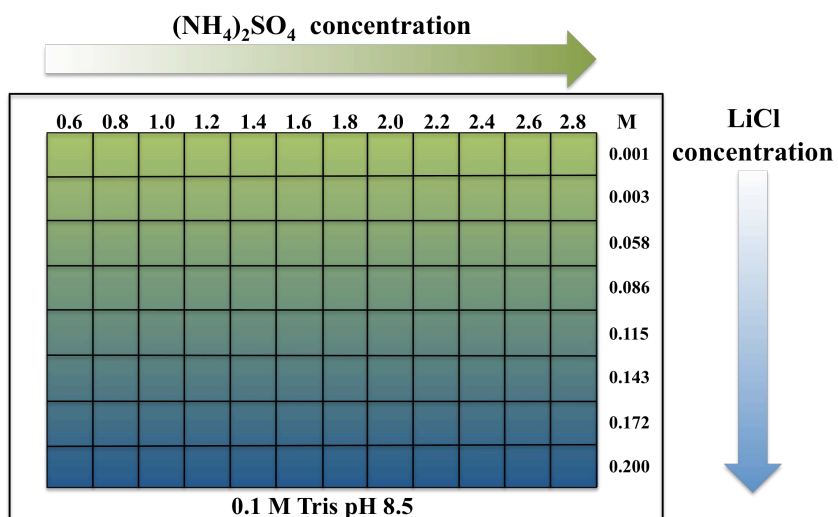


Figure 5.5: Homemade screen II for the test of salt combinations for the crystallisation of XylH. Ammonium sulphate in concentrations from 0.6–2.8 M was screened with the addition of 0.001–0.200 M LiCl. Buffer concentration and pH and protein concentration remained constant.

Increasing precipitation with XylH was observed in the homemade screen II, at ammonium sulphate concentrations of 2.6 M or higher. In screen conditions with a concentration of LiCl higher than 0.115, light precipitation with XylH was observed for ammonium sulphate concentrations of 2.4 M and higher. However, no further XylH crystals could be obtained. The complete list of optimisation screens targeting protein concentration, pH range, salt concentrations and combinations of salts as well as additives can be found below. Unfortunately it was not possible to reproduce the first obtained crystal.

Screen	Format	Prot. conc. [mg/mL]	Drop size [μL]	Additives
Peg/Ion 1/2	96	9.5	0.5	
Detergent 1	24	9.5	5	
pH/concentration	24	9.5	2	
Protein concentration	24	10.0–28.0	2	
Protein concentration	24	38.0	2	1,2,3-heptanetriol
Detergent 2	24	19.0	5	
Homemade I	96	9.5	1	
Homemade I	96	25.0	1	
Homemade II	96	9.5	1	
Initial condition	96	9.5	1	Hampton Crystal 1/2 1:10
Initial condition	96	9.5	1	Hampton Crystal 1/2 1:1000
Initial condition	96	9.5	1	JCSGplus 1/2 1:10
Initial condition	96	9.5	1	JCSGplus 1/2 1:1000
Initial condition	96	25.0	1	Hampton Crystal 1/2 1:10

Table 5.4: Complete list of optimisation screens for XylH. The drops in Detergent screens 1 and 2 were based on the initial condition and contained 2 μL protein sample, 0.5 μL detergent additive and 2.5 μL reservoir solution. All other screens were prepared with a 1:1 ratio of protein sample and reservoir. Heptanetriol was added to one half of the crystallisation drops in the protein concentration screen.

5.4 Crystallisation of PgpB

PgpB was monodisperse with the initial solubilisation detergent DDM. The first crystallisation trials with PgpB were set up with the screens MemStart/Sys, Peg/Ion 1/2, MemGold and Hampton Crystal 1/2. The PgpB concentration in the screens and the drop size are listed in Table 5.5.

Screen	Protein concentration [mg/mL]	Drop size [μL]
MemStart/Sys	8.8	0.5
Peg/Ion 1/2	8.8	0.5
MemGold	8.5	0.5
Hampton Crystal 1/2	8.5	0.5

Table 5.5: Initial screens for PgpB following purification with gel filtration, listed together with the used protein concentration and drop size (1:1 ratio protein sample to reservoir solution).

Plate-like crystals were observed directly after set up in MemSys condition No. 1 (0.1 M sodium citrate pH 5.5, 2.5 M magnesium sulphate), but the crystals vanished 15 min after set up and did not appear again.

The crystals seen in Fig. 5.6 were obtained after two weeks in the MemSys H10 condition (0.1 M Tris pH 8.5, 0.1 M NaCl, 0.1 M MgCl₂, and 12 % w/v PEG 4000). The crystals were exposed to X-rays in the in-house generator and to synchrotron radiation at the Diamond Light Source, but did not diffract. Therefore, the crystals were presumed to be protein rather than salt and optimisation screens were set up. Two 24-well pH optimisation screens (pH 7.5–9.0) with different protein concentrations were prepared. Furthermore, one 96-well plate of the initial condition (initial screen) was set up. However no more crystals were obtained, either with this condition or variations thereof.



Figure 5.6: Grown crystals in initial MemSys screen with PgpB in DDM. The MemSys H10 condition contains 0.1 M Tris pH 8.5, 0.1 M NaCl, 0.1 M MgCl₂ and 12 % w/v PEG 4000. The crystals did not diffract.

Initial tests showed that a protein concentration of 8.5 mg/mL was a good starting point with light precipitation in about 50 % of the drops. Detergent screens 1/2 and Additive screen 1 were tested, but were not successful in producing more crystals. All optimisation screens with PgPB are listed in Table 5.6 at the end of this section.

Growing detergent crystals of DDM made the identification of potential protein crystals in the screens difficult. Fig. 5.7 shows some of the detergent crystals, which usually appeared as discs, lacking distinct edges in most cases. A crystal with a different appearance than the DDM discs (Fig. 5.7) appeared after four weeks in the MemGold screen condition 27 (0.04 M Tris pH 8.0, 0.04 M NaCl, 27 % v/v PEG 350 MME). In contrast to detergent crystals, this crystal did not smear or break when mounted into a loop.

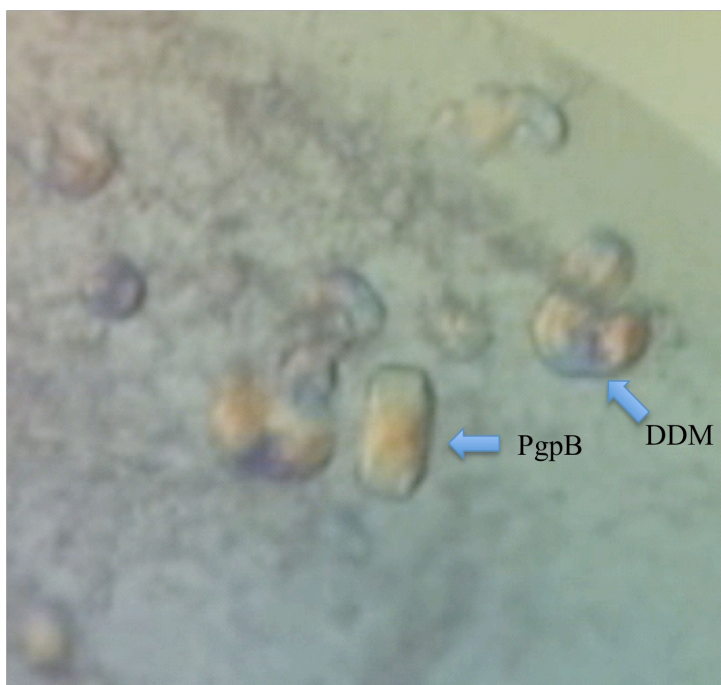


Figure 5.7: PgPB and detergent crystals in condition 27 of MemGold screen. (0.04 M Tris pH 8.0, 0.04 M NaCl, 27 % v/v PEG 350 MME)

Following tests with PEG 400 and ethylene glycol, 20 % of the latter was mixed with the reservoir solution (MemGold 27) and used as cryo-protectant. The crystal was mounted into a 0.2 μ m loop and dipped for two seconds into the cryo-protectant. The loop was immediately placed on the goniometer head, where the crystal was flash frozen by the cryo-system at -160°C . No diffraction was obtained with the in-house generator, suggesting the crystal was not salt. The crystal was stored in liquid nitrogen until exposure to stronger synchrotron radiation was possible.

The PgpB crystal from Fig. 5.7 was exposed to synchrotron radiation at the beamline I02 at the Diamond Light Source. The diffraction pattern showed characteristic low-resolution diffraction spots, which are typical for protein crystals (Rhodes 1993). The PgpB crystal diffracted to about 15 Å (Figure 5.8).

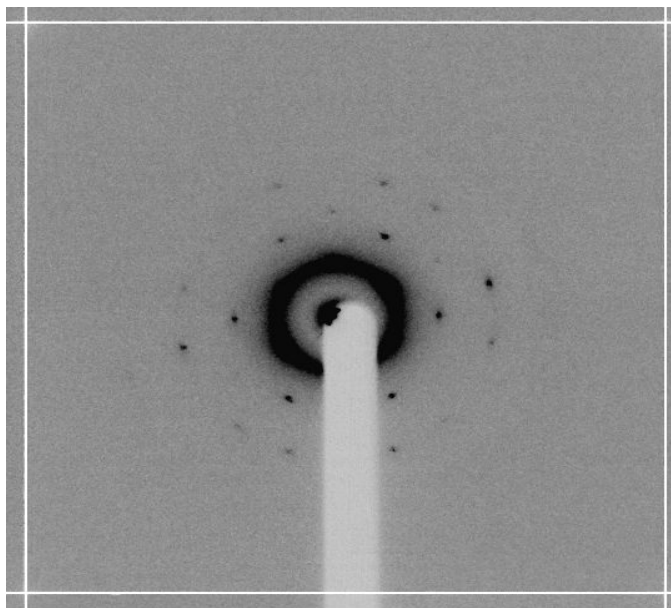


Figure 5.8: Diffraction image of the PgpB crystal obtained at the I02 beamline of the Diamond Light Source.

Optimisation screens were set-up employing the same strategies as for XylH, with the screening of additives in the initial conditions. The screens Hampton 1/2 or JCSGplus 1/2 were added in ratios of 1:10 and 1:1000. No crystallisation or trends regarding the precipitation of PgpB in the drops were obvious. The next optimisations screens aimed to test different precipitants in various concentrations. The majority of published membrane protein structures were obtained from a crystal grown in a condition containing polyethylene glycols (PEGs) or a related compound (Iwata 2003; Newstead *et al.* 2008). Particularly successful are small PEGs such as PEG 400. Larger PEGs such as PEG 3350 are often used in the crystallisation of soluble proteins, but are prone to cause phase separation in membrane protein crystallisation screens. Small PEGs are commonly used as precipitants in a concentration range between 15–35 % (Iwata 2003). Two more homemade screens were prepared to screen different PEGs. Homemade screen III was first set-up and contained 23–33% of PEGs 200, 350, 400 and 1000 in concentrations from 23–33 % and NaCl in concentrations from 0–0.06 M. The format of homemade screen III is shown in Fig. 5.9.

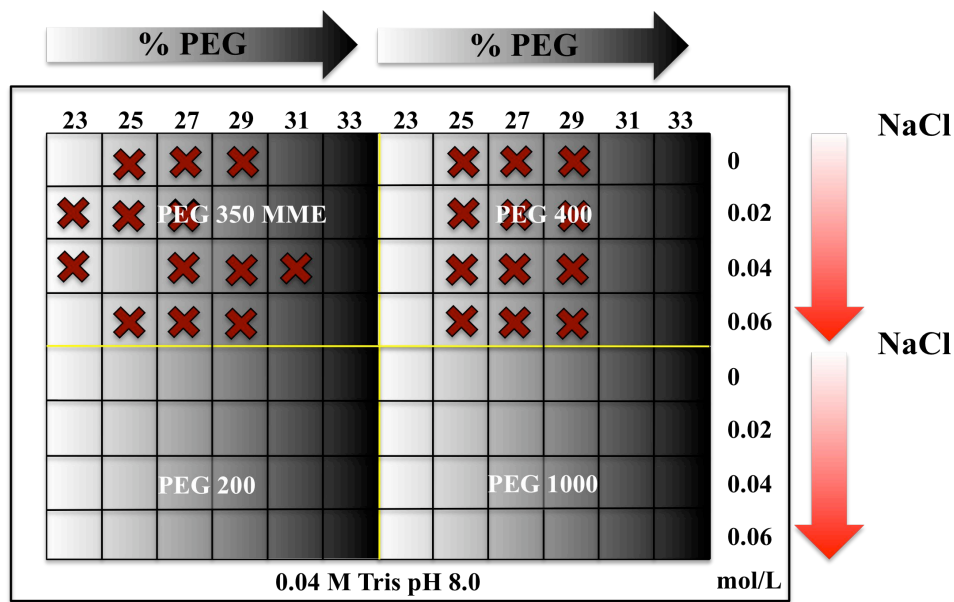


Figure 5.9: Format of the 96-well home made optimisation screen III for the screening of PgpB in different PEGs and NaCl concentrations. Red crosses mark the conditions that contained rod-like crystals. The screen is based on the successful condition with 0.04 M Tris pH 8, 0.04 M NaCl, 27 % (v/v) PEG 350 MME. Four different precipitants are screened with PEG 350 MME (MME= monomethylether), 200, 400 and 1000 in ranges from 23–33 %. NaCl concentration varied in the range of 0–0.06 M. All wells contain 0.04 M Tris pH 8.0.

Precipitate was detected in the homemade III screen after two weeks in all drops with a PEG content higher than 29 %. Detergent crystals could be observed for PEG 350 MME and PEG 400. Four weeks after set-up, small crystalline rods could be observed in conditions containing 25–29 % PEG 400 and 0–0.06 M NaCl in the homemade screen III. The rods often grew next to detergent crystals. The relevant wells are marked with red crosses in Fig. 5.9. The crystals in the original condition with PEG 350 MME appeared later and were smaller in size.

Homemade screen IV used, in contrast to homemade screen III, different buffer pH and PEG 550 MME in a similar concentration range. The Tris and NaCl concentration remained constant at 0.04 M. A schematic of the homemade screen IV for PgpB is shown in Fig. 5.10.

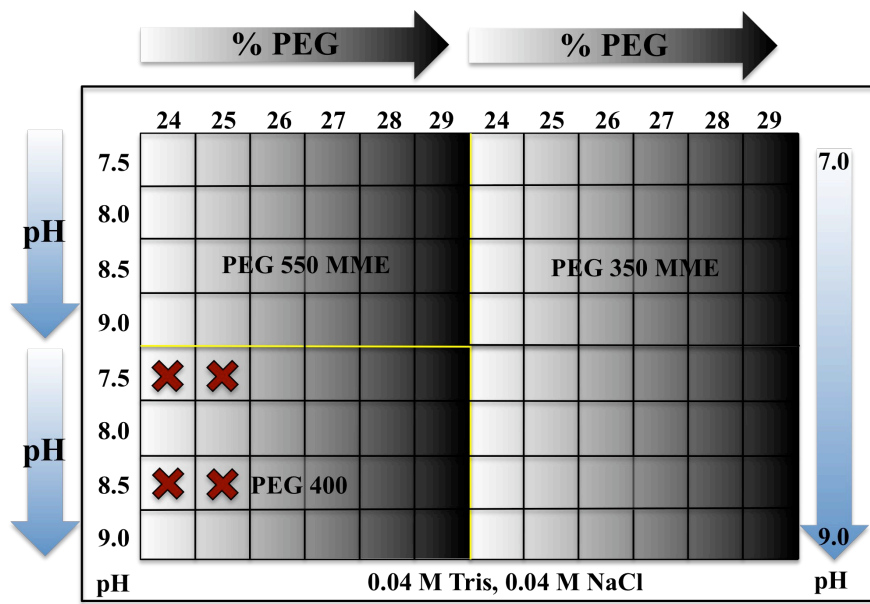


Figure 5.10: Homemade screen IV for the screening with PgpB in different PEGs and buffer pH. The screen is based on the initial crystallisation conditions (0.04 M Tris pH 8, 0.04 M NaCl, 27 % (v/v) PEG 350 MME). All wells contain 0.04 M Tris buffer and 0.04 M NaCl. The screened PEGs were PEG 550 MME, 350 MME and 400. The red crosses mark the wells containing the crystals shown in Fig. 5.11.

At the time of writing, homemade screen IV has been incubated for four weeks and has produced crystal rods in conditions with 24 and 25 % PEG 400 and a buffer pH of 7.5 and 8.5. The crystals were larger than the ones obtained with homemade screen III, which could be due to the change in buffer pH. Figure 5.11 shows two crystals from homemade screen IV. Crystal (A) grew in 0.04 M Tris pH 7.5, 0.04 M NaCl and 25 % PEG 400 while crystal (B) was obtained from 0.04 M Tris pH 8.5, 0.04 M NaCl and 24 % PEG 400. At this time, no crystals have yet been observed in the initial condition with PEG 350 MME. Combining the results of both screens crystals could be found in conditions with a PEG 400 content between 24 and 29 %, NaCl concentrations from 0-0.06 M and at pH 7.5–8.5 of 0.04 M Tris-buffer. The salt concentration did not influence the crystallisation in the range tested. Figure 5.11 shows two images of the crystal rods obtained.

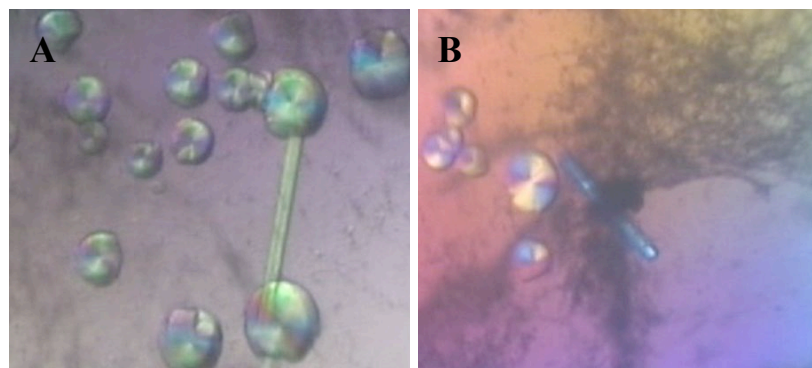


Figure 5.11: Examples of the PgpB crystals found in homemade screen III and IV. Crystal (A) grew in 0.1 M Tris pH 7.5 0.04 M NaCl 25 % PEG 400 and crystal (B) in 0.1 M Tris pH 8.5 0.04 M NaCl 24 % PEG 400 of the homemade screen IV.

PEG 400 is a cryo-protectant and present in the crystallisation condition. The crystals were therefore directly mounted in a suitable loop and flash frozen in the cold air-flow of the cryo-system. The crystals diffracted to 25 Å in the in-house X-ray source and were stored in liquid nitrogen for the exposure to stronger synchrotron radiation. A diffraction image of crystal A is shown in Fig. 5.11.

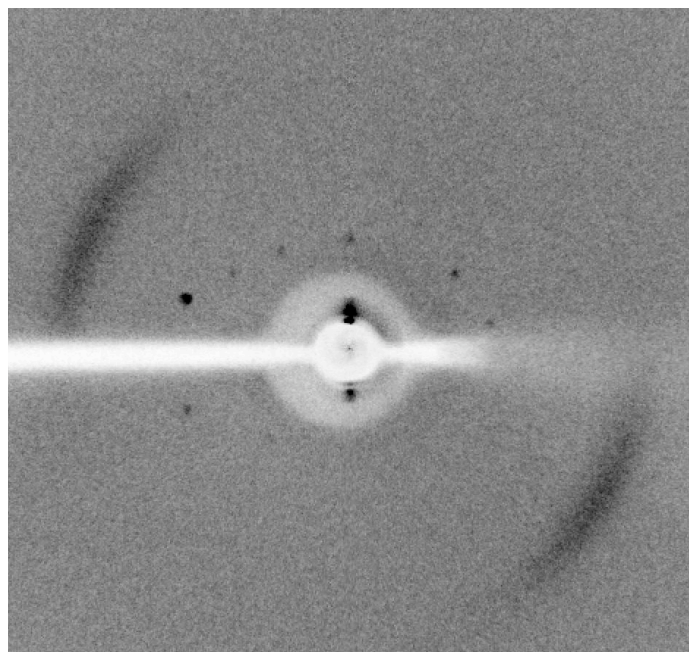


Fig. 5.12: Diffraction image of PgpB crystal (A in Fig. 5.11) from homemade screen IV in the in-house X-ray source.

In comparison to the first PgpB crystals, which did not diffract in-house, this is a good improvement. In addition not only one but several crystals grew in the drops and 15 crystals were flash frozen and stored for the next scheduled synchrotron shift.

Finally, Table 5.6 lists all the optimisation screens that were set-up for the crystallisation of PgpB.

Screen	Format	Prot. concentration [mg/mL]	Drop size [μL]	Additives
pH screen	96	8.5	1	
pH screen	24	13	2	
Det I	24	8.5	5	
Det 2	24	8.5	5	
Add 1	24	8.5	5	
Initial condition	96	8.5	1	
Initial condition	96	8.5	1	Hampton screen 1:10
Initial condition	96	8.5	1	JCSG screen 1:10
Initial condition	96	8.5	1	Hampton screen 1:1000
Initial condition	96	8.5	1	JCSG screen 1:1000
Homemade III	96	10	1	
Homemade IV	96	10	1	

Table 5.6: Optimisation screens for PgpB. The two pH screens tested a pH range of 7.5–9.0 with two different protein concentrations for the condition (0.1 M NaCl, 0.1 M MgCl₂, 0.1 M Tris pH 8.5 and 12% w/v PEG 4000), in which the first crystals were observed. Detergent and Additive screens for the above condition were set-up in a 5 μL drop consisting out of 2 μL protein, 0.5 detergent additive and 2.5 μL reservoir solution. The initial conditions yielding the diffracting crystal were 0.4 M Tris pH 8, 0.04 M NaCl and 27 % (v,v) PEG 350 MME, which were the starting point for initial screens with additives and the homemade III and IV screens.

5.5 Conclusion

The five targets Lgt, XylH, ChbC, PgpB and YdhC entered the crystallisation stage and XylH and PgpB crystallised. No crystals were observed in any trays, which were set-up with samples that had not been purified with size exclusion chromatography. A gel filtration step in the purification protocol proved to be essential to get crystals. The crystals of XylH and later PgpB were obtained early on and work then primarily dealt with the optimisation of their crystallisation conditions. Lgt did not yield any crystals in trays after the basic purification and only one protein purification including the final step of size-exclusion chromatography was performed. Monodispersity was observed for Lgt in DDM, but the protein yield of this single preparation was not sufficient to set-up crystal trays. ChbC and YdhC did not crystallise in any condition of the initial screens. In these cases, no heavy precipitation was observed in the drops. Therefore increasing the protein concentration should be the next step in crystallisation screens with ChbC and YdhC.

A strategy for all targets that did not crystallise, or with which crystals did not diffract to high resolution, is the screening of more detergents in the gel filtration step. The optimisation of detergents has already been shown to be important in the case of XylH and ChbC. In general, the choice of detergent is dependent on the solubility and stability of the target membrane protein and as there is no simple relationship between these parameters (Iwata 2003), only detergent screening can find the optimal combination. Furthermore, even if monodispersity of the protein sample is achieved, there is no guarantee that this particular detergent-protein combination is more likely to crystallise. Two crystals could be obtained in XylH crystallisation trials, of which one diffracted to 7 Å. The crystal grew in one single drop in the initial conditions out of light precipitate. None of the other drops contained crystals and neither screens with the initial condition, nor the optimisations listed in table 5.4, produced crystals again. XylH is very stable in solution with Fos-Choline 14 and even protein concentrations of 38 mg/mL did not cause heavy precipitation in crystallisation drops. The successful condition, in which XylH crystallised, does not contain any precipitant other than lithium sulphate, so an optimisation screen with a range of PEGs could be tested. Furthermore, on-column detergent screening in the gel filtration step, could assess if XylH is monodisperse in other detergents. XylH is the membrane component of the ABC transporter XylFGH (Sumiya *et al.* 1995; Wu and Mandrand-Berthelot 1995). To date six ABC transporters

have been crystallised (McLuskey *et al.* 2009). However, all of the obtained structures were crystallised together with their nucleotide binding or the substrate binding domains (McLuskey *et al.*; Rees *et al.* 2009). These domains are not located in the membrane and would enlarge the hydrophilic protein parts, which are necessary for the formation of crystal contacts. Another option would be the co-crystallisation of XylH specific antibodies or DARPINs, which would bind to the membrane protein and increase the hydrophilic surface of the complex or lock the transporter in a conformation (Hunte *et al.* 2003; Binz *et al.* 2004). However, these approaches would most likely require the optimisation of the purification protocol in regard to the new membrane protein complex.

The enzyme PgpB crystallised with DDM as detergent. A crystal grew in initial crystallisation trials, which was large enough to be mounted and exposed to X-rays. No diffraction could be detected with the in-house X-ray source, but the crystal diffracted to 15 Å at the synchrotron. PgpB crystals were, although in a different rod-like shape, reproduced in the initial condition. Crystals of the same shape were obtained in optimisation screens, targeting different precipitant concentrations. These crystals grew in a condition containing PEG 400, which is a suitable cryo-protectant. The crystal rods diffracted in-house to 25 Å and are awaiting exposure to stronger synchrotron radiation. So far optimisations for PgpB dealt mainly with the precipitant and salt concentration, therefore additives will be screened. Co-crystallisation with one of PgpB's substrates could be successful by locking the enzyme in a specific conformational state, which could improve the quality of crystals. The general strategies described before, such as the screening of different detergents, can also be employed on PgpB, if the current crystals fail to diffract to high resolution or cannot be improved.

Chapter 6

Discussion and future perspectives

The HTP approach used in this work aimed at finding the most promising target membrane proteins from a construct library, with regard to crystallisation. Every step from target selection, expression screening, purification to crystallisation tried to employ the methods and parameters providing the highest likelihood of success. The process is based on the assumption that what worked before with many membrane proteins is likely to work again. In order to increase the chances of success, targets are selected in the first step according to criteria, which fit those membrane proteins that had been previously crystallised. Most membrane structures in the PDB are from prokaryotic membrane proteins and therefore this study chooses in the first instance a target construct library of *E. coli* inner membrane proteins. The four criteria for the selection of targets from this library (see section 1.6) are based, on the one hand, on requirements by the construct design and, on the other hand, on information from databases, listing properties of crystallised membrane proteins, such as number of transmembrane helices.

The recombinant overexpression of membrane proteins is a bottleneck in membrane protein structural biology. The small-scale HTP expression screen developed in this work shows that it is possible to find optimal expression conditions for a large number of targets in a short time frame. The results show that considerable differences exist in the expression levels of membrane proteins in different cell lines, media and temperatures and that screening for the best combination of these parameters is required. All targets were later expressed in the found optimal conditions in medium-scale cell cultures. The expression levels of targets obtained were in all cases high enough to allow purification trials. Trends with regard to successful combinations of cell lines and media at different temperatures were identified and can be used to optimise the starting parameters of the screen (see section 3.7).

The question arises, why one should actually screen for conditions and not simply express all targets in the most successful condition, as for example the one identified by this screen? Examining the fluorescence data of Fig. 3.10, reveals that if all targets had been exclusively expressed in the cell line Rosetta(DE3)pLysS grown in SB medium at

25 °C, only four of the identified promising targets would have been found. However PgpB, one of the targets that yield diffracting crystals, would possibly not have been identified as promising target. PgpB is expressed in the above condition at a level nearly five-fold lower than in the determined optimal condition. Therefore, the screening of expression conditions proved to be a valuable tool to overcome the first bottleneck of membrane protein structural biology.

In contrast to the required screening for protein expression, a more restricted approach in the purification of membrane proteins is preferable. The chances are quite high that some of the tested targets will be stable in solution when solubilised with DDM. Once the promising targets are in crystallisation trials, the nucleation of protein crystals and crystal growth can require times from days to weeks or even months and the work on the remaining targets can continue in the meantime. Therefore the aim of the purification pipeline employed, was to find the targets that can be purified to monodispersity and submit these targets to crystallisation trials as fast as possible. Work on targets that precipitated heavily or completely in one of the purification steps, especially the TEVP cleavage, was halted until all targets were tested.

Two targets, PgpB and Lgt were monodisperse in solution with DDM, following the final size exclusion chromatography. PgpB was submitted to crystallisation trials. The protein yield of Lgt was too low to set up crystallisation trials. Lgt did not precipitate throughout the entire purification, therefore optimising the expression yield is required. The parameters of the small-scale HTP screen should be altered to find better expression conditions for Lgt.

On-column detergent exchange was successful for the three targets XylH, ChbC and YdhC, and their monodisperse samples were submitted to crystallisation trials. One of those targets, XylH, crystallised. Work focussed then on the two targets PgpB and XylH that had crystallised and their purification protocol was optimised. Protein yields for XylH could, for example, be doubled through the use of desalting columns instead of dialysis tubing. Finally, diffracting crystals of the two membrane proteins PgpB and XylH were obtained, showing that it is possible to find promising targets with HTP methods and with the restriction on certain parameters. At the time of writing, PgpB crystals were reproduced and optimised, leading to higher resolution (in-house).

The accumulated data from expression and purification can be analysed for trends. Table 6.1 shows next to the molecular weight, number of transmembrane domain helices and the rank in medium-scale expression, the purification status reached for each target. Furthermore, the purification steps, in which precipitation was observed are listed together with the detergents used and the suggested future strategy for each target.

	MW (kDa)	TMD H	Expr. rank.	Purification step	Precip.	Detergent	Future strategy
Unstable targets							
XylE	53.4	12	1	Cleavage	A/D/C	DDM	Detergent screening
CcmC	27.7	6	3	2 nd column	D/C	DDM	Detergent screening
FtsX	38.4	4	11	Cleavage	C	DDM	Detergent screening
YdeD	32.1	10	12	1 st column	A	DDM	Detergent screening
YhbE	34.8	10	9	1 st column	A	DDM	Detergent screening
Stable targets							
CodB	43.5	12	5	2 nd column	D/C	DDM	Optimise purification
PnuC	27.0	6	7	Cleavage	D/C	DDM	Optimise purification
Promising targets							
Lgt	33.0	5	8	Gel filtration	None	DDM	Increase yield
XylH	41.0	10	10	Gel filtration	C	DDM/FC-14	Crystals
ChbC	48.2	10	6	Gel filtration	C	DDM/Cymal-5	Crystall. screens
PgpB	28.8	6	2	Gel filtration	D/C	DDM	Crystals
YdhC	43.2	12	4	Gel filtration	D/C	DDM/FC-14	Crystall. screens

Table 6.1: Comparison of target properties with expression and purification performance. The targets are grouped according to their stability in DDM in solution. TMDH: transmembrane domain helices; Ranking when expressed in medium-scale cultures; Purification step reached in purification pipeline; Precipitation: A = affinity column, D = dialysis, C = cleavage; The future strategy describes the steps for each target in order to increase stability in solution, purification to monodispersity, crystallisation trials or the optimisation of crystals.

The identification of trends in relation to physical properties, such as size or the number of transmembrane helices, to the expression and purification behaviour, would be useful to refine the selection criteria for target proteins. However, the ranking as promising or unstable target shows no trends with the different molecular weights or the number of transmembrane domain helices. The group of promising targets has nearly the same size distribution as the group of unstable targets and with PgpB the second smallest and with XylH the third largest target crystallised. In addition, no correlation was observed with

the physical properties of the membrane proteins and their ranking in the medium-scale expression. Therefore, the expression and purification behaviour in the group of tested targets, is entirely target specific and needs to be screened and optimised. This is in accordance with the findings of structural genomics projects as discussed in the previous Chapters.

The accumulated data on the targets gives a good base for future work. After the work on the most promising targets is completed, or if time allows in between, the targets in the purification pipeline are examined in the order from its end back to the beginning. Starting with the targets that did not crystallise, despite being purified to monodispersity, more detergents should be screened with on-column detergent exchange. The stable targets in DDM of Table 6.1, CodB and PnuC, would require the optimisation of the purification protocol to reduce precipitation. The group of membrane proteins, which were found to be unstable when solubilised with DDM, should be screened for a better solubilisation detergent for purification. However, the targets YdeD and YhbE show very low expression levels and a new run of the small-scale expression screen with different conditions would be required.

Chapter 7

Appendix

7.1 DNA and protein sequences

7.1.1 CcmC

7.1.1.1 DNA sequence

ATGTGGAAAACACTGCATCAACTGGCGATCCCACCACGGCTGTCAAATCTGTGGCTGGTT
TATACCGTGGCTGGCAATTGCCAGTGTGGCTGCTTACCGTCGGCTGGATCTGGGATTG
GCTTGCTCCGGCTGATTATCAGCAGGGAAATAGCTACCGCATTATCTACCTGCATGTGCCT
GCGCGATCTGGTCGATGGCATTATGCATCAATGGCAGTGGCAGCGTTATTGGCCTTGT
CTGGCAGATGAAAATGCCAACCTGGCGGTGGCGCATGGCCCCATTGGTGCCGTGTTA
CCTTATTGCCCTGGTTACCGGCTCTGCATGGGAAAACCGATGTGGGCACCTGGTGGGTA
TGGGATGCACGTCTGACTTCTGAAGTGGTCTGCTGTTTGTATGTGGGTGTGATTGCCCTG
TGGCACGCCCTCGACGACCGCCGTCTGGCGGGCGTGCAGGTATCCTGGTCTGATTGG
CGTGGTGAATCTGCCGATTATTCACTCCGTGGAGTGGTGGAACACCCCTGCATCAGGGAT
CAACCGCGATGCAGCAAAGTATCGATCCGGCATGCGTCCGCGTGCCTGGTCGATTGG
GGCTTCCTGCTCCTGTCTGCCACGCTGACGCTGATGCGGATGCGTAATTGATTGCTGATG
GAAAAACGCCGTCCGTGGGTGAGTGAAGTGAACTGATACTGAAAAGAGGCCGTAAATGA

7.1.1.2 Protein sequence

MWKTLHQLAIPRRLYQICGWIFPWLAIASVVVLTVGWIWGFAPADYQQGNSYRIIYLHVPAI
WSMGIYASMAVAAFIGLVWQMCKMANLAVAAMAPIGAVFTFIALVTGSAWGKPMWGTWWVV
DARLTSELVLLFLYVGVIALWHAFDDRRLAGRAAGILVLIGVVLPIHYSVEWWNTLHQGSTR
MQQSIDPAMRSPLRWSIFGFLLSATLTLMRMRNLILLMEKRRPVVSELILKRGKRK

7.1.2 CodB

7.1.2.1 DNA sequence

ATGTCGCAAGATAACAACTTAGCCAGGGGCCAGTCCCGCAGTCGGCGCGAAAGGGGTAT
TGGCATTGACGTTCGTCATGCTGGATTAAACCTCTTTCCGCCAGTATGTGGACC GGCGCA
CTCTCGGAACCGGTCTTAGCTATCATGATTCTCCTCGCAGTCTCATCGTAATCTTCCT
CGGTATTACACTTCATTCTCGGTTACATTGGCGAAAAACCGGCCTGACCACTCATCTTCT
TGCTCGCTCTCGTTGGTGTAAAGGCTCATGGCTGCCTCACTGCTACTGGCGGAACCTCA
GGTGGCTGGTTGGCGTCGGTGTGGCGATGTTGCCATTCCGGTGGTAAGGCAACCGGGC
TGGATATTAATTGCTGATTGCCGTTCCGGTTACTGATGACCGTCACCGTCTTTTGGCAT
TTCGGCGCTGACGGTTCTTCGGTGATTGCGGTCCGGCTATGCCCTGCCTGGCGGTATT
CGTGTGGCTGGCTGTTAACGGCATGGCGGCCTGGACGCATTAAAAGCGGTGTTCCGCAC
AACCGTTAGATTCAATGTCGCGCTGGCGCTGGTTGTGGGTCAATTATCAGTCGGGTACG
CTCACCGCTGACTTGTCCGGTTGGTCGCAATGCCAAACTGGCGGTGCTGGTGGCGATGGT
GGCCTTTCTCGCAACTCGTGATGTTATTTCGGTGAGCAGGGCGCTCGGCACTGGG
CATGGCGGATATCTGTGATGATTGCTCAGGGCCTGCTGCCTGCGATTGTGGTGCT
GGGCTGAATATCTGGACCACCAACGATAACGCACACTATCGCTGGGTTAGGTTCGCCA
ACATTACCGGGATGTCGAGCAAACCCCTTCGTAATCAACGGTATTATCGGTACGGCTGC
GCATTATGGCTGTATAACAATTGTCGGCTGGTGACCTTCGGCAGCTATTCCCTCCA
GTGGGTGGCGTGATCATGCCGACTATCTGATGAACCGTCGCCGCTATGAGCACTTGC
CACCGTGATGATGAGTGTCAATTGGTGGCGATTCTGGCGGTGCCCTGGGATTGCTGCAG
GCCACTGGTTACCGGGATTGTCGCAACCGGTATTAGGTGGCGCGCTGAGCTATCTG
ATCCTAACCGATTGAAATCGAAAACGACAGCAGCAATGACGCATGTGGAGGCTAAC
GTGTCGAATAA

7.1.2.2 Protein Sequence

MSQDNNFSQGPVPQSARKVLALTFVMLGLTFFSASMWTGGTLGTGLSYHDFFLAVLIGNLLG
IYTSFLGYIGAKTGLTTHLLARFSFGVKGWSWPSLLLGGTQVGWFGVGVAMFAIPVGKATGLDIN
LLIAVSGLLMTVTVFFGISALTVLSVIAVPAIACLGGYSVWLAVNGMGLDALKAVVPAQPLDF
NVALALVVGSFISAGTLTADFVRFRNAKLAFLVAMVAFFLGNSLMFIFGAAGAAALGMADISD
VMIAQGLLPAIVVGLNIWTTNDNALYASGLGFANITGMSSKTLSVINGIIGTVCALWLYNNFV
GWLTFLSAAIPPVGGVIADYLMNRRRYEHFATTRMMSVNWVAILAVALGIAAGHWLPGIVPVN
AVLGGALSYLILNPILNRKTTAAMTHVEANSVE

7.1.3 FtsX

7.1.3.1 DNA sequence

ATGAATAAGCGCGATGCAATCAATCATATTGGCAGTTGGCGGGCGTCTGATCGCTCCG
TAAATCGGTGGCGGCTCAGGCACGGCGGTCTAACGCACCAAAACGCGCAAATCCTCG
CCAAAACCGTAAATCGCAAAACCAACGTTCAACGAACAGGTGCGCTATGCCCTCACGG
CGCATTGCAGGATCTGAAAAGCAAACCGTTGCCACGTTTAACGGTGATGGTTATGCCA
TTTCTCTGACGCTGCCAGCGTCTGTTATATGGTGACAAAAACGTTAACCAAGCGGCGACG
CAGTATTATCCGTACCGCAAATCACTGTTATCTGCAAAAAACGCTGGACGATGACGCTGC
TGCAGGGCGTGGTGGCACAGTTGCAGGCCAGCAAGGCAGTGGAGAAAGTGAACATCTTCT
CGTGAAGACGCACTGGGTGAGTTCCGTAACTGGTCTGGTTGGTGGTGCCTGGATATGCT
GGAAGAAAACCGCTCCGGCAGTGGCGGTGGTACCGAAACTCGATTCCAGGGGACG
GAATCACTGAATACGCTGCGTACGTATCACGAGATTACGGCATTGACGAAGTGCAGGAT
GGATGACAGCTGGTTGCCCGTCTGGCGCGTTGACCGGGCTGGTCGGCGCTGGATTCGGCGA
TGATCGGCGTGGTGTGATGGTGGCGCCGTGTTCTCGTACCGTAACAGTGTGCGTCTGAGT
ATCTTGCTCGCCGTGACTCCATTAACGTACAGAAACTGATTGGTGCACAGATGGATTCAT
CCTGCGCCCGTCTGTATGGTGGCGCACTGCTGGGATTCTGGCGCATTGTTGTCATTAAT
TTTGTCAAGAAATTCTGGTGTGCGATTGTCATCGCGGTGCGGAAGTGGCACAGGTTTCG
GAACGAAGTTGATATCAATGGCTTATCATTGATGAATGCCTGCTATTGCTGCTGGTATGCT
CGATGATTGGCTGGGTGGCAGCGTGGCTGCCACGGTACAACATTACGCCACTTACGCC
GAATAACTGGATCCGAAAACCTGTACTTCCAGGGTCAATTCAAGCAAAGGAGAAGAACCTTC
ACTGGAGTGGTCCCAGTTCTGTTGAATTAGATGGCGATGTTAATGGCAAAATTCTCTGT
CAGTGGAGAGGGTGAAGGTGATGCAACATACGGAAAACCTACCGCTTAATTGCTGCTGGT
CTGGGAAGCTACCTGTTCCATGGCAACACTGTCACTACTTCTCTTATGGTGTCAATGCT
TCTCAAGATACCCAGATCATATGAAACAGCATGACTTTCAAGAGTGCCTGCCCCGAAGGT
TATGTACAGGAAAGAACTATTTACAAAGATGACGGAAACTACAAGACACGTGCTGAAG
TCAAGTTGAAGGTGATACCCTGTTAATAGAATCGAGTTAAAGGTATTGATTTAAAGAA
GATGGAAACATTCTGGACACAAAATGGAATACAACACTACACATAATGTATACATCAT
GGGAGACAAACCAAGAATGGCATCAAAGTTAACCTCAAAATTAGACACAACATTAAAGAT
GGAAGCGTTCAATTAGCAGACCATTATCAACAAAATCTCAATTGGCGATGGCCCTGTCCT
TTTACCAACCAACCATTACCTGTCACACAATCTGCCCTTCCAAGATCCCAACGAAAAGA
GAGATCACATGATCCTCTTGAGTTGTAACAGCTGCTAGGATTACACATGGCATGGATGAG
CTCTACAAAAAGCTGCGGCCATCATCATCACCAACCACCAACTGA

7.1.3.2 Protein sequence

MNKRDAINHIRQFGGRLDRFRKSVGSGDGRNAPKRAKSSPKPVNRKTNVFNEQVRYAFHGA
LQDLKSKPFATFLTVMVIAISLTPSVCYKVNQAAATQYYPSHQITVYLQKTLDDDAAGV
VAQLQAEQGVEKVNYLSREDALGEFRNWSGFGGALDMLEENPLPAVAVVIPKLDFFQGTESLN
LRDRITQINGIDEVRMDDSWFARLAALTGLVGRVSAMIGVLMVAAVFLVIGNSVRLSIFARRDSI
NVQKLIGATDGFLRPFLYGGALLGFSGALLSLILSEILVRLSSAVAEVAVQVFGTKFDINGLSFDE
CLLLLVCMSMGWVAAWLATVQHLRHFTPE

7.1.4 Lgt

7.1.4.1 DNA sequence

ATGACCAGTAGCTATCTGCATTTCCGGAGTTGATCCGGTCATTTCTCAATAGGACCCGTG
GCGCTTCACTGGTACGGCCTGATGTATCTGGTGGGTTCATTTGCAATGTGGCTGGCAACA
CGACGGGCGAATCGTCCGGGCAGCGGCTGGACCAAAATGAAGTTGAAAACCTACTCTATG
CGGGCTTCCTCGCGTCTTCCTCGGGGACGTATTGGTTATGTTCTGTTCTACAATTCCCGC
AGTTTATGGCGATCCGCTGTATCTGTCGTCTGGGACGGCGCATGCTTCCACGGCG
GCCTGATTGGCGTTACGTGGTGTGATTATCTCGCCCCCGTACTAACGTTCTTCTCC
AGGTCTCTGATTATCGCACCACTCATTCCGTTGGTCTGGTGCCGGCGCTGGCAACT
TTATTAACGGTGAATTGTGGGCCCGCTGACCGAACCTCCGTTGCCATGCTGTTCCCTG
GCTCCCGTACAGAAGATATTGCTGCTGCAAACCAACCCGAGTGGCAATCCATTTCGAC
ACTTACGGTGTGCTGCCGCCACCCATCACAGCTTACGAGCTGCTGCTGGAAGGTGTGGT
GCTGTTATTATCCTCAACCTGTATATCGTAAACCACGCCAATGGGAGCTGTCAGGTTT
GTTCCCTGATTGGTTACGGCGCGTTCGCATATTGAGTTTCCGCCAGCCGACCGCA
GTTTACCGGTGCCTGGGTGCAGTACATCAGCATGGGCAAATTCTTCCATCCGATGATTG
TCGCGGGTGTGATCATGATGGTCTGGCATATCGTCGCAGCCCACAGCAACACGTTCTGA

7.1.4.2 Protein sequence

MTSSYLHFPEFDPVIFSIGPVALHWYGLMYLVGFIFAMWLATTRANRPGSGWTKNEVENLLYAG
FLGVFLGGRIGYVLFYNFPQFMADPLYLFRVWDGGMSFHGLIGVIVVMIIARRTKRSFFQVSD
FIAPLIPFGLGAGRLGNFINGELWGRVDPNFPFAMLFGPSRTEDILLQTNPQWQSIFDTYGVLP
HPSQLYELLLEGVVLFIILNLYIRKPRPMGAVSGLFLIGYGAFRIIVEFFRQPDAQFTGAWVQYISM
GQILSIPMIVAGVIMMVWAYRRSPQQHVS

7.1.5 PnuC

7.1.5.1 DNA sequence

ATGGATTTTTAGTGTGCAGAATATCCTGGTACATATAACCAATAGGGCAGGCGGTATGA
TCTCTCATGGATCGAACCGGTTAGGCACGATGCCGGGTTGCTGTATTGGCCTGCCAGTC
TGGAGAACATCAGCAACTACTTCTTGGCCTGATCAACGTCACCTGTTGGCATTATTTCT
TTCAGATTCACTGCTATGCCAGCCTGCTATTACAGGTGTTTCTTGCCGCAATATTACG
GTTGGTATGCGTGGCGACAAACCAGTCAGAACGAGGCGGAGTTGAAAATTGCTGGTT
GCCATTGCCGAAGGCACTCAGCTGGTGGCGGTTGCGTTGTTGATTGGCTGATGACGG
TATTATCAATCCGGTGTTCGCATTTGACCCCGTGGCAGTCATGATCATGCAAGCATTAG
GATTACAGGTTGTGATGCCCTGAACTGCAACCGGACGCTTCCCCTGTTGATTGATGCATG
ATGGTGTATCTATCGTGGCAATGATTCTGATGACCGTAAGTATGTGGAAAATGGCTGTT
GTGGGTGATTATTAACGTGATTAGCGTCGTTATTTGCACTTCAGGGCGTTACGCCATGTC
TCTGGAGTACATCATCCTGACCTTATTGCGCTAACGGCAGCCGGATGTGGATCACAGCG
CACGTGAAAGAGGCTCACGCGCGCTGTCCTAA

7.1.5.2 DNA sequence

MDFFSVQNILVHIPIGAGGYDLSWIEAVGTIAGLLCIGLASLEKISNYFFGLINVTLFGIIFQIQLYA
SLLLQVFFFANANIYGWYAWSRQTSQNEAELKIRWLPLPKALSWLAVCVVSIGLMTVFINPVFAFL
TRVAVMIMQMQLGLQVVMPELQPDAFPFWDSCMMVLSIVAMILMTRKYVENWLLWVIINVISVV
IFALQGVYAMSLEYIILTFIALNGSRMWINSARERGSRALSH

7.1.6 XylE

7.1.6.1 DNA sequence

ATGAATAACCCAGTATAATTCCAGTTATATTTCGATTACCTAGTCGCTACATTAGGTGGT
TTATTATTGGCTACGACACCGCCGTTATTCCGGTACTGTTGAGTCACTCAATACCGTCTT
GTTGCTCCACAAAACCTTAAGTGAATCCGCTGCCAACTCCCTGTTAGGGTTTGCCTGGCCAG
CGCTCTGATTGGTTGCATCATCGCGGTGCCCTCGGTGGTTATTGCAGTAACCGCTTCGGTCG
TCGTGATTCACTTAAGATTGCTGCTGTCCTGTTTTATTCTGGTGTAGGTTCTGCCTGGCCA
GAACCTGGTTTACCTCTATAAACCCGGACAACACTGTGCCCTGTTATCTGGCAGGTTATGTC
CCGGAATTGTTATTATCGCATTATTGGCGGTATTGGCGTTGGTTAGCCTCAATGCTCTCG
CCAATGTATATTGCGGAACGGCTCCAGCTCATATTGCGGGAAACTGGTCTCTTTAACCA
GTTTGCATTATTTCGGCAACCTTAGTTACTGCGTAAACTATTTATTGCCCCGTTCCGGT
GATGCCAGCTGGCTGAATACTGACGGCTGGCGTTATATGTTGCCCTCGGAATGTATCCCTGC
ACTGCTGTTCTTAATGCTGCTGTATACCGTGCCAGAAAGCCTCGCTGGCTGATGTCGCG
GCAAGCAAGAACAGGCAGGAAAGGTATCCTGCGAAAATTATGGGCAACACGCTTGCAACTCA
GGCAGTACAGGAAATTAAACACTCCCTGGATCATGGCCGAAAACCGGTGGCTGCTGCTG
ATGTTGGCGTGGCGTGATTGTAATCGCGTAATGCTCTCCATCTTCAGCAATTGTCG
ATCAATGTGGTGTGACTACGCGCCGGAAGTGTCAAACGCTGGGGCCAGCACGGATA
TCGCGCTGTTGCAGACCATTATTGTCGGAGTTATCACCTCACCTCACCGTTCTGGCAATT
TGACGGTGGATAAAATTGGTCGTAAGCCACTGCAAATTATCGCGCACTCGGAATGGCAATC
GGTATGTTAGCCTCGGTACCGCGTTTACACTCAGGCACCGGGTATTGTGGCGTACTGTCG
ATGCTGTTCTATGTTGCCGCTTGCCATGTCCTGGGTCCGGTATGCTGGTACTGCTGTCG
GAAATCTCCCGAATGCTATTGCGTAAAGCGCTGGCAATCGCGTGGCGGCCAGTGGCT
GGCGAACTACTCGTCTCCTGGACCTCCGATGATGGACAAAAACTCCTGGCTGGCG
ATTTCACACGGTTCTCCTACTGGATTACGGTTGTATGGCGTTCTGGCAGCACTGTTA
TGTGGAAATTGTCGGAAACCAAAAGGTAAAACCGTGTAGGAGCTGGAAGCGCTGGGA
ACCGGAAACGAAGAAAACACAACAAACTGCTACGCTGTAA

7.1.6.2 Protein sequence

MNTQYNSSYIFSITLVATLGGLLFGYDTAVISGTVESLNTVFVAPQNLSESAANSLLGFCVASALI
GCIIGGALGGYCSNRFGRDRSLKIAAVLFFISGVGSAWPELGFTSINPDNTPVYLAGYVPEFVIY
RIIGGIGVGLASMLSPMYIAELAPAHIRGKLVSFNQFAIFGQLLVYCNYFIARSGDASWLNTDG
WRYMFASECIPALLFLMLLYTVPESPRWLMRSRGKQEQAEGILRKIMGNTLATQAVQEIKHSLDH
GRKTGGRLLMFGVGIVIGVMLSIFQQFVGINVVLYYAPEVFKTLGASTDIALLQTIIVGVINLTFT
VLAIMTVDKFGRKPLQIIGALGMAIGMFSLGTAFYTQAPGIVALLSMLFYVAAFAMSWGPVCWV
LLSEIFPNAIRGKALAIAVAQQWLANYFVSWTFPMMDKNSWLVAHFHNGFSYWIYGCMGVLA
LFMWKFVPETKGKTLLEEALWEPETKKTQQTATL

7.1.7 XylH

7.1.7.1 DNA sequence

ATGTCGAAAAGCAATCCGTCTGAAGTGAATTGCCGTACCGACATCCGGTGGCTTCCGG
GCTGAAATCACTGAATTGCAGGTCTCGTATGATTGCAGCTATCATCGCAATCATGCTGTT
CTTACCTGGACCACCGATGGTGCCTACTTAAGCGCCGTAACGCTCTCCAACCTGTTACGCC
AGACCGCGATTACCGGCATCCTCGCGTAGGAATGGTGTTCGTATAATTCTGCTGAAATC
GACCTTCGGCTCAATGATGGGCTGTTAGGTGGCGTCGCGCGATTGTGACGTCTG
GTTAGGCTGGCCTTGCCACTTACCATCATTGTGACGCTGGTCTGGACTGCTCTCGGTGC
CTGGAACGGATGGTGGGTCGCGTACCGTAAAGTCCCTCATTATTGTCACCCCTCGCGGGCA
TGGTGGCATTCGCGGCATACTCATTGGCATCACCAACGGCACGACTGTATCCCCCACCAGC
GCCCGATGTCACAAATTGGCAAAGCTATCTCCCCGCCAGTACCGGCTTCATATTGGCGC
GCTTGGCTTAATGGCTTTGGTGGCAATGGCGCGGAAGAATGCGCCGTAGGCTTACCGCTATCATCGTAT
GTTTACAGTCTCCGGCCTCTACCGCAGTAGTCGGTGCAGGCTTAACCGCTATCATCGTAT
TAGGCGCAATCTGGCTGTTGAATGATTACCGTGGCGTCCACTCCTGTTGCTGCTGACGT
TGCTGTTACTCGGCGGAATGTTATGGCAACCGGACGGCATTGGACGACGCATTATGCC
ATCGGCGGAATCTGGAAGCAGCACGCTCTCCGGATTAAACGTTGAACGCACCAAACCTGC
CGTGGTCCGATTAAACGGATTAAATGGTAGCCATGCCGGATTAAATCCTAGTTCTGACTTGG
CGCTGGTTCACCTCTGCCGGAAATATGCCGAACTGGACGCAATTGCAGCATGCGTGATTG
GCCGACCAGCCTGGCTGGCGGTGGGAAGCGTTGCCGGAGCAGTAATGGGGCATTAT
CATGGCTTCACTGGATAACGGCATGAGTATGATGGATGTACCGACCTCTGGCAGTATATCG
TTAAAGGTGCGATTCTGTTGGCAGTATGGATGGACTCCGCAACCAACGCCGTTCTGA

7.1.7.2 Protein sequence

MSKSNPSEVKLAVPTSGGFSGLKSLSNLQVFVMIAIIIAIMLFFTWTTDGAYLSARNVSNLLRQTAI
TGILAVGMVFVIISAEIDLGVGSMMGLGGVAAICDVWLWPLPLTIVTLVLGLLLGAWNGWW
VAYRKVPSFIVTLAGMLAFRGILIGITNGTTSPSAAMSQIQSYLPASTGFIIGALGLMAFVGW
QWRGRMRRQALGLQSPASTAVVGRQALTAAIVLGAIWLLNDYRGVPTPVLLTLLLGGMFMA
TRTAFGRRRIYAIGGNLEAARLSGINVERTKLAVFAINGLMVAIAGLILSSRLGAGSPSAGNIAELD
AIAACVIGGTSAGGVGSVAGAVMGAFIMASLDNGMSMDVPTFWQYIVKGAILLA威MDS
ATKRRS

7.1.8 YdeD

7.1.8.1 DNA sequence

ATGTCGCGAAAAGATGGGTGTTGGCGCTACTGGTAGTGGCGTATGGGGCTAAATTGT
GGTCATCAAAGTGGGCCTCATAACATGCCACCGCTGATGCTGGCCGGTTGCGCTTATGC
TGGTCGCTTCCGGCTATCTTTGTCGCACGACCGAAAGTACCACTGAATTGCTGCTGG
GGTATGGATTAACCATCAGTTGCGCAGTTGCTTTCTTTTGCCATTAACCTCGGTAT
GCCTGCTGGACTGGCTTCGCTGGTACAGGCACAGGCCTTTACTATCATGCTGGCGC
GTTTACTTCGGGGAGCGACTGCATGGCAAACAATTGGCGGGATGCCTAGCGATTTTG
GCGTACTGGTGTAAATCGAAGATAGTCTGAACGGTCAGCATGTGGCGATGCTGGCTTATG
TTGACCCCTGGCGGCAGCATTAGTTGGCGTGTGGCAACATCTCAATAAAAGATCATGTC
GCACTCAACCGTCCGGCGGTGATGTCGCTGGTAATCTGGAGCGCTTAATCCAATCATTC
CCTTCTTGTGCCTCGCTGATTCTCGATGGTCCGCAACCATGATTCACAGTCTGGTTACTA
TCGATATGACCACCATCTTGTCTCTGATGTATCTGGCGTTGTGGCGACAATTGTTGTTATG
GGATCTGGGGACGTTACTGGGACGCTATGAAACCTGGCGGGTTGCACCGTTATGTTACTG
GTGCCCGTAGTAGGACTGGCAAGTGCAGCACTATTGTTGGATGAACGCTTAACGGGTCTGCA
ATTTTAGGTGCGGTGCTCATTATGACCGGGCTGTATATCAATGTATTGGCTGCGGTGGCG
TAAAGCGTAAAGGTGGAAAGTTAA

7.1.8.2 Protein sequence

MSRKDGVLALLVVVVWGLNFVVIKVGLHNMPPLMLAGLRFMLVAFPAIFFVARPKVPLNLLG
YGLTISFAQFAFLFCAINFGMPAGLASLVLQAQAFFTIMLGAFTFGERLHGKQLAGIALAIFGVLV
LIEDSLNGQHVAMLGFMLTLAAAFSWACGNIFNKKIMSHSTRPAVMSLVIWSALIPIPFFVASLIL
DGSATMIHSLVTIDMTTILSLMYLAFVATIVGYGIWGTLLGRYETWRVAPLSLLPVVGLASAAL
LLDERLTGLQFLGAVLIMTGLYINVGLWRKAVKVGs

7.1.9 ChbC

7.1.9.1 DNA sequence

ATGAGTAATGTTATTGCATCGCTTGAAAAGGTACTCCTCCCTTGCAGTAAAGGAAA
GCAGGCCACACGTTAATGCAATCAAAATGGCTTATTGCTTAATGCCGTTAACCTGCGG
GGGCCATGTTGATTAATTAACAACGTTCTAAGCTTGGGGAGGGTCGTTTTTATT
CCTTAGGTATTGCCTCGACGCCTCAACCATTGAAACACTTAATGGTCTGAAAGGTATTGGC
GGCACGTATATAACGGAACATTAGGAATAATGTCTTAATGGCACCGTTTATTGGCAT
GGCGCTGGCAGAAGAGCGTAAAGTCGATGCGCTGGCGCTGGGTTGTTATCCGTTGCAGCAT
TTATGACCGTCACCCATATAGTCGGTGAGGCCTATCGGGTGGTCAAACACTGGTTAGGT
GGGGCGAATATCATCTCCGGATTATTATTGGCCTGGTGGCAGAAATGTTACCTTATT
GTCCGCCGCAATTGGGTATTAAACTGCCGACAGCGTACCTGCTTCAGTATCGCTTCCCTC
TCGGCATTAAATTCCGGTTATTATTCTTCCGTATGGGATTATTGCCCTGGCGTTGAAT
ACCTGGGGCACCAACTCCATCAGATCATTATGGATACCACCTCAACCCCACGGCATCGTT
GGGTAGCGTGGTGGCTGGCCTATGTGATCTTGTCCACTGCTCTGGTTCTCGGTATTCA
TGGCGCGCTGGCGCTGACCGCACTGGACAACGGCATTATGACGCCGTGGCACTGGAAAAT
ATCGCGACCTATCAGCAATATGGTCCGTCGAAGCGCGCTGGCAGCGGTAAAGACCTTCCA
TATCTGGCCAAGCCGATGCTGGACTCCTTATTTCCTGGGGCAGTGGTGCAGCTTAGG
CCTGATCCTGGCTATCTTATGCCCTCGCGTGCTGATTATCGTCAGGTGGCAAATTATCATGAA
GCTGCCGTCCGGCATCTCCAGATTAACGAACCGATTCTGGCGCAATCACCCTCGCAGC
CCCGGTGATGTTATCCGTTACTGGTACAACCGATTCTGGCGCAATCACCCTCGCAGC
GTACTACATGGCATTATTCCCTCCGGTGACCAATTGACCGTGGACCATGCCAACCGGTC
TGGGAGCCTTCTTAACACCAACGGTAGCGTCGCCGATTGCTGGTGCACCTTCAACCTTG
GCATCGCAACGTTAATTATGCCCTTGTGGCTAACAAAGCACAAATGCGATT
GATAAAGAAGAGAGCGAAGAAGATATCGCTAACGCCCTGAAATTAA

7.1.9.2 Protein sequence

MSNVIASLEKVLLPFAVKIGKQPHVNAIKNGFIRLMPLTLAGAMFVLINNVFLSFGEFSFFYSLGI
RLDASTIETLNGLKIGGNVYNGTLGIMSLMAPFFIGMALAEERKVVDALAAGLLSVAAFMTVTP
YSVGEAYAVGANWLGGANIISGIIIGLVVAEMFTFIVRRNWVIKLPDSVPASRSFSALIPGFIILS
VMGIIAWALNTWGTNFHQIIMDTISTPLASLGSVVGWAYVIFVPLLWFFGIH GALALTALDNGIM
TPWALENIATYQQYGSVEAALAAGKTFHIWAKPMLDSFIFLGSGATLGLILAIFIASRRADYRQ
VAKLALPSGIFQINEPILFGLPIIMNPVMFIPFVLVQPILAITLAAYYMGHIPPVTNIAPWTMPTGLG
AFFNTNGSVAALLVALFNLGIATLIYLPFVVVANKAQNAIDKEESEEDIANALKF

7.1.10 PgpB

7.1.10.1 DNA sequence

ATGCGTTGATTGCCAGACGTACCGCAGTGGAGCTGCACATTGCTTGTATGCCAGTAGC
CGTATGGATTCTGGCTGGCGTTGGCAACCTGGAGAACAAAGTTGGCTACTAAAAGCGGCTT
TTGGGTTACTGAAACTGTACCCAGCCCTGGGGCGTCATTACACATTGATTTATCGGCT
GGTTTCTCTGGTGTCTCGTTCGCATTAAGGCTGCCTTGATTATTCGCCATTCTGGCGGC
CGCAATCCTTGTGGACAAGGCCTAAATCCTGGATCAAAGACAAAGTCCAGGAACCACGA
CCTTTGTTATCTGGCTGGAAAAAACACATCATATTCCGGTTGATGAGTTCTACACTTAAAG
CGAGCAGAACCGCGAAATCTAGTGAAAGAACAGTTGGCTGAAGAGAAAAATATCCCACAAT
ATTTGCGTTCACACTGGCAGAAAGAGACGGGGTTGCCTTCCTCCGGTCACACGATGTTT
GCTGCCAGTTGGCACTGCTGGCCGTTGGCTGTGGCCCGTCGGCGAACGTTAACCAT
TGCTATCTGCTGGCTGGCAACGGGAGTCATGGGAAGCCGCTGCTCGGGATGCATT
GGCCACCGCGATCTGGTAGTAGCTACGTTGATTCGTGGCGCTGGTGGCGGTGGCAACGTGG
CTTGCACACGAATTGTGGGCCATTAACACCACCTGCGGAAGAAAATCGCGAAATAGCGC
AACGAGAACAGAAAGTTAA

7.1.10.2 Protein sequence

MRSIARRTAVGAALLVMPAVWISGWRWQPGEQSWLLKAAFWVTETVTQPWGVITHLILFG
WFLWCLRFRIKAAFVLFAILAAAILVGQGVKSWikDKVQEPRPFVIWLEKTHHIPVDEFYTLKRA
ERGNLVKEQLAEEKNIPQYLRSHWQKETGFAPSHTMFAASWALLAVGLLWPRRRTLTIAILL
VWATGVMGSRLLMHWPRDLVVATLISWALVAVATWLAQRICGPLTPPAEENREIAQREQES

7.1.11 YhbE

7.1.11.1 DNA sequence

ATGAAGCAGCAGGCAGGCATTGGCATTCTTGGCGCTCACACAGCAATTGCTGGGGGC
GTTGCCAATCGCAATGAAGCAGGTGCTGGAGGTGATGGAACCTCCGACAATCGTGTTCACC
GTTTCTTGATGGCGAGTATTGGCTGGGTGCCATTCTGCGGTGAAGAAGAGGTTGCCGCCA
TTACCGTGTTCGTAAGCCACGCTGGTTGATTGTTGGCAGTGGCGACCGCCGGCTGTT
GGGAACCTCATCCTGTTCACTCAGCTCATCCTGCAATACCTGAGTCCGACCGCTCGCAGGTGATT
GGGCAACTCTCGCCAGTTGGCATGATGGTGCCAGCGTATTATCCTCAAAGAGAAAATGCG
CAGCACTCAGGTTGAGGGCATTGATGCTCCTGAGCGGCCTGGTGTGATGTTTTAACACCA
GTCTGGTCGAGATATTACAAAGCTCACCGATTACACCTGGGAGTTATCTTGGGTCGGT
GCGCGACGGTTGGGTGAGTTATGGCGTGGCGAAAAGGTTTATTGCGTCGGCTGGCCTC
ACCGCAGATCCTGTTTACTGTACACTTATGTACAATTGCGCTTCCCTGGCAAAGCC
TGGAGTGTAGCGCAGCTTAGCCACTGGCAGCTCGATGTTAATTGGCGACTGAATA
CCTTGGTAGGATATGGCGCCCTGGCGGAAGCGATGGCTCGCTGGCAGGCAGCGCAGGTGAG
CGCGATCATCACGCTACCCACTGTTACGCTGTTTCAGATCTTATCACTGGCCTG
GCCGATTCTCGCCAGACCGATGTTAACCTTTAGGTATCTGGTGCCTTGTGTT
TGCAGGCGCGATGTATTCCGCCATTGGTCATCGTATTGGGCGGATTACGTAAGCATACAA
CGGTGGTATCGCAACCCCGCGCAGGCGAATGA

7.1.11.2 Protein sequence

MKQQAGIGILLALTTAICWGALPIAMKQVLEVMEPPTIVFYRFLMASIGLGAILAVKKRLPPLRVF
RKPRWLILLAVATAGLFGN FILFSSSLQYLSPTASQVIGQLSPVGMMVASV FILKEKMRSTQVVG
ALMLLSGLVMFFNTSLVEIFTKLTDYT WGVIFGVGAATVVVSYGVAQKVLLRRLASPQILFLY
TLCTIALFPLAKPGVIAQLSHWQLACLIFCGLNTLVGYGALAEAMARWQAAQVSAIITLPLFTLF
FSDLLSLAWPDFFARPMLNLLGYLGAFVVVAGAMYSAIGHRIWGGLRKHTTVVSQPRAGE

7.1.12 YdhC

7.1.12.1 DNA sequence

ATGCAACCTGGAAAAGATTAGTCTGGCTGGCGGGTTGAGCGTACTCGGTTCTGGC
AACCGATATGTATCTGCCTGCTTCGCCATACAGGCCGACCTGCAAACGCCCTGCGTCTG
CTGTCAGTGCCAGCCTAGTCTGTCCTGCCGGTTGCCGCAGCCCAGCTCTGTGGGGGC
CGCTCTCCGACCGTTATGGTCGTAACCGGTATTATTAATCGGCCTGACAATTTCGCTTAG
GTAGTCTGGGATGCTGTGGTAGAAAACGCCGCTACGCTGCTGGTATTGCGTTTGACAG
GCTGTGGGTCTGCGCCGCCGGTTATCTGGCAAGCATTAGTGACAGATTATTATCCTTC
ACAGAAAGTTAACCGTATTTCGCGGCCATCATGCCGCTGGTGGCTATCTCCGGCACTGG
CTCCTCTGTTAGGAAGCTGGCTGCTGGCCATTTCCTGGCAGGCATTTGCCACCCCTGT
TTGCCATTACCGTGGTGCTGATTCTGCCTATTCTGGCTCAAACCCACGACGAAGGCCGTA
ACAATAGTCAGGATGGCTGACCTTACCGACCTGCTACGTTCTAAACCTATCGCGCAAC
GTGCTGATATACGCAGCCTGTTCAGCCAGTTTGCTGACCGGTTCACCGTTCATC
CTTAGTGAAATGGCTACAGCCCGCAGTTATTGGTTAAGTTATGTCGGCAAACATCGC
GTTCTGATTGGTGGTTATGGCTGTCGCCGCCGCTGCAGAAATGGCAAGGCAAGCAGTTAT
TACCGTGGGTGCTGGTGCTGTCAGCGTCATTGCGACCTGGCTGCCGGCTTCATTA
GCCATGTGCGCTGGTCGAAATCCTGATCCCATTCTGTGATGGCGATTGCCAATGGCG
ATCTACCCATTGTTGTCGCCAGGCCTGCGTCCCTCCACACGCAACTGGTCGCCGCA
GCGTTGAGAACACTCTCAACTGGGTCTGTGCTTCCTCGCAAGTCTGGTAGTTCTGGCTG
ATCAGTATCAGCACGCCATTGCTACCACCACAGCGTGATGTTATCAACAGTAATGCTGGT
CGCGCTGGGTTACATGATGCAACGTTGTGAAGAAGTTGGCTGCCAGAATCATGGCAATGCCG
AAGTCGCTCATAGCGAATCACACTGA

7.1.12.2 Protein sequence

MQPGKRLFVWLAGLSVLGFLATDMYLPFAAIQADLQTPASA VSASLSLFLAGFAAAQLLWGP
LSDRYGRKPVLIGLTIFALGSLGMLWVENAATLLVLRFVQAVGVCAAIVWQALVTDYYP
KVNRIFAIMPLVGLSPALAPLLGSWLLVHSWQAIFATLFAITVVLILPIFWLKPTTKARNNSQD
GLTFTDLLRSKTYRGNVLIYAACSASFFAWLTGSPFILSEMGYSPAIVLSYVPQTIAFLIGGYGCR
AALQKWQGKQLLPWLLVLFAVSVIATWAAGFISHVSLVEILIPFCVMAIANGAIYPIVVAQALRP
FPHATGRAALQNTLQLGLCFLASLVVSWLISISTPLLTTSQLSTVVLVALGYMMQRCEEVG
CQNHGNAEVAHS ESH

7.2 Mass spectrometry peptide sequencing results

7.2.1 PgpB

{**MATRIX**} **SCIENCE** Mascot Search Results

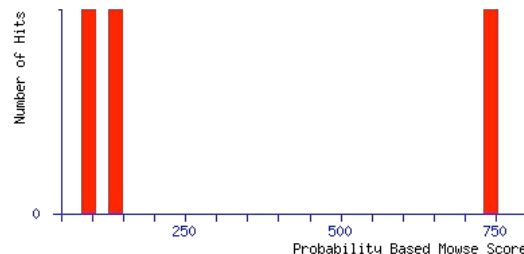
```
User : KABattie
Email :
Search title : Submitted from Frank-029-2009-NCBI by Mascot Daemon on XCALIBUR
MS data file : D:\RAW Files for Conversion\2009\090309\PYPB1.msm
Database : NCBInr (7969746 sequences; 2747354109 residues)
Taxonomy : Escherichia coli (80117 sequences)
Timestamp : 9 Mar 2009 at 12:28:27 GMT
Protein hits : gi|15801899 phosphatidylglycerophosphatase B [Escherichia coli O157:H7 EDL933]
                gi|15800816 outer membrane protein A [Escherichia coli O157:H7 EDL933]
                gi|15799851 30S ribosomal protein S2 [Escherichia coli O157:H7 EDL933]
```

Probability Based Mowse Score

Ions score is $-10 \log(P)$, where P is the probability that the observed match is a random event.

Individual ions scores > 34 indicate identity or extensive homology ($p<0.05$).

Protein scores are derived from ions scores as a non-probabilistic basis for ranking protein hits.



Peptide Summary Report

Format As **Peptide Summary** Help

Significance threshold p< Max. number of hits

Standard scoring MudPIT scoring Ions score or expect cut-off Show sub-sets

Show pop-ups Suppress pop-ups Sort unassigned Require bold red

Error tolerant

1. [gi|15801899](#) Mass: 29003 Score: 740 Queries matched: 38 emPAI: 3.75
phosphatidylglycerophosphatase B [Escherichia coli O157:H7 EDL933]
 Check to include this hit in error tolerant search or archive report

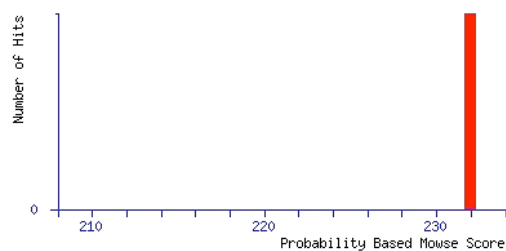
7.2.2 XyI^H

{MATRIX} SCIENCE Mascot Search Results

```
User : KABeattie
Email :
Search title : Submitted from Frank-029-2009-NCBI by Mascot Daemon on XCALIBUR
MS data file : D:\RAW Files for Conversion\2009\090309\XYLL.msm
Database : NCBI nr (7969746 sequences; 2747354109 residues)
Taxonomy : Escherichia coli (80117 sequences)
Timestamp : 9 Mar 2009 at 12:27:36 GMT
Protein hits : gi|15804114 putative xylose transport, membrane component [Escherichia coli O157:H7 EDL933]
```

Probability Based Mowse Score

Ions score is $-10 \log(P)$, where P is the probability that the observed match is a random event.
Individual ions scores > 34 indicate identity or extensive homology ($p < 0.05$).
Protein scores are derived from ions scores as a non-probabilistic basis for ranking protein hits.



Peptide Summary Report

Format As [Peptide Summary](#) [Help](#)

Significance threshold p< Max. number of hits

Standard scoring MudPIT scoring Ions score or expect cut-off Show sub-sets

Show pop-ups Suppress pop-ups Sort unassigned [Decreasing Score](#) Require bold red

[Select All](#) [Select None](#) [Search Selected](#) Error tolerant [Archive Report](#)

1. [gi|15804114](#) Mass: 41004 Score: 232 Queries matched: 7 emPAI: 0.45
putative xylose transport, membrane component [Escherichia coli O157:H7 EDL933]
 Check to include this hit in error tolerant search or archive report

7.3 Formulations of crystallisation screens

7.3.1 MemStart



MemStart™

MD1-21

Tube #	Salt	Buffer	pH	Precipitant
1	None	0.1 M sodium acetate	4.6	2 M ammonium sulfate
2	None	0.1 M ADA	6.5	1 M ammonium sulfate
3	None	None	-	2 M ammonium sulfate
4	None	0.1 M Tris	8.5	2 M ammonium sulfate
5	None	0.1 M Na HEPES	7.5	1.5 M lithium sulfate
6	None	0.1 M sodium acetate	4.6	1 M magnesium sulfate
7	None	0.1 M tri-sodium citrate	5.6	1 M magnesium sulfate
8	0.1 M lithium sulfate	0.1 M ADA	6.5	1 M magnesium sulfate
9	None	0.1 M ammonium dihydrogen phosphate	6.5	None
10	0.1 M ammonium sulfate	0.5 M di-potassium hydrogen phosphate/ 0.5 M di-sodium hydrogen phosphate	7.5	None
11	0.1M lithium sulfate	0.1 M sodium acetate	4.6	1 M ammonium dihydrogen phosphate
12	None	0.1 M tri-sodium citrate	5.6	1 M ammonium dihydrogen phosphate
13	None	0.1 M Tris	8.5	2 M ammonium dihydrogen phosphate
14	None	None	4.6	2 M sodium formate
15	None	None	-	4 M sodium formate
16	None	0.1 M MES	6.5	1.4 M sodium acetate
17	None	0.1 M Na HEPES	7.5	1.4 M tri-sodium citrate
18	None	0.1 M Na HEPES	7.5	1 M potassium sodium tartrate
19	None	0.1 M Na HEPES	7.5	2 % v/v PEG 400/ 2 M ammonium sulfate
20	0.1M magnesium chloride	0.1 M sodium acetate	4.6	30 % v/v PEG 400
21	0.1M sodium chloride	0.1 M tri-sodium citrate	5.6	30 % v/v PEG 400
22	0.1M lithium sulfate	0.1 M tri-sodium citrate	5.6	30 % v/v PEG 400
23	0.3 M lithium sulfate	0.1 M ADA	6.5	30 % v/v PEG 400
24	0.1 M magnesium chloride	0.1 M Na HEPES	7.5	30 % v/v PEG 400
25	0.1 M ammonium sulfate	0.1 M Na HEPES	7.5	30 % v/v PEG 400
26	0.2 M tri-sodium citrate	0.1 M Tris	8.5	30 % v/v PEG 400
27	0.1 M zinc acetate	0.1 M sodium acetate	4.6	12 % w/v PEG 4K
28	0.2 M ammonium sulfate	0.1 M sodium acetate	4.6	12 % w/v PEG 4K
29	None	0.1 M sodium acetate	4.6	12 % w/v PEG 4K
30	0.1 M lithium sulfate	0.1 M tri-sodium citrate	5.6	12 % w/v PEG 4K
31	0.1 M sodium chloride	0.1 M tri-sodium citrate	5.6	12 % w/v PEG 4K
32	0.1 M lithium sulfate	0.1 M ADA	6.5	12 % w/v PEG 4K
33	0.1 M sodium chloride	0.1 M Na HEPES	7.5	12 % w/v PEG 4K
34	0.1 M ammonium sulfate	0.1 M Na HEPES	7.5	12 % w/v PEG 4K
35	0.2 M magnesium chloride	0.1 M Tris	8.5	12 % w/v PEG 4K
36	0.2 M lithium sulfate hydrate	0.1 M Tris	8.5	12 % w/v PEG 4K
37	0.2 M ammonium sulfate	None	-	12 % w/v PEG 4K
38	0.1 M sodium chloride	0.1 M sodium acetate	4.6	12 % w/v PEG 6K
39	0.1 M magnesium chloride	0.1 M sodium acetate	4.6	12 % w/v PEG 6K
40	0.1 M magnesium chloride	0.1 M ADA	6.5	12 % w/v PEG 6K
41	0.1 M di-ammonium hydrogen phosphate	0.1 M Tris	8.5	12 % w/v PEG 6K
42	1 M lithium sulfate	None	-	2 % w/v PEG 8K
43	0.2 M sodium acetate	0.1 M MES	6.5	10 % w/v PEG 8K
44	0.2 M zinc acetate	0.1 M MES	6.5	10 % w/v PEG 8K
45	0.2 M calcium acetate	0.1 M MES	6.5	10 % w/v PEG 8K
46	None	0.1 M Tris	8.5	10 % w/v PEG 8K
47	0.2 M ammonium sulfate	None	-	10 % w/v PEG 8K
48	0.5 M lithium sulfate	None	-	10 % w/v PEG 8K

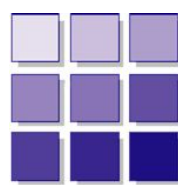
Abbreviations:

ADA: N-(2-Acetamido)iminodiacetic Acid, **HEPES:** N-(2-hydroxyethyl)-piperazine-N'-2-ethanesulfonic acid, **MES:** 2-(N-morpholino)ethanesulfonic acid, **MME:** Monomethyl ether, **PEG:** Polyethylene glycol (4K, 6K and 8K correspond to the molecular weight, in thousands of Daltons, of PEG), **Tris:** 2-Amino-2-(hydroxymethyl)propane-1,3-diol.

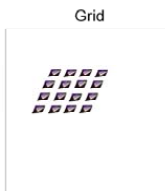
Note: The pH of each final reagent is checked and adjusted back to the stated pH of the buffer (± 0.2 pH units) as appropriate.

Manufacturer's datasheets are available on request

7.3.2 MemSys



moleculardimensions.com



MemSys MD1-25

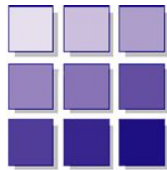
Tube No.	Salt 1	Salt 2	Buffer	pH	Precipitant
1.	None	None	0.1 M Na citrate	5.5	2.5 M ammonium sulfate
2.	0.1 M sodium chloride	0.1 M lithium sulfate	0.1 M Na citrate	3.5	30 % v/v PEG 400
3.	0.1 M sodium chloride	0.1 M magnesium chloride	0.1 M Na acetate	4.5	30 % v/v PEG 400
4.	0.1 M sodium chloride	None	0.1 M Na citrate	5.5	30 % v/v PEG 400
5.	0.1 M sodium chloride	0.1 M lithium sulfate	0.1 M Na citrate	5.5	30 % v/v PEG 400
6.	0.1 M sodium chloride	0.1 M magnesium chloride	0.1 M Na citrate	5.5	30 % v/v PEG 400
7.	None	None	0.1 M MES	6.5	2.5 M ammonium sulfate
8.	None	None	0.1 M MES	6.5	30 % v/v PEG 400
9.	0.1 M sodium chloride	None	0.1 M MES	6.5	30 % v/v PEG 400
10.	0.1 M sodium chloride	0.1 M lithium sulfate	0.1 M MES	6.5	30 % v/v PEG 400
11.	0.1 M sodium chloride	0.1 M magnesium chloride	0.1 M MES	6.5	30 % v/v PEG 400
12.	None	None	0.1 M MOPS	7.0	30 % v/v PEG 400
13.	None	None	0.1 M Na HEPES	7.5	2.5 M ammonium sulfate
14.	0.1 M sodium chloride	None	0.1 M MOPS	7.0	30 % v/v PEG 400
15.	None	None	0.1 M Na HEPES	7.5	30 % v/v PEG 400
16.	0.1 M sodium chloride	None	0.1 M Na HEPES	7.5	30 % v/v PEG 400
17.	0.1 M sodium chloride	0.1 M lithium sulfate	0.1 M Na HEPES	7.5	30 % v/v PEG 400
18.	0.1 M sodium chloride	0.1 M magnesium chloride	0.1 M Na HEPES	7.5	30 % v/v PEG 400
19.	None	None	0.1 M Tris	8.5	1.5 M lithium sulfate
20.	0.1 M sodium chloride	None	0.1 M Tris	8.5	30 % v/v PEG 400
21.	0.1 M sodium chloride	0.1 M lithium sulfate	0.1 M Tris	8.5	30 % v/v PEG 400
22.	0.1 M sodium chloride	0.1 M magnesium chloride	0.1 M Tris	8.5	30 % v/v PEG 400
23.	0.1 M sodium chloride	0.1 M lithium sulfate	0.1 M CAPSO	9.5	30 % v/v PEG 400
24.	0.1 M sodium chloride	0.1 M magnesium chloride	0.1 M CAPSO	9.5	30 % v/v PEG 400
25.	None	None	0.1 M Na citrate	5.5	1.5 M sodium phosphate
26.	0.1 M sodium chloride	0.1 M magnesium chloride	0.1 M Na citrate	3.5	12 % w/v PEG 4K
27.	0.1 M sodium chloride	0.1 M lithium sulfate	0.1 M Na acetate	4.5	12 % w/v PEG 4K
28.	0.1 M sodium chloride	None	0.1 M Na citrate	5.5	12 % w/v PEG 4K
29.	0.1 M sodium chloride	0.1 M lithium sulfate	0.1 M Na citrate	5.5	12 % w/v PEG 4K
30.	0.1 M sodium chloride	0.1 M magnesium chloride	0.1 M Na citrate	5.5	12 % w/v PEG 4K
31.	None	None	0.1 M MES	6.5	1.5 M sodium phosphate
32.	None	None	0.1 M MES	6.5	12 % w/v PEG 4K
33.	0.1 M sodium chloride	None	0.1 M MES	6.5	12 % w/v PEG 4K
34.	0.1 M sodium chloride	0.1 M lithium sulfate	0.1 M MES	6.5	12 % w/v PEG 4K
35.	0.1 M sodium chloride	0.1 M magnesium chloride	0.1 M MES	6.5	12 % w/v PEG 4K
36.	None	None	0.1 M MOPS	7.0	12 % w/v PEG 4K
37.	None	None	0.1 M Na HEPES	7.5	1.5 M potassium phosphate
38.	0.1 M sodium chloride	None	0.1 M MOPS	7.0	12 % w/v PEG 4K
39.	None	None	0.1 M Na HEPES	7.5	12 % w/v PEG 4K
40.	0.1 M sodium chloride	None	0.1 M Na HEPES	7.5	12 % w/v PEG 4K
41.	0.1 M sodium chloride	0.1 M lithium sulfate	0.1 M Na HEPES	7.5	12 % w/v PEG 4K
42.	0.1 M sodium chloride	0.1 M magnesium chloride	0.1 M Na HEPES	7.5	12 % w/v PEG 4K
43.	None	None	0.1 M Tris	8.5	1.5 M potassium phosphate
44.	0.1 M sodium chloride	None	0.1 M Tris	8.5	12 % w/v PEG 4K
45.	0.1 M sodium chloride	0.1 M lithium sulfate	0.1 M Tris	8.5	12 % w/v PEG 4K
46.	0.1 M sodium chloride	0.1 M magnesium chloride	0.1 M Tris	8.5	12 % w/v PEG 4K
47.	0.1 M sodium chloride	0.1 M lithium sulfate	0.1 M CAPSO	9.5	12 % w/v PEG 4K
48.	0.1 M sodium chloride	0.1 M magnesium chloride	0.1 M CAPSO	9.5	12 % w/v PEG 4K

Abbreviations:

CAPSO; 3-(Cyclohexylamino)-2-hydroxy-1-propanesulfonic Acid Sodium Salt, **Na HEPES**; N-(2-hydroxyethyl)-piperazine-N'-ethanesulfonic acid sodium salt, **MES**; 2-(N-morpholino)ethanesulfonic acid, **MOPS**; 3-(N-Morpholino)-propanesulfonic acid, **PEG**; Polyethylene glycol (4K corresponds to the molecular weight, in thousands of Daltons, of PEG), **Tris**; 2-Amino-2-(hydroxymethyl)propane-1,3-diol.

Manufacturer's safety data sheets are available upon request.

7.3.3 MemGold



moleculardimensions.com



MemGold

Box 1 - Tubes 1-24

MD1-39

Tube #	Salt	Buffer	pH	Precipitant
1.1	None	0.08 M sodium citrate	5.2	2.2 M ammonium sulfate
1.2	None	0.01 M Tris	8.0	1.2 M tri-sodium citrate
1.3	None	0.015 M tricine	8.5	24 % w/v PEG 4000
1.4	0.36 M sodium chloride/0.1% w/v sodium azide	0.015 M sodium phosphate	7.0	9.9 % w/v PEG 4000
1.5	0.3 M sodium chloride	0.01 M Tris	8.0	27.5 % w/v PEG 4000
1.6	None	0.225 M MES/bis-tris	6.6	6.6 % w/v PEG 6000
1.7	0.1 M ammonium sulfate	0.1 M HEPES	7.5	12.0 % w/v PEG 4000/ 22 % v/v glycerol
1.8	0.02 M calcium chloride/0.01 M magnesium sulfate/0.02 M sodium chloride	0.02 M MES	6.5	7.7 % w/v PEG 1500
1.9	None	0.05 M HEPES	7.5	2.5 M ammonium sulfate
1.10	None	0.0665 M HEPES	7.5	1.1 M tri-sodium citrate
1.11	None	0.15 M potassium phosphate	6.5	3.3 M ammonium sulfate
1.12	0.1 M magnesium acetate	0.1 M sodium citrate	5.8	14 % w/v PEG 5000 MME
1.13	0.1 M sodium chloride	0.02 M sodium citrate	5.6	11 % w/v PEG 3350
1.14	0.1 M sodium chloride	0.02 M sodium citrate	5.6	5.5 % w/v PEG 3350
1.15	0.05 M calcium chloride/0.05 M barium chloride	0.1 M Tris	8.2	32 % v/v PEG 400
1.16	0.05 M sodium chloride	0.1 M sodium phosphate	6.2	16 % w/v PEG 4000
1.17*	0.1 M magnesium chloride	0.03 M Tris-hydrochloride	8.2	19 % w/v PEG 4000
1.18	0.2 M sodium chloride	0.025 M HEPES	7.5	13 % w/v PEG 4000
1.19	None	0.1 M HEPES	7.5	11 % w/v PEG 3350
1.20	0.1 M sodium chloride	0.02 M KMES	6.7	6.6 % w/v PEG 4000
1.21	0.1 M potassium chloride	0.02 M Tris	7.0	20 % w/v PEG 4000
1.22	0.05 M magnesium chloride/0.1% w/v sodium azide	0.1 M sodium cacodylate	6.7	6.6 % w/v PEG 3350
1.23*	0.2 M potassium chloride	0.1 M sodium citrate	5.5	37 % v/v pentaerythritol propoxylate (5/4 PO/OH)
1.24	None	0.1 M Tris	8.0	5.5 % w/v PEG 4000

MemGold**Box 1 - Tubes 25-48****MD1-39**

Tube #	Salt	Buffer	pH	Precipitant
1.25	0.1 M sodium chloride	0.02 M Tris	7.0	7.7 % w/v PEG 4000
1.26	0.1 M magnesium chloride	0.1 M Tris	7.5	22 % v/v PEG 400
1.27	0.04 M sodium chloride	0.04 M Tris	8.0	27 % v/v PEG 350 MME
1.28	0.05 M sodium chloride/0.02 M magnesium chloride	0.1 M sodium citrate	6.0	22 % v/v PEG 400
1.29	None	0.1 M sodium acetate	5.5	8.8 % w/v PEG 2000 MME
1.30	None	0.4 M ammonium acetate	8.0	13 % w/v PEG 2000 MME
1.31	None	0.02 M bis Tris	7.0	15 % w/v PEG 2000
1.32	0.1 M sodium chloride/0.1 M magnesium chloride	0.02 M Tris	7.5	11 % w/v PEG 1500
1.33	0.1 M sodium chloride/0.1 M magnesium chloride	0.1 M HEPES	8.0	11 % w/v PEG 1500
1.34	0.2 M sodium acetate/0.2 M Potassium Chloride	0.1 M HEPES	7.0	22 % w/v PEG 3000
1.35	0.02 M nickel sulfate	0.01 M HEPES	7.0	33 % v/v Jeffamine-M600
1.36	0.15 M sodium chloride	0.1 M Tris	8.0	13 % w/v PEG 6000
1.37	0.2 M calcium chloride	0.1 M HEPES	7.5	53 % v/v PEG 400
1.38	0.05 M magnesium acetate	0.05 M sodium acetate	5.0	28 % v/v PEG 400
1.39	None	0.05 M HEPES	7.5	22 % v/v PEG 4000
1.40	0.2 M calcium chloride	0.1 M Tris hydrochloride	8.0	44 % v/v PEG 400
1.41	0.05 M magnesium acetate	0.05 M sodium acetate	5.4	24 % v/v PEG 400
1.42	0.2 M calcium chloride	0.1 M MES	6.5	26 % v/v PEG 350 MME
1.43	0.1 M potassium chloride	0.1 M Tris	8.5	39 % v/v PEG 400
1.44	0.05 M magnesium chloride	0.1 M glycine	9.0	22 % v/v PEG 400
1.45	0.1 M ammonium sulfate	0.1 M glycine	3.8	28 % w/v tri-ethylene glycol
1.46	0.15 M sodium formate	0.1 M HEPES	7.2	18 % w/v PEG 3350
1.47	None	0.2 M sodium acetate	6.8	8.8 % w/v PEG 6000
1.48	0.2 M potassium chloride	0.1 M MES	6.5	18 % w/v PEG 6000

MemGold**Box 2 - Tubes 1-24****MD1-39**

Tube #	Salt	Buffer	pH	Precipitant
2.1	0.22 M sodium citrate	0.1 M Tris	8.0	35 % v/v PEG 400
2.2	None	0.1 M sodium acetate	4.5	17 % v/v PEG 400
2.3	None	0.02 M Tris	8.5	1.0 M lithium sulfate/1.8 % w/v PEG 8000
2.4	None	0.02 M Tris	7.5	22 % v/v PEG 550 MME
2.5	0.05 M sodium chloride	0.02 M glycine	10.0	33 % w/v PEG 1000
2.6	0.2 M magnesium chloride	0.1 M Tris	8.5	25 % w/v PEG 4000
2.7	0.2 M magnesium chloride	0.1 M sodium cacodylate	6.5	31 % w/v PEG 2000
2.8	None	0.64 M sodium acetate	4.6	18 % w/v PEG 3350
2.9	0.1 M sodium chloride/0.1 M cadmium chloride	0.1 M Tris hydrochloride	8.0	33 % v/v PEG 400
2.10	None	0.1 M Bicine	8.9	31 % w/v PEG 2000
2.11	0.05 M sodium sulfate/0.05 M lithium sulfate	0.05 M Tris	8.5	35 % v/v PEG 400
2.12	0.1 M sodium chloride	0.05 M glycine	9.5	33 % v/v PEG 300
2.13	0.3 M magnesium nitrate	0.1 M Tris	8.0	23 % w/v PEG 2000
2.14	0.12 M lithium sulfate	0.02 M Tris/0.1 M sodium citrate	7.5/ 5.0	20 % v/v PEG 300
2.15	0.1 M sodium chloride	0.12 M Tris	9.4	20 % v/v PEG 400
2.16	0.2 M sodium chloride	0.1 M HEPES	7.0	22 % v/v PEG 550 MME
2.17	0.1 M sodium chloride/0.325 M sodium acetate	0.1 M Tris	8.0	21 % v/v PEG 400
2.18	0.02 M sodium citrate	0.08 M sodium phosphate	6.2	18 % w/v PEG 2000
2.19	0.02 M potassium nitrate	0.03 M potassium citrate	6.5	7.7 % w/v PEG 4000
2.20	0.1 M sodium chloride/0.005 M magnesium chloride	0.1 M Tris	8.5	30 % w/v PEG 2000 MME
2.21	0.2 M calcium chloride	0.1 M HEPES	7.0	33 % v/v PEG 400
2.22	0.1 M calcium chloride	0.1 M Tris	6.5	13 % w/v PEG 2000 MME
2.23	0.2 M ammonium sulfate/0.02 M sodium chloride	0.02 M sodium acetate	4.0	33 % v/v PEG 200
2.24	0.07 M sodium chloride	0.05 M sodium citrate	4.5	22 % v/v PEG 400

MemGold**Box 2 - Tubes 25-48****MD1-39**

Tube #	Salt	Buffer	pH	Precipitant
2.25	0.2 M ammonium sulfate	0.1 M sodium acetate	4.6	28 % v/v PEG 550 MME
2.26	None	0.05 M glycine	9.0	55 % v/v PEG 400
2.27	0.1 M magnesium chloride/0.1M sodium chloride	0.1 M Tris	8.5	33 % v/v PEG 400
2.28	0.1 M lithium sulfate/0.05 M disodium hydrogen phosphate	0.05 M citric acid	None	19 % w/v PEG 1000
2.29	0.2 M magnesium chloride/ 0.1 M potassium chloride	0.025 M sodium citrate	4.0	33 % v/v PEG 400
2.30	0.05 M zinc acetate	0.05 M MES	6.1	11 % w/v PEG 8000
2.31	0.3 M magnesium nitrate	0.1 M Tris	8.0	22 % w/v PEG 8000
2.32	0.1 M sodium chloride/4% v/v ethylene glycol	0.1 M MES	6.5	33 % v/v PEG 400
2.33	0.05 M sodium chloride	0.1 M sodium citrate	5.5	26 % v/v PEG 400
2.34	0.1 M lithium sulfate	0.1 M glycine	9.3	30 % v/v PEG 400
2.35*	0.15 M potassium citrate/ 0.05 M lithium citrate	0.1 M sodium phosphate	-	22 % w/v PEG 6000
2.36	0.001 M zinc sulfate	0.05 M HEPES	7.8	28 % v/v PEG 600
2.37	0.1 M sodium chloride	0.1 M sodium phosphate	7.0	33 % v/v PEG 300
2.38	0.1 M sodium chloride	0.05 M Bicine	9.0	33 % v/v PEG 300
2.39	0.05 M zinc acetate/6% v/v ethylene glycol	0.1 M sodium cacodylate	6.0	6.6 % w/v PEG 8000
2.40	0.2 M lithium sulfate	0.1 M sodium citrate	3.5	28 % v/v PEG 400
2.41	0.1 M sodium chloride	0.1 M Tris	7.5	11 % w/v PEG 4000
2.42*	0.05 M lithium sulfate	0.1 M tricine	7.4	7 % w/v PEG 3000
2.43*	0.2 M calcium chloride	0.1 M MES	6.5	33% v/v PEG 400
2.44*	1 M sodium chloride	0.1 M sodium citrate	6.0	28% w/v PEG 4000
2.45*	None	0.1 M HEPES	7.5	11% w/v PEG 4000
2.46*	0.002 M zinc sulfate	0.08 M HEPES	7.0	25 % v/v Jeffamine ED2001
2.47*	0.001 M cadmium chloride/0.03 M magnesium chloride	0.1 M MES	6.5	30 % v/v PEG 400
2.48*	None	0.1 M bis-tris-propane	7.0	3.0 M sodium chloride

*These conditions have been changed from the pre-release (prior to June 2007) beta version of MemGold. The pre-release conditions have been moved to the sister screen MemPlus (MD1-44), a new screen for Outer Membrane protein crystallisation."

Abbreviations:

ADA; N-(2-Acetamido)iminodiacetic Acid, **Bicine**; N,N-Bis(2-hydroxyethyl)glycine, **CHES**; 2-(N-Cyclohexylamino)ethane sulfonic Acid, **HEPES**; N-(2-hydroxyethyl)-piperazine-N'-2-ethanesulfonic acid, **KMES**; 2-(N-morpholino)ethanesulfonic acid potassium salt, **MES**; 2-(N-morpholino)ethanesulfonic acid, **MME**; Monomethylether, **PEG**; Polyethylene glycol, **Tricine**; N-[Tris(hydroxymethyl)methyl]glycine, **Tris**; 2-Amino-2-(hydroxymethyl)propane-1,3-diol, **Tris HCl**; 2-Amino-2-(hydroxymethyl)propane-1,3-diol, hydrochloride.]

7.3.4 Peg/Ion 1/2

PEG/Ion Screen™

HR2-126 Reagent Formulation

Tube #	Salt	Tube #	Polymer	Tube #	pH \diamond	F ⁻ Fluoride	Cl ⁻ Chloride	I ⁻ Iodide	N — O ⁻ Nitrate
1.	0.2 M Sodium fluoride	1.	20% w/v Polyethylene glycol 3,350	1.	7.3				
2.	0.2 M Potassium fluoride	2.	20% w/v Polyethylene glycol 3,350	2.	7.3				
3.	0.2 M Ammonium fluoride	3.	20% w/v Polyethylene glycol 3,350	3.	6.2				
4.	0.2 M Lithium chloride	4.	20% w/v Polyethylene glycol 3,350	4.	6.8				
5.	0.2 M Magnesium chloride hexahydrate	5.	20% w/v Polyethylene glycol 3,350	5.	5.9	O			
6.	0.2 M Sodium chloride	6.	20% w/v Polyethylene glycol 3,350	6.	6.9				
7.	0.2 M Calcium chloride dihydrate	7.	20% w/v Polyethylene glycol 3,350	7.	5.1	N — O ⁻			Nitrate
8.	0.2 M Potassium chloride	8.	20% w/v Polyethylene glycol 3,350	8.	7.0				
9.	0.2 M Ammonium chloride	9.	20% w/v Polyethylene glycol 3,350	9.	6.3	O			
10.	0.2 M Sodium iodide	10.	20% w/v Polyethylene glycol 3,350	10.	7.0				
11.	0.2 M Potassium iodide	11.	20% w/v Polyethylene glycol 3,350	11.	7.0				
12.	0.2 M Ammonium iodide	12.	20% w/v Polyethylene glycol 3,350	12.	6.2				
13.	0.2 M Sodium thiocyanate	13.	20% w/v Polyethylene glycol 3,350	13.	6.9				
14.	0.2 M Potassium thiocyanate	14.	20% w/v Polyethylene glycol 3,350	14.	7.0				
15.	0.2 M Lithium nitrate	15.	20% w/v Polyethylene glycol 3,350	15.	7.1				
16.	0.2 M Magnesium nitrate hexahydrate	16.	20% w/v Polyethylene glycol 3,350	16.	5.9				
17.	0.2 M Sodium nitrate	17.	20% w/v Polyethylene glycol 3,350	17.	6.8				
18.	0.2 M Potassium nitrate	18.	20% w/v Polyethylene glycol 3,350	18.	6.8				
19.	0.2 M Ammonium nitrate	19.	20% w/v Polyethylene glycol 3,350	19.	6.2				
20.	0.2 M Magnesium formate dihydrate	20.	20% w/v Polyethylene glycol 3,350	20.	7.0				
21.	0.2 M Sodium formate	21.	20% w/v Polyethylene glycol 3,350	21.	7.2				
22.	0.2 M Potassium formate	22.	20% w/v Polyethylene glycol 3,350	22.	7.3				
23.	0.2 M Ammonium formate	23.	20% w/v Polyethylene glycol 3,350	23.	6.6				
24.	0.2 M Lithium acetate dihydrate	24.	20% w/v Polyethylene glycol 3,350	24.	7.9				
25.	0.2 M Magnesium acetate tetrahydrate	25.	20% w/v Polyethylene glycol 3,350	25.	7.9				
26.	0.2 M Zinc acetate dihydrate	26.	20% w/v Polyethylene glycol 3,350	26.	6.4				
27.	0.2 M Sodium acetate trihydrate	27.	20% w/v Polyethylene glycol 3,350	27.	8.0				
28.	0.2 M Calcium acetate hydrate	28.	20% w/v Polyethylene glycol 3,350	28.	7.5				
29.	0.2 M Potassium acetate	29.	20% w/v Polyethylene glycol 3,350	29.	8.1				
30.	0.2 M Ammonium acetate	30.	20% w/v Polyethylene glycol 3,350	30.	7.1				
31.	0.2 M Lithium sulfate monohydrate	31.	20% w/v Polyethylene glycol 3,350	31.	6.0				
32.	0.2 M Magnesium sulfate heptahydrate	32.	20% w/v Polyethylene glycol 3,350	32.	6.0				
33.	0.2 M Sodium sulfate decahydrate	33.	20% w/v Polyethylene glycol 3,350	33.	6.7				
34.	0.2 M Potassium sulfate	34.	20% w/v Polyethylene glycol 3,350	34.	6.8				
35.	0.2 M Ammonium sulfate	35.	20% w/v Polyethylene glycol 3,350	35.	6.0				
36.	0.2 M Sodium tartrate dibasic dihydrate	36.	20% w/v Polyethylene glycol 3,350	36.	7.3				
37.	0.2 M Potassium sodium tartrate tetrahydrate	37.	20% w/v Polyethylene glycol 3,350	37.	7.4				
38.	0.2 M Ammonium tartrate dibasic	38.	20% w/v Polyethylene glycol 3,350	38.	6.6				
39.	0.2 M Sodium phosphate monobasic monohydrate	39.	20% w/v Polyethylene glycol 3,350	39.	4.7				
40.	0.2 M Sodium phosphate dibasic dihydrate	40.	20% w/v Polyethylene glycol 3,350	40.	9.1				
41.	0.2 M Potassium phosphate monobasic	41.	20% w/v Polyethylene glycol 3,350	41.	4.8				
42.	0.2 M Potassium phosphate dibasic	42.	20% w/v Polyethylene glycol 3,350	42.	9.2				
43.	0.2 M Ammonium phosphate monobasic	43.	20% w/v Polyethylene glycol 3,350	43.	4.6				
44.	0.2 M Ammonium phosphate dibasic	44.	20% w/v Polyethylene glycol 3,350	44.	8.0				
45.	0.2 M Lithium citrate tribasic tetrahydrate	45.	20% w/v Polyethylene glycol 3,350	45.	8.4				
46.	0.2 M Sodium citrate tribasic dihydrate	46.	20% w/v Polyethylene glycol 3,350	46.	8.3				
47.	0.2 M Potassium citrate tribasic monohydrate	47.	20% w/v Polyethylene glycol 3,350	47.	8.3				
48.	0.2 M Ammonium citrate dibasic	48.	20% w/v Polyethylene glycol 3,350	48.	5.1				

\diamond Measured pH at 25 ° C

PEG/Ion Screen contains forty-eight unique reagents. To determine the formulation of each reagent, simply read across the page.

34 Journey
Aliso Viejo, CA 92656-3317 U.S.A.
Tel: (949) 425-1321 • Fax: (949) 425-1611
E-mail: tech@hrmail.com
Website: www.hamptonresearch.com



Solutions for Crystal Growth

© 2000-2006 Hampton Research Corp. all rights reserved
Printed in the United States of America. This guide or
parts thereof may not be reproduced in any form without
the written permission of the publishers.

PEG/Ion 2 Screen™

HR2-098 Reagent Formulation

Tube	Salt	Tube	Buffer [◊]	Tube	Polymer
#		#		#	
1.	0.1 M Sodium malonate pH 4.0	1.	None	1.	12% w/v Polyethylene glycol 3,350
2.	0.2 M Sodium malonate pH 4.0	2.	None	2.	20% w/v Polyethylene glycol 3,350
3.	0.1 M Sodium malonate pH 5.0	3.	None	3.	12% w/v Polyethylene glycol 3,350
4.	0.2 M Sodium malonate pH 5.0	4.	None	4.	20% w/v Polyethylene glycol 3,350
5.	0.1 M Sodium malonate pH 6.0	5.	None	5.	12% w/v Polyethylene glycol 3,350
6.	0.2 M Sodium malonate pH 6.0	6.	None	6.	20% w/v Polyethylene glycol 3,350
7.	0.1 M Sodium malonate pH 7.0	7.	None	7.	12% w/v Polyethylene glycol 3,350
8.	0.2 M Sodium malonate pH 7.0	8.	None	8.	20% w/v Polyethylene glycol 3,350
9.	4% v/v Tacsimate pH 4.0	9.	None	9.	12% w/v Polyethylene glycol 3,350
10.	8% v/v Tacsimate pH 4.0	10.	None	10.	20% w/v Polyethylene glycol 3,350
11.	4% v/v Tacsimate pH 5.0	11.	None	11.	12% w/v Polyethylene glycol 3,350
12.	8% v/v Tacsimate pH 5.0	12.	None	12.	20% w/v Polyethylene glycol 3,350
13.	4% v/v Tacsimate pH 6.0	13.	None	13.	12% w/v Polyethylene glycol 3,350
14.	8% v/v Tacsimate pH 6.0	14.	None	14.	20% w/v Polyethylene glycol 3,350
15.	4% v/v Tacsimate pH 7.0	15.	None	15.	12% w/v Polyethylene glycol 3,350
16.	8% v/v Tacsimate pH 7.0	16.	None	16.	20% w/v Polyethylene glycol 3,350
17.	4% v/v Tacsimate pH 8.0	17.	None	17.	12% w/v Polyethylene glycol 3,350
18.	8% v/v Tacsimate pH 8.0	18.	None	18.	20% w/v Polyethylene glycol 3,350
19.	0.1 M Succinic acid pH 7.0	19.	None	19.	12% w/v Polyethylene glycol 3,350
20.	0.2 M Succinic acid pH 7.0	20.	None	20.	20% w/v Polyethylene glycol 3,350
21.	0.1 M Ammonium citrate tribasic pH 7.0	21.	None	21.	12% w/v Polyethylene glycol 3,350
22.	0.2 M Ammonium citrate tribasic pH 7.0	22.	None	22.	20% w/v Polyethylene glycol 3,350
23.	0.1 M DL-Malic acid pH 7.0	23.	None	23.	12% w/v Polyethylene glycol 3,350
24.	0.2 M DL-Malic acid pH 7.0	24.	None	24.	20% w/v Polyethylene glycol 3,350
25.	0.1 M Sodium acetate trihydrate pH 7.0	25.	None	25.	12% w/v Polyethylene glycol 3,350
26.	0.2 M Sodium acetate trihydrate pH 7.0	26.	None	26.	20% w/v Polyethylene glycol 3,350
27.	0.1 M Sodium formate pH 7.0	27.	None	27.	12% w/v Polyethylene glycol 3,350
28.	0.2 M Sodium formate pH 7.0	28.	None	28.	20% w/v Polyethylene glycol 3,350
29.	0.1 M Ammonium tartrate dibasic pH 7.0	29.	None	29.	12% w/v Polyethylene glycol 3,350
30.	0.2 M Ammonium tartrate dibasic pH 7.0	30.	None	30.	20% w/v Polyethylene glycol 3,350
31.	2% v/v Tacsimate pH 4.0	31.	0.1 M Sodium acetate trihydrate pH 4.6	31.	16% w/v Polyethylene glycol 3,350
32.	2% v/v Tacsimate pH 5.0	32.	0.1 M Sodium citrate tribasic dihydrate pH 5.6	32.	16% w/v Polyethylene glycol 3,350
33.	2% v/v Tacsimate pH 6.0	33.	0.1 M BIS-TRIS pH 6.5	33.	20% w/v Polyethylene glycol 3,350
34.	2% v/v Tacsimate pH 7.0	34.	0.1 M HEPES pH 7.5	34.	20% w/v Polyethylene glycol 3,350
35.	2% v/v Tacsimate pH 8.0	35.	0.1 M Tris pH 8.5	35.	16% w/v Polyethylene glycol 3,350
36.	None	36.	0.07 M Citric acid, 0.03 M BIS-TRIS propane / pH 3.4	36.	16% w/v Polyethylene glycol 3,350
37.	None	37.	0.06 M Citric acid, 0.04 M BIS-TRIS propane / pH 4.1	37.	16% w/v Polyethylene glycol 3,350
38.	None	38.	0.05 M Citric acid, 0.05 M BIS-TRIS propane / pH 5.0	38.	16% w/v Polyethylene glycol 3,350
39.	None	39.	0.04 M Citric acid, 0.06 M BIS-TRIS propane / pH 6.4	39.	20% w/v Polyethylene glycol 3,350
40.	None	40.	0.03 M Citric acid, 0.07 M BIS-TRIS propane / pH 7.6	40.	20% w/v Polyethylene glycol 3,350
41.	None	41.	0.02 M Citric acid, 0.08 M BIS-TRIS propane / pH 8.8	41.	16% w/v Polyethylene glycol 3,350
42.	0.02 M Calcium chloride dihydrate, 0.02 M Cadmium chloride hydrate, 0.02 M Cobalt(II) chloride hexahydrate	42.	None	42.	20% w/v Polyethylene glycol 3,350
43.	0.02 M Magnesium chloride hexahydrate 0.02 M Nickel(II) chloride hexahydrate	43.	0.1 M HEPES sodium pH 7.0	43.	20% w/v Polyethylene glycol 3,350
44.	0.02 M Zinc chloride	44.	None	44.	20% w/v Polyethylene glycol 3,350
45.	0.15 M Cesium chloride	45.	None	45.	15% w/v Polyethylene glycol 3,350
46.	0.2 M Sodium bromide	46.	None	46.	20% w/v Polyethylene glycol 3,350
47.	1% w/v Tryptone	47.	0.05 M HEPES sodium pH 7.0	47.	12% w/v Polyethylene glycol 3,350
48.	1% w/v Tryptone	48.	0.05 M HEPES sodium pH 7.0	48.	20% w/v Polyethylene glycol 3,350

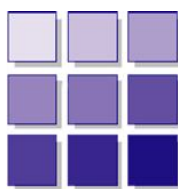
◊ Buffer pH is that of a 1.0 M stock prior to dilution with other reagent components: pH with HCl or NaOH.

PEG/Ion 2 Screen contains forty-eight unique reagents. To determine the formulation of each reagent, simply read across the page.

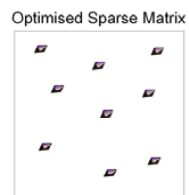
34 Journey
Aliso Viejo, CA 92656-3317 U.S.A.
Tel: (949) 425-1321 • Fax: (949) 425-1611
E-mail: tech@hrmail.com
Website: www.hamptonresearch.com

HAMPTON
RESEARCH
Solutions for Crystal Growth
© 2007 Hampton Research Corp. all rights reserved
Printed in the United States of America. This guide or
parts thereof may not be reproduced in any form without
the written permission of the publishers.

7.3.5 JCSG 1/2



moleculardimensions.com



JCSG-plus

Box 1 of 2

MD1-37

Tube No.	Salt	Buffer	pH	Precipitant
1.1	0.2 M lithium sulfate	0.1 M sodium acetate	4.5	50 % v/v PEG 400
1.2	None	0.1 M sodium citrate	5.5	20 % w/v PEG 3000
1.3	0.2 M di-ammonium hydrogen citrate	None	-	20 % w/v PEG 3350
1.4	0.02 M calcium chloride	0.1 M sodium acetate	4.6	30 % v/v MPD
1.5	0.2 M magnesium formate	None	-	20 % w/v PEG 3350
1.6	0.2 M lithium sulfate	0.1 M phosphate/citrate	4.2	20 % w/v PEG 1000
1.7	None	0.1 M CHES	9.5	20 % w/v PEG 8000
1.8	0.2 M ammonium formate	None	-	20 % w/v PEG 3350
1.9	0.2 M ammonium chloride	None	-	20 % w/v PEG 3350
1.10	0.2 M potassium formate	None	-	20 % w/v PEG 3350
1.11	0.2 M ammonium dihydrogen phosphate	0.1 M Tris	8.5	50 % v/v MPD
1.12	0.2 M potassium nitrate	None	-	20 % w/v PEG 3350
1.13	None	0.1 M citrate	4.0	0.8 M ammonium sulfate
1.14	0.2 M sodium thiocyanate	None	-	20 % w/v PEG 3350
1.15	None	0.1 M Bicine	9.0	20 % w/v PEG 6000
1.16	None	0.1 M HEPES	7.5	10 % w/v PEG 8000/ 8 % v/v Ethylene glycol
1.17	None	0.1 M sodium cacodylate	6.5	40 % v/v MPD/ 5 % w/v PEG 8000
1.18	None	0.1 M phosphate/citrate	4.2	40 % v/v Ethanol/ 5 % w/v PEG 1000
1.19	None	0.1 M sodium acetate	4.6	8 % w/v PEG 4000
1.20	0.2 M magnesium chloride	0.1 M Tris	7.0	10 % w/v PEG 8000
1.21	None	0.1 M citrate	5.0	20 % w/v PEG 6000
1.22	0.2 M magnesium chloride	0.1 M sodium cacodylate	6.5	50 % v/v PEG 200
1.23	None	None	6.5	1.6 M tri-sodium citrate
1.24	0.2 M tri-potassium citrate	None	-	20 % w/v PEG 3350
1.25	0.2 M sodium chloride	0.1 M phosphate/citrate	4.2	20 % w/v PEG 8000
1.26	1.0 M lithium chloride	0.1 M Na citrate	4.0	20 % w/v PEG 6000
1.27	0.2 M ammonium nitrate	None	-	20 % w/v PEG 3350
1.28	None	0.1 M Na HEPES	7.0	10 % w/v PEG 6000
1.29	None	0.1 M Na HEPES	7.5	0.8 M sodium dihydrogen phosphate 0.8 M potassium dihydrogen phosphate
1.30	None	0.1 M phosphate/citrate	4.2	40 % v/v PEG 300
1.31	0.2 M zinc acetate	0.1 M sodium acetate	4.5	10 % w/v PEG 3000
1.32	None	0.1 M Tris	8.5	20 % v/v Ethanol
1.33	None	0.1 M Na/K phosphate	6.2	25 % v/v 1,2-propanediol 10 % v/v Glycerol
1.34	None	0.1 M Bicine	9.0	10 % w/v PEG 20,000/ 2% v/v Dioxane
1.35	None	0.1 M sodium acetate	4.6	2.0 M ammonium sulfate
1.36	None	None	-	10 % w/v PEG 1000/ 10 % w/v PEG 8000
1.37	None	None	-	24 % w/v PEG 1500/ 20 % v/v Glycerol
1.38	0.2 M magnesium chloride	0.1 M Na HEPES	7.5	30 % v/v PEG 400
1.39	0.2 M sodium chloride	0.1 M Na/K phosphate	6.2	50 % v/v PEG 200
1.40	0.2 M lithium sulfate	0.1 M sodium acetate	4.5	30 % w/v PEG 8000
1.41	None	0.1 M HEPES	7.5	70 % v/v MPD
1.42	0.2 M magnesium chloride	0.1 M Tris	8.5	20 % w/v PEG 8000
1.43	0.2 M lithium sulfate	0.1 M Tris	8.5	40 % v/v PEG 400
1.44	None	0.1 M Tris	8.0	40 % v/v MPD
1.45	0.17 M ammonium sulfate	None	-	25.5 % w/v PEG 4000/ 15 % v/v Glycerol
1.46	0.2 M calcium acetate	0.1 M sodium cacodylate	6.5	40 % v/v PEG 300
1.47	0.14 M calcium chloride	0.07 M sodium acetate	4.6	14 % v/v 2-propanol/ 30 % v/v Glycerol
1.48	0.04 M potassium dihydrogen phosphate	None	-	16 % w/v PEG 8000/ 20 % v/v Glycerol

JCSG-plus**Box 2 of 2****MD1-37**

Tube	Salt	Buffer	pH	Precipitant
2.1	None	0.1 M sodium cacodylate	6.5	1.0 M tri-sodium citrate
2.2	0.2 M sodium chloride	0.1 M sodium cacodylate	6.5	2.0 M ammonium sulfate
2.3	0.2 M sodium chloride	0.1 M HEPES	7.5	10 % v/v 2-propanol
2.4	0.2 M lithium sulfate	0.1 M Tris	8.5	1.26 M ammonium sulfate
2.5	None	0.1 M CAPS	10.5	40 % v/v MPD
2.6	0.2 M zinc acetate	0.1 M imidazole	8.0	20 % w/v PEG 3000
2.7	0.2 M zinc acetate	0.1 M sodium cacodylate	6.5	10 % v/v 2-propanol
2.8	None	0.1 M sodium acetate	4.5	1.0 M di-ammonium hydrogen phosphate
2.9	None	0.1 M MES	6.5	1.6 M magnesium sulfate
2.10	None	0.1 M Bicine	9.0	10 % w/v PEG 6000
2.11	0.16 M calcium acetate	0.08 M sodium cacodylate	6.5	14.4 % w/v PEG 8000/ 20 % v/v glycerol
2.12	None	0.1 M imidazole	8.0	10 % w/v PEG 8000
2.13	0.05 M caesium chloride	0.1 M MES	6.5	30 % v/v Jeffamine M-600
2.14	None	0.1 M Na Citrate	5.0	3.2 M ammonium sulfate
2.15	None	0.1 M Tris	8.0	20 % v/v MPD
2.16	None	0.1 M HEPES	7.5	20 % v/v Jeffamine M-600
2.17	0.2 M magnesium chloride	0.1 M Tris	8.5	50 % v/v ethylene glycol
2.18	None	0.1 M Bicine	9.0	10 % v/v MPD
2.19	None	None	7.0	0.8 M succinic acid
2.20	None	None	7.0	2.1 M DL-malic acid
2.21	None	None	7.0	2.4 M sodium malonate
2.22	1.1 M sodium malonate	0.1 M HEPES	7.0	0.5 % v/v Jeffamine ED-2001
2.23	1.0 M succinic acid	0.1 M HEPES	7.0	1 % w/v PEG 2000 MME
2.24	None	0.1 M HEPES	7.0	30 % v/v Jeffamine M-600
2.25	None	0.1 M HEPES	7.0	30 % v/v Jeffamine ED-2001
2.26	0.02 M magnesium chloride	0.1 M HEPES	7.5	22 % w/v polyacrylic acid 5100 sodium salt
2.27	0.01 M cobalt chloride	0.1 M Tris	8.5	20 % w/v polyvinylpyrrolidone K15
2.28	0.2 M tri-methylamine N-oxide	0.1 M Tris	8.5	20 % w/v PEG 2000 MME
2.29	0.005 M cobalt chloride 0.005 M cadmium chloride 0.005 M magnesium chloride 0.005 M nickel chloride	0.1 M HEPES	7.5	12 % w/v PEG 3350
2.30	0.2 M sodium malonate	None	7.0	20 % w/v PEG 3350
2.31	0.1 M succinic acid	None	7.0	15 % w/v PEG 3350
2.32	0.15 M DL - malic acid	None	7.0	20 % w/v PEG 3350
2.33	0.1 M potassium thiocyanate	None	-	30 % w/v PEG 2000 MME
2.34	0.15 M potassium bromide	None	-	30 % w/v PEG 2000 MME
2.35	None	0.1 M Bis Tris	5.5	2.0 M ammonium sulfate
2.36	None	0.1 M Bis Tris	5.5	3.0 M sodium chloride
2.37	None	0.1 M Bis Tris	5.5	0.3 M magnesium formate
2.38	1.0 M ammonium sulfate	0.1 M Bis Tris	5.5	1 % w/v PEG 3350
2.39	None	0.1 M Bis Tris	5.5	25 % w/v PEG 3350
2.40	0.2 M calcium chloride	0.1 M Bis Tris	5.5	45 % v/v MPD
2.41	0.2 M ammonium acetate	0.1 M Bis Tris	5.5	45 % v/v MPD
2.42	0.1 M ammonium acetate	0.1 M Bis Tris	5.5	17 % w/v PEG 10000
2.43	0.2 M ammonium sulfate	0.1 M Bis Tris	5.5	25 % w/v PEG 3350
2.44	0.2 M sodium chloride	0.1 M Bis Tris	5.5	25 % w/v PEG 3350
2.45	0.2 M lithium sulfate	0.1 M Bis Tris	5.5	25 % w/v PEG 3350
2.46	0.2 M ammonium acetate	0.1 M Bis Tris	5.5	25 % w/v PEG 3350
2.47	0.2 M magnesium chloride	0.1 M Bis Tris	5.5	25 % w/v PEG 3350
2.48	0.2 M ammonium acetate	0.1 M HEPES	7.5	45 % v/v MPD

Abbreviations: **Bis Tris**; Bis-(2-hydroxyethyl)imino-tris(hydroxymethyl)methane, **CAPS**; N-Cyclohexyl-3-aminopropanesulfonic acid, **CHES**; 2-(N-Cyclohexylamino)ethane Sulfonic Acid, **HEPES**; 2-(4-(2-Hydroxyethyl)-1-piperazinyl)ethanesulfonic Acid, **Na HEPES**; 2-(4-(2-Hydroxyethyl)-1-piperazinyl)ethanesulfonic Acid Sodium Salt, **MES**; 2-(N-morpholino)ethanesulfonic acid, **MPD**; 2,4-methyl pentanediol, **PEG**; Polyethylene glycol, **Tris**; 2-Amino-2-(hydroxymethyl)propane-1,3-diol.

Manufacturer's safety data sheets are available upon request.

7.3.6 Hampton Crystal Screen 1/2

Crystal Screen™

Tube #	Salt	Tube #	Buffer ◊	Tube #	Precipitant
1.	0.02 M Calcium chloride dihydrate	1.	0.1 M Sodium acetate trihydrate pH 4.6	1.	30% v/v (+/-)-2-Methyl-2,4-pentanediol
2.	None	2.	None	2.	0.4 M Potassium sodium tartrate tetrahydrate
3.	None	3.	None	3.	0.4 M Ammonium phosphate monobasic
4.	None	4.	0.1 M TRIS hydrochloride pH 8.5	4.	2.0 M Ammonium sulfate
5.	0.2 M Sodium citrate tribasic dihydrate	5.	0.1 M HEPES sodium pH 7.5	5.	30% v/v (+/-)-2-Methyl-2,4-pentanediol
6.	0.2 M Magnesium chloride hexahydrate	6.	0.1 M TRIS hydrochloride pH 8.5	6.	30% w/v Polyethylene glycol 4,000
7.	None	7.	0.1 M Sodium cacodylate trihydrate pH 6.5	7.	1.4 M Sodium acetate trihydrate
8.	0.2 M Sodium citrate tribasic dihydrate	8.	0.1 M Sodium cacodylate trihydrate pH 6.5	8.	30% v/v 2-Propanol
9.	0.2 M Ammonium acetate	9.	0.1 M Sodium citrate tribasic dihydrate pH 5.6	9.	30% w/v Polyethylene glycol 4,000
10.	0.2 M Ammonium acetate	10.	0.1 M Sodium acetate trihydrate pH 4.6	10.	30% w/v Polyethylene glycol 4,000
11.	None	11.	0.1 M Sodium citrate tribasic dihydrate pH 5.6	11.	1.0 M Ammonium phosphate monobasic
12.	0.2 M Magnesium chloride hexahydrate	12.	0.1 M HEPES sodium pH 7.5	12.	30% v/v 2-Propanol
13.	0.2 M Sodium citrate tribasic dihydrate	13.	0.1 M TRIS hydrochloride pH 8.5	13.	30% v/v Polyethylene glycol 400
14.	0.2 M Calcium chloride dihydrate	14.	0.1 M HEPES sodium pH 7.5	14.	28% v/v Polyethylene glycol 400
15.	0.2 M Ammonium sulfate	15.	0.1 M Sodium cacodylate trihydrate pH 6.5	15.	30% w/v Polyethylene glycol 8,000
16.	None	16.	0.1 M HEPES sodium pH 7.5	16.	1.5 M Lithium sulfate monohydrate
17.	0.2 M Lithium sulfate monohydrate	17.	0.1 M TRIS hydrochloride pH 8.5	17.	30% w/v Polyethylene glycol 4,000
18.	0.2 M Magnesium acetate tetrahydrate	18.	0.1 M Sodium cacodylate trihydrate pH 6.5	18.	20% w/v Polyethylene glycol 8,000
19.	0.2 M Ammonium acetate	19.	0.1 M TRIS hydrochloride pH 8.5	19.	30% v/v 2-Propanol
20.	0.2 M Ammonium sulfate	20.	0.1 M Sodium acetate trihydrate pH 4.6	20.	25% w/v Polyethylene glycol 4,000
21.	0.2 M Magnesium acetate tetrahydrate	21.	0.1 M Sodium cacodylate trihydrate pH 6.5	21.	30% v/v (+/-)-2-Methyl-2,4-pentanediol
22.	0.2 M Sodium acetate trihydrate	22.	0.1 M TRIS hydrochloride pH 8.5	22.	30% w/v Polyethylene glycol 4,000
23.	0.2 M Magnesium chloride hexahydrate	23.	0.1 M HEPES sodium pH 7.5	23.	30% v/v Polyethylene glycol 400
24.	0.2 M Calcium chloride dihydrate	24.	0.1 M Sodium acetate trihydrate pH 4.6	24.	20% v/v 2-Propanol
25.	None	25.	0.1 M Imidazole pH 6.5	25.	1.0 M Sodium acetate trihydrate
26.	0.2 M Ammonium acetate	26.	0.1 M Sodium citrate tribasic dihydrate pH 5.6	26.	30% v/v (+/-)-2-Methyl-2,4-pentanediol
27.	0.2 M Sodium citrate tribasic dihydrate	27.	0.1 M HEPES sodium pH 7.5	27.	20% v/v 2-Propanol
28.	0.2 M Sodium acetate trihydrate	28.	0.1 M Sodium cacodylate trihydrate pH 6.5	28.	30% w/v Polyethylene glycol 8,000
29.	None	29.	0.1 M HEPES sodium pH 7.5	29.	0.8 M Potassium sodium tartrate tetrahydrate
30.	0.2 M Ammonium sulfate	30.	None	30.	30% w/v Polyethylene glycol 8,000
31.	0.2 M Ammonium sulfate	31.	None	31.	30% w/v Polyethylene glycol 4,000
32.	None	32.	None	32.	2.0 M Ammonium sulfate
33.	None	33.	None	33.	4.0 M Sodium formate
34.	None	34.	0.1 M Sodium acetate trihydrate pH 4.6	34.	2.0 M Sodium formate
35.	None	35.	0.1 M HEPES sodium pH 7.5	35.	0.8 M Sodium phosphate monobasic monohydrate 0.8 M Potassium phosphate monobasic
36.	None	36.	0.1 M TRIS hydrochloride pH 8.5	36.	8% w/v Polyethylene glycol 8,000
37.	None	37.	0.1 M Sodium acetate trihydrate pH 4.6	37.	8% w/v Polyethylene glycol 4,000
38.	None	38.	0.1 M HEPES sodium pH 7.5	38.	1.4 M Sodium citrate tribasic dihydrate
39.	None	39.	0.1 M HEPES sodium pH 7.5	39.	2% w/v Polyethylene glycol 400 2.0 M Ammonium sulfate
40.	None	40.	0.1 M Sodium citrate tribasic dihydrate pH 5.6	40.	20% v/v 2-Propanol 20% w/v Polyethylene glycol 4,000
41.	None	41.	0.1 M HEPES sodium pH 7.5	41.	10% v/v 2-Propanol 20% w/v Polyethylene glycol 4,000
42.	0.05 M Potassium phosphate monobasic	42.	None	42.	20% w/v Polyethylene glycol 8,000
43.	None	43.	None	43.	30% w/v Polyethylene glycol 1,500
44.	None	44.	None	44.	0.2 M Magnesium formate dihydrate
45.	0.2 M Zinc acetate dihydrate	45.	0.1 M Sodium cacodylate trihydrate pH 6.5	45.	18% w/v Polyethylene glycol 8,000
46.	0.2 M Calcium acetate hydrate	46.	0.1 M Sodium cacodylate trihydrate pH 6.5	46.	18% w/v Polyethylene glycol 8,000
47.	None	47.	0.1 M Sodium acetate trihydrate pH 4.6	47.	2.0 M Ammonium sulfate
48.	None	48.	0.1 M TRIS hydrochloride pH 8.5	48.	2.0 M Ammonium phosphate monobasic
49.	1.0 M Lithium sulfate monohydrate	49.	None	49.	2% w/v Polyethylene glycol 8,000
50.	0.5 M Lithium sulfate monohydrate	50.	None	50.	15% w/v Polyethylene glycol 8,000

◊ Buffer pH is that of a 1.0 M stock prior to dilution with other reagent components: pH with HCl or NaOH.

Crystal Screen contains fifty unique reagents. To determine the formulation of each reagent, simply read across the page.

34 Journey
Aliso Viejo, CA 92656-3317 U.S.A.
Tel: (949) 425-1321 • Fax: (949) 425-1611
E-mail: tech@hrmail.com
Website: www.hamptonresearch.com



Solutions for Crystal Growth

© 2000-2007 Hampton Research Corp. all rights reserved
Printed in the United States of America. This guide or parts thereof may not be reproduced in any form without the written permission of the publishers.

Crystal Screen 2™**HR2-112 Reagent Formulation**

Tube #	Salt	Tube #	Buffer ◊	Tube #	Precipitant
1. None	2.0 M Sodium chloride	1. None	None	1. 10% w/v Polyethylene glycol 6,000	
2. None	0.5 M Sodium chloride	2. None	None	2. 0.01 M Hexadecyltrimethylammonium bromide	
3. None	0.01 M Magnesium chloride hexahydrate	3. None	None	3. 25% v/v Ethylene glycol	
4. None		4. None	None	4. 35% v/v 1,4-Dioxane	
5. None	2.0 M Ammonium sulfate	5. None	None	5. 5% v/v 2-Propanol	
6. None		6. None	None	6. 1.0 M Imidazole pH 7.0	
7. None		7. None	None	7. 10% w/v Polyethylene glycol 1,000	
8. 1.5 M Sodium chloride		8. None	None	10% w/v Polyethylene glycol 8,000	
9. None		9. 0.1 M Sodium acetate trihydrate pH 4.6		8. 10% v/v Ethanol	
10. 0.2 M Sodium chloride		10. 0.1 M Sodium acetate trihydrate pH 4.6		9. 2.0 M Sodium chloride	
11. 0.01 M Cobalt (II) chloride hexahydrate		11. 0.1 M Sodium acetate trihydrate pH 4.6		10. 30% v/v (+/-)-2-Methyl-2,4-pentanediol	
12. 0.1 M Cadmium chloride hydrate		12. 0.1 M Sodium acetate trihydrate pH 4.6		11. 1.0 M 1,6-Hexanediol	
13. 0.2 M Ammonium sulfate		13. 0.1 M Sodium acetate trihydrate pH 4.6		12. 30% v/v Polyethylene glycol 400	
14. 0.2 M Potassium sodium tartrate tetrahydrate		14. 0.1 M Sodium citrate tribasic dihydrate pH 5.6		13. 30% w/v Polyethylene glycol monomethyl ether 2,000	
15. 0.5 M Ammonium sulfate		15. 0.1 M Sodium citrate tribasic dihydrate pH 5.6		14. 2.0 M Ammonium sulfate	
16. 0.5 M Sodium chloride		16. 0.1 M Sodium citrate tribasic dihydrate pH 5.6		15. 1.0 M Lithium sulfate monohydrate	
17. None		17. 0.1 M Sodium citrate tribasic dihydrate pH 5.6		16. 2% v/v Ethylene imine polymer	
18. 0.01 M Iron (III) chloride hexahydrate		18. 0.1 M Sodium citrate tribasic dihydrate pH 5.6		17. 35% v/v tert-Butanol	
19. None		19. 0.1 M Sodium citrate tribasic dihydrate pH 5.6		18. 10% v/v Jeffamine M-600®	
20. None		20. 0.1 M MES monohydrate pH 6.5		19. 2.5 M 1,6-Hexanediol	
21. 0.1 M Sodium phosphate monobasic monohydrate		21. 0.1 M MES monohydrate pH 6.5		20. 1.6 M Magnesium sulfate heptahydrate	
0.1 M Potassium phosphate monobasic				21. 2.0 M Sodium chloride	
22. None		22. 0.1 M MES monohydrate pH 6.5			
23. 1.6 M Ammonium sulfate		23. 0.1 M MES monohydrate pH 6.5		22. 12% w/v Polyethylene glycol 20,000	
24. 0.05 M Cesium chloride		24. 0.1 M MES monohydrate pH 6.5		23. 10% v/v 1,4-Dioxane	
25. 0.01 M Cobalt (II) chloride hexahydrate		25. 0.1 M MES monohydrate pH 6.5		24. 30% v/v Jeffamine M-600®	
26. 0.2 M Ammonium sulfate		26. 0.1 M MES monohydrate pH 6.5		25. 1.8 M Ammonium sulfate	
27. 0.01 M Zinc sulfate heptahydrate		27. 0.1 M MES monohydrate pH 6.5		26. 30% w/v Polyethylene glycol monomethyl ether 5,000	
28. None		28. None		27. 25% v/v Polyethylene glycol monomethyl ether 550	
29. 0.5 M Ammonium sulfate		29. 0.1 M HEPES pH 7.5		28. 1.6 M Sodium citrate tribasic dihydrate pH 6.5	
30. None		30. 0.1 M HEPES pH 7.5		29. 30% v/v (+/-)-2-Methyl-2,4-pentanediol	
31. None		31. 0.1 M HEPES pH 7.5		30. 10% w/v Polyethylene glycol 6,000	
32. 0.1 M Sodium chloride		32. 0.1 M HEPES pH 7.5		5% v/v (+/-)-2-Methyl-2,4-pentanediol	
33. None		33. 0.1 M HEPES pH 7.5		31. 20% v/v Jeffamine M-600®	
34. 0.05 M Cadmium sulfate hydrate		34. 0.1 M HEPES pH 7.5		32. 1.6 M Ammonium sulfate	
35. None		35. 0.1 M HEPES pH 7.5		33. 2.0 M Ammonium formate	
36. None		36. 0.1 M HEPES pH 7.5		34. 1.0 M Sodium acetate trihydrate	
37. None		37. 0.1 M HEPES pH 7.5		35. 70% v/v (+/-)-2-Methyl-2,4-pentanediol	
38. None		38. 0.1 M HEPES pH 7.5		36. 4.3 M Sodium chloride	
39. 0.2 M Magnesium chloride hexahydrate		39. 0.1 M Tris pH 8.5		37. 10% w/v Polyethylene glycol 8,000	
40. None		40. 0.1 M Tris pH 8.5		8% v/v Ethylene glycol	
41. 0.01 M Nickel (II) chloride hexahydrate		41. 0.1 M Tris pH 8.5		38. 20% w/v Polyethylene glycol 10,000	
42. 1.5 M Ammonium sulfate		42. 0.1 M Tris pH 8.5		39. 3.4 M 1,6-Hexanediol	
43. 0.2 M Ammonium phosphate monobasic		43. 0.1 M Tris pH 8.5		40. 25% v/v tert-Butanol	
44. None		44. 0.1 M Tris pH 8.5		41. 1.0 M Lithium sulfate monohydrate	
45. 0.01 M Nickel (II) chloride hexahydrate		45. 0.1 M Tris pH 8.5		42. 12% v/v Glycerol	
46. 0.1 M Sodium chloride		46. 0.1 M BICINE pH 9.0		43. 50% v/v (+/-)-2-Methyl-2,4-pentanediol	
47. None		47. 0.1 M BICINE pH 9.0		44. 20% v/v Ethanol	
48. None		48. 0.1 M BICINE pH 9.0		45. 20% w/v Polyethylene glycol monomethyl ether 2,000	
				46. 20% v/v Polyethylene glycol monomethyl ether 550	
				47. 2.0 M Magnesium chloride hexahydrate	
				48. 2% v/v 1,4-Dioxane	
				10% w/v Polyethylene glycol 20,000	

◊ Buffer pH is that of a 1.0 M (0.5 M for MES monohydrate) stock prior to dilution with other reagent components:
pH with HCl or NaOH.

Crystal Screen 2 contains forty-eight unique reagents. To determine the formulation of each reagent, simply read across the page.

34 Journey
Aliso Viejo, CA 92656-3317 U.S.A.
Tel: (949) 425-1321 • Fax: (949) 425-1611
E-mail: tech@hrmail.com
Website: www.hamptonresearch.com



Solutions for Crystal Growth

© 2000-2007 Hampton Research Corp. all rights reserved
Printed in the United States of America. This guide or
parts thereof may not be reproduced in any form without
the written permission of the publishers.

7.3.7 Detergent Screen 1/2

Detergent Screen 1™

HR2-410 Reagent Formulation

Tube #	Detergent	Classification	MW	CMC (mM)	[Actual]	Type ¹
1. C ₁₂ E ₉	Polyoxyethylene(9)dodecyl ether / Thesit® / α-Dodecyl-ω-hydroxy-poly(oxy-1,2-ethanediyl)	avg. 583.0	0.05	0.5	N	
2. C ₁₂ E ₈	Octaethylene glycol Mono-n-dodecyl Ether	538.8	0.11	1.1	N	
3. n-Dodecyl-β-D-maltoside	n-Dodecyl-β-D-maltopyranoside	510.6	0.17	1.7	N	
4. Sucrose monolaurate	β-D-Fructopyranosyl-α-D-glucopyranoside monododecanoate / Lauroyl sucrose / Dodecanoyl sucrose / Sucrose monododecanoate	524.6	0.3	3.0	N	
5. CYMAL®-6	6-Cyclohexyl-1-hexyl-β-D-maltoside	508.5	0.56	5.6	N	
6. TRITON® X-100	Octylphenoxy polyethoxyethanol / Polyethylene Glycol-p-isooctylphenyl Ether	650.0	0.90	9.0	N	
7. CTAB	Hexadecyltrimethylammonium bromide / Cetyltrimethylammonium bromide / Cetrimonium bromide / Palmitytrimethylammonium bromide	364.46	1.00	10.0	I	
8. Big CHAP, Deoxy	N,N-bis-(3-D-Gluconamidopropyl)deoxycholamide	862.1	1.4	14.0	N	
9. n-Decyl-β-D-maltoside	n-Decyl-β-D-maltopyranoside	482.6	1.80	18.0	N	
10. LDAO	Lauryldimethylamine-N-oxide / DDAO / N,N-Dimethyl-1-dodecanamine-N-oxide / n-Dodecyl-N,N-dimethylamine-N-oxide	229.41	2.0	20.0	N	
11. CYMAL®-5	5-Cyclohexyl-1-pentyl-β-D-maltoside	494.5	5.0	50.0	N	
12. ZWITTERGENT® 3-12	n-Dodecyl-N,N-dimethyl-3-ammonio-1-propanesulfonate	335.6	4.0	40.0	Z	
13. n-Nonyl-β-D-glucoside	n-Nonyl-β-D-glucopyranoside	306.4	6.50	65.0	N	
14. n-Octyl-β-D-thioglucoside	n-Octyl-β-D-thioglucopyranoside / 1-s-Octyl-β-D-thioglucoside	308.4	9.00	90.0	N	
15. DDAO	N,N-Dimethyldecylamine-N-oxide	201.35	10.4	104.0	N	
16. HECAMEG®	Methyl-6-O-(N-heptylcarbamoyl)-α-D-glucopyranoside	335.4	19.5	195.0	N	
17. n-Octanoylsucrose	Sucrose monocaproylate / n-Octanoyl-β-D-fructofuranosyl-α-D-glucopyranoside	468.5	24.4	244.0	N	
18. n-Heptyl-β-D-thioglucopyranoside	Heptyl-β-D-thioglucoside	294.4	30.0	300.0	N	
19. n-Octyl-β-D-glucoside	n-Octyl-β-D-glucopyranoside	292.4	20.0	200.0	N	
20. CYMAL®-3	3-Cyclohexyl-1-propyl-β-D-maltoside	466.5	34.5	345.0	N	
21. C-HEGA®-10	Cyclohexylbutanoyl-N-hydroxyethylglucamide	377.5	35.0	350.0	N	
22. ZWITTERGENT® 3-10	n-Decyl-N,N-dimethyl-3-ammonio-1-propanesulfonate	307.6	40.0	400.0	Z	
23. MEGA®-8	Octanoyl-N-methylglucamide	321.4	79.0	790.0	N	
24. n-Hexyl-β-D-glucopyranoside	n-Hexyl-β-D-glucoside	264.3	250.0	2500.0	N	

¹ N=NON-IONIC, I=IONIC, Z=ZWITTERIONIC

34 Journey
Aliso Viejo, CA 92656-3317 U.S.A.
Tel: (949) 425-1321 • Fax: (949) 425-1611
E-mail: tech@hrmail.com
Website: www.hamptonresearch.com



Solutions for Crystal Growth
© 2000-2007 Hampton Research Corp. all rights reserved
Printed in the United States of America. This guide or
parts thereof may not be reproduced in any form without
the written permission of the publishers.

Detergent Screen 2™**HR2-411 Reagent Formulation**

Tube #	Detergent	Classification	MW	CMC (mM)	[Actual]	Type ¹
1.	Pluronic® F-68	Polyoxyethylene-polyoxypropylene Block Copolymer / Methyl-oxirane, polymer with oxirane, $(C_2H_5O)_n$ / Poloxamer 188	~ 8400	17.9	10% w/v	N
2.	ANAPOE®-35	BRIJ®-35 / $C_{12}E_{23}$ / α -Dodecyl-w-hydroxy-poly(oxy-1,2-ethanediyl) / Polyethylene glycol (23) monododecyl ether	~ 1198	0.091	10% w/v	N
3.	2,6-Dimethyl-4-heptyl- β -D-maltopyranoside	n-Dodecyl- β -D-maltopyranoside	468.5	27.5	275 mM	N
4.	ANAPOE®-58	BRIJ®-58 / $C_{16}E_{20}$ / α -Hexadecyl-w-hydroxy-poly(oxy-1,2-ethanediyl) / Polyethylene glycol (20) monohexadecyl ether	~ 1122	0.004	10% w/v	N
5.	ANAPOE®-X-114	TRITON® X-114 / α -[(1,1,3,3-Tetramethylbutyl)phenyl]-w-hydroxy-poly(oxy-1,2-ethanediyl)	~ 536	0.2	10% w/v	N
6.	ANAPOE®-X-305	TRITON® X-305 / α -[4-(1,1,3,3-Tetramethylbutyl)phenyl]-w-hydroxy-poly(oxy-1,2-ethanediyl)	~ 1526	None	10% w/v	N
7.	ANAPOE®-X-405	TRITON® X-405 / α -[4-(1,1,3,3-Tetramethylbutyl)phenyl]-w-hydroxy-poly(oxy-1,2-ethanediyl)	~ 1967	0.81	10% w/v	N
8.	ANAPOE®-20	TWEEN® 20 / Polyoxyethylene(20)sorbitan monolaurate / Poly(oxy-1,2-ethanediyl) derivs., sorbitan monododecanoate	~ 1228	0.059	10% w/v	N
9.	ANAPOE®-80	TWEEN® 80 / Polyoxyethylene(80)sorbitan monolaurate / Poly(oxy-1,2-ethanediyl) derivs., (Z)-sorbitan mono-9-octadecanoate	~ 1310	0.012	10% w/v	N
10.	ANAPOE®-C ₁₀ E ₆	Polyoxyethylene(6)decyl ether / 3,6,9,12,15,18-hexaoxaocacosan-1-ol	~ 423	0.9	10% w/v	N
11.	ANAPOE®-C ₁₀ E ₉	Polyoxyethylene(9)decyl ether / α -Decyl-w-hydroxy-poly(oxy-1,2-ethanediyl)	~ 555	1.3	10% w/v	N
12.	ANAPOE®-C ₁₂ E ₁₀	Polyoxyethylene(10)dodecyl ether / 3,6,9,12,15,18,24,27,30-decaoxadotetracontan-1-ol	~ 627	0.2	10% w/v	N
13.	ANAPOE®-C ₁₃ E ₈	Polyoxyethylene(8)tridecyl ether	~ 553	0.1	10% w/v	N
14.	IPTG	Isopropyl- β -D-thiogalactopyranoside, ANAGRADE® / 1-Methylethyl-1-thio- β -D-galactopyranoside	238.31	None	10% w/v	N
15.	n-Dodecyl-N,N-dimethylglycine	None	271.4	1.5	15.0 mM	Z
16.	HEGA®-10	Decanoyl-N-hydroxyethylglucamide	379.5	7.0	70.0 mM	N
17.	C ₈ E ₅	Pentaethylene glycol monooctyl ether, ANAGRADE® / Octyl pentaethylene glycol ether / Octylpentaglycol / 3,6,9,12,15-Pentaoxatricosan-1-ol	350.5	7.1	71.0 mM	N
18.	CHAPS	3-[(3-Cholamidopropyl)-dimethylammonio]-1-propane sulfonate / N,N-Dimethyl-3-sulfo-N-[3-[(3 α ,5 β ,7 α ,12 α)-3,7,12-trihydroxy-24-oxocholan-24-yl]amino]propyl]-1-propanaminium hydroxide, inner salt	614.9	8.0	80.0 mM	Z
19.	CHAPSO	3-[(3-Cholamidopropyl)dimethylammonio]-2-hydroxy-1-propanesulfonate	630.9	8.0	80.0 mM	Z
20.	C-HEGA®-11	Cyclohexylpentanoyl-N-hydroxyethylglucamide	391.5	11.5	115.0 mM	N
21.	HEGA®-9	Nonanoyl-N-hydroxyethylglucamide	365.5	39.0	390.0 mM	N
22.	C-HEGA®-9	Cyclohexylpropanoyl-N-hydroxyethylglucamide	363.5	108.0	1.08 M	N
23.	HEGA®-8	Octanoyl-N-hydroxyethylglucamide	351.5	109.0	1.09 M	N
24.	C-HEGA®-8	Cyclohexylethanoyl-N-hydroxyethylglucamide	349.5	277	6.6% w/v	N

¹ N=NON-IONIC, I=IONIC, Z=ZWITTERIONIC

Solutions for Crystal Growth

© 2000-2007 Hampton Research Corp. all rights reserved
 Printed in the United States of America. This guide or
 parts thereof may not be reproduced in any form without
 the written permission of the publishers.

34 Journey
 Aliso Viejo, CA 92656-3317 U.S.A.
 Tel: (949) 425-1321 • Fax: (949) 425-1611
 E-mail: tech@hrmail.com
 Website: www.hamptonresearch.com

7.3.8 Additive screen

Additive Screen™

HR2-428 Reagent Formulation

Tube #	Salt	Tube #	Classification	Tube #	Suggested Drop Concentration
1. (A1)	0.1 M Barium chloride dihydrate	1. (A1)	Multivalent	1. (A1)	0.01 M (10 mM)
2. (A2)	0.1 M Cadmium chloride hydrate	2. (A2)	Multivalent	2. (A2)	0.01 M (10 mM)
3. (A3)	0.1 M Calcium chloride dihydrate	3. (A3)	Multivalent	3. (A3)	0.01 M (10 mM)
4. (A4)	0.1 M Cobalt(II) chloride hexahydrate	4. (A4)	Multivalent	4. (A4)	0.01 M (10 mM)
5. (A5)	0.1 M Copper(II) chloride dihydrate	5. (A5)	Multivalent	5. (A5)	0.01 M (10 mM)
6. (A6)	0.1 M Magnesium chloride hexahydrate	6. (A6)	Multivalent	6. (A6)	0.01 M (10 mM)
7. (A7)	0.1 M Manganese(II) chloride tetrahydrate	7. (A7)	Multivalent	7. (A7)	0.01 M (10 mM)
8. (A8)	0.1 M Strontium chloride hexahydrate	8. (A8)	Multivalent	8. (A8)	0.01 M (10 mM)
9. (A9)	0.1 M Yttrium(III) chloride hexahydrate	9. (A9)	Multivalent	9. (A9)	0.01 M (10 mM)
10. (A10)	0.1 M Zinc chloride	10. (A10)	Multivalent	10. (A10)	0.01 M (10 mM)
11. (A11)	0.1 M Iron(III) chloride hexahydrate	11. (A11)	Multivalent	11. (A11)	0.01 M (10 mM)
12. (A12)	0.1 M Nickel(II) chloride hexahydrate	12. (A12)	Multivalent	12. (A12)	0.01 M (10 mM)
13. (B1)	0.1 M Chromium(III) chloride hexahydrate	13. (B1)	Multivalent	13. (B1)	0.01 M (10 mM)
14. (B2)	0.1 M Praseodymium(III) acetate hydrate	14. (B2)	Multivalent	14. (B2)	0.01 M (10 mM)
15. (B3)	1.0 M Ammonium sulfate	15. (B3)	Salt	15. (B3)	0.1 M (100 mM)
16. (B4)	1.0 M Potassium chloride	16. (B4)	Salt	16. (B4)	0.1 M (100 mM)
17. (B5)	1.0 M Lithium chloride	17. (B5)	Salt	17. (B5)	0.1 M (100 mM)
18. (B6)	2.0 M Sodium chloride	18. (B6)	Salt	18. (B6)	0.2 M (200 mM)
19. (B7)	0.5 M Sodium fluoride	19. (B7)	Salt	19. (B7)	0.05 M (50 mM)
20. (B8)	1.0 M Sodium iodide	20. (B8)	Salt	20. (B8)	0.1 M (100 mM)
21. (B9)	2.0 M Sodium thiocyanate	21. (B9)	Salt	21. (B9)	0.2 M (200 mM)
22. (B10)	1.0 M Potassium sodium tartrate tetrahydrate	22. (B10)	Salt	22. (B10)	0.1 M (100 mM)
23. (B11)	1.0 M Sodium citrate tribasic dihydrate	23. (B11)	Salt	23. (B11)	0.1 M (100 mM)
24. (B12)	1.0 M Cesium chloride	24. (B12)	Salt	24. (B12)	0.1 M (100 mM)
25. (C1)	1.0 M Sodium malonate pH 7.0	25. (C1)	Salt	25. (C1)	0.1 M (100 mM)
26. (C2)	0.1 M L-Proline	26. (C2)	Amino Acid	26. (C2)	0.01 M (10 mM)
27. (C3)	0.1 M Phenol	27. (C3)	Dissociating Agent	27. (C3)	0.01 M (10 mM)
28. (C4)	30% v/v Dimethyl sulfoxide	28. (C4)	Dissociating Agent	28. (C4)	3.0%
29. (C5)	0.1 M Sodium bromide	29. (C5)	Dissociating Agent	29. (C5)	0.01 M (10 mM)
30. (C6)	30% w/v 6-Aminohexanoic acid	30. (C6)	Linker	30. (C6)	3.0%
31. (C7)	30% w/v 1,5-Diaminopentane dihydrochloride	31. (C7)	Linker	31. (C7)	3.0%
32. (C8)	30% w/v 1,6-Diaminohexane	32. (C8)	Linker	32. (C8)	3.0%
33. (C9)	30% w/v 1,8-Diaminoctane	33. (C9)	Linker	33. (C9)	3.0%
34. (C10)	1.0 M Glycine	34. (C10)	Linker	34. (C10)	0.1 M (100 mM)
35. (C11)	0.3 M Glycyl-glycyl-glycine	35. (C11)	Linker	35. (C11)	0.03 M (30 mM)
36. (C12)	0.1 M Taurine	36. (C12)	Linker	36. (C12)	0.01 M (10 mM)
37. (D1)	0.1 M Betaine hydrochloride	37. (D1)	Linker	37. (D1)	0.01 M (10 mM)
38. (D2)	0.1 M Spermidine	38. (D2)	Polyamine	38. (D2)	0.01 M (10 mM)
39. (D3)	0.1 M Spermine tetrahydrochloride	39. (D3)	Polyamine	39. (D3)	0.01 M (10 mM)
40. (D4)	0.1 M Hexammine cobalt(III) chloride	40. (D4)	Polyamine	40. (D4)	0.01 M (10 mM)
41. (D5)	0.1 M Sarcosine	41. (D5)	Polyamine / Osmolyte	41. (D5)	0.01 M (10 mM)
42. (D6)	0.1 M Trimethylamine hydrochloride	42. (D6)	Chaotrope	42. (D6)	0.01 M (10 mM)
43. (D7)	1.0 M Guanidine hydrochloride	43. (D7)	Chaotrope	43. (D7)	0.1 M (100 mM)
44. (D8)	0.1 M Urea	44. (D8)	Chaotrope	44. (D8)	0.01 M (10 mM)
45. (D9)	0.1 M β -Nicotinamide adenine dinucleotide hydrate	45. (D9)	Co-factor	45. (D9)	0.01 M (10 mM)
46. (D10)	0.1 M Adenosine-5'-triphosphate disodium salt hydrate	46. (D10)	Co-factor	46. (D10)	0.01 M (10 mM)
47. (D11)	0.1 M TCEP hydrochloride	47. (D11)	Reducing Agent	47. (D11)	0.01 M (10 mM)
48. (D12)	0.01 M GSH (L-Glutathione reduced), 0.01 M GSSG (L-Glutathione oxidized)	48. (D12)	Reducing Agent	48. (D12)	0.001 M (1 mM)

Additive Screen contains ninety-six unique reagents beginning at position A1.

To determine the formulation of each reagent, simply read across the page.

34 Journey
Aliso Viejo, CA 92656-3317 U.S.A.
Tel: (949) 425-1321 • Fax: (949) 425-1611
E-mail: tech@hrmail.com
Website: www.hamptonresearch.com



Solutions for Crystal Growth
© 2000-2008 Hampton Research Corp. all rights reserved
Printed in the United States of America. This guide or
parts thereof may not be reproduced in any form without
the written permission of the publishers.

Additive Screen™

HR2-428 Reagent Formulation

Tube #	Salt	Tube #	Classification	Tube #	Suggested Drop Concentration
49.(E1)	0.1 M Ethylenediaminetetraacetic disodium salt dihydrate	49.(E1)	Chelating Agent	49.(E1)	0.01 M (10 mM)
50.(E2)	5% w/v Polyvinylpyrrolidone K15	50.(E2)	Polymer	50.(E2)	0.5%
51.(E3)	30% w/v Dextran sulfate sodium salt (M _r 5,000)	51.(E3)	Polymer	51.(E3)	3.0%
52.(E4)	40% v/v Pentaerythritol ethoxylate (3/4 EO/OH)	52.(E4)	Polymer	52.(E4)	4.0%
53.(E5)	10% w/v Polyethylene glycol 3,350	53.(E5)	Polymer	53.(E5)	1.0%
54.(E6)	30% w/v D-(+)-Glucose monohydrate	54.(E6)	Carbohydrate	54.(E6)	3.0%
55.(E7)	30% w/v Sucrose	55.(E7)	Carbohydrate	55.(E7)	3.0%
56.(E8)	30% w/v Xylitol	56.(E8)	Carbohydrate	56.(E8)	3.0%
57.(E9)	30% w/v D-Sorbitol	57.(E9)	Carbohydrate	57.(E9)	3.0%
58.(E10)	12% w/v myo-Inositol	58.(E10)	Carbohydrate	58.(E10)	1.2%
59.(E11)	30% w/v D-(+)-Trehalose dihydrate	59.(E11)	Carbohydrate	59.(E11)	3.0%
60.(E12)	30% w/v D-(+)-Galactose	60.(E12)	Carbohydrate	60.(E12)	3.0%
61.(F1)	30% v/v Ethylene glycol	61.(F1)	Polyol	61.(F1)	3.0%
62.(F2)	30% v/v Glycerol	62.(F2)	Polyol	62.(F2)	3.0%
63.(F3)	3.0 M NDSB-195	63.(F3)	Non-detergent	63.(F3)	0.3 M (300 mM)
64.(F4)	2.0 M NDSB-201	64.(F4)	Non-detergent	64.(F4)	0.2 M (200 mM)
65.(F5)	2.0 M NDSB-211	65.(F5)	Non-detergent	65.(F5)	0.2 M (200 mM)
66.(F6)	2.0 M NDSB-221	66.(F6)	Non-detergent	66.(F6)	0.2 M (200 mM)
67.(F7)	1.0 M NDSB-256	67.(F7)	Non-detergent	67.(F7)	0.1 M (200 mM)
68.(F8)	0.15 mM CYMAL® -7	68.(F8)	Amphiphile	68.(F8)	0.000015 M (0.015 mM)
69.(F9)	20% w/v Benzamidine hydrochloride hydrate	69.(F9)	Amphiphile	69.(F9)	2.0%
70.(F10)	5% w/v n-Octyl-N,N-dimethylamine-N-oxide, (LDAO, DDAO)	70.(F10)	Detergent	70.(F10)	0.5%
71.(F11)	5% w/v n-Octyl-β-D-glucoside	71.(F11)	Detergent	71.(F11)	0.5%
72.(F12)	5% w/v n-Dodecyl-β-D-maltoside	72.(F12)	Detergent	72.(F12)	0.5%
73.(G1)	30% w/v Trimethylamine N-oxide dihydrate	73.(G1)	Osmolyte	73.(G1)	3.0%
74.(G2)	30% w/v 1,6-Hexanediol	74.(G2)	Organic, Non-volatile	74.(G2)	3.0%
75.(G3)	30% v/v (+/-)-2-Methyl-2,4-pentanediol	75.(G3)	Organic, Non-volatile	75.(G3)	3.0%
76.(G4)	50% w/v Polyethylene glycol 400	76.(G4)	Organic, Non-volatile	76.(G4)	5.0%
77.(G5)	50% v/v Jeffamine M-600® pH 7.0	77.(G5)	Organic, Non-volatile	77.(G5)	5.0%
78.(G6)	40% v/v 2,5-Hexanediol	78.(G6)	Organic, Non-volatile	78.(G6)	4.0%
79.(G7)	40% v/v (±)-1,3-Butanediol	79.(G7)	Organic, Non-volatile	79.(G7)	4.0%
80.(G8)	40% v/v Polypropylene glycol P 400	80.(G8)	Organic, Non-volatile	80.(G8)	4.0%
81.(G9)	30% v/v 1,4-Dioxane	81.(G9)	Organic, Volatile	81.(G9)	3.0%
82.(G10)	30% v/v Ethanol	82.(G10)	Organic, Volatile	82.(G10)	3.0%
83.(G11)	30% v/v 2-Propanol	83.(G11)	Organic, Volatile	83.(G11)	3.0%
84.(G12)	30% v/v Methanol	84.(G12)	Organic, Volatile	84.(G12)	3.0%
85.(H1)	40% v/v 1,4-Butanediol	85.(H1)	Organic, Volatile	85.(H1)	4.0%
86.(H2)	40% v/v tert-Butanol	86.(H2)	Organic, Volatile	86.(H2)	4.0%
87.(H3)	40% v/v 1,3-Propanediol	87.(H3)	Organic, Volatile	87.(H3)	4.0%
88.(H4)	40% v/v Acetonitrile	88.(H4)	Organic, Volatile	88.(H4)	4.0%
89.(H5)	40% v/v Formamide	89.(H5)	Organic, Volatile	89.(H5)	4.0%
90.(H6)	40% v/v 1-Propanol	90.(H6)	Organic, Volatile	90.(H6)	4.0%
91.(H7)	5% v/v Ethyl acetate	91.(H7)	Organic, Volatile	91.(H7)	0.5%
92.(H8)	40% v/v Acetone	92.(H8)	Organic, Volatile	92.(H8)	4.0%
93.(H9)	0.25% v/v Dichloromethane	93.(H9)	Organic, Volatile	93.(H9)	0.025%
94.(H10)	7% v/v 1-Butanol	94.(H10)	Organic, Volatile	94.(H10)	0.7%
95.(H11)	40% v/v 2,2,2-Trifluoroethanol	95.(H11)	Organic, Volatile	95.(H11)	4.0%
96.(H12)	40% v/v 1,1,1,3,3,3-Hexafluoro-2-propanol	96.(H12)	Organic, Volatile	96.(H12)	4.0%

Additive Screen contains ninety-six unique reagents beginning at position A1.

To determine the formulation of each reagent, simply read across the page.

34 Journey
 Aliso Viejo, CA 92656-3317 U.S.A.
 Tel: (949) 425-1321 • Fax: (949) 425-1611
 E-mail: tech@hamptonmail.com
 Website: www.hamptonresearch.com



Solutions for Crystal Growth
 © 2000-2008 Hampton Research Corp. all rights reserved
 Printed in the United States of America. This guide or
 parts thereof may not be reproduced in any form without
 the written permission of the publishers.

References

- Abramson, J., Smirnova, I., Kasho, V., Verner, G., Kaback, H.R., and Iwata, S. 2003. Structure and Mechanism of the Lactose Permease of *Escherichia coli*. *Science* **301**(5633): 610-615.
- Agostiano, A., Mavelli, F., Milano, F., Giotta, L., Trotta, M., Nagy, L., and Maroti, P. 2004. pH-sensitive fluorescent dye as probe for proton uptake in photosynthetic reaction centers. *Bioelectrochemistry* **63**(1-2): 125-128.
- Ahuja, U. and Thony-Meyer, L. 2003. Dynamic features of a heme delivery system for cytochrome C maturation. *J Biol Chem* **278**(52): 52061-52070.
- Alberts, B., Bray, D., Lewis, J., Raff, M., Roberts, K., and Watson, D. 1983. *Molecular Biology of the Cell (fourth edition 2002)*. Garland Publishing Inc., New York.
- Almgren, M. 2000. Mixed micelles and other structures in the solubilization of bilayer lipid membranes by surfactants. *Biochim Biophys Acta* **1508**(1-2): 146-163.
- Ames, G.F., Mimura, C.S., Holbrook, S.R., and Shyamala, V. 1992. Traffic ATPases: a superfamily of transport proteins operating from *Escherichia coli* to humans. *Adv Enzymol Relat Areas Mol Biol* **65**: 1-47.
- Anatrace. 2008. *Detergents and their uses in membrane protein science*. Anatrace, Inc.
- Baneyx, F. 1999. Recombinant protein expression in *Escherichia coli*. *Current Opinion in Biotechnology* **10**(5): 411-421.
- Baumgart, T., Hammond, A.T., Sengupta, P., Hess, S.T., Holowka, D.A., Baird, B.A., and Webb, W.W. 2007. Large-scale fluid/fluid phase separation of proteins and lipids in giant plasma membrane vesicles. *Proc Natl Acad Sci U S A* **104**(9): 3165-3170.
- Baumgart, T., Hess, S.T., and Webb, W.W. 2003. Imaging coexisting fluid domains in biomembrane models coupling curvature and line tension. *Nature* **425**(6960): 821-824.
- Berrow, N.S., Bussow, K., Coutard, B., Diprose, J., Ekberg, M., Folkers, G.E., Levy, N., Lieu, V., Owens, R.J., Peleg, Y. et al. 2006. Recombinant protein expression and solubility screening in *Escherichia coli*: a comparative study. *Acta Crystallographica Section D* **62**(10): 1218-1226.
- Bertani, G. 1951. Studies on lysogenesis. I. The mode of phage liberation by lysogenic *Escherichia coli*. *J Bacteriol* **62**(3): 293-300.
- Biemans-Oldehinkel, E., Doeven, M.K., and Poolman, B. 2006. ABC transporter architecture and regulatory roles of accessory domains. *FEBS Lett* **580**(4): 1023-1035.

-
- Binz, H.K., Amstutz, P., Kohl, A., Stumpp, M.T., Briand, C., Forrer, P., Grutter, M.G., and Pluckthun, A. 2004. High-affinity binders selected from designed ankyrin repeat protein libraries. *Nat Biotechnol* **22**(5): 575-582.
- Breyton, C., Haase, W., Rapoport, T.A., Kuhlbrandt, W., and Collinson, I. 2002. Three-dimensional structure of the bacterial protein-translocation complex SecYEG. *Nature* **418**(6898): 662-665.
- Brown, D.A. and London, E. 1998. Functions of lipid rafts in biological membranes. *Annu Rev Cell Dev Biol* **14**: 111-136.
- Buchanan, S.K. 1999. Beta-barrel proteins from bacterial outer membranes: structure, function and refolding. *Curr Opin Struct Biol* **9**(4): 455-461.
- Carpenter, E.P., Beis, K., Cameron, A.D., and Iwata, S. 2008. Overcoming the challenges of membrane protein crystallography. *Current Opinion in Structural Biology* **18**(5): 581-586.
- Collinson, I. 2005. The structure of the bacterial protein translocation complex SecYEG. *Biochem Soc Trans* **33**(Pt 6): 1225-1230.
- Daßler, T., Maier, T., Winterhalter, C., and Böck, A. 2000. Identification of a major facilitator protein from *Escherichia coli* involved in efflux of metabolites of the cysteine pathway. *Molecular Microbiology* **36**(5): 1101-1112.
- Dalbey, R.E. and Chen, M. 2004. Sec-translocase mediated membrane protein biogenesis. *Biochim Biophys Acta* **1694**(1-3): 37-53.
- Daley, D.O., Rapp, M., Granseth, E., Melen, K., Drew, D., and von Heijne, G. 2005. Global topology analysis of the *Escherichia coli* inner membrane proteome. *Science* **308**(5726): 1321-1323.
- Danielli, J.F. and Davson, H. 1935. A contribution to the theory of permeability of thin films. *J Cell Comp Phys* **5**(4).
- Danielsen, S., Boyd, D., and Neuhard, J. 1995. Membrane topology analysis of the *Escherichia coli* cytosine permease. *Microbiology* **141**(11): 2905-2913.
- Danielsen, S., Kilstrup, M., Barilla, K., Jochimsen, B., and Neuhard, J. 1992. Characterization of the *Escherichia coli* codBA operon encoding cytosine permease and cytosine deaminase. *Mol Microbiol* **6**(10): 1335-1344.
- Daumas, F., Destainville, N., Millot, C., Lopez, A., Dean, D., and Salome, L. 2003. Confined diffusion without fences of a g-protein-coupled receptor as revealed by single particle tracking. *Biophys J* **84**(1): 356-366.
- Davis, E.O. and Henderson, P.J. 1987. The cloning and DNA sequence of the gene *xylE* for xylose-proton symport in *Escherichia coli* K12. *J Biol Chem* **262**(29): 13928-13932.

-
- Dean, M., Rzhetsky, A., and Allikmets, R. 2001. The human ATP-binding cassette (ABC) transporter superfamily. *Genome Res* **11**(7): 1156-1166.
- Deisenhofer, J., Epp, O., Miki, K., Huber, R., and Michel, H. 1985. Structure of the protein subunits in the photosynthetic reaction center of *Rhodopseudomonas-viridis* at 3 Å resolution. *Nature* **318**(6047): 618-624.
- Destainville, N., Dumas, F., and Salome, L. 2008. What do diffusion measurements tell us about membrane compartmentalisation? Emergence of the role of interprotein interactions. *J Chem Biol* **1**(1-4): 37-48.
- Dillon, D.A., Wu, W.I., Riedel, B., Wissing, J.B., Dowhan, W., and Carman, G.M. 1996. The *Escherichia coli* pgpB gene encodes for a diacylglycerol pyrophosphate phosphatase activity. *J Biol Chem* **271**(48): 30548-30553.
- Drew, D., Froderberg, L., Baars, L., and de Gier, J.W. 2003. Assembly and overexpression of membrane proteins in *Escherichia coli*. *Biochim Biophys Acta* **1610**(1): 3-10.
- Drew, D.E., von Heijne, G., Nordlund, P., and de Gier, J.W.L. 2001. Green fluorescent protein as an indicator to monitor membrane protein overexpression in *Escherichia coli*. *Febs Letters* **507**(2): 220-224.
- Driessens, A.J. and Nouwen, N. 2008. Protein translocation across the bacterial cytoplasmic membrane. *Annu Rev Biochem* **77**: 643-667.
- Edelhoch, H. 1967. Spectroscopic determination of tryptophan and tyrosine in proteins. *Biochemistry* **6**(7): 1948-1954.
- Feigenson, G.W. 2006. Phase behavior of lipid mixtures. *Nat Chem Biol* **2**(11): 560-563.
- Feilmeier, B.J., Iseminger, G., Schroeder, D., Webber, H., and Phillips, G.J. 2000. Green Fluorescent Protein Functions as a Reporter for Protein Localization in *Escherichia coli*. *J Bacteriol* **182**(14): 4068-4076.
- Foster, J.W., Park, Y.K., Penfound, T., Fenger, T., and Spector, M.P. 1990. Regulation of NAD metabolism in *Salmonella typhimurium*: molecular sequence analysis of the bifunctional nadR regulator and the nadA-pnuC operon. *J Bacteriol* **172**(8): 4187-4196.
- Fujiwara, T., Ritchie, K., Murakoshi, H., Jacobson, K., and Kusumi, A. 2002. Phospholipids undergo hop diffusion in compartmentalized cell membrane. *J Cell Biol* **157**(6): 1071-1081.
- Garavito, R.M. and Ferguson-Miller, S. 2001. Detergents as Tools in Membrane Biochemistry. *J Biol Chem* **276**(35): 32403-32406.
- Geertsma, E.R., Groeneveld, M., Slotboom, D.J., and Poolman, B. 2008. Quality control of overexpressed membrane proteins. *Proc Natl Acad Sci U S A* **105**(15): 5722-5727.

-
- Geller, B.L. 1991. Energy requirements for protein translocation across the *Escherichia coli* inner membrane. *Mol Microbiol* **5**(9): 2093-2098.
- Gorter, E. and Grendel, F. 1925. On Bimolecular Layers of Lipoids on the Chromocytes of the Blood. *J Exp Med* **41**(4): 439-443.
- Graslund, S., Nordlund, P., Weigelt, J., Hallberg, B.M., Bray, J., Gileadi, O., Knapp, S., Oppermann, U., Arrowsmith, C., Hui, R. *et al.* 2008. Protein production and purification. *Nat Methods* **5**(2): 135-146.
- Griffith, J.K., Baker, M.E., Rouch, D.A., Page, M.G., Skurray, R.A., Paulsen, I.T., Chater, K.F., Baldwin, S.A., and Henderson, P.J. 1992. Membrane transport proteins: implications of sequence comparisons. *Curr Opin Cell Biol* **4**(4): 684-695.
- Grigorieff, N., Ceska, T.A., Downing, K.H., Baldwin, J.M., and Henderson, R. 1996. Electron-crystallographic refinement of the structure of bacteriorhodopsin. *J Mol Biol* **259**(3): 393-421.
- Hanahan, D. 1983. Studies on transformation of *Escherichia coli* with plasmids. *J Mol Biol* **166**(4): 557-580.
- Heijne, G.v. 1999. Recent advances in the understanding of membrane protein assembly and structure. *Q Rev Biophys* **32**(4): 285-307.
- Heijne, G.v. 2007. The membrane protein universe: what's out there and why bother? *Journal of Internal Medicine* **261**(6): 543-557.
- Helenius, A., McCaslin, D.R., Fries, E., and Tanford, C. 1979. Properties of detergents. *Methods Enzymol* **56**: 734-749.
- Higgins, C.F. 1992. ABC transporters: from microorganisms to man. *Annu Rev Cell Biol* **8**: 67-113.
- Higgins, C.F. 2007. Multiple molecular mechanisms for multidrug resistance transporters. *Nature* **446**(7137): 749-757.
- Hollenstein, K., Dawson, R.J., and Locher, K.P. 2007. Structure and mechanism of ABC transporter proteins. *Curr Opin Struct Biol* **17**(4): 412-418.
- <http://www.uniprot.org>.
- Huang, Y., Lemieux, M.J., Song, J., Auer, M., and Wang, D.N. 2003. Structure and mechanism of the glycerol-3-phosphate transporter from *Escherichia coli*. *Science* **301**(5633): 616-620.
- Hunte, C., Michel, H., Carola, H., Gebhard Von, J., and Hermann, S.g. 2003. Membrane Protein Crystallization. In *Membrane Protein Purification and Crystallization (Second Edition)*, pp. 143-160. Academic Press, San Diego.

Hutchings, M.I., Palmer, T., Harrington, D.J., and Sutcliffe, I.C. 2009. Lipoprotein biogenesis in Gram-positive bacteria: knowing when to hold 'em, knowing when to fold 'em. *Trends Microbiol* **17**(1): 13-21.

Hvorup, R.N., Goetz, B.A., Niederer, M., Hollenstein, K., Perozo, E., and Locher, K.P. 2007. Asymmetry in the Structure of the ABC Transporter-Binding Protein Complex BtuCD-BtuF. *Science* **317**(5843): 1387-1390.

Hwang, P.M., Choy, W.Y., Lo, E.I., Chen, L., Forman-Kay, J.D., Raetz, C.R., Prive, G.G., Bishop, R.E., and Kay, L.E. 2002. Solution structure and dynamics of the outer membrane enzyme PagP by NMR. *Proc Natl Acad Sci U S A* **99**(21): 13560-13565.

Icho, T. 1988. Membrane-bound phosphatases in *Escherichia coli*: sequence of the *pgpB* gene and dual subcellular localization of the *pgpB* product. *J Bacteriol* **170**(11): 5117-5124.

Iwata, S. 2003. Crystallization Informatics of Membrane Proteins. In *Methods and Results in Crystallization of Membrane Proteins*, Vol 4 (ed. S. Iwata), pp. 281-294. International University Line.

Jana, S. and Deb, J.K. 2005. Strategies for efficient production of heterologous proteins in *Escherichia coli*. *Appl Microbiol Biotechnol* **67**(3): 289-298.

Jolly, C. and Sattentau, Q.J. 2005. Human immunodeficiency virus type 1 virological synapse formation in T cells requires lipid raft integrity. *J Virol* **79**(18): 12088-12094.

Keyhani, N.O. and Roseman, S. 1997. Wild-type *Escherichia coli* grows on the chitin disaccharide, N,N'-diacetylchitobiose, by expressing the cel operon. *Proc Natl Acad Sci U S A* **94**(26): 14367-14371.

Kido, M., Yamanaka, K., Mitani, T., Niki, H., Ogura, T., and Hiraga, S. 1996. RNase E polypeptides lacking a carboxyl-terminal half suppress a mukB mutation in *Escherichia coli*. *J Bacteriol* **178**(13): 3917-3925.

Kinch, L.N., Saier, M.H., Jr., and Grishin, N.V. 2002. Sec61beta--a component of the archaeal protein secretory system. *Trends Biochem Sci* **27**(4): 170-171.

King, L.S., Kozono, D., and Agre, P. 2004. From structure to disease: the evolving tale of aquaporin biology. *Nat Rev Mol Cell Biol* **5**(9): 687-698.

Koch, A.L. 1970. Turbidity measurements of bacterial cultures in some available commercial instruments. *Anal Biochem* **38**(1): 252-259.

Kolbe, M., Besir, H., uuml, seyin, Essen, L.-O., and Oesterhelt, D. 2000. Structure of the Light-Driven Chloride Pump Halorhodopsin at 1.8Å Resolution. *Science* **288**(5470): 1390-1396.

Krogh, A., Larsson, B., von Heijne, G., and Sonnhammer, E.L. 2001. Predicting transmembrane protein topology with a hidden Markov model: application to complete genomes. *J Mol Biol* **305**(3): 567-580.

-
- Kusumi, A., Sako, Y., and Yamamoto, M. 1993. Confined lateral diffusion of membrane receptors as studied by single particle tracking (nanovid microscopy). Effects of calcium-induced differentiation in cultured epithelial cells. *Biophys J* **65**(5): 2021-2040.
- Lacapère, J.-J., Pebay-Peyroula, E., Neumann, J.-M., and Etchebest, C. 2007. Determining membrane protein structures: still a challenge! *Trends in Biochemical Sciences* **32**(6): 259-270.
- Laemmli, U.K. 1970. Cleavage of structural proteins during the assembly of the head of bacteriophage T4. *Nature* **227**(5259): 680-685.
- Lamanna, C., Mallette M. F. 1973. *Basic bacteriology*. The Williams and Wilkins Co., Baltimore.
- Landau, E.M. and Rosenbusch, J.P. 1996. Lipidic cubic phases: a novel concept for the crystallization of membrane proteins. *Proc Natl Acad Sci U S A* **93**(25): 14532-14535.
- Lau, F.W. and Bowie, J.U. 1997. A method for assessing the stability of a membrane protein. *Biochemistry* **36**(19): 5884-5892.
- Law, C.J., Maloney, P.C., and Wang, D.N. 2008. Ins and outs of major facilitator superfamily antiporters. *Annu Rev Microbiol* **62**: 289-305.
- Lawrence, J.V. and Maier, S. 1977. Correction for the inherent error in optical density readings. *Appl Environ Microbiol* **33**(2): 482-484.
- le Maire, M., Champeil, P., and Moller, J.V. 2000. Interaction of membrane proteins and lipids with solubilizing detergents. *Biochim Biophys Acta* **1508**(1-2): 86-111.
- Lee, G.M., Zhang, F., Ishihara, A., McNeil, C.L., and Jacobson, K.A. 1993. Unconfined lateral diffusion and an estimate of pericellular matrix viscosity revealed by measuring the mobility of gold-tagged lipids. *J Cell Biol* **120**(1): 25-35.
- Lemieux, M.J., Huang, Y., and Wang, D.N. 2004. Glycerol-3-phosphate transporter of *Escherichia coli*: structure, function and regulation. *Res Microbiol* **155**(8): 623-629.
- Linton, K.J. and Higgins, C.F. 1998. The *Escherichia coli* ATP-binding cassette (ABC) proteins. *Mol Microbiol* **28**(1): 5-13.
- Locher, K.P., Lee, A.T., and Rees, D.C. 2002. The *E. coli* BtuCD structure: a framework for ABC transporter architecture and mechanism. *Science* **296**(5570): 1091-1098.
- Loll, P.J. 2003. Membrane protein structural biology: the high throughput challenge. *Journal of Structural Biology* **142**(1): 144-153.

-
- Lopez, P.J., Marchand, I., Joyce, S.A., and Dreyfus, M. 1999. The C-terminal half of RNase E, which organizes the *Escherichia coli* degradosome, participates in mRNA degradation but not rRNA processing *in vivo*. *Molecular Microbiology* **33**(1): 188-199.
- Luecke, H., Schobert, B., Lanyi, J.K., Spudich, E.N., and Spudich, J.L. 2001. Crystal Structure of Sensory Rhodopsin II at 2.4 Angstroms: Insights into Color Tuning and Transducer Interaction. *Science* **293**(5534): 1499-1503.
- Luirink, J., Heijne, G.v., Houben, E., and Gier, J.-W.d. 2005. Biogenesis of Inner Membrane Proteins in *Escherichia coli*. *Annual Review of Microbiology* **59**(1): 329-355.
- Luirink, J., ten Hagen-Jongman, C.M., van der Weijden, C.C., Oudega, B., High, S., Dobberstein, B., and Kusters, R. 1994. An alternative protein targeting pathway in *Escherichia coli*: studies on the role of FtsY. *EMBO J* **13**(10): 2289-2296.
- Lundbäck, A.-K., van den Berg, S., Hebert, H., Berglund, H., and Eshaghi, S. 2008. Exploring the activity of *tobacco etch virus* protease in detergent solutions. *Analytical Biochemistry* **382**(1): 69-71.
- Lundstrom, K. 2006. Structural genomics for membrane proteins. *Cellular and Molecular Life Sciences* **63**(22): 2597-2607.
- Marger, M.D. and Saier Jr, M.H. 1993. A major superfamily of transmembrane facilitators that catalyse uniport, symport and antiport. *Trends in Biochemical Sciences* **18**(1): 13-20.
- McKeegan, K.S., Borges-Walmsley, M.I., and Walmsley, A.R. 2002. Microbial and viral drug resistance mechanisms. *Trends Microbiol* **10**(10 Suppl): S8-14.
- McLuskey, K., Gabrielsen, M., Kroner, F., Black, I., Cogdell, R.J., and Isaacs, N.W. 2008. A protocol for high throughput methods for the expression and purification of inner membrane proteins. *Mol Membr Biol* **25**(8): 599-608.
- McLuskey, K., Roszak, A., Zhu, Y., and Isaacs, N. 2009. Crystal structures of all-alpha type membrane proteins. *European Biophysics Journal*, <http://www.springerlink.com/content/c785214508570616> (published online).
- Michel, H. 1983. Crystallization of membrane proteins. *Trends in Biochemical Sciences* **8**(2): 56-59.
- Miroux, B. and Walker, J.E. 1996. Over-production of proteins in *Escherichia coli*: mutant hosts that allow synthesis of some membrane proteins and globular proteins at high levels. *J Mol Biol* **260**(3): 289-298.
- Mittal, K.L. 1972. Determination of CMC of polysorbate 20 in aqueous solution by surface tension method. *Journal of Pharmaceutical Sciences* **61**(8): 1334-1335.

-
- Mohanty, A.K., Simmons, C.R., and Wiener, M.C. 2003. Inhibition of *tobacco etch virus* protease activity by detergents. *Protein Expression and Purification* **27**(1): 109-114.
- Neugebauer, J.M. 1990. Detergents: an overview. *Methods Enzymol* **182**: 239-253.
- Newstead, S., Ferrandon, S., and Iwata, S. 2008. Rationalizing alpha-helical membrane protein crystallization. *Protein Sci* **17**(3): 466-472.
- Nouwen, N., Berrelkamp, G., and Driessens, A.J. 2007. Bacterial sec-translocase unfolds and translocates a class of folded protein domains. *J Mol Biol* **372**(2): 422-433.
- Ono, A. and Freed, E.O. 2001. Plasma membrane rafts play a critical role in HIV-1 assembly and release. *Proc Natl Acad Sci USA* **98**(24): 13925-13930.
- Ostermeier, C., Iwata, S., Ludwig, B., and Michel, H. 1995. Fv fragment-mediated crystallization of the membrane protein bacterial cytochrome c oxidase. *Nat Struct Mol Biol* **2**(10): 842-846.
- Oxenoid, K. and Chou, J.J. 2005. The structure of phospholamban pentamer reveals a channel-like architecture in membranes. *Proc Natl Acad Sci USA* **102**(31): 10870-10875.
- Pace, C.N., Vajdos, F., Fee, L., Grimsley, G., and Gray, T. 1995. How to measure and predict the molar absorption coefficient of a protein. *Protein Sci* **4**(11): 2411-2423.
- Pebay-Peyroula, E., Rummel, G., Rosenbusch, J.P., and Landau, E.M. 1997. X-ray structure of bacteriorhodopsin at 2.5 angstroms from microcrystals grown in lipidic cubic phases. *Science* **277**(5332): 1676-1681.
- Peti, W. and Page, R. 2007. Strategies to maximize heterologous protein expression in *Escherichia coli* with minimal cost. *Protein Expr Purif* **51**(1): 1-10.
- Phillips, R. and Quake, S.R. 2006. The Biological Frontier of Physics. *Physics Today* **59**(5): 38-43.
- Pike, L.J. 2006. Rafts defined: a report on the Keystone Symposium on Lipid Rafts and Cell Function. *J Lipid Res* **47**(7): 1597-1598.
- Privè, G.G. 2007. Detergents for the stabilization and crystallization of membrane proteins. *Methods* **41**(4): 388-397.
- Rapoport, T.A. 2007. Protein translocation across the eukaryotic endoplasmic reticulum and bacterial plasma membranes. *Nature* **450**(7170): 663-669.
- Rapoport, T.A., Jungnickel, B., and Kutay, U. 1996. Protein transport across the eukaryotic endoplasmic reticulum and bacterial inner membranes. *Annu Rev Biochem* **65**: 271-303.

-
- Rapp, M., Drew, D., Daley, D.O., Nilsson, J., Carvalho, T., Melen, K., De Gier, J.W., and Von Heijne, G. 2004. Experimentally based topology models for *E. coli* inner membrane proteins. *Protein Sci* **13**(4): 937-945.
- Rath, A., Glibowicka, M., Nadeau, V.G., Chen, G., and Deber, C.M. 2009. Detergent binding explains anomalous SDS-PAGE migration of membrane proteins. *Proc Natl Acad Sci U S A* **106**(6): 1760-1765.
- Rawicz, W., Olbrich, K.C., McIntosh, T., Needham, D., and Evans, E. 2000. Effect of Chain Length and Unsaturation on Elasticity of Lipid Bilayers. *Biophysical Journal* **79**(1): 328-339.
- Rees, D.C., Johnson, E., and Lewinson, O. 2009. ABC transporters: the power to change. *Nat Rev Mol Cell Biol* **10**(3): 218-227.
- Rhodes, G. 1993. *Crystallography Made Crystal Clear: A Guide for Users of Macromolecular Models*. Academic Press Ltd. London, London.
- Rosen, M.J. 2004. *Surfactants and interfacial phenomena*. Hoboken: John Wiley & Sons, Inc.
- Sahdev, S., Khattar, S.K., and Saini, K.S. 2008. Production of active eukaryotic proteins through bacterial expression systems: a review of the existing biotechnology strategies. *Mol Cell Biochem* **307**(1-2): 249-264.
- Saier, M.H., Jr. 2003. Tracing pathways of transport protein evolution. *Mol Microbiol* **48**(5): 1145-1156.
- Saier, M.H., Ma, C.H., Rodgers, L., Tamang, D.G., Yen, M.R., Allen I. Laskin, S.S., and Geoffrey, M.G. 2008. Chapter 6 Protein Secretion and Membrane Insertion Systems in Bacteria and Eukaryotic Organelles. In *Advances in Applied Microbiology*, Vol Volume 65, pp. 141-197. Academic Press.
- Sambrook, J., Fritsch, E.F., and Maniatis, T. 1989. *Molecular Cloning: A Laboratory Manual*. . Cold Spring Harbour Laboratory Press, New York.
- Schein, C.H. and Noteborn, M.H.M. 1988. Formation of Soluble Recombinant Proteins in *Escherichia Coli* is Favored by Lower Growth Temperature. *Nat Biotech* **6**(3): 291-294.
- Schmidt, K.L., Peterson, N.D., Kustusch, R.J., Wissel, M.C., Graham, B., Phillips, G.J., and Weiss, D.S. 2004. A Predicted ABC Transporter, FtsEX, Is Needed for Cell Division in *Escherichia coli*. *J Bacteriol* **186**(3): 785-793.
- Schulz, G.E. 2000. beta-Barrel membrane proteins. *Curr Opin Struct Biol* **10**(4): 443-447.
- Schulz, H., Fabianek, R.A., Pellicoli, E.C., Hennecke, H., and Thony-Meyer, L. 1999. Heme transfer to the heme chaperone CcmE during cytochrome c maturation requires

the CcmC protein, which may function independently of the ABC-transporter CcmAB. *Proc Natl Acad Sci U S A* **96**(11): 6462-6467.

Scotti, P.A., Valent, Q.A., Manting, E.H., Urbanus, M.L., Driessens, A.J., Oudega, B., and Luirink, J. 1999. SecA is not required for signal recognition particle-mediated targeting and initial membrane insertion of a nascent inner membrane protein. *J Biol Chem* **274**(42): 29883-29888.

Seddon, A.M., Curnow, P., and Booth, P.J. 2004. Membrane proteins, lipids and detergents: not just a soap opera. *Biochim Biophys Acta* **1666**(1-2): 105-117.

Sehgal, P., Mogensen, J.E., and Otzen, D.E. 2005. Using micellar mole fractions to assess membrane protein stability in mixed micelles. *Biochim Biophys Acta* **1716**(1): 59-68.

Serek, J., Bauer-Manz, G., Struhalla, G., van den Berg, L., Kiefer, D., Dalbey, R., and Kuhn, A. 2004. *Escherichia coli* YidC is a membrane insertase for Sec-independent proteins. *EMBO J* **23**(2): 294-301.

Shaikh, S.R., Dumaual, A.C., Jenski, L.J., and Stillwell, W. 2001. Lipid phase separation in phospholipid bilayers and monolayers modeling the plasma membrane. *Biochim Biophys Acta* **1512**(2): 317-328.

Shultis, D.D., Purdy, M.D., Banchs, C.N., and Wiener, M.C. 2006. Outer membrane active transport: structure of the BtuB:TonB complex. *Science* **312**(5778): 1396-1399.

Sijbrandi, R., Urbanus, M.L., ten Hagen-Jongman, C.M., Bernstein, H.D., Oudega, B., Otto, B.R., and Luirink, J. 2003. Signal recognition particle (SRP)-mediated targeting and Sec-dependent translocation of an extracellular *Escherichia coli* protein. *J Biol Chem* **278**(7): 4654-4659.

Simons, K. and van Meer, G. 1988. Lipid sorting in epithelial cells. *Biochemistry* **27**(17): 6197-6202.

Singer, S.J. and Nicolson, G.L. 1972. The fluid mosaic model of the structure of cell membranes. *Science* **175**(23): 720-731.

Skou, J.C. 1998. Nobel Lecture. The identification of the sodium pump. *Biosci Rep* **18**(4): 155-169.

Smirnova, I., Kasho, V., Choe, J.Y., Altenbach, C., Hubbell, W.L., and Kaback, H.R. 2007. Sugar binding induces an outward facing conformation of LacY. *Proc Natl Acad Sci U S A* **104**(42): 16504-16509.

Sofia, H.J., Burland, V., Daniels, D.L., Plunkett, G., III, and Blattner, F.R. 1994. Analysis of the *Escherichia coli* genome. V. DNA sequence of the region from 76.0 to 81.5 minutes. *Nucl Acids Res* **22**(13): 2576-2586.

-
- Song, S. and Park, C. 1998. Utilization of D-ribose through D-xylose transporter. *FEMS Microbiol Lett* **163**(2): 255-261.
- Sprong, H., van der Sluijs, P., and van Meer, G. 2001. How proteins move lipids and lipids move proteins. *Nat Rev Mol Cell Biol* **2**(7): 504-513.
- Stevens, R.C. 2000. Design of high-throughput methods of protein production for structural biology. *Structure* **8**(9): R177-R185.
- Strop, P. and Brunger, A.T. 2005. Refractive index-based determination of detergent concentration and its application to the study of membrane proteins. *Protein Sci* **14**(8): 2207-2211.
- Studier, F.W. 2005. Protein production by auto-induction in high-density shaking cultures. *Protein Expression and Purification* **41**(1): 207-234.
- Studier, F.W. and Moffatt, B.A. 1986. Use of bacteriophage T7 RNA polymerase to direct selective high-level expression of cloned genes. *J Mol Biol* **189**(1): 113-130.
- Sumiya, M., Davis, E.O., Packman, L.C., McDonald, T.P., and Henderson, P.J. 1995. Molecular genetics of a receptor protein for D-xylose, encoded by the gene *xylF*, in *Escherichia coli*. *Receptors Channels* **3**(2): 117-128.
- Sun, X. and Whittaker, G.R. 2003. Role for influenza virus envelope cholesterol in virus entry and infection. *J Virol* **77**(23): 12543-12551.
- Surade, S., Klein, M., Stolt-Bergner, P.C., Muenke, C., Roy, A., and Michel, H. 2006. Comparative analysis and "expression space" coverage of the production of prokaryotic membrane proteins for structural genomics. *Protein Sci* **15**(9): 2178-2189.
- Swaisgood, M. and Schindler, M. 1989. Lateral diffusion of lectin receptors in fibroblast membranes as a function of cell shape. *Exp Cell Res* **180**(2): 515-528.
- Takamatsu, H., Bunai, K., Horinaka, T., Oguro, A., Nakamura, K., Watabe, K., and Yamane, K. 1997. Identification of a region required for binding to presecretory protein in *Bacillus subtilis* Ffh, a homologue of the 54-kDa subunit of mammalian signal recognition particle. *Eur J Biochem* **248**(2): 575-582.
- Teng, T.-Y. 1990. Mounting of crystals for macromolecular crystallography in a free-standing thin film. *Journal of Applied Crystallography* **23**(5): 387-391.
- Terpe, K. 2006. Overview of bacterial expression systems for heterologous protein production: from molecular and biochemical fundamentals to commercial systems. *Appl Microbiol Biotechnol* **72**(2): 211-222.
- Touze, T., Blanot, D., and Mengin-Lecreulx, D. 2008. Substrate specificity and membrane topology of *Escherichia coli* PgpB, an undecaprenyl pyrophosphate phosphatase. *J Biol Chem* **283**(24): 16573-16583.

-
- Van den Berg, B., Clemons, W.M., Jr., Collinson, I., Modis, Y., Hartmann, E., Harrison, S.C., and Rapoport, T.A. 2004. X-ray structure of a protein-conducting channel. *Nature* **427**(6969): 36-44.
- van Meer, G., Voelker, D.R., and Feigenson, G.W. 2008. Membrane lipids: where they are and how they behave. *Nat Rev Mol Cell Biol* **9**(2): 112-124.
- Varela, A.S., Macho, M.I.S., and González, A.G. 1995. The size of sodium dodecyl sulfate micelles in the presence of alcohols as determined by fluorescence quenching measurements. *Colloid & Polymer Science* **273**(9): 876-880.
- Veesler, D., Blangy, S., Cambillau, C., and Sciara, G. 2008. There is a baby in the bath water: AcrB contamination is a major problem in membrane-protein crystallization. *Acta Crystallogr Sect F Struct Biol Cryst Commun* **64**(Pt 10): 880-885.
- Vereb, G., Szollosi, J., Matko, J., Nagy, P., Farkas, T., Vigh, L., Matyus, L., Waldmann, T.A., and Damjanovich, S. 2003. Dynamic, yet structured: The cell membrane three decades after the Singer-Nicolson model. *Proc Natl Acad Sci U S A* **100**(14): 8053-8058.
- Vincentelli, R., Bignon, C., Gruez, A., Canaan, S., Sulzenbacher, G., Tegoni, M., Campanacci, V., and Cambillau, C. 2003. Medium-Scale Structural Genomics: Strategies for Protein Expression and Crystallization. *Accounts of Chemical Research* **36**(3): 165-172.
- Voet, D., Voet, J.G., and Pratt, C.W. 2002. *Biochemie*. Wiley-VCH Verlag GmbH Weinheim.
- Wagner, S., Baars, L., Ytterberg, A.J., Klussmeier, A., Wagner, C.S., Nord, O., Nygren, P.A., van Wijk, K.J., and de Gier, J.W. 2007. Consequences of membrane protein overexpression in *Escherichia coli*. *Mol Cell Proteomics* **6**(9): 1527-1550.
- Waldo, G.S., Standish, B.M., Berendzen, J., and Terwilliger, T.C. 1999. Rapid protein-folding assay using green fluorescent protein. *Nature Biotechnology* **17**(7): 691-695.
- White, S. 2008. Membrane Proteins of known 3D structures. Available from http://blanco.biomol.uci.edu/Membrane_Proteins_xtal.html.
- Wu, L.F. and Mandrand-Berthelot, M.A. 1995. A family of homologous substrate-binding proteins with a broad range of substrate specificity and dissimilar biological functions. *Biochimie* **77**(9): 744-750.
- Yin, Y., He, X., Szewczyk, P., Nguyen, T., and Chang, G. 2006. Structure of the multidrug transporter EmrD from *Escherichia coli*. *Science* **312**(5774): 741-744.
- Yoshikawa, S., Shinzawa-Itoh, K., and Tsukihara, T. 1998. Crystal Structure of Bovine Heart Cytochrome c Oxidase at 2.8 Å Resolution. *Journal of Bioenergetics and Biomembranes* **30**(1): 7-14.

Zhu, N., Olivera, B.M., and Roth, J.R. 1991. Activity of the nicotinamide mononucleotide transport system is regulated in *Salmonella typhimurium*. *J Bacteriol* **173**(3): 1311-1320.

Zulauf, M. 1991. Detergent Phenomena in membrane protein crystallization. In *Crystallization of Membrane Proteins*, (ed. H. Michel), pp. 53-72. CEC Press.